Starved Holes and Active Nuclei

The Central Engine in Galactic Centers

Hungernde Löcher und aktive Kerne

Die zentrale Maschine in galaktischen Zentren

Inaugural-Dissertation
zur Erlangung der Doktorwürde
der Mathematisch-Naturwissenschaftlichen Fakultät
der Rheinischen Friedrich-Wilhelms-Universität
zu Bonn

vorgelegt von

Heino Falcke

aus Köln

Juni 1994
Max-Planck-Institut für Radioastronomie
Bonn

Angefertigt mit Genehmigung der

Math.-Nat. Fakultät der Universität Bonn

Referent: Prof. Dr. P.L. Biermann
Koreferent: Prof. Dr. H.J. Fahr

Tag der Promotion: 4. Juli 1994

This whole way of thinking and acting rests on the assumption that reality is reliable, not that disasters, and failures, and evil things will never happen, but that the world in which they happen ultimately makes sense. It is not just 'buzzing, booming confusion' but springs from the will of a creator whose purposes are trustworthy and whose ultimate aim is glorious however dark and mysterious the way to it.

(John Habgod in "Can Scientists Believe?", Ed. Sir Nevill Mott, 1991)

Abstract

In this thesis the standard paradigm for the explanation of activity in galaxies is tested and extended. It is proposed that most galaxies harbor a massive black hole in their nuclei with a closely coupled accretion disk/jet system. The level of activity is mainly determined by the overall accretion flow. A model is developed to describe the broad-band (radio to X-ray) emission of a coupled jet/disk system and it is shown that a sample of radio loud *and* radio quiet quasars as well as the Galactic Center source Sgr A* can be explained by such a model the latter resembling an "AGN on a starvation diet". The parameters for jets in luminous AGN are consistent with previously found values and there is evidence for the presence of relativistic jets also in radio weak quasars. An important mechanism for injecting synchrotron emitting particles in radio loud jets could be secondary pair production in hadronic cascades following *pp*-collisions leading to an electron distribution with low-energy cut-off. Finally, it is proposed that the difference between radio loud and radio weak quasars, the rarity of FR I type quasars and the difference between FR I and FR II radio galaxies is simply due to a different environment on the pc-scale ('obscuring torus') the jet/disk system is interacting with. It is postulated that the opening angle of obscuring tori in AGN depend on the power of the central engine and the host galaxy type where the tori in elliptical galaxies narrow to the jet beaming angle at $L_{\rm disk} \leq 10^{46}$ erg/sec.

Vorwort

Diese Dissertation ist ein reines Zufallsprodukt – geplant war ein ganz anderes Thema. Am Anfang dieser Arbeit stand daher ein thematischer Seitensprung, nämlich der Versuch, neuere Daten über das Zentrum der Milchstraße, gewonnen am MPIfR in Bonn und dem MPE in Garching, besser zu verstehen. Es war mehr der Spieltrieb, der uns dazu brachte, die schon etwas verstaubten Modelle für AGN – gigantische Monster in den Zentren weit entfernter Galaxien mit unvorstellbar hohen Energieausstößen – auch auf unser kümmerliches Galaktisches Zentrum anzuwenden. Dabei bot sich auch noch einmal die Möglichkeit, das sogenannte Standardparadigma für AGN in verschiedene Richtungen hin auszuloten und darin neue Wege zu entdecken oder zumindest Begradigungen vorzunehmen, wo historischer Wildwuchs gelegentlich den Blick verstellte.
Wichtig war uns, daß jeder Schritt, wenn er schon nicht beweisbar war, so doch konzeptuell plausibel und durchschaubar sein sollte. Bei der Abwägung zwischen aufwendiger Modellierung einzelner Schritte oder Diskussion vieler Einzelpunkte in Blick auf ein Gesamtkonzept haben wir uns für letzteres entschieden. Mein Vorteil dabei war, daß ich dies unbelastet von den Diskussionen der letzten 30 Jahre tun konnte, gleichzeitig aber immer wieder durch meinen Doktorvater auf die alten Fragestellungen gestoßen wurde. Beeinflußt hat diese Arbeit sicher auch die höchst aktuelle Sehnsucht der Physiker (und Physikerinnen) nach einer "großen vereinheitlichten Theorie", die in den letzten Jahren auch die Astronomen gepackt zu haben scheint – wobei mich nur wundert, daß es so lange gedauert hat.
Das Resultat ist nicht nur ein Modell für das Galaktische Zentrum, sondern auch eine Reihe von Vorschlägen zum Verständnis aktiver Galaxien und eine Modifikation, ja eine Zusammenfassung der Vereinheitlichungstheorien für den Zoo extragalaktischer Objekte die sogar eine Erklärung für das alte Rätsel der Dichotomie zwischen radio-lauten und radio-leisen Quasaren anbietet. Grundphilosophie ist dabei, daß die Physik des die Aktivität hervorrufenden schwarzen Loches – sozusagen das Atom der AGN Physik – überall dieselbe ist, daß aber die Erscheinungsformen der Aktivität von den Zufälligkeiten der Umgebung abhängen.
Nun sind bekanntlich fast 90% der bei der wissenschaftlichen Arbeit entstehenden Ideen falsch, nicht anwendbar oder gar überflüssig. Und wenn ich mir die exponentiell wachsenden Regale mit Journalen anschaue, befürchte ich, daß auch 90% der publizierten Arbeiten falsch, nicht anwendbar oder überflüssig sind — aber wer möchte von vorneherein entscheiden, welche Arbeiten und Ideen das im einzelnen sind. Insofern blicke ich mit ruhiger Gelassenheit auf diese Arbeit hier; schlimmer als falsch, nicht anwendbar und überflüssig kann sie nicht sein auch wenn ich zur Zeit das Gegenteil hoffe.
Zum Schluß noch ein paar Worte zur äußeren Form. Ich werde fast durchgängig das Wort "wir" gebrauchen, nicht nur, um den Leser mit einzubeziehen, sondern auch, um deutlich zu machen, daß jeder Teil in einer (auch internationalen) Kollaboration entstanden ist, insbesondere aber auch in ungezählten Diskussionen in unserer Arbeitsgruppe, wo ein freier und ungeschützter Austauch von Gedanken notwendig und möglich war. Wissenschaft muß sich mitteilen – sonst ist es keine – und da Wissenschaft international ist, muß man sich auf eine gemeinsame Sprache einigen. Mit Blick auf meine Schulzeit stelle ich erleichtert fest, daß Latein den einstigen Status einer Lingua Franca verloren hat. Deutsch ging als internationale Wissenschaftssprache mit der Weimarer Republik im nationalen Größenwahn unwiederbringbar unter. Bleibt am Ende, auch für diese Promotion, nur das Schulenglisch: nicht schön, aber verständlich für die, die ihre Gedanken und Daten mit eingebracht haben und für die, die es noch tun möchten.

Heino Falcke, im Juni 1994

Contents

Chapter 1

Zusammenfassung – Summary

1.1 Zusammenfassung

1.1.1 Die Scheibe im Galaktischen Zentrum

Neuere Beobachtungen von Sgr A* im Galaktischen Zentrum erlauben es, Modelle über die Natur dieser Quelle besser zu determinieren und legen die Existenz eines massereichen Schwarzen Loches ($M \leq 2 \cdot 10^6 M_\odot$) nahe, das von einer Akkretionsscheibe umgeben ist. Die Leuchtkraft dieser Quelle liegt bei $< 7 \cdot 10^5 L_\odot$, wobei davon auszugehen ist, daß der größte Teil der zentralen Leuchtkraft von Sternen produziert wird. Diese niedrige Leuchtkraft steht im krassen Widerspruch zu sphärischen Akkretionsmodellen für Sgr A*. Wir berechnen daher Spektren von Akkretionsscheiben um Scharze Löcher in der Kerr Geometrie. Leuchtktraft und Effektiv-Temperatur dieser Spektren machen es möglich, den Parameterbereich für die Masse, die Akkretionsrate und den Drehimpuls des Schwarzen Loches in Sgr A* einzugrenzen.
Ein Strahlungsfeld von $L \simeq 7 \cdot 10^4 - 7 \cdot 10^5 L_\odot$ und $T_{\rm eff} \simeq 2 - 4 \cdot 10^4$K kann durch ein stark rotierendes Kerr Loch und eine Akkretionsrate von $10^{-8.5} M_\odot/\mathrm{yr} < \dot{M} < 10^{-7} M_\odot/\mathrm{yr}$ beschrieben werden. Ein Schwarzes Loch mit $M \ll 2 \cdot 10^6\,\mathrm{M}_\odot$ erscheint unwahrscheinlich. Die Heizung des Gases innerhalb einer Bogensekunde um Sgr A* Spektrum von Sgr A* hängt sehr stark von den Parametern des Schwarzen Loches ab, was wir durch Photoionisationsrechnungen belegen.

1.1.2 Der Jet im Galaktischen Zentrum

Die Entdeckung einer elongierten Struktur von Sgr A* bei 43 GHz und die Hinweise auf eine mögliche Akkretionsscheibe legen die Vermutung nahe, daß – wie bei AGN – Jet und Scheibe im Galaktischen Zentrum vorhanden und physikalisch gekoppelt sind. Wir modellieren die Radio Emission von Sgr A* mit einem Blandford & Königl Jet und analysieren den Energiehaushalt des gekoppelten Jet/Scheibe Systems, welches durch die Akkretionsenergie parametrisiert wird. Auf diese Weise können wir die untere Grenze $\dot{M} \gg 10^{-8.5} M_\odot$ für die Akkretionsrate von Sgr A* bestätigen. Aus den Beobachtungdaten läßt sich mit Hilfe des Modelles ableiten, daß die Leistungen im Jet und in der Scheibe von gleicher Größenordnung sind. Das Jet Modell, unter Annahme eines zentralen $10^6 M_\odot$ Schwarzen Loches, ist auch qualitativ in der Lage, den sub-mm Excess und das Fehlen nicht-thermischer IR Strahlung zu erklären. Die geringe Größe des Radiokernes ist eine natürliche Folge der niedrigen Akkretionsrate von Sgr A*.

1.1.3 Jet/Scheibe Symbiose – Breitband Spektrum des Monsters

Wir starten mit dem grundlegenden Ansatz, daß Radiojets und Akkretionsscheiben symbiotische Gebilde sind, die beide mit der Akkretionsrate skalieren und in radio-lauten und radio-schwachen Quasaren zu finden sind. Dazu erweitern wir das Blandford & Königl Jet Modell ganz allgemein mit der Bedingung von Energie- und Massenerhaltung im Jet/Scheibe System. Der Jet wird als konisch expandierender Plasmastrom mit maximaler Schallgeschwindigkeit $c/\sqrt{3}$ beschrieben, welcher magnetische Felder und relativistische Teilchen transportiert. Relativistische Geschwindigkeiten ($\gamma_{\rm j}\beta_{\rm j} \geq 5$) machen eine zusätzliche Kollimation überflüssig, so daß die Geometrie der Strömung allein durch den Mach-Kegel bestimmt wird.

Das Modell hängt nur von wenigen Parametern ab, die durch Beobachtung bestimmbar sind. Wir können zeigen, daß Radio und Röntgen Spektren der Kerne und Radiokeulen, sowie typische Dimensionen eines radio-lauten Quasars mit einem solchen Modell zu beschreiben sind; dabei berechnen wir konsistent ein synthetisches Breitbandspektrum eines Jet/Scheibe Systems.
Die hohe Effizienz radio-lauter Quasare kann nur erklärt werden, wenn man 'totale Equipartition' fordert, wobei Magnetfeld und Teilchen gleiche Energiedichten haben, der Poyntingfluß vergleichbar der kinetischen Energie ist und die gesamte Leistung im Jet vergleichbar der Scheibenleuchtkraft ist. Da aber die Anzahl der Elektronen im Plasma begrenzt ist, kann eine solche Situation nur eintreten, wenn entweder massiv $e^{\pm}$ Paare erzeugt werden oder die Elektronenpopulation einen niederenergetischen Cut-off bei ≥ 50 MeV zeigt. Letzteres wäre eine natürliche Konsequenz, wenn die Elektronen/Positronen durch hadronische Wechselwirkungen erzeugt und injiziert werden.
Die Emission radio-leiser Quasare kann im Prinzip mit dem gleichen Typ eines relativistischen und energetischen Jets erklärt werden, wobei der Unterschied zwischen radio-laut und radio-leise durch eine unterschiedliche Effizienz der Elektronen Injektion auf der sub-Parsec Skala erklärt werden kann.
Schließlich untersuchen wir noch die Bedeutung des hohen Energiebedarfes des Jets für die Akkretionsscheibe. Offensichtlich kann nur ein Prozeß, welcher in direktem Zusammenhang mit dem Dissipationsprozeß in der Scheibe steht, die Jet-Entstehung erklären.

1.1.4 Jet und Scheibe in Quasaren

Im Lichte der zuvor entwickelten theoretischen Grundlagen untersuchen wir Korrelationen zwischen Akkretionsscheiben und Radio Kern Leuchtkraft in einem Quasar Sample, welches alle PG Quasare einschließt. Dabei leiten wir empirische Konversionsfaktoren zwischen Scheibenleuchtkraft und Emissionslinienleucktkräften her. In einem Radio gegen $L_{\rm disk}$ Diagramm teilen sich die Quasare in vier unterschiedlich Klassen: Core Dominated Quasars (CDQ), Lobe Dominated Quasars (LDQ), Radio-Intermediate Quasar (RIQ) und radio-leise Quasare. In jeder Unterklasse, und insbesondere bei den radio-leisen Quasaren, skaliert die Radioemission mit der Scheibenleuchtkraft. Dies macht deutlich, daß Radio und UV Emission einen gemeinsamen Ursprung haben und daß die Aufspaltung in radio laut und radio-leise schon auf der Parsec Skala passiert. Beim Vergleich mit unserem Jet/Scheibe Modell finden wir, daß der Jet eine Gesamtleistung von ca. einem Drittel der Scheibenleuchtkraft benötigt. Streuung und Verlauf der UV-Radio Korrelation von LDQ und CDQ begrenzt den Parameterbereich des Jet Lorentzfaktors auf einen engen Bereich ($3 \leq \gamma_{\rm j} \leq 10$). Die, relativ zur Scheibenleuchtkraft gesehene, starke Emission des Radio Kernes ist kaum mit normaler Schockbeschleunigung thermischer Elektronen in eine Potenzverteilung zu erklären. Viel eher muß man die Erzeugung von $e^{\pm}$ Paaren und/oder Injektion von Elektronen oberhalb einer Schwelle von 50 MeV fordern – Erzeugung sekundärer Paare in hadronischen Kaskaden könnte solch ein Prozess sein.
Die Radioemission radio-leiser Quasare kann mit denselben Parametern für einen leistungsstarken, relativistischen Jet – wie in radio-lauten Quasaren – erklärt werden, wenn die Erzeugung von Sekundärteilchen unterdrückt ist. So ließen sich auch die RIQ als geboostete radio-leise Quasare erklären.
Unser Diagramm bietet darüberhinaus einen direkten Test für die FR II/Quasar Vereinheitlichungstheorie. Aus dem Verhältnis $Q_{\rm jet}/L_{\rm disk}$ können wir die versteckte Scheibenleuchtkraft von FR II Galaxien aus ihren Radioeigenschaften abschätzen und mit Quasaren vergleichen. Wie erwartet, fallen Lobe- und Kernleuchtkräfte der beiden Populationen zusammen.

1.1.5 Vereinheitlichung der Vereinheitlichungstheorien

In dem zuvor erstellten *Radio*/$L_{\rm disk}$ Diagramm ist auffällig, daß unterhalb einer kritischen Leuchtkraft von $\sim 10^{46}$ erg/sec keine radio-lauten Quasare mehr auftreten. Wir bringen dies in Zusammenhang mit dem völligen Fehlen von Quasaren mit FR I Radiomorphologie und schlagen vor, daß die Wechselwirkung des Jets mit einem optisch dicken Torus mit kleinem Öffnungswinkel diesen Effekt erklären könnte. Das FR I/BL Lac Phänomen käme dadurch zustande, daß ein quasi geschlossener Torus die zentrale Leuchtkraft fast vollständig absorbiert und gleichzeitig den Jet rapide abbremst. Überhalb einer kritischen Jet-Energie gelänge es dem Jet, den Torus abzutragen und zu öffnen. Dies würde einen ungestörten Blick auf die zentrale Maschine erlauben und einen relativistischen (FR II) Jetstrom ermöglichen. Die Wechselwirkung mit dem Torus könnte immer noch zur Kollimation des Jets dienen. Darüberhinaus wäre ein mit dem Jet wechselwirkender Torus ein gutes Target für pp Kollisionen, die gebraucht werden, um über Paarerzeugung die hohe Radioleuchtkraft radio-lauter Jets zu erklären.

Für den Fall, daß der optisch dicke Torus in Spiralgalaxien aufgrund höheren Drehimpules viel leichter zu öffnen wäre, hätte man zusätzlich noch eine Erklärung für den Unterschied zwischen radio-laut und radio-leise: Die viel schwächere Wechselwirkung zwischen Jet und Torus würde weder den Jet kollimieren können, noch genügend $e^{\pm}$ Paare erzeugen, um einen radio-lauten Kern zu produzieren.

1.2 Summary

1.2.1 The Disk in the Galactic Center

Recent observations of the Galactic Center source Sgr A* give strong constraints for possible models of its physical nature and suggest the presence of a massive black hole with $M \leq 2 \cdot 10^6 M_\odot$ surrounded by an accretion disk which we estimate to radiate at a luminosity of $< 7 \cdot 10^5 L_\odot$; we argue that most of the luminosity of the Galactic Center is due to stars. This low luminosity is a strong argument against recently proposed spherical accretion scenarios which predict higher values. We therefore calculate the appearance of a standard accretion disk around a Kerr hole in Sgr A* following from general relativity and a few fundamental assumptions. Effective temperature and luminosity of the disk spectra do not depend on the unknown viscosity mechanism but instead are quite sensitive to variations of intrinsic parameters: the mass, the accretion rate, the angular momentum of the accreting hole and the inclination angle.
A radiation field of $L \simeq 7 \cdot 10^4 - 7 \cdot 10^5 L_\odot$ and $T_{\rm eff} \simeq 2 - 4 \cdot 10^4$K ascribed to the central object is naturally explained by a rapidly rotating Kerr hole ($a > 0.9$) accreting $10^{-8.5} M_\odot/{\rm yr} < \dot{M} < 10^{-7} M_\odot/{\rm yr}$ at a black hole mass of $M \leq 2 \cdot 10^6\,{\rm M}_\odot$ seen almost edge on. A low mass black hole of $M \leq 10^3 M_\odot$ seems to be very unlikely. We also shortly discuss the possibility to further constrain parameters by analyzing the heating of the ambient medium around Sgr A* by the central source.

1.2.2 The jet in the Galactic Center

The discovery of an elongated structure of Sgr A* at 43 GHz and the evidence for an accretion disk surrounding a black hole lead us to assume that both, an accretion disk and a jet, are present in the Galactic Center and are physically linked. We model the radio emission of Sgr A* successfully with a Blandford & Königl type jet and analyze the energetics of the coupled jet-disk system where jet and disk are parametrized in terms of the accretion power. With this method we are able to confirm independently the lower limit of the Sgr A* accretion rate $\dot{M} \gg 10^{-8.5} M_\odot$ found previously. Moreover, using the limits imposed by observational data, we show that within such a jet-disk model, the total jet power $Q_{\rm jet}$ is of comparable order as the radiated disk luminosity $L_{\rm disk}$. A jet model together with the assumption of an $10^6 M_\odot$ black hole also qualitatively explains the submm excess and the lack of non-thermal IR radiation. The small size of the visible part of the jet (< 1 mas) is due to the low accretion rate of Sgr A*.

1.2.3 The jet-disk symbiosis – broadband spectrum of the monster

Starting from the assumption that radio jets and accretion disks are symbiotic features present in radio loud and radio quiet quasars we scale the bulk power of radio jets with the accretion power by adding mass- and energy conservation of the whole jet-disk system to the standard Blandford & Königl theory for compact radio cores. The jet is described as a conically expanding plasma with maximal sound speed $c/\sqrt{3}$ enclosing relativistic particles and a magnetic field. Relativistic speeds of $\gamma_{\rm j}\beta_{\rm j} \geq 5$ make an additional confinement unnecessary and the shape is solely given by the Mach cone. The model depends on only few parameters and can be constrained by observations. Thus we are able to show that radio and X-ray fluxes (SSC emission) of cores and lobes and typical dimensions of radio loud quasars are consistent with a jet being produced in the central engine. We present a synthetic broadband spectrum from radio to X-ray for a jet-disk system. The only way to explain the high efficiency of radio loud objects is to postulate that these objects consist of 'maximal jets' with 'total equipartition', where the magnetic energy flow of the jet is comparable to the kinetic jet power and the total jet power is a large fraction of the disk power. As the number of electrons is limited by the accretion flow, such a situation is only possible when the minimum Lorentz factor of the electron distribution is $\gamma_{\rm e,min} \geq 100$ ($E \geq 50$MeV) or/and a large number of pairs are present. Such an electron/positron population would be a necessary consequence of hadronic interactions and may lead to some interesting effects in the low frequency self-absorbed spectrum. Emission from radio weak quasars can be explained with an initially identical jet. The difference between radio loud and radio weak could be due to a different efficiency in accelerating relativistic electrons on the sub-parsec scale only. Finally we demonstrate that in order to appease the ravenous hunger of radio loud jets its production must be somehow linked to the dissipation process in the inner part of the disk.

1.2.4 Jet and disk in quasars

We investigate the correlations between accretion disk luminosity (UV) and radio core of an extended quasar sample, containing all PG quasars, also deriving empirical conversion factors from emission line luminosities to disk luminosities. This method allows us to investigate the radio properties of AGN on the absolute scale set by the accretion power. In a radio vs. $L_{\rm disk}$ plot we find the quasars to be separated into four classes: core dominated quasars (CDQ), lobe dominated quasars (LDQ), radio-intermediate quasars (RIQ) and radio weak quasars. In general the radio core emission scales with the disk luminosity, especially in the radio weak quasars. This shows that radio and UV emission have a common energy source and that the difference between radio loud and radio weak is established already on the parsec scale. Comparing our data with a simple jet emission model that takes the limits imposed by energy and mass conservation in a coupled jet-disk system into account, we find that radio loud jets carry a total power $Q_{\rm jet}$ that is at least 1/3 of the observed disk luminosity $L_{\rm disk}$. The strong radio core emission in radio loud quasars relative to $L_{\rm disk}$ is difficult to explain by normal acceleration of thermal electrons into a non-thermal powerlaw distribution. One rather is forced to postulate an efficient process producing a large number of pairs and/or a distribution with low-energy cut-off around 50 MeV – secondary pair production in hadronic cascades could be such a process. Width and shape of the UV-radio correlation of LDQ and CDQ limit the parameter range for the bulk Lorentz factor of the jet to a narrow region ($3 \leq \gamma_{\rm j} \leq 10$). The radio emission of radio weak quasars can be explained with exactly the same parameters for a powerful relativistic jet if secondary pair production, as suggested for radio loud jets, is inhibited. There is evidence that RIQ are the relativistically boosted population of radio weak quasar jets. Our diagram provides also a test for the unification of FRII radio galaxies with quasars. From the ratio $Q_{\rm jet}/L_{\rm disk}$ we can estimate the hidden disk luminosity of FR II galaxies from their radio properties alone and compare them with quasars. As expected core as well as lobe luminosities of both populations coincide.

1.2.5 Unified unification

We note that in our optically selected quasar sample below a critical power of $\sim 10^{46}$ erg/sec no radio loud quasars are found and link this to the absence of FRI type quasars. We suggest that jet/torus interaction could explain this and variety of related AGN properties. Following the logic of current unification schemes we propose that the FRI/BL Lac phenomenon is caused by a nearly closed torus that completely absorbes the optical emission while its interaction with the jet leads to a disruption and slow-down of the relativistic outflow. Above a certain power the jet is able to carry away most of the obscuring material. This opens the viewing cone for observing the quasar and allows an undisturbed propagation of a jet up to large distances. The interaction might also serve to collimate the jet. Via pp collisions of relativistic protons in the jet with target material from the dense torus the large number of $e^{\pm}$ pairs required for the intense radio emission can be produced. The difference between radio loud and radio quiet quasars is explained if in spiral galaxies the obscuring material is always disk like. The lack of jet/torus interaction would neither lead to a collimation of the jet nor to the production of an enhanced $e^{\pm}$ population.

Chapter 2

Introduction

Research on active galactic nuclei (AGN) is a field born in this century starting with the observations of emission lines in NGC 1068 (Fath 1908, Slipher 1917) and the discovery of the M87 jet. But at that time it was not clear at all, that this and other 'spiral nebulae' were distant galaxies (Hubble 1926) like the Milky Way. Funnily enough the key for our current understanding of AGN was already implied in Schwarzschilds (1916) solution of Einsteins field equations for the gravitational field around a spherical mass.
But what is an AGN? Today this term comprises a large variety of phenomena seen in the sky beyond the limits of our own galaxy in a vast frequency range from long radio wavelength (10^8 Hz) to $\gamma-$rays (10^{23} Hz) and above. All AGN have in common that a large amount of energy is released in a relatively compact ($R \ll 1\,\mathrm{pc} \simeq 3.1 \cdot 10^{18}$cm) region in the center of a galaxy not primarily produced by stars – although the latter is already interpretation and occasionally questioned (Terlevich & Melnick 1985). The actitvity manifests itself in various ways:

- a featureless optical continuum,
- ionization and heating of line emitting plasma,
- heating of huge amounts of gas and dust masses,
- compact non-thermal radio and high-energy emission,
- production of ultra-high energy (cosmic ray) particles with energies up to $3 \cdot 10^{20}$ eV,
- energetic bipolar outflows and relativistic jets.

A different combination and appearance of some or all of these elements has lead to a confusing zoo of AGN. There is a huge amount of reviews on this popular topic (to mention only a few: Osterbrock 1991; Wilson 1992; Antonucci 1993; Gopal-Krishna 1994) and we will not repeat this here or leave it to the discussions in subsequent chapters and merely give a short general overview over the specimen crowding the zoo and their standard interpretation:

2.1 The zoo

Seyfert galaxies were identified by Seyfert (1943) as galaxies with many high-ionization emission lines in the spectra of the nucleus of a normal galaxy. Usually two types (type 1 and type 2) of Seyfert galaxies are distinguished where type 1 galaxies show narrow (200-700 km/s) permitted lines of H I, HeI, He II and forbidden lines [O III] $\lambda\lambda 4959, 5007$ and [N II] $\lambda\lambda 5648, 6583$ plus broad (500-7000 km/s FWHM) lines of H I, He I, He II and Fe II. The full widths at nearly zero intensity can range up to 30000 km/s. This is generally interpreted as being due to clouds in two separate regions, one being very close to a central black hole and hence showing strong Doppler broading as a consequence of high rotational and turbulent velocities and the other one being further away and hence with smaller Doppler broadening. Accordingly the regions are called broad line region (BLR) and narrow line region (NLR). The spectra of Seyfert 2 galaxies show no broad lines, however, Antonucci & Miller (1985) discovered broad spectral lines in the polarized light of the Seyfert 2 NGC 1068 – light which apparently is scattered by a kind of mirror into the line of sight. This has lead to the Seyfert unification scheme

which assumes that Seyfert 2 and Seyfert 1 are basically the same objects seen under different aspect angles. An obscuring torus surrounding the nucleus is thought to be responsible for blocking the view of the optical continuum and the BLR for galaxies which are edge on to the observer. High resolution studies of Seyfert 2 galaxies have indeed shown that the gas is ionized within a narrow cone originating in the center (e.g. Pogge 1989a&b).
Active nuclei at the lowest end of the luminosity distribution like in M81 were called LINER (Low Ionization Narrow Emission-Line Region) by T. Heckman (1978). They show spectra like those of Seyfert 2 galaxies with a generally lower level of ionization. Interestingly some ellipticals show LINER spectra as well.

Quasars seem to be the more luminous siblings of Seyfert 1 galaxies. They were discovered as starlike objects (Quasi Stellar Objects = QSO) by M. Schmidt (1963) with unusual emission lines, when it became clear that these lines resemble an ordinary emission line spectrum which, however, was highly redshifted. The first quasar discovered this way was 3C 273 which until these days is often referred to as the archetype of a quasar. This may be true in the sense that almost all phenomena expected in quasars can be found in 3C 273, but this is mainly due to its high intrinsic luminosity and a small alignment between the jet axis and the line of sight (see Chap. 6) making it rather a very unusual object in the sky. The high redshift of quasars is usually attributed to their large distances (many 100 Mpc) in an expanding universe. In recent years it became more and more possible to obtain high resolution images of quasars, for nearer ones it can be shown that they reside in the nuclei of galaxies – mostly spiral galaxies. Although there seems to be a continuity from Seyferts to quasars a few sources ($\sim 10\%$) are different in that they exhibit very strong radio emission[1]. In fact there seems to be a dichotomy between quasars with strong radio emission (radio loud) and weak (radio weak) radio emission. The former seem to be exclusively associated with ellipticals while the latter reside mostly in spirals. Among the radio loud quasars one finds another subdivision between flat-spectrum (radio spectral index $\alpha > -0.5$, $S_\nu \propto \nu^\alpha$) and steep spectrum ($\alpha < -0.5$) quasars. The most likely explanation is that the flat spectrum radio core in quasars is caused by a relativistic jet (Chap. 5), which in sources well aligned with the line of sight is relativistically boosted and dominates the total spectrum. The steep spectrum is caused by isotropically radiating giant lobes and hot-spots at the termination point of the jet.

Radio galaxies were discovered already 1946 by J.S. Hey and collaborators (Cygnus A). These are almost exclusively giant elliptical galaxies with strong radio emission ($L_\nu(1.4\mathrm{GHz}) \geq 10^{30}$ erg/sec/Hz), most of them showing an extended radio structure. As usual, they come in two different classes. Considering the radio morphology and luminosity one distinguishes between Fanaroff-Riley type I and type II. The discovery of Fanaroff & Riley (1974) was that a critical radio luminosity at 178 MHz of $5 \cdot 10^{33}$ erg/sec/Hz exists which separates two clearly distinct morphological classes. The high power sources (FR II) are edge brightened showing two bright regions on both sides of a compact radio core. These lobes and hotspots are the brightest constituents of the radio maps. In low power sources (FR I) the situation is different where one sees a radio structure with a prominent central emission and lobes having declining radio emission with increasing distance from the center and resembling a chimney's smoke trail.

Blazars and BL Lac objects are the most unusual objects in this list of AGN. Their main characteristic is that they do not have any, except a strong featureless continuum that seems to extend from radio to optical wavelengths. The flux is polarized and highly variable. Due to the EGRET experiment on board the Gamma-Ray Observatory (GRO) we now know that blazars belong to a class of sources with the strongest high energy emission, extending beyond several 100-1000 MeV. The name BL Lac indicates that the archetype of this class was first identified as a variable star and not as an extragalactic object. It is now generally assumed that the strong featureless continuum in BL Lacs is strongly Doppler-boosted synchrotron emission from a relativistic jet (the flat spectrum core) pointing into the direction of the observer and giving the source the 'core dominated' look. This is mostly supported by the work of radioastronomers (see Witzel 1992): the radio spectrum of these sources is flat with variability timescales occasionally as short as a few hours and multi-epoch VLBI observations exhibit superluminal motion of VLBI blobs which is readily interpreted as being due to relativistic speeds. One distinguishes between several classes: BL Lacs themselves show no or only weak emission lines while blazars have quasar like emission lines with a highly variable and polarized continuum – the highly-polarizes quasars (HPQ). There is also a class of X-ray selected BL Lacs which show strong X-ray emission and only moderate radio emission.

[1] That was the point where the 'r' entered the term quasar (from quasi-stellar radio source)

2.2 The standard interpretation

It seems to be clear that some of the emission seen in AGN is produced by jets which can be seen directly in radio maps. Indications are very strong that these jets have bulk relativistic velocities and contain a magnetized relativistic gas of electrons (or pairs) in strong magnetic fields, producing synchrotron emission. The estimated Lorentz factors of the jets are ususally in the range $\gamma_{\rm j} \sim 5^{+30}_{-3}$ (see Chap. 6). Hence in some of the objects the observed radiation is strongly anisotropic and boosted. As the so called boosting cone is only a few degrees wide, boosting can not eplain all types of emission and there is an appreciable amount of energy in the spectral energy distribution (SED) of quasars left, mainly radiated in the optical-UV regime ('UV-bump'), that seems to be relatively isotropic. Therefore one comes to the conclusion that quasars emit total energies in the range 10^{44-48} erg/sec (see Chap. 6) and from variability studies we know that this incredible amount of energy is liberated in an extremely compact region smaller than 1 pc. By looking at the VLBI maps we can directly see that the large radio jets and lobes, carrying a kinetic powers of similar orders of magnitude (Rawlings & Saunders 1991), are produced at these small scales.

The best explanation so far for the underlying energy source of AGN is accretion of matter in a strong gravitational potential. The compactness of the region, however, requires also a very compact mass distribution, most likely a supermassive black hole. From the condition that outwards directed radiation pressure has to be smaller than the gravitational attraction for the matter to fall inwards (Eddington criterion) one derives masses for the central black hole of the order $10^6 - 10^{10}$ times the solar mass ($M_\odot$) and accretion rates of $0.01 - 100 M_\odot$/yr. The length scales for black holes corresponding to these masses are $3 \cdot 10^{11} - 3 \cdot 10^{15}$ cm. From the observation of a rotational axis (the jets) in active galaxies and the existence of disk like structure in astrophysical system (e.g. galaxies and solar sytem) it was proposed to assume accretion within a disk rather than spherical accretion onto the black hole. In fact the theory of disk accretion, which was already derived in the late fourties bei v. Weizsäcker and others, can explain the blue bump (Malkan & Sargen 1982) in quasars, X-ray emission of binary systems, and the Galactic Center source Sgr A* (see Chap. 3).

In order to spiral in, the gas in the disk dissipates $\sim 50\%$ of its potential energy and becomes heated to temperatures of several 10^4 K in typical AGN. This energy is radiated in the optical-UV regime and serves to ionize the BLR and NLR. Probably through amplification of magnetic fields a jet is formed in the inner region of the disk. The details of this processes are not understood to date, primarily because of the small, unresolved size of the region and the contribution of many different effects. For example it is not really clear where the X-ray emission, seen in AGN, is produced. It could be due to an optically thin corona above the disk, effects of the inner boundary layer between disk and black hole or irradiation of the disk from an external source (corona, clouds, jet etc.). It is also not understood how the dust beyond the central parsec is heated by the central source producing the so called IR-bump, e.g. either by particle heating (Niemeyer & Biermann 1993) or direct interception of photons (Sanders et al. 1989). Even the production and ionization of the BLR clouds is not yet understood although elaborated computer codes for investigation of photionization are available.

Despite all these uncertainties there has been considerable progress in the last 10 years in determining the principles governing the different appearances of AGN which has lead to the so called unification schemes. Besides the boosting due to relativistic beams, for which fairly solid evidence now exists, absorption by dense material in a torus-like geometry has become the second important ingredient that is assumed to be responsible for changing the look of an AGN. Stimulated by the Seyfert scheme, where a molecular torus inhibits a direct view of the central source, it was proposed that FRII radio galaxies (obscured), radio loud quasars and HPQs (beamed) are basically identical objects. A similar idea was proposed to unify FRI radio galaxies (obscured) and BL Lac objects (beamed). Curiously, this scheme, in contrast to the FRII/quasars/HPQ scheme, lacks a transitional population (like quasars) which is not obscured and not strongly beamed. Finally, although generally not called a unification scheme, it is believed that LINERs, Seyferts and radio weak quasars are basically similar and only differ by their accretion rates.

At present this leaves us with three species: FRI radio galaxies, FRII radio galaxies and radio weak quasars/Seyferts. The former two are associated with elliptical galaxies and the latter mostly with spiral galaxies, the latter two show evidence for an accreton disk while only the former two show direct evidence for a jet. What is the reason for this remaining trichotomy? Have we identified three fundamentally different engines working in the center of galaxies? Is the notion of black hole/jet/disk only true for the radio loud quasars species and intrinsically different for the other two? However, for esthetical reasons it would please theorists much better if they could use Occam's razor and argue that in fact the central engines are similiar in all of the three classes.

2.3 The approach

The purpose of this thesis now is to test the applicability of the black hole/disk/jet model in galacic nuclei over a wide range of parameters, disregarding any bias introduced by observational classification schemes. We will start with discussing the center of our own galaxy as this might be the 'AGN' with the lowest level of activity we can observe. Fortunately, one finds in the Galactic Center evidence for a massive black hole, an accretion disk and non-thermal radio (jet) emission which can successfully be explained as an AGN like system (Chap. 3&4). In Chap. 5&6 we will apply a similar analysis to samples of AGN and find that the same type of model yields a consistent picture for radio loud and radio weak quasars as well. From the Galactic Center to AGN we will cover a range of ~ 9 orders of magnitude in luminosity with basically one model engine – which is of course no proof but makes one confident that the standard paradigm of a super massive black hole plus disk and jet provides a solid base to explain the activity in the center of galaxies. Finally, this will lead us in Chapter 7 to propose a picture that might unify even the three remaining classes of AGN in to one general scheme by assuming that the central engines in AGN are intrinsically similar — from a starved hole like in Sgr A* up the spectacular active nuclei in quasars.

Chapter 3

The disk in the Galactic Center

3.1 Introduction

There is mounting evidence for the presence of a black hole surrounded by an accretion disk at the center of our Galaxy, provided by the following observations:

i) The kinematics of gas and stars in the inner parsecs requires an enclosed mass of a few $10^6 M_\odot$ within a galacto-centric radius of $R \leq 0.1\,\mathrm{pc}$ (see Genzel & Townes 1987, Sellgren 1988 and references therein).

ii) Morphology and kinematics of the layer of interstellar matter between the inner Lindblad resonance (i.e. $R \leq 2.5\,\mathrm{pc}$) and $R \simeq 1 - 0.1\,\mathrm{pc}$ show the expected characteristics of accretion disks in active galactic nuclei (AGN) (Zylka, Mezger & Lesch 1992 (hereafter ZML92), and references therein)

iii) Close to, or at the dynamical center of the Galaxy is the variable radio source Sgr A* interpreted as synchroton emission.

iv) The luminosity of the compact central object is $L \leq 7 \cdot 10^5 L_\odot$, far below the Eddington limit of $\simeq 2 - 4 \cdot 10^{10} L_\odot$ for a black hole with $M \simeq 1 - 2 \cdot 10^6 M_\odot$. A cavity in the Sgr A East core could be due to an explosive event in the past, when this accretion rate was several magnitudes higher (Zylka et al 1990).

v) The radio emission of Sgr A* could be explained as emission from a small scale nuclear jet, stressing the analogy to AGN (Falcke, Mannheim & Biermann 1993) where a massive black hole with an accretion disk is still the best explanation for the central engine. 7 mm (Krichbaum et al. 1993) and 3 mm VLBI observations of Sgr A* therefore give a firm test for the whole scenario.

Hence if there is a black hole surrounded by a hot accretion disk in the center of the Galaxy it would be underfed at present with an accretion rate of $\dot{M} \ll 10^{-6} M_\odot/\mathrm{yr}$ as compared with an accretion rate of $\simeq 0.03 M_\odot/\mathrm{yr}$ in the Eddington limit. The luminosity of $\leq 7 \cdot 10^5 L_\odot$ of the starved black hole would be mainly contributed by thermal emission from a $T_\mathrm{e} \simeq 2 - 4 \cdot 10^4\mathrm{K}$ plasma at the inner edge of an accretion disk (ZML92) in agreement with recent NIR observations by Eckart et al. (1992).
Various other attempts fail to explain these features of Sgr A*. Therefore here we propose to test the black hole concept in more detail by calculating the appearance of a disk around a rotating black hole, considering specifically the effects of the Kerr metric on the spectrum. We will demonstrate that a black hole mass of about $2 \cdot 10^6\ \mathrm{M}_\odot$ and the radiation field described above require a strongly rotating Kerr black hole with a low accretion rate and seen almost edge on.
However, at the moment the observational basis is too weak to give an unambiguous answer to the question whether such a configuration exists in the Galactic Center, since most of these observations are at the limit of what is technically possible. For an observer it should therefore be of highest interest to know, which the crucial observations are for a confirmation of a black hole/accretion disk configuration and for a determination of its parameters. We therefore compute in this chapter the characteristics of such a configuration for a parameter range suggested by the observations above. We find that a refined measurement of the effective temperature and the luminosity of the central object together with our grid of parameters should make it possible to differentiate between parameter combinations for a black hole/accretion disk model of the Galactic Center and even gives an estimate for the angular momentum of the hole.

3.2 A critical review of the crucial observations

The crucial observations related to the nature of the central compact object and its surrounding disk are: the kinematics of gas and stars, the mm-to-MIR spectrum of the central arcseconds, the NIR spectrum of Sgr A* and its effective temperature and luminosity.

Genzel & Townes (1987) and Sellgren (1988) – based on the same observational results – arrive at somewhat contradictory interpretations. Genzel & Townes state that the data are best approximated by a star cluster and a central point mass of $\simeq 2.5 - 3 \cdot 10^6 M_\odot$. Sellgren states that – if the core-radius of the star cluster is $\leq 0.1\,\mathrm{pc}$ – no central point mass is required, although in our opinion the model fit shown in her Fig. 4 requires a point mass of the order of $\sim 10^6 M_\odot$.

How well are the effective temperature and luminosity of the central object known? The dereddened spectrum (Eckart et al. (1991) adopt $A_K = 3.4$ and $A_H = 5.4$ corresponding to $A_v = 27$ mag) can be approximated by a Rayleigh-Jeans spectrum. Hence, if the radiation is thermal free-free emission from an opaque plasma, its electron temperature must be $T_\mathrm{e} > 10^4$K. This sets a lower limit for both T_e and L. Combining the Rayleigh-Jeans approximation $S_\mathrm{NIR} \propto \Omega_\mathrm{s} T_\mathrm{e}$ (Ω_s is the source solid angle) with the integrated Planck spectrum $L \propto \Omega_\mathrm{s} T_\mathrm{e}^4$ yields[1]

$$L = 7.5 \cdot 10^4 (T_\mathrm{e}/20\,000\mathrm{K})^3 L_\odot. \tag{3.1}$$

ZML92 obtained the luminosity of the central 30" by integrating the observed spectrum

$$L_\mathrm{IR}(30"; \lambda \geq 10\mu\mathrm{m}) = L_\mathrm{IR}(\text{star cluster}) + L_\mathrm{IR}(\text{central object}) \simeq 1.5 \cdot 10^6 L_\odot \tag{3.2}$$

This assumes that heating of the dust is due to contributions from both the star cluster and a central object. The contribution from the star cluster can be estimated from IRAS observations (Cox & Laureijs 1989). Fig. 14 of Cox & Mezger (1989) shows the accumulated bolometric luminosities of the star cluster (derived by Sanders and Lowinger (1972) from the $\lambda 2.2\mu$m surface brightness) and IRAS. Within $10 \leq R_\mathrm{pc} \leq 200$ both have the same functional dependence $L \propto R_\mathrm{pc}^{1.2}$. Specifically, the accumulated IRAS dust luminosity is

$$L_\mathrm{IRAS}(R) = 1.5 \cdot 10^6 R_\mathrm{pc}^{1.2} L_\odot \tag{3.3}$$

yielding $L_\mathrm{IR}(30"; \text{star cluster}, \lambda \geq 10\mu\mathrm{m}) \simeq 8 \cdot 10^5 L_\odot$ and leading to $L_\mathrm{IR}(\text{central object}) \simeq 7 \cdot 10^5 L_\odot$.

On the assumption that all radiation from the inner disk is absorbed by dust in the central 30" we can substitute the above luminosity in Eq. (3.1) and obtain an electron temperature $T_\mathrm{e} \simeq 42\,000$K. This is an upper limit since all other effects – e.g. a substantial contribution of the "He I emission-line stars" detected by Krabbe et al. (1991) in the inner parsec or a probable increase of dust extinction beyond $A_v = 27$ mag – tend to decrease T_e but increase L for a given T_e. Thus

$$20\,000\mathrm{K} < T_\mathrm{e} < 42\,000\mathrm{K} \tag{3.4}$$

and

$$7 \cdot 10^4 L_\odot < L(\text{central object}) < 7 \cdot 10^5 L_\odot \tag{3.5}$$

seem to be reasonable limits for T_e and L of the central object. *This implies that most of the central luminosity is from stars and not from the central obejct.*

Although our estimate of the effective temperature falls exactly in the regime derived before from the ionization state of gas in the inner 3 pc (Genzel & Townes 1987, Sect. 3, Roberts et al. 1991) it is doubtful whether one can use these estimates as observational parameters to fit accretion disk models to the central object. Firstly, one should expect that with such low luminosities the ionization of the gas is dominated mainly by hot stars in the central star cluster (Krabbe et al. 1991) and secondly, because the spectrum of an accretion disk – being a superposition of black body spectra – is usually flatter than $S_\nu \propto \nu^2$. Only for high inclination angles, nearly edge on, the disk spectrum comes close to a black body type. The fit of a one-component Planck function to a flatter spectrum thus can lead to an underestimate of the actual effective temperature of the inner edge of the disk. The uncertainties in the observations still allow a broader range of spectral indices.

[1]This is the relation given by Eckart et al. (1991) for a disk distribution of the surface brightness, which is more likely than the gaussian distribution adopted by ZML92, yielding $L = 2 \cdot 10^5 (T_\mathrm{e}/35\,000\mathrm{K}) L_\odot$.

3.3 Spherical accretion vs. disk accretion

3.3.1 Arguments against purely spherical accretion in Sgr A*

One has to admit that there are alternative models to explain the phenomena seen in Sgr A*. There are two main scenarios competing with each other. One is the standard paradigm for AGN scaled down to the Galactic Center with black hole, jet and accretion disk (Zylka et al. 1992, Falcke et al. 1993a&b). Here it is assumed that the matter accretes through a disk structure onto the black hole, part of this matter is then expelled again by a jet formed in the very inner parts of the disk close to the black hole.

The other model – the spherical wind accretion scenario – put forward by Melia (1992a & 1994), Melia et al. (1992) and Ozernoy (1989) assumes that Sgr A* accretes in a Bondi-Hoyle type accretion from the wind of the IRS 16 complex, a small subcluster of NIR bright stars with possible temperatures of some $10,000$ K. Radio and X-ray emission is then produced in onion-like shells around the central black hole with the highest frequencies produced close to the black hole. The spectral characteristics of this accretion process are then used to obtain mass estimates for Sgr A*, but despite using similar approaches both authors come to contrary conclusions. Melia confirms a supermassive balck hole of mass $\sim 10^6 M_\odot$ while Ozernoy denies it and allows only $10^3 M_\odot$ for the central mass. In the disk models a value of $10^6 M_\odot$ is favoured.

The main difference between the spherical and the disk scenario therefore does not concern the central mass but the accretion rate. Both, Melia and Ozernoy need a very high accretion rate which is $10^{-4} M_\odot/\mathrm{yr}$. For a low mass black hole, as proposed by Ozernoy, this accretion rate would be close or even above the Eddington limit (in contrast to our claim in the introduction) and it would take only some 10^8 years to increase the black hole mass by a factor 10 to a much higher value. It appears difficult to explain how Sgr A* could have kept its low mass over the whole history of the Galaxy and there is no reason to believe that we are currently in an outstandingly short and active period.

The model by Melia does not have this problem but faces another. He argues that the spherical infall will still have a net angular momentum which will lead to the formation of a small disk inside a certain radius. Thus he is able to account for the NIR source at the position of Sgr A*; to reduce the efficiency of the black hole in producing the visible luminosity Melia considers only a Schwarzschild hole, but still with the high accretion rate the total disk luminosity would be well above the observed limits for the luminosity of the central object. He therefore presents the spectrum of a highly inclined Newtonian disk which brings down the apparent disk luminosity by more than a factor 10.

Disregarding that relativistic effects would diminish this effect drastically the comparison of apparent disk luminosity and observed luminosities is highly misleading. The luminosity estimates from the central source are obtained by making use of the fact that most of the nuclear luminosity at optical wavelengths gets absorbed in the dust of the central region and is reradiated in the IR, therefore one has to use *total* and not *apparent* luminosity of the disk for the comparison. Inclination effects will make no difference in this number. Falcke et al. 1993a and Zylka et al. 1992 have shown that from the IR luminosities and taking the stellar light contributions into account, Sgr A* can not have a total luminosity $L_{\rm tot}$ larger than $\sim 7 \cdot 10^5 L_\odot$ which is also consistent with estimates for the NIR source. If one relaxes all limits and postulates clumpiness and a special geometry of the dust distribution Davidson et al. (1992) get as a very strict upper limit $L_{\rm tot} < 10^7 L_\odot$ for the nuclear luminosity which still is almost an order of magnitude below the luminosity which would be produced by central disk in the Melia model ($\sim 10^8 L_\odot$) and a rotating black hole would make this even worse. Hence, in order to reproduce the radio and X-ray emission of Sgr A* correct the spherical accretion model of Melia (1992a & 1994) is in serious conflict with observational constraints in the energetically dominant NIR-UV regime.

3.3.2 Fossil disk and wind accretion

Now, we do not deny that there are indications for a strong wind in the Galactic Center (e.g. Yussef-Zadeh & Melia 1992) but first of all the inferred accretion rate of Sgr A* depends very sensitively on the wind parameters at the position of Sgr A*, the overall geometry of the wind and the real distance between wind source and black hole. Secondly, the question is if the wind has indeed the parameters quoted by Melia will this wind affect the accretion rate in the energetically important innermost region?

Imagine that there is a fossil disk in the center of the Galaxy – a remainder of past activity or even of galaxy formation. In how far does it influence current accretion flows? If there is no significant mass supply for the central region from larger scales those fossil disks will appear as the starving disks discussed in this paper. As we will show these disks are very stable and slowly evolving structures that may last for a long time. The disks themselves still have a large amount of angular momentum, mass and kinetic energy. A spherically infalling wind will sooner or later hit the disk which definitively leads to a strong distortion and even disruption of the spherical infall. Especially in the inner regions the wind will be incorporated into the general disk accretion and mainly lead to a local enhancement of the accretion rate. It will take a long viscous time scale until this enhanced accretion rate reaches the black hole and becomes "visible".

Such a concept has several advantages, firstly, a fossil disk will preserve the memory of the initial orientation of the galactic plane. This makes it more likely for an accretion disk like in Sgr A* to be somehow aligned with the galactic plane, as indicated by the radio observations (Krichbaum et al. 1993), although it is so small that the disk potential of the Galaxy is irrelevant to the dynamics of this region. Secondly, the problem of the mass supply in the central parsec is no longer important. A few stars could provide enough fuel to keep the central engine alive. First of all it supplies mass and secondly, the lower angular momentum of the more or less spherically infalling matter will counteract the tendency of the fossil accretion disk to transport its original angular momentum outwards. Wind accretion will simply lead to a shrinking of the fossil disk down to an equilibrium radius – the angular momentum of the disk is conserved, but the matter is increased – and a mass reservoir at the outer edges of the disk will develop. Hence, wind accretion can conserve angular momentum and orientation of a fossil disk for a long time and refill empty mass stores. Different epochs of star formation may then also lead to different stages of activity in the center of galaxies.

For Sgr A* we can make some simple arguments. The parameters assumed for a possible wind produced by nearby stars are a total mass loss rate $\dot{M}_{\mathrm{w}*} = \dot{m}_{-2.5}\ 3.5\cdot 10^{-3} M_{\odot}/\mathrm{yr}$, a wind velocity $V_{\mathrm{w}*} = v_{600}\ 600$ km/sec and a distance of the wind sources from Sgr A* of $D_* = d_{0.1} 0.1$ pc (Melia 1992a). The accretion radius is $R_{\mathrm{acc}} = 2GM_\bullet/V_{\mathrm{w}*}^2$ which is for a black hole of mass $M_\bullet = m_6\ 10^6 M_\odot$ approximately $R_{\mathrm{acc}} \approx 7.3\cdot 10^{16}\mathrm{cm}\ m_6/v_{600}^2$. The wind accretion rate onto the black hole is $\dot{M}_{\mathrm{w}\bullet} = 5\cdot 10^{-5} M_\odot/\mathrm{yr}$ and the mass flow per area through a disk with radius R_{acc} (disregarding inclination effects) would be $\dot{\Sigma}_{\mathrm{w}\bullet} \approx 1.8\cdot 10^{-13}\,\mathrm{g/sec/cm^2}\ \dot{m}_{-2.5} d_{0.1}^{-2}$. We can compare this with the radial accretion flow in the inner region $\dot{M}_{\mathrm{disk}}/4\pi R_{\mathrm{disk}}$ and see that the wind accretion becomes important at a scale $R_{\mathrm{disk,out}} \geq 3\cdot 10^{15}\,\mathrm{cm}\ d_{0.1}\dot{m}_{-2.5}$. This is much larger than the inner hot disk which is smaller than 10^{14} cm with viscous timescales of the order $> 10^7$ years, thus larger than the expected lifetime of such a wind.

Of course the whole argument rests on the assumption that a cold, molecular fossil disk indeed extends to radii comparable to $R_{\mathrm{disk,out}}$ which is able to catch the wind before it reaches the small scales. The enclosed mass in the molecular disk can easily be of the order of a few 100 solar masses and should be seen at infrared wavelengths below $\lambda 18\mu m$ (see Zylka et al. 1993 for discussion of this topic). Another prediction of this concept would be an increased activity in some 10^7 years which, unfortunately, is slightly longer than an astronomers lifetime and certainly longer than a PhD thesis time.

3.4 The signature of a rotating black hole

Fortunately the main results for standard accretion disks theory (von Weizsäcker 1948, Shakura & Sunyaev 1973) and its general relativistic extension (Novikov & Thorne 1973) follow from fundamental physics with only a few assumptions:

- The gravitational field is dominated by the central black hole and the metric is described by a Kerr metric (Kerr 1963) allowing for rotation of the black hole. Parameters of the metric are mass $M_\bullet$ and Kerr parameter $0 \leq a \leq 1$ of the black hole ($a \propto$ angular momentum of black hole).
- Matter flows along direct, nearly circular, geodesic orbits in the equatorial plane of the black hole.
- Angular momentum is transported outwards due to a turbulent viscosity mechanism resulting in a radial velocity of the matter towards the center, which is much smaller than the circular velocity of the matter.
- The disk is thin (height $<$ radius/3) and steady.
- At the inner edge of the disk, angular momentum, mass and energy of the inflowing matter are swallowed completely by the black hole.

Having such an accretion disk the amount of gravitational energy which has to be dissipated per surface area and time (dissipation rate D_0) at each radius can be calculated simply from conservation of energy and angular momentum, yielding

$$D_0 = \frac{3GM\dot{M}}{8\pi R^3}\frac{\mathcal{Q}}{\mathcal{B}\sqrt{\mathcal{C}}} = 6.8\cdot 10^{37}\frac{\dot{m}_{-8}}{r^3}\frac{\mathcal{Q}}{\mathcal{B}\sqrt{\mathcal{C}}}\frac{\text{erg}}{\text{s}\,R_{\text{g}}^2} \tag{3.6}$$

which is *independent of the viscosity parameter* α defined by Shakura & Sunyaev (1973). Assuming black-body radiation this can be translated to an effective temperature via

$$T_{\text{eff}} = (D_0/\sigma)^{1/4} \tag{3.7}$$

which in turn defines a characteristic frequency

$$\nu_{\max} = 8.2\cdot 10^{10}\ (T_{\text{eff}}/\text{K})\ \text{Hz} \tag{3.8}$$

where the black-body radiation of this temperature has a maximum in νF_ν:

$$\nu_{\max} = 7\cdot 10^{15}\,\frac{\dot{m}_{-8}^{1/4}}{m_6^{1/2}}\left(\frac{1}{r^3}\frac{\mathcal{Q}}{\mathcal{B}\sqrt{\mathcal{C}}}\right)^{1/4}\ \text{Hz} \tag{3.9}$$

Here $m_6 = M_\bullet/10^6 M_\odot$ and $\dot{m}_{-8} = \dot{M}/10^{-8}(M_\odot/\text{yr})$ are the dimensionless mass and accretion rate of the black hole. $r = R/R_{\text{g}}$ is the dimensionless radius in units of the gravitational radius $R_g = GM_\bullet/c^2 = 1.48\cdot 10^5 M_\bullet/M_\odot\text{cm}$ which is half the Schwarzschild radius. The inner edge of an accretion disk lies at the radius $r_{\text{ms}}(a)\cdot R_{\text{g}}$ of the last, marginally stable orbit, which is 6 R_{g} for a nonrotating ($a = 0$) and 1.232 R_{g} for a maximal rotating black hole ($a = 0.9981$). The relativistic correction factors $\mathcal{B}, \mathcal{C}$ and $\mathcal{Q}$ are functions of r and a with the limits such that $D_0 \propto r^{-3}$ for $r \to \infty$ and $D_0 \to 0$ for $r \to r_{\text{ms}}$. They are given explicitly in Page & Thorne (1974). Note that the dependence of the disk properties on the Kerr parameter a is contained completely in these correction factors and in the marginally stable radius r_{ms}. For fast rotating black holes luminosity and effective temperature of the disk may be up to 5 times higher than in the non-rotating case mainly because the disk extends to lower radii. The radiation field of the disk is most sensitive to changes of the holes angular momentum in the regime $a > 0.9$. Because of this sensitivity one has for given black hole mass and inclination angle an unequivocal translation from the two observables effective temperature and luminosity (T_{eff}, L) to a new pair of intrinsic properties, namely angular momentum and accretion rate $(a, \dot{M})$ of the hole.

3.4.1 Inner boundary conditions for a Kerr accretion disk

Standard accretion disk theory assumes that at the inner boundary of the accretion disk the effective temperature goes to zero. In the stellar case a finite boundary layer has to exist which can produce an appreciable part of the total luminosity, and which may also encompass a non-negligible part of the accretion disk near the inner boundary (Duschl & Tscharnuter 1991). In the case of black hole accretion, one expects a similar phenomenon (Kato 1982). But as it is not necessary for the matter to slow down before being swallowed by the hole as in the stellar case we neglect all such effects and use the standard Novikov & Thorne (1973) boundary condition described at the beginning of Sect. 3. And even if there is a luminous boundary layer most of the emitted photons will not be able to escape from the very edge of the black hole – the relativistic transferfunction tends to zero (Cunningham 1975; next section) – but the radial structure of the disk may change in the inner region.

3.5 Calculation of relativistic disk spectra

In this section we shortly revisit the method used by Cunningham (1975) to calculate the relativistic transfer functions for light-rays in the Kerr metric to ease programming of the neccessary algorithms. This algorithm will be used to calculate the spectra of accretion disks around rotating black holes. Here we use units which are appropiate for the black hole scenario and set $G = M_\bullet = c = 1$.

3.5.1 Equation of motion

The equation of motion for photons in the Kerr metric can be written in integral form (Carter 1968) as

$$I_{\text{r}}^{\pm} - I_{\mu}^{\pm} = I^{(\pm,\pm)} = 0 \tag{3.10}$$

with

$$V_\mathrm{r} = \left(a^2 - \lambda a + r^2\right)^2 - \left((a-\lambda)^2 + q^2\right)\left(a^2 - 2r + r^2\right) \tag{3.11}$$

$$V_\mu = -a^2\mu^4 + \left(a^2 - \lambda^2 - q^2\right)\mu^2 + q^2 \tag{3.12}$$

$$I_\mathrm{r}^\pm = \int_{r_\mathrm{min}}^{r_\mathrm{o}} \frac{1}{\sqrt{V_\mathrm{r}}}\mathrm{d}r \pm \int_{r_\mathrm{e}}^{r_\mathrm{min}} \frac{1}{\sqrt{V_\mathrm{r}}}\mathrm{d}r \tag{3.13}$$

$$I_\mu^\pm = \int_{\mu_\mathrm{min}}^{\mu_\mathrm{o}} \frac{1}{\sqrt{V_\mu}}\mathrm{d}\mu \pm \int_{\mu_\mathrm{e}}^{\mu_\mathrm{min}} \frac{1}{\sqrt{V_\mu}}\mathrm{d}\mu \tag{3.14}$$

V_r and V_μ contain angular and radial information of the position of the photon, (q,λ) are the constants of motion, a is the Kerr Parameter, $\mu = \cos\theta$ and (r,θ) are Boyer-Lindquist coordinates with subscripts e and o denoting where the photon is emitted or observed respectively. For the infinitively thin disk is $\mu_\mathrm{e} = 0$, $r_\mathrm{e} = r_\mathrm{d}$, $\mu_\mathrm{o} = \cos i_\mathrm{o}$ and $r_\mathrm{o} = \infty$. The integrals $I^\pm_{\mu\|\mathrm{r}}$ are integrals along the trajectory of a photon.
Cunningham noted that the integrals (3.13,3.14) can be expressed in terms of elliptical integrals of the first kind $F(\Phi|m)$ (Abramowitz & Stegun 1972, 17.2.6). As the derivation is a little bit tedious, we give here the explicit form. The polynomials can be factored and from the limits $\lim_{r\to 0} V_\mathrm{r} = -(aq)^2$ and $\lim_{r\to\infty} V_\mathrm{r} = +\infty$ we know that there are either 2 or 4 real roots for this 4th-order polynomial. If 2 of the roots coincide (saddle point) so that one has exactly 3 different roots left. Following from the condition that V_r is real for every r we know that the 2 complex roots, if present, are conjugate complex numbers. The same logic applied to V_μ tells us that this polynom has always 2 real roots. The roots are the so called turning points of the photon trajectories; at these points the sign in $I^\pm_{\mu\|\mathrm{r}}$ changes accordingly. Knowing the properties of the roots we can write

$$V_\mathrm{r} = \begin{cases} (r-y_1)(r-y_2)(r-y_3)(r-y_4) & \text{4 roots} \\ \left((r-\Re(y_2))^2 + \Im(y_2)^2\right)(r-y_{1/3})(r-y_4) & \text{2 roots} \end{cases}$$

$$V_\mu = (\mu^2 + x_1^2)(x_2^2 - \mu^2). \tag{3.15}$$

The roots are defined by

$$x_{1/2}^2 = \frac{1}{2} - \frac{\lambda^2 + q^2 \pm \sqrt{-4a^2\lambda^2 + (a^2+\lambda^2+q^2)^2}}{2a^2} \tag{3.16}$$

$$y_{1/2} = \left(\pm\sqrt{y_{10} - 864^{\frac{1}{2}} y_5 y_8^{\frac{3}{2}}} + y_9^{\frac{3}{4}}\right) / \sqrt{24 y_8 y_9^{\frac{1}{2}}}$$

$$y_{3/4} = \left(-\sqrt{y_{10} + 864^{\frac{1}{2}} y_5 y_8^{\frac{3}{2}}} \pm y_9^{\frac{3}{4}}\right) / \sqrt{24 y_8 y_9^{\frac{1}{2}}} \tag{3.17}$$

with

$$\begin{aligned}
y_5 &= aq \\
y_6 &= 2\left((a-\lambda)^2 + q^2\right) \\
y_7 &= a^2 - \lambda^2 - q^2 \\
y_8 &= \Big(27\,y_6^2 + 72\,y_5^2\,y_7 + 2\,y_7^3 + 3^{\frac{3}{2}}\ \big(256\,y_5^6 + 27\,y_6^4 \\
&\quad +144\,y_5^2\,y_6^2\,y_7 + 128\,y_5^4\,y_7^2 + 4\,y_6^2\,y_7^3 + 16\,y_5^2\,y_7^4\big)^{\frac{1}{2}}\Big)^{\frac{1}{3}} \\
y_9 &= -3\cdot 2^{\frac{10}{3}}\,Y_5^2 + 2^{\frac{4}{3}}\,y_7^2 - 4y_7y_8 + 2^{\frac{2}{3}}y_8^2 \\
y_{10} &= \sqrt{y_9}\left(3\cdot 2^{\frac{10}{3}}y_5^2 - 2^{\frac{4}{3}}y_7^2 - 8y_7y_8 - 2^{\frac{2}{3}}y_8^2\right)
\end{aligned} \tag{3.18}$$

The integrals in the equation of motion

$$I_\mu(\tilde{\mu}) = \int_{\mu_\mathrm{min}}^{\tilde{\mu}} V_\mu^{-\frac{1}{2}} \quad \text{and} \quad I_\mathrm{r}(\tilde{r}) = \int_{r_\mathrm{min}}^{\tilde{r}} V_\mathrm{r}^{-\frac{1}{2}} \tag{3.19}$$

can be evaluated analytically and yield

$$
\begin{aligned}
I_\mu &= \frac{F\left(\arccos\frac{\tilde{\mu}}{x_2}\middle|\frac{x_2^2}{x_2^2+\Im(x_1)^2}\right)}{a\sqrt{\Re(x_1)^2+x_2^2}} && (3.20)\\
I_\mathrm{r} &= \begin{cases} \dfrac{2F\left(\arcsin\sqrt{\frac{(y_1-y_4)(\tilde{r}-y_1)}{(y_1-y_4)(\tilde{r}-y_2)}}\middle|\frac{(y_2-y_3)(y_1-y_4)}{(y_1-y_3)(y_2-y_4)}\right)}{\sqrt{(y_1-y_3)(y_2-y_4)}} & \text{4 roots}\\ \dfrac{F\left(2\arctan\sqrt{\frac{w(\tilde{r}-y_{1/3})}{v(\tilde{r}-y_4)}}\middle|\frac{(v+w)^2-(y_{1/3}-y_4)^2}{4vw}\right)}{\sqrt{vw}} & \text{2 roots}\end{cases} && (3.21)\\
v &= \sqrt{\left(\Re(y_2)-y_{1/3}\right)^2+\Im(y_2)^2} && (3.22)\\
w &= \sqrt{\left(\Re(y_2)-y_4\right)^2+\Im(y_2)^2}. && (3.23)
\end{aligned}
$$

Given the constants of motion one now has an analytic expression of the equation of motion and could obtain the trajectory of the photon by solving Eq. (3.10) for $\tilde{r}$ and $\tilde{\mu}$ implicitly.

3.5.2 Calculating the spectrum

Knowing the photon trajectories, we can calculate the observed spectrum of an accretion disk. The flux of a luminous disk with inner and outer radius r_in and r_out and a limb-darkening law with limb-darkening factor a_ld, inclined by $\cos i_\mathrm{o} = \mu_\mathrm{o}$ towards an observer ($\mu_\mathrm{o} = 1$ means face on) at a distance $r_\mathrm{o} \gg r_\mathrm{out}$ is obtained by integrating the locally emitted intensity $I(\nu, r_\mathrm{d})$ folded with the relativistic transfer function $\mathcal{T}$ (Cunningham 1975).

$$F_{\nu_\mathrm{o}} = \frac{2\mu_\mathrm{o}}{r_\mathrm{o}^2}\int_{r_\mathrm{in}}^{r_\mathrm{out}}\int_0^1 I\left(\nu_\mathrm{o}/g, r_\mathrm{d}\right)\frac{g^2}{\sqrt{g_\star-g_\star^2}}\mathcal{T}\,\mathrm{d}g_\star\, r_\mathrm{d}\,\mathrm{d}r_\mathrm{d}. \qquad (3.24)$$

The transfer function is defined as

$$
\begin{aligned}
\mathcal{T} &= \mathcal{T}_1+\mathcal{T}_2 && (3.25)\\
\mathcal{T}_{1\|2} &= c_\mathrm{ld}\, g\sqrt{g_\star-g_\star^2}\left(g_\mathrm{max}-g_\mathrm{min}\right)S_{1\|2}/\left(2\mu_\mathrm{o}r_\mathrm{d}\right) && (3.26)\\
c_\mathrm{ld} &= \frac{1+a_\mathrm{ld}gq/r_\mathrm{d}}{1+0.5a_\mathrm{ld}} && (3.27)\\
S_{1\|2} &= q/\left(\beta\sqrt{1-\mu_\mathrm{o}^2}\sqrt{V_\mathrm{r}}\frac{\partial I^{(\pm,\pm)}}{\partial q}\frac{\partial g}{\partial\lambda}\right) && (3.28)\\
g_\star &= \frac{g-g_\mathrm{min}}{g_\mathrm{max}-g_\mathrm{min}} && (3.29)\\
g^2 &= \left(1-\frac{\lambda}{a+r^{\frac{3}{2}}}\right)^{-2}\left(\left(a+r^{\frac{3}{2}}\right)^2\left(a^2\mu^2+r^2\right)^2\left(a^2-2\,r+r^2\right)\right.\\
&+ \left.\left(\mu^2-1\right)\left(a^4\mu^2-2\,a^2\mu^2 r+a^2r^2+a^2\mu^2r^2-2\,a\,r^{\frac{5}{2}}+r^4\right)^2\right)\\
&\cdot \left(\left(a^2+r^2\right)^2+a^2\left(\mu^2-1\right)\left(a^2-2\,r+r^2\right)\right)^{-1}\\
&\cdot \left(a+r^{\frac{3}{2}}\right)^{-2}\left(a^2\mu^2+r^2\right)^{-1} && (3.30)
\end{aligned}
$$

This definition of the transfer function[2] was derived for differentially rotating disk with circular equatorial geodesics (i.e. Keplerian orbits in the Newtonian limit). It contains all relativistic effects like boosting, light bending, gravitational redshift etc.

[2] Note that the disk surface element S containing the Jacobian $\partial(g, r_\mathrm{e})/\partial(\lambda, g)$ was simplified via the therorem for differentiating implicit functions. As one can express the equation of motion in terms of the incomplete elliptical integral of the first kind (see above) calculating the derivatives of the equation of motion is straightforward and there is no need to use finite differences as in Cunnningham (1975).

The task now is to find for a given ring with radius r_e all trajectories that reach the observers eye. The trajectories are fixed by specifying the constants of motion and thus we have to find all combinations of λ and q that solve Eq. (3.10) by fixing endpoints r_e, r_o, $\mu_{\min}$ and μ_o. The set of (λ,q) then found represents the set of photon trajectories from a ring in the disk to the observer. The ϕ-coordinate is parametrized by the redshift parameter g_*. Consequently Eq. (3.10) defines a smooth – usually closed – line in the (λ,q) plane. This contourline $s(\lambda, q)$ is defined by solving the differential equation $\mathrm{d}I^{(\pm,\pm)}/\mathrm{d}s(\lambda, q) = 0$ and Eq. (3.10).
Depending on the position in the ring, the trajectories will have different numbers of turning points $\mu_{\min}$ and $r_{\min}$ defined by the equations $V_r(r_{\min}) = 0$ and $V_\mu(\mu_{\min}) = 0$ but there is at maximum one turning point per trajectory. One can now easily separate the ring in up to 4 branches according to the signs used in Eq. (3.10). The branching points can be found at the positions, where the turning point coincides with the emitting position ($V_\mu(\mu_e) = 0$ or $V_r(r_e) = 0$). This branching points should be calculated first and then they can be used to find the "contourline" of the ring $s(\lambda, q)$ by solving up to 4 separate boundary value problems. The minimum and maximum λ and thus the minimum and maximum g needed for the definition of g_* are given by Eq. (3.10) and $\partial I^{(\pm,\pm)}/\partial q = 0$. Between these extrema one has two solutions of $\mathcal{T}$ for each value of λ defining $\mathcal{T}_1$ and $\mathcal{T}_2$. The re-calculated transfer functions are shown in Figure 3.1 which we then used to calculate the relativistic disk spectra.

3.6 Radiation field in the Kerr metric

To build up a translation table from $(T_{\rm eff}, L)$ to $(a, \dot{M})$ we used the method described above to calculate the full general relativistic geodesic transformation of radiation in the Kerr-metric (i.e. gravitational redshift, boosting, light bending). We assumed that the disk radiates locally as a black-body with an additional limb-darkening law $I_\nu(\theta) = (1 + 1.5\cos\theta)/1.75 \cdot B_\nu$. B_ν is the Planck function with $T_{\rm eff}$ taken from Eqs. (3.6,3.7). In our scenario, where $M \sim 2 \cdot 10^6 M_\odot$ and $\dot{M} \ll 10^{-5} M_\odot/\mathrm{yr}$, the standard theory predicts an accretion disk which is dominated entirely by gas pressure (Novikov & Thorne 1973, Eqs. (5.9.6+8)) so that these assumptions are justified with the exception of a possible weak modification of the spectrum in the inner region of the disk due to electron scattering, which was neglected. But since we are mainly interested in the energetics of the disk radiation, we do not require elaborate disk spectra at this stage.
Using the more detailed accretion disk theory (Novikov & Thorne 1973) – including the visocsity paramter α – one finds that the disk is optically thick everywhere, for a low viscosity parameter $\alpha \leq 10^{-4}$ as used for the modeling of comparable disks for FU Orionis events (Hessman 1991, Clarke et al. 1990). Using improved opacities Falcke & Heinrich (1994) find that even for higher values of α the assumptions of a thin and optically thick disk remain valid. Anyway, this does not affect the outcome of our of the order estimates drastically. The results do also not depend crucially on the assumed limb-darkening law.
A variety of spectra were calculated as viewed by an observer at infinity from different inclination angles for a black hole with $M = 2 \cdot 10^6 M_\odot$, angular momentum ranging from $a = 0.1$ to $a = 0.9981$. Because of relativistic boosting the effective temperature of these spectra is maximal at high (edge on) and minimal at low (face on) inclination angles, whereas the aparent luminosity is lower at large and higher at low inclination angles. The temperature effect is much more pronounced in the case of rotating black holes while the luminosity effect is stronger for non-rotating holes.
From each spectrum we took the maximum in νF_ν and converted the corresponding frequency via Eq. (3.7) to an effective temperature. This corresponds to the effective temperature of the energetically dominant part of the disk – usually within a few gravitational radii from the black hole. The results are shown in Fig. 3.3 (left) where we plotted these effective temperatures versus the 4π integrated flux (i.e. total luminosity) of the disk for a grid of angular momenta and accretion rates. Also shown are our observational constraints for the Galactic Center. Some selected spectra for different parameters are shown in Fig. 3.3 (right) and Fig. 3.6 gives an overwiew of the whole parameter range relevant in astrophysics.
The spectral form of the disk radiation (exponential cut-off) ensures that – unless further hot components are present – the effective temperature is also very close to the high-energy cut-off for the overall photon spectrum. That is very important vor the impact of the disk radiation on the ambient medium, i.e. ionization and heating. Different black hole/accretion disk models may lead to different temperatures in the surrounding gas due to photoionization. This diagnostic tool will be shortly considered in Chapter 3.7.
We took a canonical black hole mass of $2 \cdot 10^6 M_\odot$ as our reference model but one can easily obtain a similar grid for different masses simply by using the Relations (3.6) and (3.9). As one can see the luminosity scales with $L = 2\int_{r_{\rm ms}} D_0 2\pi dr \propto \dot{M}$ and is independent of the black hole mass M, while the effective temperature scales

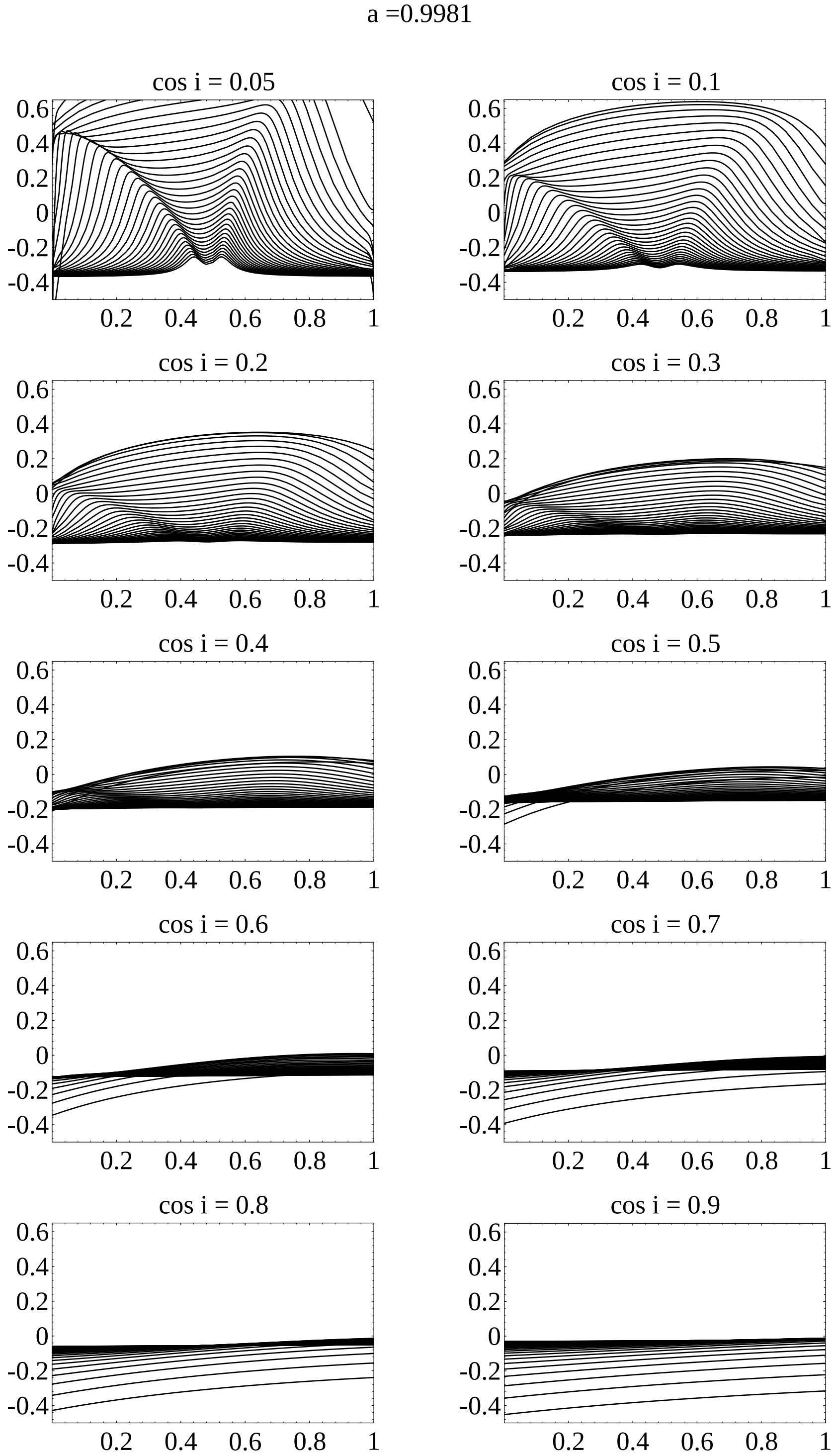

Figure 3.1a: Logarithm of the transfer function $\mathcal{T}$ as a function of g_* for different inclination angles of the disk. Each plot contains the transferfunction at different radii in logarithmic steps. Here the limb-darkening factor is $a_{\rm ld} = 1.5$, the Kerr parameter is $a = 0.9981$ and the transfer functions are given for rings with radius $r = 2.1 - 1000$.

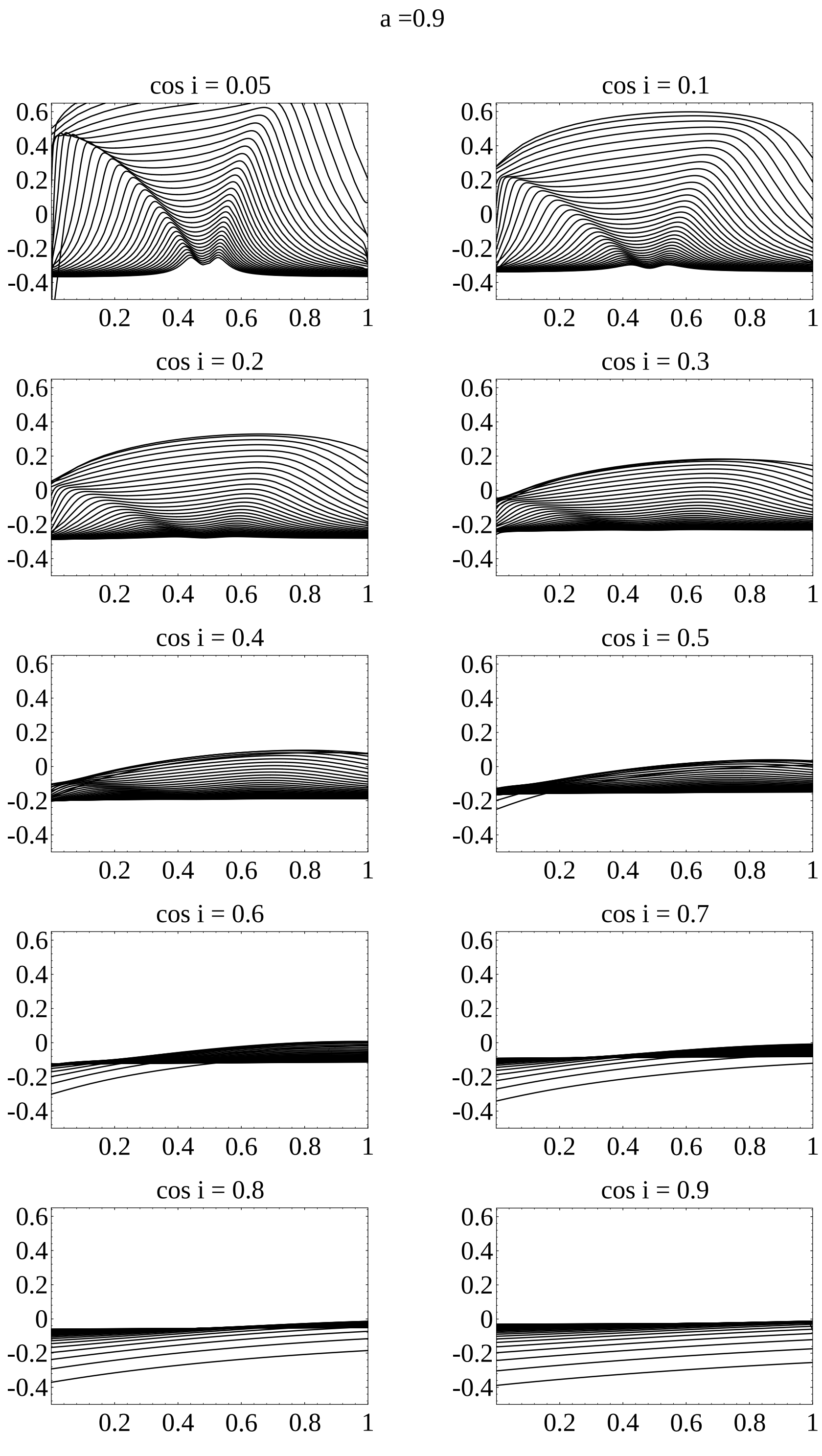

Figure 3.1b: Logarithm of the transfer function $\mathcal{T}$ as a function of g_* for different inclination angles of the disk. Each plot contains the transferfunction at different radii in logarithmic steps. Here the limb-darkening factor is $a_{\rm ld} = 1.5$, the Kerr parameter is $a = 0.9$ and the transfer functions are given for rings with radius $r = 2.55 - 1000$.

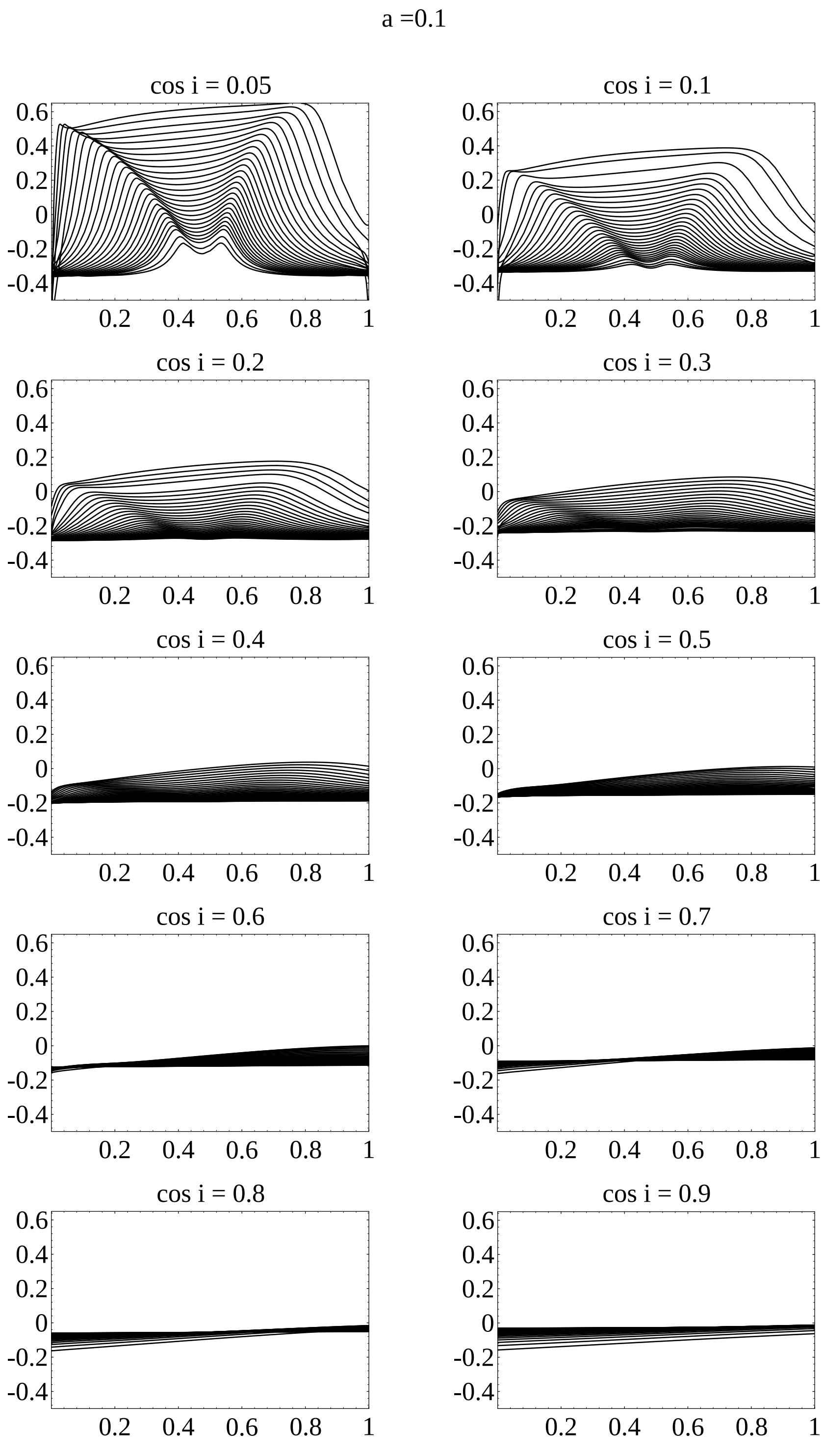

Figure 3.1c: Logarithm of the transfer function $\mathcal{T}$ as a function of g_* for different inclination angles of the disk. Each plot contains the transferfunction at different radii in logarithmic steps. Here the limb-darkening factor is $a_{\rm ld} = 1.5$, the Kerr parameter is $a = 0.1$ and the transfer functions are given for rings with radius $r = 6.24 - 1000$.

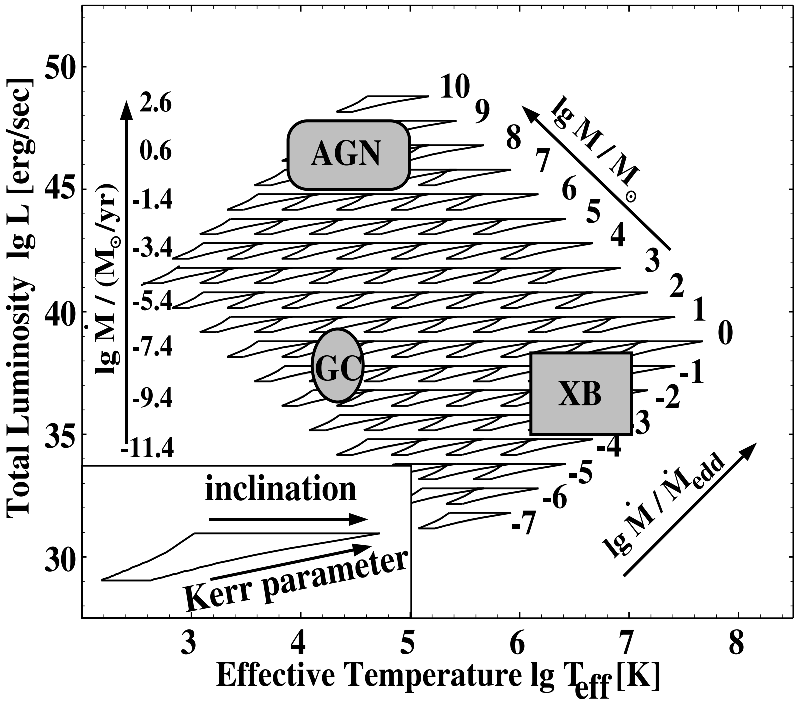

Figure 3.2: Hertzsprung-Russell-Escher diagram for black holes. The figure gives an overwiev for the whole parameter range of astrophysically relevant black holes. The small areas cover all possible values for effective temperature and luminosity of a black hole of given mass and accretion rate but different inclination angles and angular momenta a. Areas at the same horizontal line have the same absolute accretion rate, areas at the same diagonal line from lower left to upper right have the same mass and areas at the same diagonal from the lower right to the upper left have the same accretion rate in terms of their Eddington rate. The boxes denote schematically the position of AGN, Sgr A* and stellar mass black holes.

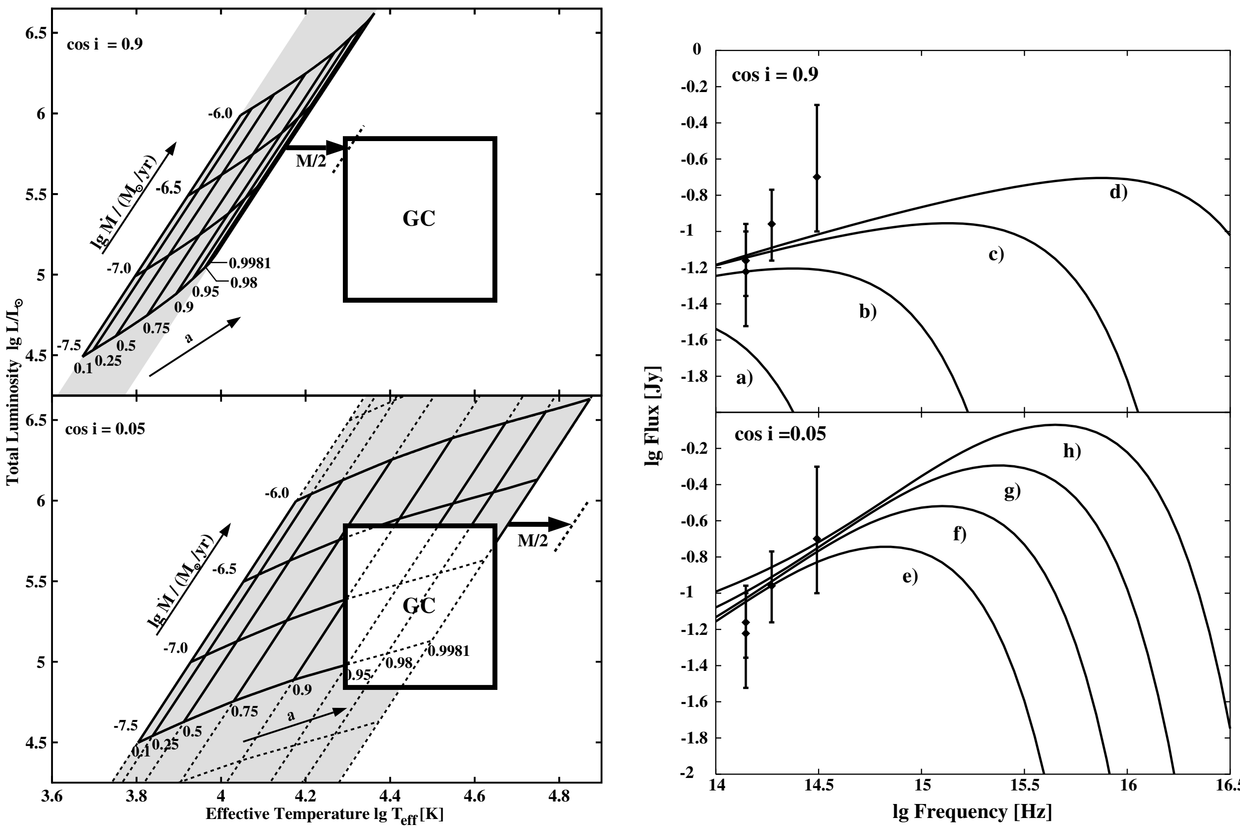

Figure 3.3: *On the left:* "Hertzsprung-Russell diagram for a black hole" of $2 \cdot 10^6 M_\odot$. Plotted is the effective temperature of the radiation flux (maximum in νF_ν) for a disk seen almost face on (cos i= 0.9) and a disk seen almost edge on ($\cos i = 0.05$) versus the *total* luminosity of the disk for a grid of angular momenta and accretion rates. The rectangle represents the observational constraints from Sgr A*. The arrow indicates how the whole grid shifts if one divides the black hole mass by a factor of 2.
On the right: Sample spectra of an accretion disk around a Kerr hole ($a = 0.9981$) together with the λ =2.2, 1.6 and 1μm data from Eckart et al., Close et al. and Rosa et al. (1992). The labels refer to different values of mass and accretion rate. Spectra a)-d): face on disk with $M = (2 \cdot 10^6, 2 \cdot 10^5, 2 \cdot 10^4, 2 \cdot 10^3) M_\odot$ and $\dot{M} = (10^{-10.5}, 10^{-9.5}, 10^{-8.5}, 10^{-7.5}) M_\odot$/yr. Spectra e)-h): edge on disk with $M = (2 \cdot 10^6, 10^6, .5 \cdot 10^6, .25 \cdot 10^6) M_\odot$ and $\dot{M} = (10^{-8.5}, 10^{-8.}, 10^{-7.5}, 10^{-7.}) M_\odot$/yr. The total luminosity for a maximal Kerr hole is given by $L_{\rm tot} = 2 \cdot 10^{38} \dot{m}_{-8}$erg/s.

with $T_{\rm eff} \propto \dot{M}^{1/4}/\sqrt{M}$. Thus one can obtain further models for different parameters of M and $\dot{M}$ by simple linear extrapolation.

3.7 Heating of the ambient medium

To learn more about the hidden UV spectrum of Sgr A*, one has to apply indirect methods, i.e. the heating and ionization of ambient gas by the disk spectrum. From the HR diagram one can see, that the disk is at the edge of producing an appreciable amount of ionizing UV photons, therefore the state of the ambient gas will be very sensitive towards changes of the parameters in the BH/accretion disk system. To test this we took the photoionization code HOTGAS developed by Schmutzler (1987; Schmutzler & Tscharnuter 1993) to calculate gas temperatures of a test cloud with constant density at different spatial positions around Sgr A* neglecting all dynamical and optical depth effects (Fig. 2).
For a set of parameters with $M_\bullet = 10^6 M_\odot$, $\dot{M} = 10^{-7} M_\odot/{\rm yr}$ and a maximally rotating BH, we find a very anisotropic temperature distribution, which reflects the relativistic beaming of the disk spectrum at high inclination angles, heating the gas to temperatures of $T_{\rm gas} \geq 10.000$ K. A moderate change of the angular momentum of the BH from $a = 0.9981$ to $a = 0.9$ is enough to suppress the heating almost completely. On the other hand, a low mass BH (e.g. $10^3 M_\odot$) inevitably leads to much higher temperatures ($10^5 - 10^6$ K) in the inner arcsec of the Galactic Center because of the higher effective temperature. No configuration is able to heat the total H II region around Sgr A*. Nevertheless, once we are able to determine temperature and density distribution of the gas in the inner arcsecond of the GC we will have a powerful tool to discriminate between different models.

3.8 Conclusions

If the observational constraints could be confirmed then Fig. 3.3 requires a fast rotating Kerr hole ($a > 0.9$) with a fairly low accretion rate of $\dot{M} < 10^{-7} M_\odot/{\rm yr}$ seen almost edge on.
In fact if we fit the disk spectra directly to the NIR spectrum than an even lower accretion rate of $\dot{M} \sim 10^{-8.5} M_\odot/{\rm yr}$ seems also possible (Fig.3.3e), giving also a lower limit, because an even lower accreting disk would not be capable of reproducing the NIR data. From this figure one can also se¡e – like in the HR-diagram – that a low mass black hole with $M \ll 10^6$ (e.g. $\sim 10 M_\odot$ as proposed by Sanders (1992)) and an edge on disk fitted to this data would produce a luminosity exceeding the limit from the dust observations, whereas the face on disk models produce spectra which are obviously too flat.
So if the central disk really is edge on, then it is suggestive to assume that it is also roughly aligned with the galactic plane, with the rotation axis perpendicular to it. This, however, can not be confirmed by NIR observation, but has to await further mm VLBI experiments to strengthen the non-spherical structure of Sgr A* possibly caused by jet parallel to the disk axis. Thus one could fix the orientation of the disk in the observers plane.
If the constraint on the mass of the putative black hole could be relaxed then a lower black hole mass could also fit into the Hertzsprung-Russell diagram, with no particular constraint on the Kerr parameter. But during the evolution process of a black hole it is quite natural to expect an evolution towards strong rotation to a maximum at $a \approx 0.9981$ (Bardeen 1970, Thorne 1974). From Fig.3.3 one can see that a maximal Kerr Hole of $M = 10^6$ would then require at least $10^{-8} M_\odot/{\rm yr}$.
Therefore the Galactic Center could become an important laboratory to study general relativity and the Kerr metric. This model gives some firm predictions

- strong anisotropies of the effective temperature of the radiation field for a strongly rotating black hole resulting in an anisotropic ionization of the ambient medium, and
- strong anisotropies for the luminosity of the radiation field for non-rotating black holes.

The results are summarized in Fig. 3.5, where we show accretion rate versus black hole mass with the parameters Kerr parameter and inclination angle. We obtained this grid by applying the scaling laws $\dot{M} \propto \tilde{L}/L \cdot \dot{M}_0$ and $M = (\tilde{T}/T_{\rm eff})^2 \cdot \sqrt{L/\tilde{L}} \cdot M_0$ where $\tilde{L} = \tilde{L}(a,i)$ and $\tilde{T} = \tilde{T}(a,i)$ are the calculated functions for luminosity and effective temperature of the disk at arbitrary but fixed values of $M = M_0$ and $\dot{M} = \dot{M}_0$. $T_{\rm eff}$ and L are the observed values of the radiation field for which we took $T_{\rm eff} = 4 \cdot 10^4$K and $L = 3 \cdot 10^5 L_\odot$ as our reference frame

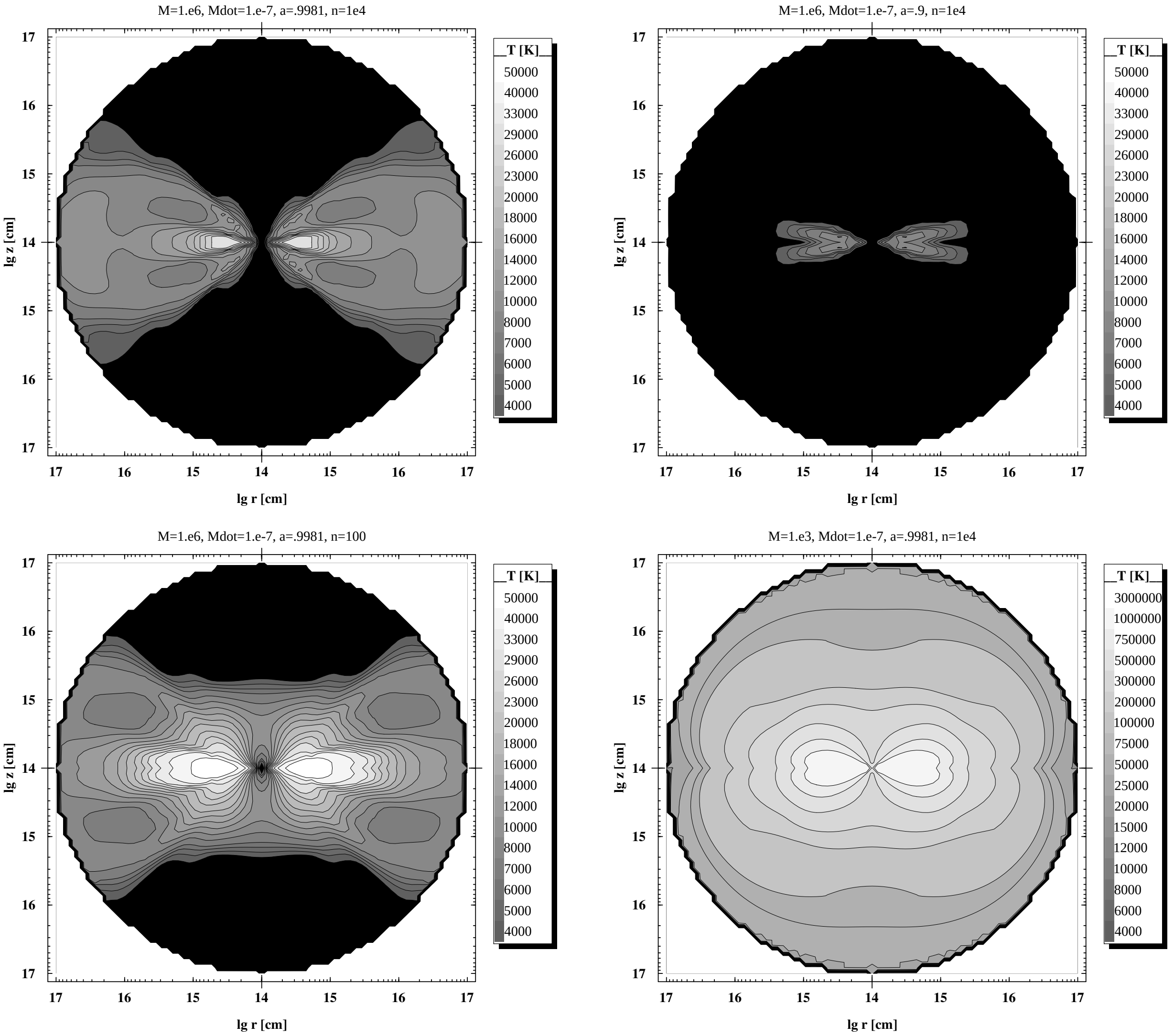

Figure 3.4:
Top left: The temperatures of a test cloud of constant density ($n = 10^4/\mathrm{cm}^3$) exposed to a disk spectrum for an accretion rate of $10^{-7} M_\odot/\mathrm{yr}$ around maximally rotating BHs of mass $10^6 M_\odot$.
Top right: As top left but for a slightly less rotating black hole ($a = 0.9$).
Bottom left: As top left but with lower density ($n = 10^2/\mathrm{cm}^3$).
Bottom right: As top left but for a low mass black hole ($M_\bullet = 10^3 M_\odot$).
The disk lies horizontally in the center and is seen edge on. Black means that the gas is almost neutral and too cold for obtaining a reliable equilibrium temperature with the program.

for the Galactic Center. Again, with better observational data at hand, one can easily adapt this grid by simple interpolation to test the black hole scenario for Sgr A*.

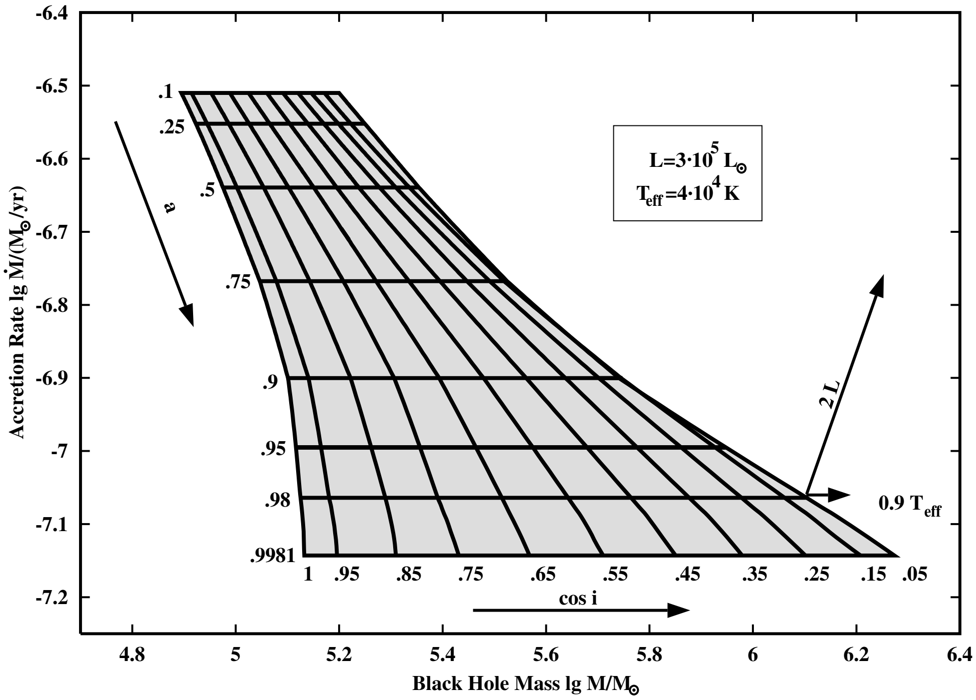

Figure 3.5: The shaded area limits the possible parameters M and $\dot{M}$ for a black hole that matches a luminosity of $L = 3 \cdot 10^5 L_\odot$ and an effective temperature $T_{\rm eff} = 4 \cdot 10^4$K for a grid of angular momenta a and inclination angles i. The thick arrows indicate how the whole grid shifts if one increases the luminosity by a factor 2 or reduces the effective temperature by one tenth respectively.

Chapter 4

The jet in the Galactic Center

4.1 What is Sgr A*?

The Galactic Center is a quiet little corner in the universe, yet from studying this region we may learn something about the largest and most violently active regions we know – the active galactic nuclei (AGN) of distant galaxies. Firstly, there is increasing evidence that the very Center of the Galaxy at the position of the radio source Sgr A* contains the same ingredients as are proposed to exist in AGN, namely a supermassive black hole with mass $M_\bullet \sim 10^6 M_\odot$ (see Genzel & Townes 1987), a thin accretion disk (Zylka et al. 1992, Falcke et al. 1993a, hereafter FBDM; Falcke & Heinrich 1994; Chapter 3) and a radio jet (Krichbaum et al. 1993; Falcke et al. 1993, hereafter FMB), but due to a disenchantingly low accretion rate (5 orders of magnitude below the Eddington limit) the activity is not very pronounced and our galaxy resembles an AGN on a starvation diet (Falcke & Biermann 1993) rather than a powerful quasar or Seyfert galaxy. On the other hand this gives us the unique opportunity to study such a system in the low-power regime which in other galaxies would escape our attention. Moreover, 'increasing evidence' does not mean 'proof' and we have to apply further tests to this scenario which then may be able to discriminate between the jet/disk model and alternative picture, e.g. the spherical accretion models proposed by Melia et al. 1992 and Ozernoy 1993.

4.1.1 Observations of Sgr A*

A prominent phenomenon in the Galactic Center is the compact, non-thermal radio source Sgr A* (Balick & Brown 1974, Lo et al. 1985), showing a fairly flat ($S_\nu \propto \nu^{0\ldots0.3}$) spectrum in the range 1 to 230 GHz (eg. Zylka & Mezger 1988, Duschl & Lesch 1994). Eckart et al. (1992) and Rosa et al. (1992, Müller et al. 1994) have detected Sgr A* at $\lambda 2.2\mu$m and $\lambda 1\mu$m wavelengths providing evidence for a luminous central object radiating also at optical wavelength. Zylka et al. (1992) explain their $\lambda 1300\mu$m and $\lambda 870\mu$m continuum observations of the Sgr A* region by the existence of a thermal dust disk surrounding Sgr A* or a self-absorbed compact synchroton source. Falcke et al. (1993) explain the NIR data with a rotating black hole of mass $M_\bullet \sim 10^6 M_\odot$ surrounded by a hot accretion disk seen edge-on. And finally, as another breakthrough, Krichbaum et al. (1993) succeeded in detecting Sgr A* with VLBI at 7mm. For the first time a resolved picture of this non-thermal radio source suggests an elongated structure on a scale of a few mas corresponding to an observed linear size of several 10^{14}cm inclined at $\sim 55°$ to the galactic plane.

4.1.2 Jet or homogenous blob?

The real spectrum of Sgr A* is difficult to obtain, due to a high degree of confusion in single dish observations and substantial variability; real simultaneous multifrequency spectra are rare. Recently Duschl & Lesch (1994) combined various data sets and claimed that the *time averaged* spectrum of Sgr A* has an inverted spectrum with spectral index $\alpha_{\rm s} = 0.35 - 0.38$ ($S_\nu \propto \nu^{\alpha_{\rm s}}$). They interpret this as a signature of a blob with radius $4 \cdot 10^{13}$ cm filled with monoenergetic electrons with Lorentz factor $\gamma_{\rm e} \sim 160$. The prediction of such a model is that the spectrum is optically thin synchrotron emission that should vary simultaneously over the whole frequency range from 200 GHz to 1 GHz. Another way to test the homogenous blob hypothesis are sources size measurements. At wavelengths ($\leq$ 7 mm) where the intrinsic size dominates the source size and the effects of broadening through scattering in the interstellar medium is not important, a homogenous blob should show the same size at all wavelengths (i.e. 7mm and 3mm), whereas for an expanding jet one expects an approximate linear decline of the source size with wavelength. Moreover, if Sgr A* indeed is a jet, as suggested by its elongated structure (Krichbaum et al. 1993) and also needed if Sgr A* is the source of the electrons in the Bridge and Arc (Lesch et al. 1988), this conceptually already implies a gradient in the magnetic field rather then a single homogenous blob. It should be noted that the values given by Duschl & Lesch are very similar to the ones used in our jet model and the electron Lorentz factor is very close to the low energy cut-off predicted by Falcke & Biermann (1994b) as a consequene of pp collisions and $\pi^{\pm}$ decay.

4.2 The jet-disk coupling

4.2.1 Parametrization of the jet-disk model

We now want to investigate whether the elongated radio structure in Sgr A* can be interpreted as a radio jet where in this chapter we only outline the basic concept for the Sgr A* jet and leave a more detailed discussion of the underlying theory to the next chapter.

It is commonly believed that radio jets originate from an accretion disk surrounding a star, neutron star or a black hole. As there are also strong hints for emission from an accretion disk in Sgr A* (see Chap. 3) that assumption may be valid for the Galactic Center as well, providing us with observational information for both systems. We therefore develop a jet model with regard to the coupling of jet and disk and the constraints imposed by observation.

Within such a jet-disk model, we express the basic properties of the radio jet in units of the disk accretion rate $\dot{M}_{\rm disk}$ of Sgr A*. The maximum accretion power $Q_{\rm accr}$ is given by the rest energy at infinity of the matter $\dot{M}_{\rm disk}c^2$. The total radiated disk luminosity $L_{\rm disk}$ is an appreciable fraction $q_{\rm d}$ of this accretion power and in the case of a black hole as the central object will be in the range $q_{\rm d} \sim 5\% - 30\%$ (Thorne 1974). Likewise, the total jet power $Q_{\rm jet}$ – including the rest energy of the expelled matter – should be a fraction $q_{\rm j} < 1$ of the accretion power and also the mass loss rate due to the jet $\dot{M}_{\rm jet}$ is a fraction $q_{\rm m} < 1$ of the mass accretion rate in the disk. Thus we define

$$Q_{\rm accr} = \dot{M}_{\rm disk}c^2, \qquad q_{\rm j} = \frac{Q_{\rm jet}}{Q_{\rm accr}}, \qquad q_{\rm d} = \frac{L_{\rm disk}}{Q_{\rm accr}}, \qquad q_{\rm m} = \frac{\dot{M}_{\rm jet}c^2}{Q_{\rm accr}}. \tag{4.1}$$

The $q_{\rm d,j,m}$ are dimensionless parameters, while $Q_{\rm accr}$ defines the physical scale of the system; c denotes the speed of light. We neglect all other energy consuming processes so that the remaining energy $(1 - q_{\rm j} - q_{\rm d})Q_{\rm accr}$ is swallowed by the black hole.

4.2.2 Basic assumptions of the jet-disk model

The above quantities are all measured in the observer's frame; we now switch to the rest frame of the jet and use this parametrization to calculate the radio emission of Sgr A* as emission from a radio jet and analyze its possible link to the accretion process. As the structural information about the Sgr A* radio emssion is still uncertain, we will use the simplified Blandford & Königl (1979) jet model which was developed initially for the unresolved core of AGN jets. The basic idea is that the radio emission is produced by a supersonic, freely expanding, therefore conical jet with semi-opening angle ϕ and constant velocity $\beta_{\rm j}$, convecting a tangled magnetic field dominating the internal gas pressure and producing a powerlaw energy distribution of relativistic electrons via shock acceleration. It is assumed that there is an approximate equipartition between the magnetic energy density $u_{\rm mag} = B^2/8\pi$ and the relativistic particle energy density $u_{\rm rel}$. In the following we will use cylindrical coordinates, denoting the axis along the jet as z and the distance from the axis to the boundary surface of the jet-cone as $r = z \sin\phi$. We discuss only the part of the jet far away from its footpoint.

For this model one usually takes an electron distribution of the form $N(\gamma_{\rm e}) = K\gamma_{\rm e}^{-2}$ for relativistic electron Lorentz factors in the range $\gamma_{\rm min} \leq \gamma_{\rm e} \leq \gamma_{\rm max}$. From $u_{\rm rel} \simeq u_{\rm mag}$ we get $K = B^2/(8\pi m_{\rm e}c^2\Lambda)$,where $m_{\rm e}$ is the electron mass and $\Lambda = \ln(\gamma_{\rm max}/\gamma_{\rm min})$ yielding a number density for electrons of $n = B^2/(8\pi\Lambda\gamma_{\rm min}m_{\rm e}c^2)$.

The energy density and the pressure in the jet is assumed to be mainly due to the magnetic field and the relativistic particles $p = p_{\rm mag} + p_{\rm rel} \simeq (B^2/8\pi)(1 + \frac{1}{3})$. Actually the factor $\frac{1}{3}$ is valid only for the extreme relativistic case where $p_{\rm rel} = \frac{1}{3}u_{\rm rel}$ and exact equipartition, however, it can only be as high as $\frac{2}{3}$ in the nonrelativstic case or negligible for $u_{\rm rel} \ll u_{\rm mag}$. Thus our choice of p is a fair approximation.

An important parameter of the jet flow is its proper Mach number $\mathcal{M} = \beta_{\rm j}\gamma_{\rm j}/\beta_{\rm s}\gamma_{\rm s}$. For a free jet the minimum opening angle is given by its Mach angle, which is defined as $\sin\phi_{\rm min} = 1/\mathcal{M}$ (Königl 1980). For a perfect gas we have: $\gamma_{\rm j} = 1/\sqrt{1-\beta_{\rm j}}$, $\beta_{\rm s} = \sqrt{\Gamma p/\omega} < 1$, $\gamma_{\rm s} \simeq 1$, the adiabatic index $\frac{4}{3} \leq \Gamma \leq \frac{5}{3}$, and the enthalpy density $\omega = m_{\rm p}nc^2 + \Gamma p/(\Gamma-1)$ if we demand equal numbers of thermal protons and relativistic electrons (cnf. last paragraph of this section). For $\Lambda\gamma_{\rm min} \ll \frac{m_{\rm p}}{m_{\rm e}}$ we have

$$\mathcal{M} = \gamma_{\rm j}\beta_{\rm j}/\sqrt{\frac{4m_{\rm e}}{3m_{\rm p}}\Gamma\Lambda\gamma_{\rm min}}, \tag{4.2}$$

while for the other extreme we would get a maximum sound velocity $\beta_{\rm s,max} = \sqrt{(\Gamma-1)}$ and the condition $\mathcal{M} > \gamma_{\rm j}\beta_{\rm j}/\beta_{\rm s,max}$.

Considering that the particle flux of the jet is given by $q_{\rm m}Q_{\rm accr}/m_{\rm p}c^2 = \gamma_{\rm j}n\beta_{\rm j}c\pi r^2$ we can now express the magnetic field in the jet in terms of the numbers $q_{\rm m}$ and $\mathcal{M}$, obtaining the familiar $B \propto z^{-1}$ behaviour.

$$B = \sqrt{\frac{6\gamma_{\rm j}\beta_{\rm j}q_{\rm m}Q_{\rm accr}}{\Gamma\mathcal{M}^2z^2\sin\phi^2c}}, \tag{4.3}$$

The assumption of Blandford & Königl that all electrons are relativistic and all protons are thermal is very crude and we would rather expect to have a mixture of a thermal and a relativistic plasma both containing electrons and protons. But if the ratio of thermal protons to nonthermal electrons is constant throughout the jet, this effect will cancel out in the final equations and only the definition of Λ and $\mathcal{M}$ in Eq. (4.2) will change. We therefore will not use Eq. (4.2) in this chapter and rather consider $\mathcal{M}$ and Λ as free parameter which in principle contain all the unknown microphysics (e.g. the electron to proton ratio). We leave a more elaborated discussion of this point to Chapter 5 but note already here that low Mach numbers require high electron Lorentz factors of $\gamma_{\rm min} \gg 1$.

4.2.3 Energy equation of the the jet-disk model

To investigate how much energy is extracted by the jet relative to the disk, we have to write down the basic energy equation for the jet-disk system. This is simply the relativistic Bernoulli equation for the jet

$$\gamma\omega/n = \omega/n|_\infty \tag{4.4}$$

with the left hand side parametrized by the quantities $q_{\rm m}$ and $\mathcal{M}$ and the right hand side determined by the energy supply from the accretion process and parametrized by $q_{\rm j}$. Algebraic transformations then lead to

$$\gamma_{\rm j}q_{\rm m}\left(1+\frac{\gamma_{\rm j}^2\beta_{\rm j}^2}{(\Gamma-1)\mathcal{M}^2}\right) = q_{\rm j}. \tag{4.5}$$

If we subtract the rest energy from both sides and take the non-relativistic limit, this equation simply states that the total power in the jet consists of the power in relativistic particles and the magnetic field plus the kinetic energy of the matter.

4.2.4 Radio emission from the jet

To deduce some of the parameters of the jet-disk system from the observation we now have to calculate the synchroton emission from the jet described above. Angle averaged emissivity and absorption coefficient are given by $\epsilon_{\rm sync} = 2450\,(B/{\rm Gauss})^{7/2}(\nu/{\rm GHz})^{-1/2}\Lambda^{-1}{\rm Jy/cm\,ster}$ and $\kappa_{\rm sync} = 2.25\cdot10^{-12}(B/{\rm Gauss})^4(\nu/{\rm GHz})^{-3}\Lambda^{-1}{\rm cm}^{-1}$ respectively using the equipartition assumption for magnetic field and relativistic particles. At a given frequency the jet will become optically thin and thus visible for a comoving observer at a jet position $z_{\tau_\nu=1}$ where the optical depth along the line of sight, inclined by the angle i to the jet axis, is unity. For a ray right through the central axis of the jet and $i \gg \phi$ we can approximate this by $2\sin\phi\, z_{\tau_\nu=1}\,\kappa_{\rm sync}(z_{\tau_\nu=1})/\sin i \simeq 1$ neglecting the gradient in the magnetic field along the line of sight for $i \neq \pi/2$. To obtain the total flux at this frequency we then have to integrate the jet emission from $z_{\tau_\nu=1}$ to infinity (or whatever one considers to be the outer

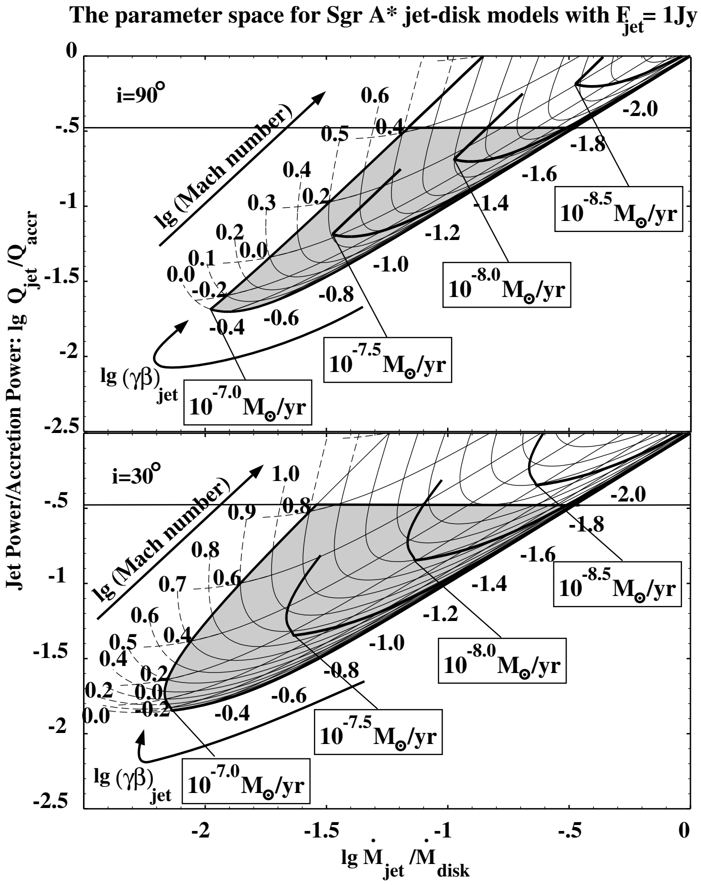

Figure 4.1: The shaded area limits the parameter space for a coupled jet-disk system in Sgr A* producing a flat radio spectrum with $F_\nu = 1.1 Jy$ and a NIR-UV disk luminosity $\leq 5 \cdot 10^5 L_\odot$. The vertical axis gives the log of the total power extracted by the jet from the accretion disk normalized by the total accretion power $Q_{\rm accr} = \dot{M}_{\rm disk} c^2$; for comparison: the radiative power of the accretion disk is $0.05 - 0.3 Q_{\rm accr}$. The horizontal axis gives the log of the relative mass loss due to the jet compared to the mass accretion rate of the disk. Strongly bended lines in the plot represent models of equal Mach number $\mathcal{M}$ whereas the less bended lines represent models of constant proper jet velocity $\gamma_{\rm jet}\beta_{\rm jet}$. The left figure is plotted for a jet seen side on with inclination angle $i = 90°$, while the figure on the right is plotted for a jet with an axis inclined to the line of sight by 30°. A shift of the parameter grid with different accretion rates is indicated by text boxes and the shape of the shifted bounding lines of the parameter grid.

edge of the jet) yielding a flat spectrum. Transforming the equation into the observer's frame, we have for the continuous, optically thin part of a jet (Lind & Blandford 1985)

$$\begin{aligned} &\mathcal{D} = 1/\gamma_{\rm j}(1 - \beta_{\rm j}\cos i_{\rm obs}), \quad F_{\rm obs}(\nu_{\rm obs}) = \mathcal{D}^2 F_{\rm obs}(\mathcal{D}\nu) \\ &\nu = \nu_{\rm obs}/\mathcal{D}, \quad \sin i = \mathcal{D}\sin i_{\rm obs}, \quad \phi = \phi_{\rm obs}\sin i_{\rm obs} \end{aligned} \tag{4.6}$$

and obtain as the observed flux from one jet cone

$$F_{\rm obs,1|2}(\nu_{\rm obs}) = 1\ {\rm Jy}\cdot\mathcal{D}^{13/6}\sin i^{1/6}\left(\frac{\mathcal{M}}{3}\right)^{-11/6}\left(\frac{\Lambda}{9}\right)^{-5/6}\cdot\left(\gamma_{\rm j}\beta_{\rm j}\frac{q_{\rm m}}{3\%}\frac{\dot{M}_{\rm disk}}{10^{-7}M_\odot/{\rm yr}}\right)^{17/12} \tag{4.7}$$

which is the original Blandford & Königl equation only with a new parametrization and the assumption that the opening angle of the jet is given by the Mach angle. We adopted a Galactic Center distance of $D = d_{8.5}8.5$ kpc and a central accretion rate of $\dot{M}_{\rm disk} = \dot{m}_{-7}10^{-7}M_\odot/{\rm yr}$. The total flux from both cones is $F_{\rm obs} = F_{\rm obs,1}|_{i_{\rm obs}} + F_{\rm obs,2}|_{\pi - i_{\rm obs}}$.

4.2.5 Size of the emitting region

To find out whether the central core of the jet can be resolved, we transform the source size in the rest frame given approximately by $z_{\tau_\nu=1}$ into the observed size $z_{\tau_\nu=1,{\rm obs}}$ which is

$$z_{\tau_\nu=1,{\rm obs}} = 2\cdot 10^{13}{\rm cm}\left(\frac{43GHz}{\nu}\right)\cdot\left(\frac{\gamma_{\rm j}\beta_{\rm j}}{\sqrt{1+(\gamma_{\rm j}\beta_{\rm j})^2}}\sqrt{\frac{9}{\Lambda}\frac{3}{\mathcal{M}}}\frac{q_{\rm m}}{3\%}\frac{\dot{M}_{\rm disk}}{10^{-7}M_\odot/{\rm yr}}\right)^{2/3}. \tag{4.8}$$

We see that even at high frequencies the size of the jet is smaller than current VLBI resolution. If we go even further, i.e. to submm wavelengths, the size of the emitting region approaches the minimal size, which is the size of a black hole of mass $\sim 10^6 M_\odot$. This scale then should correspond to the 'nozzle' of the jet, producing the highest frequencies and fluxes and explaining the rise of the spectrum in the submm range (Zylka et al. 1992) as a very compact, hence variable synchroton source at the footpoint of the jet (and not as thermal dust emission). At higher frequencies (IR) non-thermal jet emission should not be detectable because of the large size of the black hole (Falcke & Biermann 1993).

4.2.6 Parameter space of jet-disk models

Now we can limit the parameter space for possible models of the jet-disk system in the Galactic Center. We know from observation that the flux from Sgr A* at 43 GHz is $F_{\rm obs} \simeq 1.1$ Jy (Krichbaum et al. 1993). Inserting this into equation (4.7) we get an equation for the relative mass loss $q_{\rm m}$ in Sgr A* as a function of the opening angle, the velocity, the inclination angle and the Mach number of the jet. With $q_{\rm m}$ specified, we can calculate the energy consumption $q_{\rm j}$ of the jet relative to the disk from the energy equation (4.5). As a free jet should have an opening angle $\sin\phi \geq 1/\mathcal{M}$ and the radiative efficiency of the jet decreases with increasing opening angle the equality $\sin\phi = 1/\mathcal{M}$ used in Eq. (4.7) gives a lower limit for the energy demand $q_{\rm j}$ of the Sgr A* jet. Moreover we are not free to choose the other parameters completely arbitrarily. For a free jet the Mach number should be greater than unity and as stated above for a given Mach number the jet velocity can not exceed $\gamma_{\rm j,max}\beta_{\rm j,max} = \mathcal{M}\sqrt{(\Gamma-1)}$. Because of mass conservation in the jet-disk system we have $q_{\rm m} < 1$ and from energy conservation we get the limit $q_{\rm j} < 1$. The latter is probably too generous, as there is at least some energy loss through the disk radiation and could be reduced to 2/3 or even 1/3 – the maximum efficieny of the disk.

Lastly, we need to specify the accretion rate of Sgr A*. Falcke et al. (1993) deduced a range of $10^{-7}M_\odot/{\rm yr} > \dot{M} > 10^{-8.5}M_\odot/{\rm yr}$ from standard accretion disk models and IR/NIR luminosities. The upper limit is obtained by assuming that most of the disk luminosity is absorbed in the surrounding dust and thus the disk luminosity can not exceed the dust luminosity. But as the dust is probably also heated by stars of the central cluster, the real disk luminosity will be much lower. On the other hand these models did not include the influence of a jet on the disk structure and efficiency. This may change the estimate of the accretion rate if $q_{\rm j}$ is comparable to the radiative efficiency of the disk $q_{\rm l}$.

4.3 Results

In Figure 1 we have plotted the lower limit of the relative energy demand $q_{\rm j}$ and the relative mass loss rate $q_{\rm m}$ of the Sgr A* jet compared to the accretion power and mass accretion rate of the disk as functions of the jet velocity and Mach number for two inclination angles and different accretion rates. The shaded area limits the possible parameter space for a Sgr A* jet-disk system being capable to produce 1.1 Jy radio emission. For our calculations we took as adiabatic index $\Gamma = 4/3$ and a fairly low logarithmic factor $\Lambda = 9$ which corresponds to a ratio of $\gamma_{\rm max}/\gamma_{\rm min} \sim 10^4$. These values are completely arbitrary, but a higher Λ would again reduce the radiative efficiency, increase the energy demand and thus strengthen our conclusion. Note that the models with extremely low Mach number $\mathcal{M} \leq 3$ require unrealistic large opening angles and the lowest part of the parameter grid is only plotted for completeness.

One can see that even for the highest disk accretion rates allowed by the IR dust observations the *minimum* energy requirements for a Blandford & Königl type jet are at least several per cent of the total accreted rest mass energy $q_{\rm j} > 2\%$. If one compares this with the radiative disk efficiency $q_{\rm l} \sim 5\% - 30\%$ one can say that within this model the Sgr A* jet could extract as much energy from the disk – in form of kinetic and magnetic energy – as is radiated by dissipative processes in the disk itself.

The minimum energy demands for the Sgr A* jet are found for low Mach numbers – this means high magnetic energy compared to the kinetic energy – and moderate relativistic velocities with $\gamma_{\rm j}\beta_{\rm j} \sim 0.1 - 6$. The Mach-number is limited to be $\mathcal{M} < 40$. Higher γ-factors or nonrelativistic velocities seem to be excluded. This is well within the range of parameters which is found in extragalactic jets.

On the other hand our analysis also gives a strict lower limit for the Sgr A* accretion rate namely $\dot{M} \gg 10^{-8.5} M_\odot/{\rm yr}$ which is independent of the disk luminosity. Any lower accretion rates are not capable of producing such a strong radio emission. This agrees well with the lower limit given by Falcke et al. (1993) deduced earlier. And finally it should be noted that if one accepts the high energy extraction efficiency of the jet – despite our ignorance of the exact physical process being responsible for this – there is ample space in the parameter space left to positively state that the radio spectrum of Sgr A* can be understood as emission from a radio jet which is barely resolved due to a small spatial scale and a small power, both limited by the low disk accretion rate.

4.4 Variability of Sgr A*

In this section we want to review observational and theoretical arguments concerning the variability of Sgr A*. What are the intrinsic timescales for variability expected in the jet/disk model? The answer has to be given on different levels. First there is the large scale variation caused by the accretion process itself. As discussed earlier (FBDM; Chap. 3) the viscosity parameter may be very low and of the order $\alpha \leq 10^{-3}$ for an accretion rate of $\dot{M} = m_7 \cdot 10^{-7} M_\odot/yr$. The disk therefore is gas pressure dominated at all radii, with the exception of some small regions very close to the center(Falcke & Heinrich 1994).

4.4.1 Long-term variability

The radial velocity of the accretion flow

$$V_{\rm r} = 4\,\frac{\rm cm}{\rm sec}\left(\frac{\alpha}{10^{-3}}\right)^{0.8}\frac{\dot{m}_7^{0.3}}{r^{0.25} m_6^{0.2}}\,\frac{\mathcal{B}^{0.8}\mathcal{E}^{0.05}}{\mathcal{A}^{0.1}\mathcal{C}^{1.2}} \tag{4.9}$$

is extremely low and of the order 20-3 cm/sec in the very inner region and of ther order 0.5 cm/sec further out (10^{14-15} cm). This corresponds to timescales $\tau_{\rm accr} = r R_{\rm g}/V_{\rm r}$ of several 10 to 100 years in the very inner region and to 10^{7-8} years at 10^{14-15} cm from the black hole. This means that the time averaged fluxdensity of Sgr A* which is solely determined by the accretion rate should change only slightly in a few decades. And indeed it appears as if Sgr A* has on average a fairly constant radio flux at usual radio frequencies around 1 Jy. This is valid for instabilities of the accretion in the inner region; changes of the total accretion rate affecting the whole disk will take millions of years so it is conceivable that Sgr A* was generally more active in past times as indicated by possible starburst activities 10^8 years ago (Tamblyn & Rieke 1993) and today is only finishing up stored reserves from stellar winds (Melia 1993).

4.4.2 Short-term variability

Besides the long term variability there may be a shorter variability due to internal instabilities in the disk/jet interface. This variabilities, however, should vary around an equilibrium state determined by the total accretion rate as discussed above. The velocity to be identified with this processes is the sound speed of the plasma in the inner region. As shown in Chapter 5 the disk has to produce the magnetic field driving the jet locally. We suggest that in this case probably dynamo processes produce a magnetic field exceeding the gas pressure and therefore leading to a break out of the jet in the inner region. Anyhow, the magnetic field at the radial boundary between disk and jet will be extremal and thus approximately equal to the gas pressure. We find from Eq. 5.9.6g of NT73

$$B_{\rm disk} = 60\,{\rm kG}\,\frac{\alpha^{0.05}\dot{m}_7^{0.425}}{r^{1.3}m_6^{0.45}}\frac{\mathcal{B}^{0.05}\mathcal{E}^{0.24}\mathcal{Q}^{0.43}}{\mathcal{A}^{0.48}\mathcal{D}^{0.21}}. \tag{4.10}$$

For Sgr A* this implies magnetic fields in the disk of the order 10-1.5 kG in the region $r = 2 - 10$. We note that the magnetic field needed in the jet is of the order 120-25 Gauss and therefore well below the disk value. Possible instabilities in the disk should be mainly associated with variations in the magnetic field and as gas and magnetic field pressure are assumed to be equal, the magnetic sound speed is the characteristic speed for the short term variability in the jet nozzle yielding

$$\tau_{\rm jet} = 16\,{\rm days}\,\left(\frac{\alpha}{10^{-3}}\right)^{-0.4}\frac{r^{1.4}m_6^{1.1}}{\dot{m}_7^{0.15}}\frac{\mathcal{A}^{0.05}\mathcal{B}^{0.1}\mathcal{D}^{0.075}}{\mathcal{E}^{0.025}\mathcal{Q}^{0.15}}. \tag{4.11}$$

We see that the derived timescale in the inner region $r = 2-10$ is of the order 50-400 days. This is in agreement with the observed variation in the high frequency range. It has been found that Sgr A* is not variable on very short time scale of few days to one week (Zylka p.c.), but that significant changes are found within 2 month to half a year, e.g. Krichbaum et al. 1993 not only found an elongated structure of Sgr A* contrary to an observation 2 months later (Backer et al. 1993), they also found a significantly lower flux.
We note that the same kind of estimate for AGN disks (radiation pressure dominated) with $M_\bullet = 10^8$ and $\dot{M}_{\rm disk} = 1 M_\odot/{\rm yr}$ yields variability timescales of the order one half to 10 days, assuming a canonical viscosity parameter for this disks of $\alpha = 0.1$ – again not far from actually observed timescales.
The variations described above are assumed to be due to changes in the jet/disk interface but there might also be fluctuations in the jet itself due to inhomogenities leading to a flickering of the emission with the smallest amplitude. The scale for this is given by the jet sound and flow speed – both close to the speed of light. As the size of the emitting region gets larger with the observed wavelength, the timescale of such an internal flickering should be wavelength dependent and increase roughly linear with wavelength. If the typical scale for Sgr A* at 7 mm is $\leq 10^{14}$ cm (1 mas), than flickering could be as fast as 5 minutes to 1 hour. It is questionable if this is observable, not only because of the small amplitude but also because of the flickering produced externally by interstellar gas.

4.5 Conclusions

Together with the spectra discussed in the preceding chapter (see also Zylka et al. 1992) we can explain the spectrum of Sgr A* from radio to NIR in a consistent manner, including the flat radio spectrum (jet) and its variability, the upturn in the submm range ('nozzle'), the break in the IR (black hole) and a new component in the NIR (disk). It shows that such an AGN like scenario with black hole, accretion disk and jet may explain the inner part of the Galactic Center as well, but on a much lower level of activity. This is caused by a very low central accretion rate in the range $10^{-7} M_\odot/{\rm yr} > \dot{M} > 10^{-8.5} M_\odot/{\rm yr}$ making the Galactic Center an AGN on a starvation diet.
The elongated structure found by Krichbaum et al. (1993) on the mas scale is well explained as a weak radio jet. On the kpc scale Sofue et al. (1989) found a large structure ('Galactic Center Spur') pointing at the Galactic Center which could well be the final smoke trail of our Galactic Center jet.
Our finding that the energy extracted by the jet in Sgr A* is comparable to the energy radiated by the accretion disk is not unique. Rawlings & Saunders (1991) came to a similar conclusions from a purely observational analysis of jet and disk emission of a large variety of radio galaxies. What is striking here, is that these radio galaxies are ususally steep-spectrum radio sources associated with an active galactic nucleus inside elliptical galaxies. If indeed an ordinary spiral like our Milky Way shows a similiar $Q_{\rm jet}/L_{\rm disk}$ ratio as these AGN, than

the ratio of jet power to disk luminosity is a consequence of fundamental jet-disk physics and not special to any type of galaxy, whereas the absolute powers of jets and disks are a consequence of different host galaxies, i.e. the different processes of feeding. Interestingly our equation (4.7) predicts a certain scaling of radio emission from the central radio core with accretion rate which should hold for AGN as well – this is tested in Chapter 6. The combined jet-disk system for the GC we have sketched here, is of course very simplified, but as we have concentrated on the basic energetics this seems to be justified. Moreover, the statement that the jet extracts a non negligible part of the accretion power is fairly robust, as we always used lower limits for the energy demand of the jet.

Nevertheless, some assumptions of the Blandford & Königl model may be violated but only a few of them making a lower $Q_{\rm jet}/L_{\rm disk}$ possible. For example the jet could be additionally confined with an opening angle smaller than the Mach angle, and therefore be more efficient. Perhaps with better data at hand (e.g. velocity and opening angle of the jet or the mass accretion rate) such an additional confinement may even be required to explain the high efficiency of the Sgr A* radio jet compared to the luminosity of the accretion disk. On the other hand, the jet could extract additional rotational energy from the black hole (Blandford & Znajek 1977) or reduce the disk luminosity by its influence on the accretion process, which we have not included in our model. Finally there could be a less efficient central object – other than a black hole – or a not fully dissipative disk changing the estimates for the accretion rate.

Chapter 5

The jet-disk symbiosis – broadband spectrum of the monster

5.1 Introduction

Some of the most spectacular objects in astrophysics are the giant radio lobes and jets found in many active galaxies. Today it is fairly well established that these structures are due to a collimated outflow from the nuclear region. High resolution studies show jet-like structures on all scales with a common alignment (Bridle & Perley 1984), suggesting that indeed the jet is accelerated on small scales and proceeds through the galaxy until it is stopped far from the nucleus. In the most active galaxies – the quasars – the radio spectrum of the jet may dominate the whole radio emission of the galaxy. However, only $\sim 10\%$ of the quasars show radio jets on large (> 10 kpc) scales, even though nuclear radio emission is found in many more objects (Kellermann et al. 1989).

Another feature of active galactic nuclei (AGN) is an enormous energy output in other wavelengths as well, coming from an extremely compact core. An average spectrum consists of two important components, an infrared (IR) bump and an ultraviolet (UV) bump (Sanders et al. 1989). The latter can be fitted by emission from a standard accretion disk (Shakura & Sunyaev 1973, Novikov & Thorne 1973) around a supermassive black hole with mass $M_\bullet > 10^7 M_\odot$ accreting $0.1 - 10 M_\odot$/yr (Sun & Malkan 1989). In recent years it became clear that beyond these parts also in the X-ray and γ-ray region important contributions to the overall AGN luminosity can be found (e.g. Hartman et al. 1992). The presence of reflected components in the disk spectra leads to a modification of the simple accretion disk scenario, where the disk is additionally heated by an external source, probably powered by the nuclear jet (Niemeyer & Biermann 1993) or a disk corona (Haardt et al. 1991).

An obvious consequence of the presence of accretion disk and radio jet is the idea that both are intimately linked: the jet is produced in the inner parts of the disk and flows along its rotation axis outwards. And indeed, Rawlings & Saunders (1991) found a remarkable correlation between a disk luminosity indicator and the power of the large scale jet structures in FR II galaxies.

But despite many attempts to model this, the origin and acceleration mechanism of jets is still uncertain. This is mainly due to the fact that the acceleration region is hidden deep inside the quasar, so that the boundary conditions for any theory are arbitrary over a wide range. Our approach now is to construct a more descriptive model based on the standard theory for the emission from compact radio cores by Blandford & Königl (1979, see also Marscher 1992 for a recent review) to which we simply add mass and energy conservation of the jet-disk system. This model can be constrained by observations and provides us with information about possible physical states of the jet plasma.

In this chapter we discuss the underlying model of an electron(/positron)/proton plasma jet linked to an accretion disk within a standard set of parameters. Section 5.2 describes the properties of the jet plasma and defines model parameters. In Sec. 5.3 we calculate the observable consequences in radio wavelengths of such models which are discussed in Section 5.6. Section 5.4 discusses the expected X-ray signature from SSC emission and Sec. 5.5 contains some remarks concerning the standard accretion disk theory and possible mechanisms for the jet production. In the next chapter (Falcke et al. 1994) we test the predictions of our model with the optically selected PG sample of bright quasars. A later work (Falcke & Biermann 1994) will test our hypothesis for galactic sources.

5.2 Jet-disk symbiosis

The basic idea was already outlined in Chap. 5 (FBDM; Falcke et al. 1993b) where we have learned that even in Sgr A* a jet might be comparable in power to the accretion disk. We now want to extend this analysis to other objects as well and generalize our hypothesis to make it even stronger. Here we start with the basic ansatz that *jet and disk are symbiotic features*. This makes the link hypothesis bi-directional: not only is a disk required to produce a jet, also does the disk need a jet to fulfill its inner boundary conditions. One has to admit, there is no strong physical justification for this assumption, besides the perception that indeed standard accretion disk theory breaks down in the very inner region close to the black hole, but we rather start with the most comprehensive approach, calculate the expected observational signatures and then let observation decide when, where and how far one has to step back to get more specific theories. Our 'symbiosis' ansatz thereby implies that also the radio weak quasars produce powerful relativistic radio jets in which energetic particles are accelerated as was proposed earlier to explain IR observations (Chini et al. 1989a, Niemeyer & Biermann 1993).

5.2.1 The link

Within such a jet-disk model, we express the basic properties of the radio jet in units of the disk accretion rate $\dot{M}_{\rm disk}$ and the mass $M_\bullet$ of the black hole. We use the same notation as in Chap. 5, defining

$$Q_{\rm accr} = \dot{M}_{\rm disk}\,c^2; q_{\rm j} = \frac{Q_{\rm jet}}{\dot{M}_{\rm disk}\,c^2}, q_{\rm l} = \frac{L_{\rm disk}}{\dot{M}_{\rm disk}\,c^2}, q_{\rm m} = \frac{\dot{M}_{\rm jet}}{\dot{M}_{\rm disk}}. \tag{5.1}$$

To scale the equations for AGN, we will refer to the following standard masses and accretion rates:

$$m_8 = \frac{M_\bullet}{10^8 M_\odot} \tag{5.2}$$

$$\dot{m}_{\rm disk} = \frac{\dot{M}_{\rm disk}}{1\,M_\odot/{\rm yr}}. \tag{5.3}$$

The total luminosity of a disk around a maximally rotating black hole with Kerr parameter $a = 0.9981$ is $L_{\rm disk} = 1.7\cdot 10^{46}\dot{m}_{\rm disk}$ erg/sec and the (spherical) Eddington luminosity of the black hole is $L_{\rm edd} = 1.26\cdot 10^{46}\,m_8$ erg/sec.

In our model the base of the jetflow is close to or at the boundary layer between accretion disk and black hole. The characteristic length scale of the jet-disk system is the characteristic scale of the Black Hole: the gravitational radius $R_{\rm g} = GM_\bullet/c^2 = 1.48\cdot 10^{13}\,m_8$cm. In the following we will use small letters to represent dimensionless variables, e.g. we will write the radial coordinate R and the vertical (along the jet) coordinate Z as

$$r_{\rm jet} = R_{\rm jet}/R_{\rm g}, \quad z_{\rm jet} = Z_{\rm jet}/R_{\rm g} \tag{5.4}$$

The jet will split in four basic parts. First, the flow will be accelerated in a nozzle close to the disk, then it will expand adiabatically, enclosing the magnetic field and showing up as the flat spectrum core, after that we expect an intermediate phase, where ordered magnetic fields and shocks dominate the structure which can be seen as a jet like in M87 and finally the flow will either become subsonic and terminate in the interstellar medium (ISM) or further out in the intergalactic medium (IGM) producing lobes and hotspots. Accordingly we will refer to the four regions as jet nozzle, inner jet cone, outer jet cone and lobe.

5.2.2 Initial conditions of the jet plasma

In this subsection we discuss the initial conditions of the supersonic jetflow in or right after the nozzle. The prerequisite of this model is that the jet is described by a plasma accelerated close to the disk, containing a magnetic field and a population of relativistic electrons and protons with a power-law distribution. The acceleration zone is assumed to be very small as is the case in most hydrodynamical winds, so that the jet velocity $\beta_{\rm j}c$ is treated as being constant. The magnetic field is produced in or close to the disk. Relativistic particles are assumed to be produced in the jet somewhere between the disk and the first visible emission ($\le 10^{18}$ cm) by a process related to the magnetic field; diffusive shock acceleration is just one example of such a process. Hereafter, all hydrodynamical quantites will be measured in the rest frame of the jet. If not distinguished explicitly the term 'electron' may include positrons as well.

The total energy density $U_{\rm jet}$ in the jet is the sum of magnetic field energy density $U_{\rm B} = B^2/8\pi$, turbulent kinetic plasma energy density $U_{\rm turb} \simeq U_{\rm B}$ assumed to be in equipartition with the magnetic field and the energy density of relativistic particles $U_{\rm e+p} = k_{\rm e+p} U_{\rm B}$.

$$\begin{aligned} U_{\rm jet} &= U_{\rm B} + U_{\rm turb} + U_{\rm e+p} = u_{\rm j_0} B^2/8\pi && (5.5)\\ u_{\rm j_0} &\simeq (2 + k_{\rm e+p}) && (5.6) \end{aligned}$$

As $k_{\rm e+p}$ can have any value we also allow discussion of non-equipartition situations and especially any small value $k_{\rm e+p} \ll 1$ where the plasma is dominated by the magnetic field. Nevertheless, we will refer to this equation as the equipartition assumption.
The number densities of relativistic particles in the jet are described by a power law distribution of the form

$$dN_{\rm e|p} = K_{\rm e|p}\, \gamma_{\rm e|p}^{-p}\, d\gamma \qquad (5.7)$$

where $\gamma_{\rm e|p}$ is the Lorentz factor of electrons and protons respectively. For simplicity we will assume, that the exponent p is the same for both species. The constants $K_{\rm e|p}$ can be evaluated with help of Eq.(5.5), where we assume that the particles are within a factor $k_{\rm e+p}$ in equilibrium with the magnetic energy density.

$$\begin{aligned} k_{\rm e+p} B^2/8\pi &= K_{\rm e}\int_{\gamma_{\min,e}}^{\gamma_{\max,e}} \gamma m_{\rm e} c^2 \gamma^{-p}\, d\gamma + K_{\rm p}\int_{\gamma_{\min,p}}^{\gamma_{\max,p}} \gamma m_{\rm p} c^2 \gamma^{-p}\, d\gamma && (5.8)\\ \Rightarrow K_{\rm e} &= B^2/\left(8\pi f m_{\rm e} c^2\right) && (5.9) \end{aligned}$$

where we have defined the integration factors $\Lambda_{\rm e}$ and $\Lambda_{\rm p}$ as

$$\Lambda_{\rm e|p} = \begin{cases} \left(\gamma_{\min,e|p}^{2-p} - \gamma_{\max,e|p}^{2-p}\right)/(p-2) & : \; p \neq 2 \\ \ln \gamma_{\max,e|p}/\gamma_{\min,e|p} & : \; p = 2 \end{cases}, \qquad (5.10)$$

the relativistic p/e ratio (plus one)

$$\mu_{\rm p/e} = \left(1 + \frac{K_{\rm p}\Lambda_{\rm p} m_{\rm p}}{K_{\rm e}\Lambda_{\rm e} m_{\rm e}}\right) \qquad (5.11)$$

and a fudgefactor

$$f = \Lambda_{\rm e}\mu_{\rm p/e}/k_{\rm e+p}. \qquad (5.12)$$

To ease understanding, we will discuss meaning, limits and expected values of our parameters in a special subsection (5.2.5).
Having the normalization specified it is now straightforward to integrate the powerlaw Eq.(5.7) and obtain the total number density of relativistic electrons and protons.

$$\begin{aligned} n_{\rm e} &= B^2/\left(8\pi\gamma_{\rm min,e}^{p-1} f m_{\rm e} c^2 (p-1)\right), && (5.13)\\ n_{\rm p} &= (\mu_{\rm p/e} - 1)\gamma_{\rm min,e}^{p-1} n_{\rm e}\frac{\Lambda_{\rm e} m_{\rm e}}{\Lambda_{\rm p} m_{\rm p}}. && (5.14) \end{aligned}$$

For small $\mu_{\rm p/e}$ the number of relativistic protons will be negligible compared to the number of either relativistic electrons or thermal protons, whereas the fraction $x_{\rm e} = n_{\rm e}/n_{\rm tot}$ of relativistic electron density $n_{\rm e}$ compared to the total number density of protons $n_{\rm tot}$ (relativistic + thermal protons) might be fairly high. For simplicity we define a modified electron ratio

$$x'_{\rm e} = x_{\rm e}\gamma_{\rm min,e}^{p-1}. \qquad (5.15)$$

and obtain as total density from Eq.(5.13)

$$n_{\rm tot} = B^2/\left(8\pi x'_{\rm e} f m_{\rm e} c^2 (p-1)\right). \qquad (5.16)$$

Considering the disk in-flow as primary source for mass out-flow, the values for density and magnetic field are not arbitrary but are fixed by the jet parameters, i.e. the proper velocity $\gamma_{\rm j}\beta_{\rm j}$, the width of the nozzle $r_{\rm nozz}$ and the mass loss rate of the jet $\dot{M}_{\rm jet}$ which in turn is constrained by the maximum mass supply from the disk.

$$\dot{M}_{\rm jet} = q_{\rm m}\dot{M}_{\rm disk} = \gamma_{\rm j}\beta_{\rm j} c n_{\rm tot} m_{\rm p}\pi\left(r_{\rm nozz}R_{\rm g}\right)^2 \qquad (5.17)$$

By comparing the number density following from this equation

$$n_{\rm tot} = 5.5 \cdot 10^{10}{\rm cm}^{-3} \left(\frac{q_{\rm m}}{0.03}\right) \frac{\dot{m}_{\rm disk}}{\gamma_{\rm j}\beta_{\rm j} m_8^2 r_{\rm nozz}^2} \tag{5.18}$$

with the number density needed to establish equipartition between magnetic field and relativistic particles (Eq. 5.16) we can express the magnetic field in terms of the dimensionless parameters described above.

$$B_{\rm nozz} = 1064\,{\rm G}\sqrt{\frac{f x_{\rm e}'(p-1)}{\gamma_{\rm j}\beta_{\rm j} r_{\rm nozz}^2} \frac{\dot{m}_{\rm disk}}{m_8^2} \left(\frac{q_{\rm m}}{0.03}\right)} \tag{5.19}$$

With this information at hand we can fix the initial conditions in the plasma flow under the additional assumption that the magnetic field can be included in the overall equation of state of a perfect gas with pressure

$$P_{\rm jet} = (\Gamma - 1)U_{\rm jet} = u_{\rm j_0}(\Gamma - 1)B^2/8\pi. \tag{5.20}$$

A turbulent and almost isotropic magnetic field gas has the ratio 1/3 between pressure and energy density ($\Gamma = 4/3$). For an ordered magnetic field (e.g. a toroidal component only) this ratio would be unity. In the following we give some basic equations for the plasma, following the description developed by Königl (1980). The enthalpy density plus rest mass energy of the plasma for a constant adiabatic index Γ is

$$\omega = m_{\rm p} n_{\rm tot} c^2 + \Gamma P_{\rm jet}/(\Gamma - 1); \tag{5.21}$$

pressure and enthalpy combined tell us the local sound speed of the plasma in its local rest frame

$$\beta_{\rm s} = \sqrt{\Gamma P/\omega} \tag{5.22}$$

$$\simeq \min\left(\sqrt{u_{\rm j_0}(\Gamma^2 - \Gamma) f x_{\rm e}'(p-1) m_{\rm e}/m_{\rm p}}, \beta_{\rm s,max}\right) \tag{5.23}$$

where the maximum sound speed is

$$\beta_{\rm s,max} = \sqrt{\Gamma - 1}. \tag{5.24}$$

For usual adiabatic indices the latter will be well below 1, so that it is fairly safe to assume $\gamma_{\rm s} = 1/\sqrt{1-\beta_{\rm s}^2} \approx 1$. In this case we can write the relativistic Mach number of the flow as

$$\mathcal{M} = \gamma_{\rm j}\beta_{\rm j}/\beta_{\rm s} \tag{5.25}$$

which gives the ratio between the proper flow speed and the internal sound speed. One consequence of relativistic gas dynamics and the upper limit for the sound speed is that any flow with bulk relativistic motion is supersonic and needs no collimation. For a free plasma stream the Mach number defines the semi-opening angle unless we have a situation where the field lines are arranged such that they confine the flow. Such a confinement is more likely to happen in the nozzle region and in the following we will ignore this possibility, rather take the photon gas approximation and set the adiabatic index of the plasma flow to

$$\Gamma = 4/3. \tag{5.26}$$

The underlying picture is a turbulent magnetic field in the inner jet cone. However, the whole description remains valid, if one considers an ordered magnetic field. In case of a solely toroidal magnetic field only a few factors will change slightly but the vertical ($1/z$, see below) dependence of B will be the same as in the turbulent case. Only for a predominantly poloidal magnetic field, we will get a different (steeper) z depependence of B. Polarizaton measurement do show different orientations of the magnetic field along the jets, suggesting different orientations of a net magnetic field as well (sometimes poloidal, sometimes toroidal). This is not a problem as long as the turbulent component of the magnetic field dominates the internal energy, otherwise some of our conclusions could change.

5.2.3 Energy equation

We now investigate the energy demand of the jet as described above. The energy equation describing our jet-disk system was derived already in Chap. 4 from the relativistic Bernoulli equation:

$$\gamma_{\rm j} q_{\rm m} \left(1 + \frac{\beta_{\rm s}^2}{\Gamma - 1}\right) = q_{\rm j}. \tag{5.27}$$

In case the internal sound speed reaches its maximum $\beta_{\rm s} = \sqrt{\Gamma - 1}$ the bracket evaluates to 2 and the internal power equals the kinetic power of the jet

$$2\gamma_{\rm j} q_{\rm m} = q_{\rm j} \quad \Rightarrow \quad q_{\rm m} = \frac{q_{\rm j}}{2\gamma_{\rm j} q_{\rm l}} \frac{L_{\rm disk}}{\dot{M}_{\rm disk} c^2}. \tag{5.28}$$

In most other cases ($\mathcal{M} \gg \gamma_{\rm j}\beta_{\rm j}/\sqrt{\Gamma - 1}$) we may use the approximation

$$\gamma_{\rm j} q_{\rm m} \simeq q_{\rm j} \quad \Rightarrow \quad q_{\rm m} = \frac{q_{\rm j}}{\gamma_{\rm j} q_{\rm l}} \frac{L_{\rm disk}}{\dot{M}_{\rm disk} c^2}. \tag{5.29}$$

5.2.4 Maximal jets

Obviously this energy equation limits the internal power to a maximum, which is set by the kinetic power (both in the observers frame). The case $\beta_{\rm s} = \beta_{\rm s,max}$ is the most extreme case in any model. Equation (5.28) transformed into the restframe of the gas tells us that in a given volume the enthalpy equals the rest mass energy of the protons – which is the microscopic equivalent to the statement that bulk kinetic power equals bulk internal power. We therefore will refer to this case as the 'maximal case' or the 'maximal jet'. Usually the kinetic power dominates the total energy but as soon as the magnetic field contributes a significant fraction to the total jet power, energy conservation provides us with a strict upper limit for the maximal magnetic field. Increasing the internal power would then increase the total power as well beyond the value $Q_{\rm jet}$ assigned to the jet. Even by dropping the assumption of a 'heavy' jet and taking out the protons from the energy balance (decreasing the kinetic power) we would gain only a negligible factor $\sqrt{2}$ for the magnetic field.
We have to make sure that this limit is not violated and formulate it as an additional condition for the plasma parameters involved. The total energy flow

$$\mathrm{EF} = \gamma_{\rm j}^2 \beta_{\rm j} c \omega \pi (r R_{\rm g})^2 \leq q_{\rm j} Q_{\rm accr} \tag{5.30}$$

is smaller than or equal to the total jet power, which leads to

$$\mu_{\rm p/e} \leq 100 \frac{k_{\rm e+p}}{\ln\left(\frac{\gamma_{\rm max,e}}{\gamma_{\rm min,e}} \frac{1}{100}\right) u_3 \gamma_{\rm min,e} x_{\rm e}} \tag{5.31}$$

We can turn this argument around and ask, what combination of parameters always gives the equality between internal and kinetic power, i.e. a maximal jet, and find

$$\mu_{\rm p/e} = 1.0 \frac{k_{\rm e+p}}{\ln\left(\frac{\gamma_{\rm max,e}}{\gamma_{\rm min,e}} \frac{1}{100}\right) u_3 \gamma_{\rm e,100} x_{\rm e}} \tag{5.32}$$

Equation (5.32) will be used to eliminate the proton/electron ratio in all subsequent equations for maximal jets. We will mark these equations with an asterisk ensuring that whatever parameters are used one still has a maximal jet.

$$^* = \text{“maximal case''} \tag{5.33}$$

5.2.5 Discussion of parameters

In this subsection we discuss the parameters which we introduced and their expected values and limitations.

- $r_{\rm nozz}$ is the radius of the jet at the disk/jet interface divided by the gravitational radius. It can have any value larger or equal to the inner radius of the disk, which for a maximally rotating black hole is $\simeq 1.23$ and likely values are ≥ 2 where the disk structure equations do have a maximum and the boundary layer begins, but could also be somewhat higher if one considers a rapidly rotating magnetosphere of the disk (Camenzind 1986; also Section 5.4).

- $x_{\rm e}$ is the ratio of relativistic electron density $n_{\rm e}$ to the total number density of protons $n_{\rm tot}(relativistic + thermal)$. If charge neutrality is assumed and no pair creation takes place than $x_{\rm e} \leq 1$ is a strict limit. Reaching the upper limit would mean all thermal electrons are accelerated. It is doubtful if any process can be so efficient and usually $x_{\rm e} = 0.1 - 0.5$ is already considered an extreme limit. In cases where pair creation is possible $x_{\rm e}$ could be higher than 1 but energy conservation (Eq. 5.31, $\mu_{\rm p/e} \geq 1$ and $\gamma_{\rm min,e} \geq 1$ per definitionem!) demands $x_{\rm e} \leq 100\ k_{\rm e+p}/\ln\left(\frac{\gamma_{\rm max,e}}{\gamma_{\rm min,e}}\frac{1}{100}\right) u_3 \gamma_{\rm min,e}$.

- $\gamma_{\rm min,e}$ is the minimum Lorentz factor of the relativistic electron population. As a powerlaw with low energy cut-off is only a first order approximation this could have several meanings: a simple break in the energy spectrum of the electrons with a much flatter slope than $p = 2$ below $\gamma_{\rm min,e}$, a thermal distribution with high temperatures ($T = \gamma_{\rm min,e} 6 \cdot 10^9$ K) plus powerlaw, or a real cut-off towards low energies caused by a threshold condition in the acceleration process. The only limit is $\gamma_{\rm min,e} > 1$. For energies higher than a critical value ($\gamma_{\rm min,e} \geq 100$) the electron fraction $x_{\rm e}$ has to decrease (Eq. 5.31) simultaneously. We emphasize that $\gamma_{\rm min,e} \geq 100$ is a necessary consequence of the pion decay following hadronic interactions (Biermann, Strom, Falcke 1994; Daum & Biermann in prep.).

- $x'_{\rm e}$ is defined as $\gamma_{\rm min,e}^{(p-1)} x_{\rm e}$ and is a normalized and dimensionless measure for the energy density of the relativistic electrons if $p = 2$. Again Eq.(5.31) limits $x'_{\rm e}$ to be ≤ 100.

- $\mu_{\rm p/e}$ is the cosmic ray proton/electron ratio plus one. The cosmic ray ratio is the ratio of the energy densities in relativistic protons and electrons integrated from $\gamma_{\rm min,p} = 1$ and $\gamma_{\rm min,e}$ respectively to infinity. By definition this value must be larger than unity. Exactly unity means there are no protons a all. Values discussed in the literature usually range from a few to 100 in the cosmic rays themselves and 2000 for certain acceleration theories. If the electron population is a product of hadronic interactions (secondary pairs) than one naively would expect that on average the electrons should not gain more power than the protons, i.e. $\mu_{\rm p/e} \geq 2$.

- $k_{\rm e+p}$ is the equipartition parameter. $k_{\rm e+p} = 1$ means: the energy density of the magnetic field equals exactly the energy density of all relativistic particles (electrons + protons). $k_{\rm e+p} \gg 1$ would imply that electrons and protons have gained much more energy than is stored in the magnetic field. Regarding that all likely acceleration mechanisms require a strong magnetic field, we consider this possibility unlikely and usually assumed values are in the range $k_{\rm e+p} \sim 0.01 - 1$.

- f is defined as $\Lambda_{\rm e}\mu_{\rm p/e}/k_{\rm e+p}$ and is needed in the non-maximal case as an additional parameter to describe the relative strength of the magnetic field energy density to the relativistic electron density. If one excludes $k_{\rm e+p} \gg 1$ (see above) and takes $\gamma_{\rm max,e}/\gamma_{\rm min,e} \simeq 100$ we have $f \geq 4$ for $p = 2$, whereas if $p = 3$ we have $f \geq \gamma_{\rm min,e}^{-1}$.

To shorten the equations we will also make use of the following definitions and standard parameters whose values are discussed in more detail in the next chapter.

- The ratio $Q_{\rm jet}/L_{\rm disk}$ between total jet power and disk luminosity

$$q_{\rm j/l} := q_{\rm j}/q_{\rm l} = Q_{\rm jet}/L_{\rm disk} \tag{5.34}$$

  which can have any value between zero (no jet) and infinity (no disk), but we consider $q_{\rm j/l} \leq 1$ as a sensible limit.

- The disk luminosity, which for 'typical' AGN is in the range $10^{44} - 10^{48}$ erg/sec.

$$L_{46} := L_{\rm disk}/\left(10^{46}\text{erg/sec}\right). \tag{5.35}$$

- The jet velocity and its bulk Lorentz factor $\gamma_{\rm j}$ usually assumed to be in the range $\gamma_{\rm j} \simeq 2 - 20$ (Ghisellini et al. 1993).

$$\gamma_{\rm j,5} := \gamma_{\rm j}/5 \tag{5.36}$$

  The bulk Lorentz factor (jet velocity) has a more subtle limit. In order to still have a jet and not a quasi spherical wind the Mach number should be larger than unity. For a maximal jet we need $\beta_{\rm j}\gamma_{\rm j} > 0.58$ and for lower bulk velocities $\beta_{\rm s}$ (i.e. f or $x'_{\rm e}$) also has to be lowered and one rather should use the Mach number as a parameter for sub-relativistic jets as in Chapter 4.

- The minimum Lorentz factor of the electron distribution, which may be in some cases ≥ 100 (see Discussion).
$$\gamma_{e,100} := \gamma_{\min,e}/100 \tag{5.37}$$
- Likewise, the modified electron density
$$x'_{e,100} := \gamma_{e,100}^{p-1} x_e \tag{5.38}$$
where one has to be careful if $p \neq 2$ as then we have $x'_{e,100} \neq x'_e/100$.
- The ratio u_{j_0} between total energy density in the jet and the magnetic energy density. In case we have equipartition between turbulent kinetic energy, magnetic field and relativistic particles this value is 3, neglecting turbulence gives 2 (or $1+k_{e+p}$). For high values of k_{e+p} this factor is no longer a small number and $u_{j_0} \propto k_{e+p}$.
$$u_3 := u_{j_0}/3 = (2+k_{e+p})/3 \tag{5.39}$$

Our general conclusions are qualitatively independent of the power law index p. For the observational consequences we concentrate on the canonical case $p=2$ and give some equations for $p=2.5$ in the Appendix.
Finally there is another limit we have to check. For the electrons one still could argue that they actually are pairs and therefore the electron fraction x_e may exceed unity, for protons the fraction x_p of relativistic protons in the jet must be less or equal unity otherwise mass conservation is violated. From Eqs.(5.14,5.18,5.19) we find that

$$x_p = 5.4 \cdot 10^{-4}\, \gamma_{\min,e} x_e \frac{\Lambda_e}{\Lambda_p} \left(\mu_{p/e} - 1\right) \leq 1. \tag{5.40}$$

Usually this limit is not important but in the maximal case where $\gamma_{\min,e} \geq 100$ this equation limits the proton/electron ratio $\mu_{p/e}$ to be ≤ 100. Fortunately, this limit is automatically met by virtue of Eq.(5.32), because for $k_{e+p} \gg 1$ we have $u_3 = k_{e+p}$ and a high value of $\mu_{p/e} \gg 1$ can not be obtained while keeping x'_e constant at ≥ 100.

5.3 Observational consequences

5.3.1 The cone

Beyond the nozzle the flow will expand sideways; either the jet has still a lot of angular momentum from the disk leading to an opening of the streamlines, or the strong and turbulent magnetic field dominates the internal pressure and leads to an expansion of the jet. In the latter case the semi-opening angle of the flow[1] ϕ is simply given by the relativistic Mach number $\mathcal{M}$ (Königl 1980). If, in the other case, the opening angle is given by the angular momentum, then the opening angle should be larger than this and we have

$$\phi \geq \arcsin \mathcal{M}^{-1}. \tag{5.41}$$

We will use only the equality

$$\phi \simeq 0.3^\circ \cdot \sqrt{\frac{f u_3 x'_e}{\beta_j^2 \gamma_{j,5}^2}} \tag{5.42}$$
$$\phi^* = 6.6^\circ \cdot \left(\beta_j \gamma_{j,5}\right)^{-1} \tag{5.43}$$

but one has to bear in mind that a larger opening angle will later reduce the radiative efficiency of the jet and in the final analysis therefore increase the energy demand of the jet relative to the disk. The cylinder-symmetrical shape $r(z)$ of the cone is given by

$$r_{jet}(z_{jet}) = r_{nozz} + (z_{jet} - z_{nozz})/\mathcal{M} \overset{z\to\infty}{=} z_{jet}/\mathcal{M}. \tag{5.44}$$

Considering an adiabatic jet, all quantities derived in the previous section will follow the laws of adiabatic expansion; we only have to substitute the radius r by means of the above equation (5.44) and obtain the hydrodynamical quantities as functions of the distance z from the disk. The magnetic field declines with

[1] This is defined to reflect the scale of the cone radius and is not identical with the opening angle as defined in some hydrodynamical simulations where zero pressure is reached.

$$B = B_{\rm nozz} r_{\rm j}(z)^{-\aleph}. \tag{5.45}$$

Conservation of magnetic energy leads to $\aleph = 1$ (the familiar $B_{\rm j} \propto 1/z_{\rm jet}$ decline) and a constant Mach number because particle and energy density both scale with $1/z_{\rm jet}^2$.
Note that there is no ad-hoc need for reacceleration of the relativistic particles. Likewise there is no dissipation or recreation of the magnetic field in the case $\aleph = 1$; but from synchrotron energy loss arguments we will find that acceleration of relativistic particles in the jet itself indeed is necessary. Nevertheless, our description will still be correct if this acceleration always leads to (quasi-)equipartition with the magnetic field. The same is true if one considers adiabatic losses (see Biermann et al. 1994).
We also note, that shocks will increase the magnetic field strength, taking the energy from the overall flow. Thus, in the case of semi-periodic shock structures, it is quite conceivable, that an average equilibrium between energetic particles, magnetic field energy and flow energy can be maintained. The high amount of energy in relativistic particles we need for some models is not unusual within the general picture of shock acceleration (see Drury 1983).

5.3.2 Emission from the radio core

Now we calculate the synchrotron emission of the different parts of the jet. First, we give the emission and absorption coefficients for powerlaw distributions of relativistic electrons (see Eq. 5.7) with index $p = 2$ in the rest frame. For the pitch angle of the electrons $\alpha_{\rm pitch}$ we took the values which inserted into the formulae yield the average for an isotropic turbulent medium. We get (Rybicki & Lightman 1979)

$$\begin{aligned}
\epsilon_{\rm sync} &= 5.5 \cdot 10^{-19} \, \frac{\rm erg}{\rm s\, cm^3\, Hz} \, f^{-1} \left(\frac{B}{\rm G}\right)^{3.5} \left(\frac{\nu}{\rm GHz}\right)^{-.5} && (5.46)\\
\alpha_{\langle {\rm pitch},\epsilon\rangle} &= 53.4^\circ && (5.47)\\
\kappa_{\rm sync} &= 4.5 \cdot 10^{-12} \, {\rm cm}^{-1} \, f^{-1} \left(\frac{B}{\rm G}\right)^{4} \left(\frac{\nu}{\rm GHz}\right)^{-3} && (5.48)\\
\alpha_{\langle {\rm pitch},\kappa\rangle} &= 54.7^\circ. && (5.49)
\end{aligned}$$

In Sec. 5.2 and the beginning of this section we defined the state of the emitting plasma in the freely expanding inner jet cone beyond the nozzle as a function of several dimensionless parameters. Using the synchrotron emissivity we can now calculate the total synchrotron emission from that region. The optical depth τ for a ray right through the central axis of the cone is given by

$$\tau = 2 r_{\rm j} R_{\rm g} \kappa_{\rm sync} / \sin i \tag{5.50}$$

using Eq.(5.44) to express the shape of the cone. From the condition $\tau = 1$ we find the part of the jet, where for an observed[2] frequency $\nu_{\rm s,obs}$ the jet becomes synchrotron self absorbed.

$$\begin{aligned}
Z_{\rm ssa} &= 19\,{\rm pc} \, \frac{x_{\rm e}^{1/6} \beta_{\rm j}^{1/3}}{u_3^{1/3} \gamma_{\rm j,5}^{1/3} f^{1/6} \sin i^{1/3}} \, \frac{\rm GHz}{\nu_{\rm s,obs}/\mathcal{D}} \left(q_{\rm j/l} L_{46}\right)^{2/3} && (5.51)\\
Z^*_{\rm ssa} &= 31\,{\rm pc} \left(\frac{x'_{\rm e,100} \beta_{\rm j}}{\gamma_{\rm j,5} u_3 \sin i}\right)^{1/3} \frac{\rm GHz}{\nu_{\rm s,obs}/\mathcal{D}} \left(q_{\rm j/l} L_{46}\right)^{2/3} && (5.52)
\end{aligned}$$

The size of the visible inner jet cone scales proportionally with the wavelength and the typical size of the inner jet is for AGN on the parsec scale. The size seen by an observer has to be multiplied with an additional factor $\sin i$. We can now integrate the emission of the cone from $Z_{\rm ssa}$ to infinity in the rest frame of the jet

$$L_{\nu_{\rm s}} = 4\pi \int_{Z_{\rm ssa}}^{\infty} \epsilon_{\rm sync} \pi r_{\rm j}^2(z_{\rm jet}) dz_{\rm jet} \tag{5.53}$$

[2] This means a frequency observed in the rest frame of the *quasar*, and does not include cosmological corrections.

yielding the total monochromatic luminosity of one jet cone in the rest frame. To get the observed fluxes we have to perform the transformations (Lind & Blandford 1985) already mentioned in Chap. 4

$$\begin{aligned} &\mathcal{D} = 1/\gamma_{\rm j}(1-\beta_{\rm j}\cos i_{\rm obs}), \quad L_{\nu,\rm obs}(\nu_{\rm obs}) = \mathcal{D}^2 L_\nu(\nu_{\rm obs}/\mathcal{D}) \\ &\nu_{\rm s} = \nu_{\rm s,obs}/\mathcal{D}, \quad \sin i = \mathcal{D}\sin i_{\rm obs}. \end{aligned} \tag{5.54}$$

Thus we have

$$L_{\nu_{\rm s,obs}} = 4.5\cdot 10^{31}\,\frac{\rm erg}{\rm s\,Hz}\,\left(q_{\rm j/l}L_{46}\right)^{17/12}\frac{\mathcal{D}^{13/6}\sin i_{\rm obs}^{1/6} f^{1/12} x_{\rm e}'^{11/12}}{\sqrt{u_3}\,\gamma_{\rm j,5}^{11/6}\beta_{\rm j}^{5/12}} \tag{5.55}$$

$$L^*_{\nu_{\rm s,obs}} = 1.3\cdot 10^{33}\,\frac{\rm erg}{\rm s\,Hz}\,\left(q_{\rm j/l}L_{46}\right)^{17/12}\frac{\mathcal{D}^{13/6}\sin i_{\rm obs}^{1/6} x_{\rm e,100}'^{5/6}}{\gamma_{\rm j,5}^{11/6}\beta_{\rm j}^{5/12}u_3^{7/12}} \tag{5.56}$$

Obviously the frequency cancels out in this equation (for all values of p) and the resulting spectrum of the cone is flat up to a maximum frequency (see below). The typical luminosity for cores of radio loud quasars with a disk luminosity of 10^{46} erg/sec is in the range $2\cdot 10^{31} - 6\cdot 10^{32}$ erg/sec/Hz at 5 GHz (e.g. Chap. 6). To avoid extreme parameters ($q_{\rm j/l}\gg 1$) one is forced to choose a model close to the maximal case (Eq. 5.56) in order to reproduce these high luminosities. A moderate value $2q_{\rm j/l}\approx 0.3$ seems to be sufficient in the maximal case.
Moreover, it is quite interesting that the flux emitted from the jet cone need not scale linearly with the accretion rate. This is a consequence of the nonlinearity between the magnetic energy density ($\propto B^2 \propto \dot m$) and the synchrotron emissivity ($\propto B^{3.5}$). Because of jet geometry and self-absorption this also depends slightly on the electron powerlaw. For very large p (approaching a monoenergetic distribution) radio emission and disk luminosity become proportional.
As noted before (Ghisellini et al. 1993) the brightness temperature of the cone (in the rest frame of the jet!)

$$T_{\rm b} = 1\cdot 10^{11}\,{\rm K}\left(\frac{x_{\rm e}' q_{\rm j/d} L_{46}}{f\gamma_{\rm j,5}^2\beta_{\rm j}}\right)^{1/12}\sin i^{5/6} \tag{5.57}$$

$$T_{\rm b}^* = 1.2\cdot 10^{11}\,{\rm K}\left(\frac{x_{\rm e,100}'^{\,2} u_3 q_{\rm j/l} L_{46}}{\gamma_{\rm j,5}^2\beta_{\rm j}}\right)^{1/12}\sin i^{5/6} \tag{5.58}$$

is constant along the jet axis and depends very weakly on the parameters – this is due to a self-regulation mechanism because emission and width of the jet are both governed by the magnetic field. The numbers may change between 10^{11} Kelvin for $p=2$ and 10^{10} Kelvin for $p=3$. The observational finding that there is a maximum brightness temperature of $T_{\rm b}\le 10^{12}$Kelvin (Kellermann & Pauliny-Toth 1969) might therefore not only be due to the synchrotron self-compton limit but is a natural consequence of a jet in a Mach cone. This is strongly supported by more recent investigations by Ghisellini et al. (1993), where it is found that the brightness temperature in the rest frame of VLBI jets has an extremely narrow distribution around $1.8\cdot 10^{11}$Kelvin – pointing nearer to $p=2$ in our model.

5.3.3 High frequency cut-off and maximum Lorentz factors

Until now we have neglected all radiation losses but we have to make sure that the energy loss by synchrotron radiation ($L_{\rm jet} = \int_0^{\nu_{\rm max}} L_{\nu_{\rm s}} d\nu$) does not exceed a certain fraction

$$\eta_{\rm sync} = L_{\rm jet}/\left(\gamma_{\rm j}^2\beta_{\rm j}c\pi\left(r_{\rm nozz}R_{\rm g}\right)^2\Gamma P_{\rm jet}/\left(\Gamma-1\right)\right) < 1 \tag{5.59}$$

of the internal energy flow. For reference we deliberately take a maximum efficiency of 33% for the conversion of internal energy into radiation and define $\eta_{\rm sync} = 1/3\cdot\eta_{1/3}$. Integration of the flat spectrum Eq.(5.55) in the rest frame yields a maximum frequency $\nu_{\rm max}$ where the spectrum has to cut off (or steepen substantially) to fulfill this limitation (here we ignore the anisotropy of the radiation field).

$$\nu_{\rm max,1} = 160\,{\rm GHz}\,\mathcal{D}\eta_{1/3}\frac{f^{11/12}\gamma_{\rm j,5}^{11/6}\beta_{\rm j}^{5/12}x_{\rm e}'^{1/12}u_3^{3/2}}{\left(q_{\rm j/l}L_{46}\right)^{5/12}\sin i^{1/6}} \tag{5.60}$$

$$\nu^*_{\rm max,1} = 1300\,{\rm GHz}\,\mathcal{D}\eta_{1/3}\frac{\gamma_{\rm j,5}^{5/6}\beta_{\rm j}^{5/12}u_3^{7/12}}{{x'_{\rm e,100}}^{5/6}\left(q_{\rm j/l}L_{46}\right)^{5/12}\sin i^{1/6}} \tag{5.61}$$

And indeed such a break is observed (Chini et al. 89b), where from 1.3 and 0.8 mm fluxes one can imply a turn-over of the core spectrum. A more precise determination of the break frequency would be an interesting test for this models. Because $\nu_{\rm max}$ is a function of the Doppler factor, the observed break frequency is smaller for radio galaxies (anti-boosted) than for core dominated quasars (boosted) if the unified scheme is correct.
In AGN this maximum frequency is much lower than the characteristic frequency in the very inner parts of the jet obtained by extrapolating this theory down to the nozzle. Hence we have to limit the maximum Lorentz factor of the electrons in the nozzle to prevent the jet from exhausting itself in the very beginning. The characteristic frequency of an electron with energy $\gamma_{\rm e}m_{\rm e}c^2$ in an magnetic field B is given by

$$\nu_{\rm e} = 4.2\cdot 10^6\,{\rm Hz}\;\,(B/{\rm Gauss})\,\gamma_{\rm e}^2 \tag{5.62}$$

and we can equate $\nu_{\rm max}$ with $\nu_{\rm e}$ using the magnetic field of the nozzle Eq.(5.19) to obtain the maximal initial Lorentz factor for electrons in the jet

$$\gamma_{\rm nozz,max} = 9\,\frac{\sqrt{\eta_{03}m_8 r_{\rm nozz}}\beta_{\rm j}^{11/24}\gamma_{\rm j,5}^{17/12}u_3^{3/4}}{{x'_{\rm e}}^{5/24}\left(q_{\rm j/l}L_{46}\right)^{11/24}\sin i^{1/12}} \tag{5.63}$$

$$\gamma^*_{\rm nozz,max} = 6\,\frac{\sqrt{\eta_{03}m_8 r_{\rm nozz}}\beta_{\rm j}^{11/24}\gamma_{\rm j,5}^{17/12}u_3^{13/24}}{{x'_{\rm e,100}}^{5/12}\left(q_{\rm j/l}L_{46}\right)^{11/24}\sin i^{1/12}} \tag{5.64}$$

For the maximal case this limit is inconsistent with a low energy cut-off at $\gamma_{\rm e}=100$. Unless pairs with $\gamma_{\rm min}\simeq 1$ are present, in situ acceleration of electrons is therefore necessary and the high internal energy flow in the beginning is only due to a Poynting flux with an electron distribution not in equipartition with the magnetic field and starting at low energies (model **B*** & **Bp** see Discussion). As we have not considered the effects of self-absorption (but see next section) and the turn over of the spectrum, slightly higher Lorentz factors are possible, but if they are initially much higher than these the jet would be completely dissipated by radiation losses. Starting with low Lorentz factors and shuffling the electrons towards higher energies by reacceleration in the jet into a state of equilibrium without severe radiation losses is possible only far away from the black hole and this scale is approximately given by the distance

$$Z^*_{\rm min,1} = 5\cdot 10^{16}\,{\rm cm}\;\frac{\left(q_{\rm j/l}L_{46}\right)^{13/12}x_{\rm e,100}^{7/6}}{\eta_{03}\beta_{\rm j}^{1/12}\gamma_{\rm j,5}^{13/6}u_3^{11/12}\sin i^{1/6}} \tag{5.65}$$

where the the high energy break $\nu_{\rm max,1}$ equals the peak (synchrotron self-absorption) frequency $\nu_{\rm s}$. This is the minimum scale for the beginning of the full jet emission. To ensure that the synchrotron emission in the optical thin part is not cut-off directly one also has to compare the synchrotron loss time $t_{\rm sync} = 7.7\cdot 10^8\,{\rm sec}\;(\gamma_{\rm min,e}(B/{\rm Gauss})^2)^{-1}$ of the electrons with the time scale of the local adiabatic expansion $t_{\rm exp} = z_{\rm jet}R_{\rm g}/(\gamma_{\rm j}\beta_{\rm j}c)$. Beyond a distance

$$Z^*_{\rm min,2} = 8.6\cdot 10^{17}\,{\rm cm}\;\frac{q_{\rm j/l}L_{46}\gamma_{\rm min,100}}{\beta_{\rm j}\gamma_{\rm j,5}^2 u_3} \tag{5.66}$$

the synchrotron spectrum can take its usual shape without severe radiation losses in the optically thin region around the synchrotron self absorption frequency. These scales are in agreement with the minimum size for the region where the γ-ray emission in blazars are proposed to originate (Dermer & Schlickeiser 1994, Mannheim 1993) suggesting a deeper connection between both processes. The frequency corresponding to this scale where a turnover of the flat spectrum is likely to occur is

$$\nu^*_{\rm max,2} = 70\,{\rm GHz}\,\mathcal{D}\left(\frac{\beta_{\rm j}\gamma_{\rm j}^2u_3^2x_{\rm e}}{\gamma_{100,\rm e}^2 q_{\rm j/l}L_{46}\sin i}\right)^{1/3}. \tag{5.67}$$

This is a bit lower than $\nu^*_{\rm max,1}$ which is a strict upper limit for the break in the radio spectrum.

5.3.4 Self-absorption vs. optical thin turnover

The traditional picture to obtain the flat spectrum core is based on the overlap of self-absorbed synchrotron blobs. This, however, may be a critical assumption at least in the maximal case when one demands high minimum electron Lorentz factors. To check this, we have to compare the synchrotron self-absorption frequency derived in Eq.(5.51) with the characteristic frequency

$$\nu_{\rm c}^*(\gamma=\gamma_{\rm min,e}) = 14\,{\rm GHz}\;\gamma_{\rm min,100}^2\sqrt{\frac{\beta_{\rm j}q_{\rm j/l}L_{46}}{u_3}}\left(\frac{\rm pc}{Z_{\rm jet}}\right) \tag{5.68}$$

emitted by an electron with Lorentz factor $\gamma_{\rm min,e}$ in a maximal jet. The ratio between both frequencies

$$\frac{\nu_{\rm s}^*}{\nu_{\rm c}^*} = 1.45\,\gamma_{\rm min,100}^{-5/3}\left(\frac{q_{\rm j/l}L_{46}x_{\rm e}^2}{\beta_{\rm j}\gamma_{\rm j,5}^2\sin i^2}\right)^{1/6} \tag{5.69}$$

again is only a weak function of all parameters except $\gamma_{\rm min,e}$ and constant throughout the jet. In the non-maximal case this ratio is $\sim 10^4$ and negligible, but in the maximal case this becomes an important effect. It means that for $\gamma_{\rm min,e}>120$ the spectrum will turn over already before synchrotron self-absorption sets in. One never gets a clear self absorbed $\nu^{2.5}$ spectrum but rather an optically thin $\nu^{1/3}$ spectrum which then turns over into a self-absobed 'thermal' ν^2 spectrum. The exact description will be given elsewhere.
Fortunately, both frequencies follow the same scaling along the jet and our calculations for the composite spectrum are still valid as the peaks at the two frequencies one integrates along the jet are very close. We still get a flat composite spectrum, not as an overlap of self-absorbed components but of components with an optically thin low energy turnover. This effect ensures that one always expects to see a flat to inverted spectrum. If for example one part of a variable and inhomogenous jet is enhanced and dominates the whole spectrum, we still will see a flat or even inverted spectrum at frequencies below $\nu_{\rm c}$. The spectrum of a resolved part of the jet core should be different as well; the low frequency turnover part of a VLBI blob will result in a spectrum possibly much flatter than the usual $\nu^{2.5}$.

5.3.5 Pair creation

Is the plasma in the jet optically thick, so that pair creation becomes important? To give an answer we calculate the optical depth $\tau_{\rm Th}=n\sigma_{\rm Th}2rR_{\rm g}$ of the jet for the Thomson cross section $\sigma_{\rm Th}=6.65\cdot10^{-25}{\rm cm}^2$

$$\tau_{\rm Th} = 50\,\frac{q_{\rm j/l}L_{46}}{\sqrt{f u_3}\gamma_{\rm j,5}m_8 z} \tag{5.70}$$

$$\tau_{\rm Th}^* = 1\,\frac{q_{\rm j/l}L_{46}}{\gamma_5 m_8 z} \tag{5.71}$$

and find that in all cases the jet is optically thin and $\tau_{\rm Th}$ decreases with distance. Only in the non-maximal case the very inner region of a few gravitational radii may be optically thick. The jet remains optically thin also for smaller black hole masses as than the luminosity decreases as well because of the Eddington limit.
One model very much under discussion to explain the hard X-ray spectrum of Seyfert galaxies and quasars is the idea, that there is a source of hard X-rays above the disk, which shines down on the disk. This hard radiation is then reprocessed in the disk, and reemitted with all the modifications due to interaction with the matter in the disk, thus yielding a number of spectral features, as observed. One mechanism to obtain this hard radiation is a pair creation cloud possibly connected to a putative jet. The primary source of energy could then be either a population of energetic electrons, or of energetic protons. In such models the pair creation opacity has to be fairly high to reprocess a large fraction of the primary energy (Zdziarski et al. 1990). In the context of our approach, we show here that this opacity is not high, and therefore that the notion of a pair creation cloud is not implied by our model.

5.3.6 Terminus

Now we leave the inner part of the jet and approach the same subject from the opposite side, namely the termination point. As magnetic field and particle densities expand adiabatically, the total energy density

ED= $\gamma_{\rm j}^2\omega$ in the jet as measured in the lab-frame will decline in the same way as well all the way out to kpc-scales.

$$\mathrm{ED} \simeq 8.4\cdot 10^{-7}\,\frac{\rm erg}{\rm cm^3}\,\frac{\beta_{\rm j}\gamma_{\rm j,5}^2\,(460+fu_3)\,q_{\rm j/l}L_{46}}{fx_{\rm e}'u_3}\left(\frac{\rm kpc}{Z_{\rm jet}}\right)^2 \tag{5.72}$$

$$\mathrm{ED}^* \simeq 8.4\cdot 10^{-7}\,\frac{\rm erg}{\rm cm^3}\,\gamma_{\rm j,5}^2\beta_{\rm j}q_{\rm j/l}L_{46}\left(\frac{\rm kpc}{Z_{\rm jet}}\right)^2 \tag{5.73}$$

The non-maximal jet stores most of its energy in the kinetic energy of the plasma; together with the narrow beam this gives a ram pressure acting into the forward direction being a factor 500 (for our set of parameters) higher than in the maximal case. Maximal jets have equal amounts of kinetic and internal energy, thus they will have a substantial amount of isotropic pressure. Taking only the amount of internal energy into account (dropping the factor 460 in Eq.(5.72)) we see that both types of jets have the same internaled energy density due to a self regulating process: lowering the energy density will always lead to a smaller opening angle which in turn will increase the energy density again.

If we want to calculate the typical length scale of a jet, we have at least two possibilities for non-maximal jets. First one should simply compare the ram pressure of the jet beam ($P_{\rm ram}\simeq$ ED) with the external pressure $P_{\rm ext}$, neglecting possible differences of the sound speeds in both media. For an external pressure of $P_{\rm ext}=P_{-12}10^{-12}\mathrm{erg/cm^3}$ we get a maximum scale length $Z_{\rm free}$ of the jet of

$$Z_{\rm free} = 20\,\mathrm{Mpc}\;\gamma_{\rm j,5}\sqrt{\frac{\beta_{\rm j}q_{\rm j/d}L_{46}}{fx_{\rm e}'u_3P_{-12}}} \tag{5.74}$$

This of course would be deep inside the IGM with pressures much lower than 10^{-12} erg/cm^3 and hence there is little chance to stop such a jet at all. On the other hand the jet might be distorted much earlier as the cone has to be supported sideways against the external pressure as well. The scale where strong interactions between cone and external medium are expected then is given by the condition $P_{\rm ext}=1/3$ ED* for *both* types of jets (see above) leading to

$$Z^*_{\rm free} = 530\,\mathrm{kpc}\;\gamma_{\rm j,5}\sqrt{\beta_{\rm j}q_{\rm j/l}L_{46}P_{-12}^{-1}} \tag{5.75}$$

This can easily be matched with the parameter to the observed distances of lobes, which seem to cluster around ~ 300 kpc.

Of course there are quite a few processes which are able to decrease this size (e.g. mass entrainment). On the other hand, we see that in principle there is enough power stored in these jets to proceed far into the galaxy and even beyond. In the maximal case the agreement of theoretical interaction scale and observed lobe distances is reassuring, in the non-maximal case the situation is less clear as there are no observation to compare to. The jet is either so thin that it would 'cut' through the ISM and terminate far in the IGM (Eq. 5.74) or would be disrupted at the same distance as maximal jets (Eq. 5.75). For the inner jet cones we conclude that the energy density is always so high that no ISM is able to confine this part of the jet in any way and the assumption of a free jet is really justified. The whole picture may change if the jet interacts with the dense torus believed to be present in the center of active galaxies (see Chap. 7).

These estimates also demonstrate that for higher ambient energy densities of the interstellar medium, such as observed in the Galactic Center region, or in the starburst galaxy M82, and low power jets these scales may decrease to galactic sizes. Thus there may be sources where the jet terminates inside the galaxy. Our picture is also invalid as soon as we leave the static situation and deal with young sources which still have to drill through the ISM. Here one should use the ram pressure for $P_{\rm ext}$ and by increasing this value by a factor $\sim 10^4$ one possibly could explain some of the compact steep spectrum sources (Fanti et al. 1990). In this context it would be interesting to analyze the low frequency turnover seen in this sources in light of the low-energy cut-off discussed here.

5.3.7 Lobes

What is the luminosity of the jet at the termination point? In chapter we do not intend to develop a new model for the emission of lobes and hotspots (see Meisenheimer 1992 for a review), but at least we have to check if in principle the jet is capable to transport the right portion of energy and magnetic fields outward so that it

can supply extended structures like radio lobes of FR II type jets in radio loud quasars. The general numbers should not be completely incompatible with the usually inferred numbers for this regions.
We describe the terminal region as a cylinder where the jet is first slowed down close to its internal sound speed and then terminates in a strong shock. We assume that the magnetic field in the first part is enhanced by the slow-down and then compressed by the shock with a compression ratio $v_1/v_2 = 7$ for $\Gamma = 4/3$. The magnetic field given by

$$B^*_{\rm lobe} = 7 \cdot B_{\rm nozz} \frac{r_{\rm nozz}}{r_{\rm lobe}} \sqrt{\frac{\gamma_{\rm j}\beta_{\rm j}}{\beta_{\rm s}}} = 13\mu{\rm G}\, \sqrt{\frac{\beta_{\rm j} P_{-12}}{\gamma_{\rm j,5}\, u_3}} \tag{5.76}$$

is a bit lower than canonical values and independent of the accretion rate[3] and thus fairly constant, a finding which seems to be supported by observations (Meisenheimer 1992).
Radius and length of the cylindrical lobe are given approximately by the radius of the jet cone before the termination point. For the distance from the core we take the value $Z^*_{\rm free}$ from Eq.(5.74) where the pressure of the jet equals the pressure of the external medium. Following the above arguments the jet speed after the shock is then approximately 1/7 of the sound speed i.e.

$$\beta^*_{\rm lobe} \geq 1/\sqrt{3}/7 = 0.08, \tag{5.77}$$

close to estimated speeds in hotspots (Mesenheimer 1992). We obtain an optically thin spectrum for the whole observable frequency range

$$L^*_{\rm lobe} \quad = \quad 1.8 \cdot 10^{34}\, \frac{\rm erg}{\rm s\,Hz} \left(\frac{\rm GHz}{\nu}\right)^{0.5} \frac{\beta_{\rm j}^{1/4} P_{-12}^{1/4} x'_{\rm e,100} \left(q_{\rm j/l} L_{46}\right)^{3/2}}{\gamma_{\rm j,5}^{7/4}\, u_3^{3/4}} \tag{5.78}$$

where the amplification is only due to the compression of the plasma. As expected, the extended (lobe) emission dominates the total flux at and below GHz frequencies. At these low magnetic fields we need very high Lorentz factors of the order 10^4 to 10^6 to explain the observed spectrum in the GHz range and beyond. A low-frequency turn-over could be visible at low MHz frequencies. It is noteworthy that core and lobe emission show a comparable scaling with accretion rate and $\gamma_{\rm min,e}$. The core to lobe luminosity ratio

$$\frac{L_{\nu_{\rm s}}}{L_{\rm lobe}} = 0.07\, P_{-12}^{-1/4} \left(\frac{u_3 \sin i}{\beta_{\rm j} x'_{\rm e,100} \sqrt{\gamma_{\rm j,5} q_{\rm j/l} L_{46}}}\right)^{1/6} \left(\frac{\nu}{\rm GHz}\right)^{0.5}. \tag{5.79}$$

is fairly insensitive to parameter changes. The latter as an observed quantity is of course a strong function of the Doppler factor and the luminosities and frequencies compared in Eq.(5.79) are frequencies in the rest frame of the flow. As cores probably are boosted while hotspots radiate isotropically, comparing lobe flux and core flux at the same *observed* frequency may therefore be misleading. In quasars where as a consequence of the unification scheme the Doppler factors are assumed to be of order unity, the core/lobe ratios indeed scatter around the value given above (see Chapter 6) whereas in FR II radio galaxies they are more then a factor 10 lower.
Although the values for the lobes we get are sufficiently close to the real world – especially with regard to the giant jump over several orders of magnitudes from cores to lobes – one should be very cautious in their interpretation: our equations describe the lobes as homogenous bubbles radiating uniformly, but the observed morphology is very different. Usually the brightness profiles peak towards a central hotspot. One therefore should understand our values only as crude averages and magnetic field and pressure in the central regions will definitively be higher.
Finally we want to calculate the expected luminosity of a non-maximal jet if it terminates at the same distance as a maximal one (Eq. 5.75). Using the same assumptions as before we get

$$L_{\rm lobe} \quad = \quad 2 \cdot 10^{28}\, \frac{\rm erg}{\rm s\,Hz} \left(\frac{\rm GHz}{\nu}\right)^{0.5} \frac{\beta_{\rm j}^{1/4} P_{-12}^{1/4} f^{11/8} {x'_{\rm e}}^{19/8} \left(q_{\rm j/l} L_{46}\right)^{3/2}}{\gamma_{\rm j,5}^{7/4}\, u_3^{5/8}}. \tag{5.80}$$

This is a factor 1000 fainter than the already faint cores of such a jet. Therefore it seems almost impossible to ever detect radio emission from a putative lobe of non-maximal jets.

[3] This is only valid as long the jets all see the same external pressure. A low power jet may terminate much earlier in a region, where the external pressure is slightly different.

5.4 Inverse Compton scattering

5.4.1 Compton losses

Relativistic electrons in a jet produce not only synchrotron emission but will also upscatter photons via inverse Compton scattering. This leads to energy losses in the electron population and to the appearance of high energy emission in X-ray bands and beyond. Especially the scattering of synchrotron photons (synchrotron self Compton effect – SSC) is an inevitable effect. A general result is that energy losses due to sychrotron radiation $\dot{E}_{\rm sync}$ and due to Compton scattering $\dot{E}_{\rm comp}$ are proportional where the proportionality factor is given by the ratios of the energy densities of magnetic field $U_{\rm B}$ and photons $\dot{E}_{\rm ph}$ in the rest frame of the jet

$$\frac{\dot{E}_{\rm sync}}{\dot{E}_{\rm comp}}=\frac{U_{\rm B}}{U_{\rm ph}}. \tag{5.81}$$

For the SSC effect this translates into the condition that locally the energy density of synchrotron photons $dE_{\rm sync}/dV$ has to be substantially lower than the magnetic field energy density to inhibit strong Compton losses. This condition is automatically fulfilled at distances larger than $Z^*_{\rm min,1}$ (Eq. 5.65) – the distance where a large fraction of the internal energy is dissipated by synchrotron emission. At smaller scales the energy density in synchrotron photons would locally exceed the magnetic field energy density. SSC losses would increase this energy loss even further making acceleration of relativistic particles to the desired high energies at smaller scales impossible. On the other hand Compton scattering will give an additional factor <2 at $Z^*_{\rm min,1}$ so that at larger scales ($\geq 10^{17}$ cm) SSC losses, like sychrotron losses, are no longer important for the energy budget of the electron population.
Another source for photons is of course the disk with a photon energy density $U_{\rm ph,disk}=10^{46}\,{\rm erg/sec}\;L_{46}/(4\pi z^2 R_{\rm g}^2 c)$. Comparing this with $U_{\rm B,jet}=\gamma_{\rm j}B^2/8\pi$ and Eqs.(5.19&5.45) in the laboratoy frame we find that

$$\left(\frac{U_{\rm B,jet}}{U_{\rm ph,disk}}\right)^{*}=7.5\,q_{\rm j/l}\,\frac{\gamma_{\rm j,5}\beta_{\rm j}}{u_3} \tag{5.82}$$

is a constant ratio and of the same order as $q_{\rm j/l}$. For a non-maximal jet the ratio is a factor 2 higher. This result is intuitively clear as it reflects the basic assumptions of the model. The implications of a high energy density in disk photons are already know for a long time (Abramowicz & Piran 1980, Phinney 1982) and it provides a strong limit for the Lorentz factors in the jet close to the disk. From our simple equation we can conclude that, as long as $q_{\rm j/l}$ is in the range $0.1-1$, synchrotron losses and Compton losses due to disk photons are comparable and Eqs. (5.63&5.64) state that the maximum Lorentz factor permitted by synchrotron losses in the very vicinity of the disk is of the order 10. As Compton scattering of disk radiation will energetically be at least equally important, these limits will become even more stringent if one would consider both. The limit $\gamma\leq 10$ is of the order of the bulk Lorentz factor of the jet – which usually is negligible compared to the electron Lorentz factors – so that close to the disk roughly the same process will constrain the bulk jet velocity as well (see also Melia & Königl 1989) because internal energy flow and kinetic energy flow are comparable. And indeed one finds that jet Lorentz factors usually derived are not $\gg 10$.
The scattering of the disk photons will result in a considerable gamma-ray spectrum but which can be seen only if the inclination angle is low. This point was discussed in detail by Dermer & Schlickeiser (1993). Here, we only note that the anisotropy of the disk radiation and the presence of an additional isotropic radiation field (Broad Line Region) complicate the analysis considerably. The energy loss equation (3.21) of Dermer & Schlickeiser however is basically the same as our Equation (5.82) if one considers the magnetic field gradient.
In our argumentation we have translated these loss mechanisms always into limits for jet parameters. Of course, if there is a persistent acceleration mechanism (for relativistic particles or bulk motion) at work it could be possible to dissipate a large fraction of the jet energy already at sub-parsec scales leading to strong high energy emission. On the other hand this would also lead to a reduction of the radio emission below what is seen in radio loud quasars because most of the energy would be lost before the jet starts to radiate in radio wavelengths. Radio weak quasars on the other hand do not show any signs of strongly enhanced gamma-ray emission.

5.4.2 SSC emission

Compton scattering is not only important as an energy loss mechanism but the synchrotron self Compton effect also is of great interest for the interpretation of quasar X-ray spectra (Jones et al. 1974, Königl 1981, Ghisellini et al. 1985, Marscher 1983 & 1987) where it generally is believed to be the relevant emission mechanism. In this chapter we do not intend to present a thorough study of SSC emission as this was done in depth in the papers mentioned above. Most of these models, however, invoke a large number of parameters to fit observed spectra. Our model will be contained in one of the previous SSC models as we have not changed the basic ingredients of jet models relevant for calculating the SSC spectrum; it is only that we are much more constrained in our choice of parameters by incorporating the accretion disk into a consistent physical picture of the quasar (jet-)emission. Hence, we do not expect results unheard of before. Nevertheless we briefly want to discuss the expected SSC emission from our model to get a feeling where to place it within the known jet models.

For given electron and photon distributions (Eqs. 5.7&5.46), the emissivity of inverse Compton scattering of a synchrotron powerlaw spectrum with $p=2$ is roughly given by (Blumenthal & Gould 1970; Rybicky & Lightman 1979, Eq. 7.29a)

$$\epsilon_{\rm ssc} = 0.53\,\sigma_{\rm Th} c K_{\rm j} \epsilon_{\rm sync}(\nu_{\rm x}) r_{\rm j}\,(R_{\rm g}/c)\ln\left(\nu_{\rm r,1}/\nu_{\rm r,2}\right). \tag{5.83}$$

The limits of the powerlaw are given by $\nu_{\rm x,1}=4\gamma_{\rm e,min}^2 h\nu_{\rm r,1}$ and $\nu_{\rm x,2}=4\gamma_{\rm e,max}^2 h\nu_{\rm r,2}$ where we have assumed that the synchrotron spectrum is given by a powerlaw between the two radio frequencies $\nu_{\rm r,1}$ and $\nu_{\rm r,2}$. For simplicity we set $\gamma_{\rm e,max}=100\gamma_{\rm e,min}$. The frequency of the scattered X-ray spectrum is $\nu_{\rm x}$. We ignore the corrections introduced by the Klein-Nishina cross section and also note that for a powerlaw distribution of the seed photons Eq.(5.46) overestimates the flux by a factor ~ 3 near the cut-offs.

Because we deal with a scattering process, where the total emission is given by the product of photon energy density and electron energy density, Eq. (5.83) will have a steeper gradient along the jet than the synchrotron emissivity and because of the relatively flat local SSC spectrum the total X-ray spectrum of the jet will be dominated by a single region in the jet. This is in marked contrast to the radio spectrum which is produced by different regions. If we integrate Eq. (5.83) analogous to the synchrotron emission (Eq. 5.53) along the jet, we obtain

$$L^*_{\nu_{\rm x},\rm SSC}(z_{\rm x}) \;=\; 2.0\cdot 10^{28}\,\frac{\rm erg}{\rm s\,Hz}\,\frac{{x'_{\rm e,100}}^2 (q_{\rm j/l}L_{46})^{11/4}}{\beta_{\rm j}\gamma_{\rm j,5}^3 u_3^{3/4}}\left(\frac{R_{\rm g} z_{\rm x}}{10^{17}\rm cm}\right)^{-3/2}\left(\frac{h\nu_{\rm x}}{\rm keV}\right)^{-1/2} \tag{5.84}$$

where $z_{\rm x}R_{\rm g}$ is the distance in the jet where the SSC emission starts. For the integration we have considered only the locally produced $\nu^{-1/2}$ synchrotron emission as target photons for the relativistic electrons. Consideration of non-local cone emission will introduce an additional highly anisotropic, highly energetic, but much weaker photon flux component. As limits of the photon spectrum $\nu_{\rm r,1|2}$ we took the characteristic frequencies (Eq. 5.62&5.68) of the electrons with Lorentz factors $\gamma_{\rm e,min}$ and $\gamma_{\rm e,max}$ respectively. For this calculation the synchrotron-self absorption frequency is not appropriate because the absorption length scale $1/\kappa_{\rm sync}$ is much larger than the gyroradii of the scattering electrons; but we have shown before (Eq. 5.69) that self-absorption and characteristic frequency become equal if $\gamma_{\rm e,min}\sim 100$. The electrons in the jet might also see the low frequency $\nu^{1/3}$ spectrum below $\nu_{\rm r,1}$ which may extend the SSC spectrum to lower energies. Actually the situation is very complicated (see Sec. 5.4.3) as the plasma is optically thick to synchrotron radiation at some frequencies but can cool by Compton scattering. It is not clear how the real local spectrum and the real, stationary electron distribution will look like.

To predict the SSC spectrum from a jet model one probably would have to discuss the evolution of the electron distribution along the jet to find the exact position $z_{\rm x}$ of the SSC emission region. Fortunately, we have argued above that the energetic component of the electron distribution which starts at $\gamma_{\rm e,min}\simeq 100$ can not be produced very close to the disk as it would suffer strong losses from synchrotron radiation and Compton scattering of disk photons. We thus can take the distances $Z^*_{\rm min,1}$ or $Z^*_{\rm min,2}$ (Eqs. 5.65&5.66), where synchrotron losses become negligible and the 'loud' electron distribution can be produced, as a lower limit for $z_{\rm x}R_{\rm g}$. $Z^*_{\rm min,1}$ inserted in the SSC jet emission formula (Eq. 5.84) yields

$$L^*_{\nu_{\rm x},\rm SSC} \;\leq\; 6.2\cdot 10^{28}\,\frac{\rm erg}{\rm s\,Hz}\,\eta_{03}{x'_{\rm e}}^{1/4} u_3^{5/8}\gamma_{\rm j,5}^{1/4}\beta_{\rm j}^{-1/8}(q_{\rm j/l}L_{46})^{9/8}\left(\frac{h\nu_{\rm x}}{\rm keV}\right)^{-1/2}. \tag{5.85}$$

To get the observed fluxes one has to do the same transformation from the jet frame into the observers frame (Eqs. 5.54) as for the radio emission.

This equation has the nice property that the X-ray luminosity scales with the radio core luminosity as $L^*_{\nu_{\rm x},SSC}\propto {L^*_{\nu_{\rm s}}}^{0.79}$ which is in agreement with the observational finding that $L^*_{\nu_{\rm x},X-ray}\propto {L^*_{\nu_{\rm s},\rm radio}}^{0.71\pm0.7}$ (Kembhavi et al

1986). However, the ratio between X-ray and radio flux

$$\frac{L^*_{\nu_x,SSC}}{L^*_{\nu_s}} = 5 \cdot 10^{-5} \, \frac{\beta_j^{7/24} \gamma_{j,5}^{25/12} u_3^{29/24}}{{x'_{e,100}}^{7/12} (q_{j/l} L_{46})^{7/24}} \left(\frac{h\nu_x}{\text{keV}} \right)^{-1/2}. \tag{5.86}$$

is a bit too high. Requiring that the electron loss time is reduced sufficiently we go a bit further out along the jet to the distance $Z^*_{\rm min,2}$ and find

$$L^*_{\nu_x,\rm SSC} \quad \leq \quad 7.9 \cdot 10^{26} \, \frac{\text{erg}}{\text{s Hz}} \, \gamma_{\rm e,min}^{1/2} x_e^2 u_3^{3/4} \gamma_{j,5}^{-3/2} \beta_j^{-1/8} (q_{j/l} L_{46})^{5/4} \left(\frac{h\nu_x}{\text{keV}} \right)^{-1/2}. \tag{5.87}$$

The ratio

$$\frac{L^*_{\nu_x,SSC}}{L^*_{\nu_s}} \leq 6 \cdot 10^{-7} \, \frac{\beta_j^{1/6} \gamma_{j,5}^{1/3} u_3^{4/3} x_e^{7/6}}{\gamma_{e,100}^{1/3} (q_{j/l} L_{46})^{1/6}} \left(\frac{h\nu_x}{\text{keV}} \right)^{-1/2}. \tag{5.88}$$

is now compatible with the observed ratio of a few 10^{-7} (see Brunner et al. 1994) especially if one takes the transformations into the observers frame and a more precise SSC emissivity into account.
The peak of the SSC spectrum (i.e. the lower limit of the powerlaw) corresponding to the distance $Z^*_{\rm min,2}$ is

$$\nu_{x,1} \approx 0.01 \, (\text{keV}/h) \, \gamma_{e,100}^3 \beta_j \gamma_{j,5} u_3^{1/2} \sqrt{q_{j/l} L_{46}}, \tag{5.89}$$

which means that if $\gamma_{\rm min,e}$ is only a bit higher than 100, the spectrum observed in ROSAT bands may be below the turnover of the SSC spectrum (implied by the low energy cut-off in the energy distribution). As the turnover can be very soft this could explain the very flat, sometimes inverted, (flux) spectra seen in quasars. The spectrum may well extend beyond energies of a few MeV.

5.4.3 SSC emission from the nozzle

To conclude the discussion of SSC emission we want to mention one interesting aspect of our concept. We can exclude from energy loss arguments that the highly energetic electron distribution with $\gamma_{\rm e,min} \geq 100$, that makes a jet radio loud, is produced at the base of the jet. However, it might well be that there is a primary electron distribution of the plasma electrons which starts at low energies ($\gamma_{\rm e,min} \geq 1$, $x_e \leq 1$) and was already accelerated in the nozzle. Synchrotron emission of these electrons would be completely self-absorbed in the inner regions and be dominated by a secondary electron population ($\gamma_{\rm min,e} \geq 100$) further out. The situation in the nozzle could either lead to a "synchrotron boiler" (Ghisellini et al. 1988) where electrons are cooked up to a thermal energy distribution – providing another mechanism to produce a kind of low energy cut-off – or the electrons would cool by SSC emission and produce a visible signature. If we now apply our SSC formula to a cylindrical region of radius $r_{\rm nozz}$ and height $z_{\rm nozz}$ with our parameters for the nozzle and $\gamma_{\rm e,min} \approx 1$ we find

$$L^*_{\nu_x,nozz} \quad = \quad 7.7 \cdot 10^{27} \, \frac{\text{erg}}{\text{s Hz}} \, \frac{x'_e (q_{j/l} L_{46})^2}{\beta_j^{11/4} \gamma_{j,5}^{11/2} u_3^{3/4} m_8^{3/2}} \left(\frac{z_{\rm nozz}}{r_{\rm nozz}^{5/2}} \right) \left(\frac{h\nu_x}{\text{keV}} \right)^{-1/2}. \tag{5.90}$$

Although this depends strongly on the geometry of the nozzle and the Lorentz factor of the jet one should check if such a component could be present as well. Depending on the maximal Lorentz factor of these electrons ($\leq 10 - 100$) the spectrum could extend up to a few keV and would probably be steeper than $\nu^{-1/2}$ because of energy losses. If our notion of initially identical jets in radio loud and radio weak quasars, which later develop different electron populations, is correct such a signature would be common to radio loud and radio weak jets. The former would show an additional spectral component from the region at $Z^*_{\rm min,2}$, which could well dominate the nozzle emission, while the latter are likely to show only the steeper nozzle emission. Seen under small inclination angles radio weak quasars with SSC emission from the nozzle would exhibit strongly boosted X-ray emission and a still boosted but nevertheless much weaker radio emission. An application of this idea to the explanation of the large number of X-ray selected BL Lacs if compared to radio selected BL Lacs (Maraschi et al. 1992) seems possible but remains speculative at this point.

5.5 Disk and nozzle

After analyzing the jet and its energy demand we now want to discuss possible mechanisms for the jet production in relation to standard accretion disk theory (Novikov & Thorne 1973, Shakura & Sunyaev 1973). As said in the beginning, we have no idea, how the jet nozzle works and what process is responsible for the acceleration of the plasma. Still, we can give a crude description of the most likely scenario and test its feasibility.
The jet should start somewhere in the inner region of the disk between the innermost radius of the disk $r_{\rm in}$ and a point $r_{\rm nozz}$ furter out – the footpoint of the jet. What is a characteristic value for the dimensions of this part of the jet? Following standard accretion disk theory (Novikov & Thorne 1973) the inner radius of the disk will be given by the last marginal stable radius $r_{\rm ms}$ around the black hole. Following our symbiosis assumption a natural choice for the footpoint of the jet would be a radius close to the region where the inner boundary layer becomes important. Only in this region a disk really might require the presence of a jet. One guess would be to take the radius $r_{\max}$, where in standard accretion disk theory the radial run of the dissipation rate has its maximum. This point depends only on the Kerr parameter a (angular momentum) of the BH as shown in Fig. 5.5 The region between $r_{\max}$ and $r_{\rm in}$ is only poorly described by standard accretion disk theory and is partially unphysical (e.g. gas pressure and temperature decline rapidly to zero). Here magnetic processes and boundary effects of the black hole will dominate the disk – if a jet is produced this is the most likely place where it might happen. Moreover $r_{\max}$ is also the characteristic scale of all disk properties, as close to this value all radial functions of the disk peak.

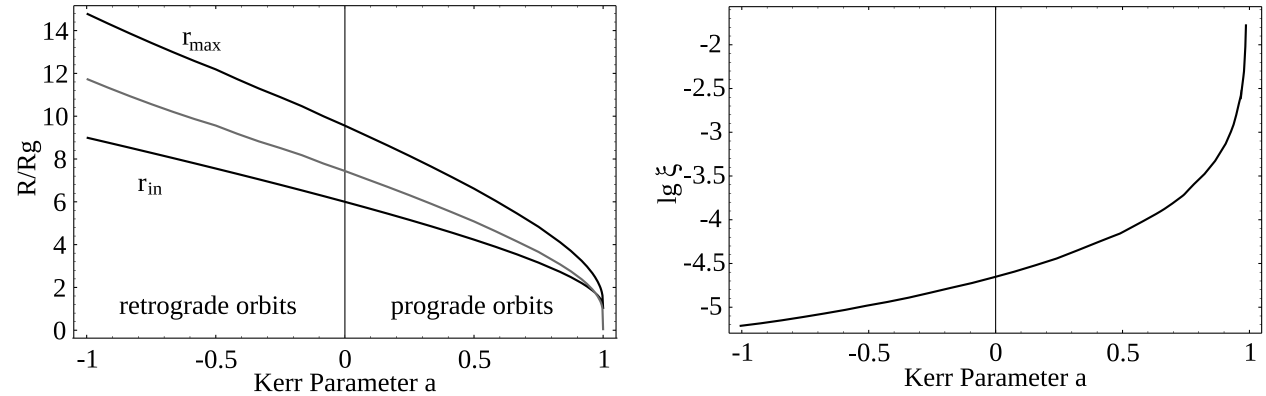

Figure 5.1: *Left:* The full lines give the inner disk radius and the radius $r_{\max}$ of the disk where the energy dissipation has its maximum as a function of the angular momentum $a \cdot R_{\rm g} M_\bullet c$ of the black hole. The grey line is an effective radius defined as $\sqrt{r_{\max}^2 - r_{\rm ms}^2}$ used to describe a filled cylinder with volume equivalent to a hollow cylinder with inner radius $r_{\max}$.
Right: The ratio ξ of the maximal radial magnetic energy flow in the disk compared to the magnetic energy flow in the jet for different Kerr parameters a and the parameters shown in Eq.(5.94).

To get a feeling for the possible feeding mechanism of the jet, we calculate the maximal radial magnetic energy flux permitted in a thin accretion disk. To have a disk, the magnetic pressure should always be smaller than the total gas pressure. An upper limit for the maximum energy density of the magnetic field is given by the maximum total gas pressure at $r_{\max}$. In the inner part of radiation pressure supported disks this is of the order $10^3 - 10^4$ Gauss and depends only on the mass of the central black hole and its angular momentum parameter a hidden in the relativistic correction factors $\mathcal{A}, \mathcal{B}$ and $\mathcal{E}$. The derivation of the equations for standard relativistic accretion disks and the definition of the correction factors can be found in Novikov & Thorne (1973) or Falcke (1992).

$$B_{\rm disk,max} = 1.2 \cdot 10^4\,{\rm Gauss}\,\frac{\sqrt{m_8}}{r^{3/4}}\frac{\mathcal{B}\sqrt{\mathcal{C}}}{\mathcal{A}} \tag{5.91}$$

This value of the magnetic field is close to the value required at the base of the maximal jet flow and for disks accreting close to the Eddington luminosity the scaling of magnetic fields in jet and disk would be the same. What is, however, more interesting is to compare the maximally possible radial magnetic energy flow through the accretion disk

$$Q_{\rm B,disk} \quad = \quad B_{\rm max}^2/(8\pi)\cdot V_{\rm r}\, 2\pi r_{\rm max}\, z_{\rm disk}\, R_{\rm g}^2 = 1.9\cdot 10^{46}\alpha \frac{\dot{m}_{\rm disk}^2}{m_8^3 r_{\rm max}^3}\frac{\mathcal{A}^2\mathcal{Q}^2}{\mathcal{B}^4\mathcal{D}^{3/2}\mathcal{E}}\frac{\rm erg}{\rm sec}, \tag{5.92}$$

where $z_{\rm disk}$ is the disk height, $V_{\rm r}$ the radial velocity of the acretion flow and α is the Shakura & Sunyaev (1973) disk parameter, with the magnetic energy flow in the maximal jet

$$Q_{\rm B,jet} = 1/6\cdot 10^{46}\,{\rm erg/sec}\; q_{\rm j/l} L_{46}/u_3 \tag{5.93}$$

yielding

$$\frac{Q_{\rm B,disk}}{Q_{\rm B,jet}} = \xi(a)\frac{\alpha u_3}{q_{\rm j} r_{\rm max}^3}\left(\frac{\dot{m}_{\rm disk}}{m_8}\right)^2. \tag{5.94}$$

The function $\xi(a)$ is evaluated and plotted in Fig. 5.5. We see that for radio loud jets the energy requirements are extremely high and exceed the maximum radial magnetic field flow allowed in the disk in all cases. Even though $q_{\rm j}$ may be as small as 0.1 and below, the limit is still very strong, as the viscosity parameter usually is assumed to be $\alpha \leq 0.1$ and in addition the accretion rate is already slightly above the Eddington limit. The Galactic Center source Sgr A* would lie more than 10 orders of magnitude above any allowed state. Thus radial accretion plus local amplification of the magnetic field seems very unlikely because it can not provide enough energy for the jet.

In this case we only have the choice to postulate that the magnetic field transported by the jet is produced locally at the footpoint of the jet in the disk by a mechanism closely related to the dissipation processes. *In its inner region the disk dissipates*[4] *into a jet and not into heat.* With our parametrization we have already ensured that this is energetically possible – even in Sgr A*. This is not a completely surprising result, because one finding of accretion disk theory is that the dominant energy transport is in the vertical (local dissipation of gravitational energy) and not in the radial direction. If the jet-energy is a high fraction of the total accretion power then only a process linked to the dissipation process itself can provide us with enough energy over a long time-scale.

Common speculations for the dissipation process in accretion disks often invoke magnetic fields. A combination of dynamo processes (creating magnetic field) and reconnection (destroying magnetic field) could be a possible mechanism. If close to the boundary layer the rate of the magnetic field produced exceeds the rate in which it can be destroyed then the only way to get rid of the energy and continue the accretion is to produce a jet.

To highlight the possible geometry of such a jet, we make a simple estimate. Suppose inside a certain disk radius $r_{\rm nozz}$ all the energy to be dissipated is diverted into the formation of a jet (calling it $Q_{\rm jet}$) and above $r_{\rm nozz}$ all energy is dissipated into heat producing the disk luminosity ($L_{\rm disk}$). To how large radii does one have to go, in order to obtain a certain value $Q_{\rm jet}/L_{\rm disk}$? We can easily answer this question by integrating the dissipation rate

$$D_0 = \frac{3GM_\bullet \dot{M}_{\rm disk}}{8\pi R_{\rm disk}^3}\frac{\mathcal{Q}}{\mathcal{B}\sqrt{\mathcal{C}}} = 6.8\cdot 10^{45}\frac{\dot{m}_{\rm disk}}{r_{\rm disk}^3}\frac{\mathcal{Q}}{\mathcal{B}\sqrt{\mathcal{C}}}\frac{\rm erg}{{\rm s}\, R_{\rm g}^2} \tag{5.95}$$

separately over the inner and outer region and defining

$$Q_{\rm jet} = \int_{r_{\rm in}}^{r_{\rm nozz}} 4\pi r_{\rm disk} D_0 R_{\rm g}^2 {\rm d}r_{\rm disk} \tag{5.96}$$

$$L_{\rm disk} = \int_{r_{\rm nozz}}^{\infty} 4\pi r_{\rm disk} D_0 R_{\rm g}^2 {\rm d}r_{\rm disk}. \tag{5.97}$$

In Fig. 5.5 we show the ratio $Q_{\rm jet}/L_{\rm disk}$ as a function of $r_{\rm nozz}$. We find that even for high jet powers where $q_{\rm j/l} \simeq 1$, the jet can still be produced in the very inner regions of the disk. Once again this is no surprise as it is well known that most energy of an accretion disk is released very close to the center.

Of course in a realistic case the situation will be somewhat different and it is more likely that also in the inner parts of the disk only a fraction of the dissipated energy is used for the jet and not 100%. Therefore the radii indicated above should be taken as lower limits for the jet size or as upper limits for $q_{\rm j/l}$.

Other pitfalls connected with this kind of argument are the unknown effects of the jet on the disk structure and the inner boundary conditions, which might change this picture quite a bit. There is also a possibility that

[4] The term *dissipation* is probably no longer appropriate in such a context.

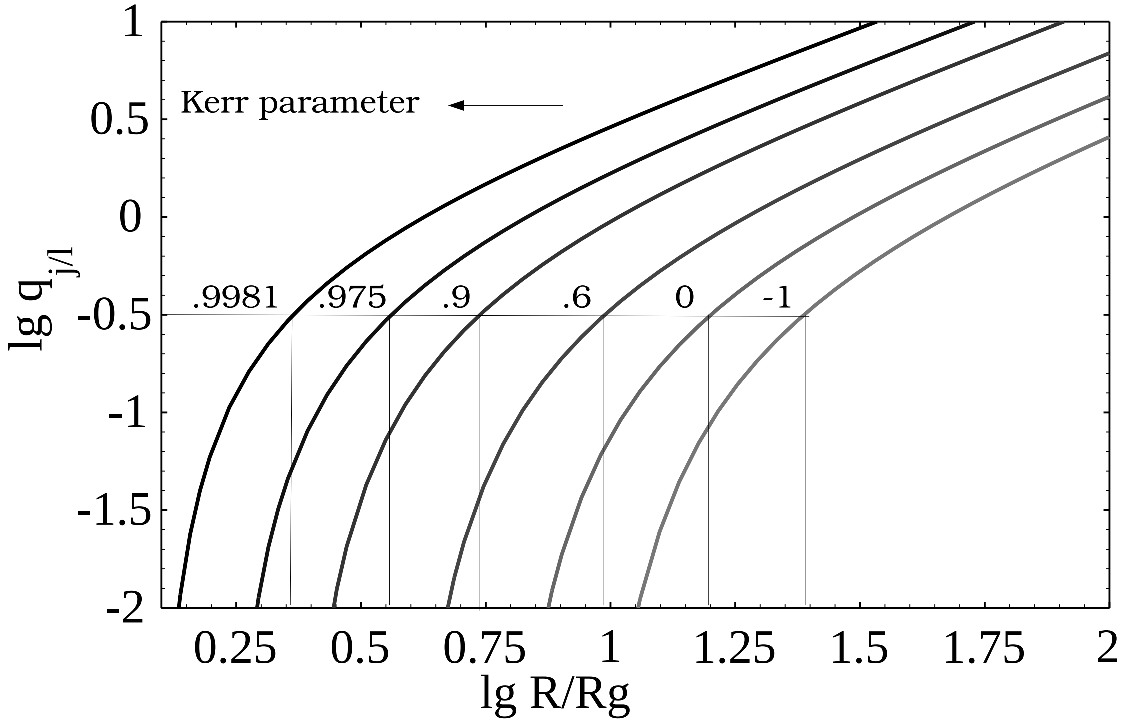

Figure 5.2: Upper limit for the value $Q_{\mathrm{jet}}/L_{\mathrm{disk}}$ for given widths r_{nozz} of the jet at the disk, assuming that the dissipation energy of the disk inside the radius r_{nozz} is diverted completely into the jet (Q_{jet}) and outside r_{nozz} is used to produce the disk luminosity (L_{disk}). If in a more realistic case the separation between disk and jet is less stringent than for a fixed value of $Q_{\mathrm{jet}}/L_{\mathrm{disk}}$, the jet width has to be larger than the value indicated here. The different curves are for different Kerr parameters a (angular momenta) of the central black hole (-1 means retrograde orbits).

the black hole itself can contribute to the jet production (Blandford & Znajek 1977) or the jet is produced in the very inner boundary layer. At the innermost orbits the particles still have a large amount of kinetic energy and it is unclear what fraction of this energy is swallowed by the black hole and what may escape. Despite this uncertainties it still seems justified to claim that for high ratios of $q_{\mathrm{j/l}}$ the jet probably is produced within a few gravitational radii from the black hole.

5.6 Discussion of the jet models

From our analysis in Sec. 5.2&5.3 we can interpret different combinations of parameters as conceptually different models for the radio emission of jets. They can be split in 5 different types as sketched in Figure 5.6. We have a subdivision between maximal jets, where the internal sound speed reaches its maximal value $\beta_{\mathrm{s}} \simeq 0.6c$ due to a large amount of magnetic energy and non-maximal jets with a sound speed substantially lower than $0.6c$. Moreover we may differentiate between radio loud and radio weak models according to their radiative efficiency or between high energy and low energy models according to their total energy. We label the individual models by a combination of letters representing their characteristic features (B=magnetic field, p=protons in equipartition, e=electrons in equipartition, Q=total energy flow).

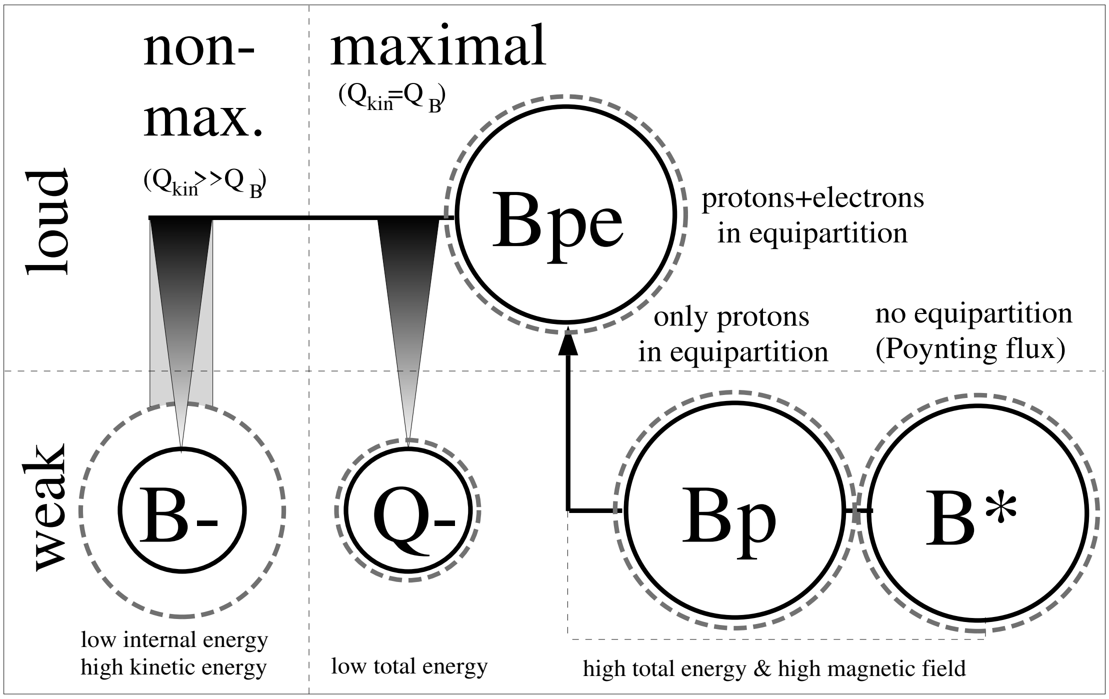

Figure 5.3: The family of jet models as described in the text. The vertical axis indicates jet luminosity relative to the disk luminosity. Large circles mean high energy content, dashed circles are used for kinetic energy and full circles for internal energy.

Bpe: The high magnetic field is in equilibrium with electrons and protons ($k_{\mathrm{p+e}} = 1$, $\mu_{\mathrm{p/e}} \geq 1$) requiring a minimum energy of the electrons of the order of 50 MeV ($\gamma_{\mathrm{min}} \simeq 100/x_{\mathrm{e}}$) or a large amount of $e^{\pm}$ pairs ($x_{\mathrm{e}} \geq 100$); maximal jet with high internal and kinetic energy flow ($q_{\mathrm{j/l}} \leq 1$), radio loud.

Bp: The high magnetic field is in equilibrium with protons only and electrons carry much less energy ($\mu_{\mathrm{p/e}} > 100$); maximal jet with high internal and kinetic energy flow ($q_{\mathrm{j/l}} \leq 1$). This is the case if all thermal electrons are accelerated ($\mathrm{x_e} \simeq 1$) but the powerlaw distribution starts at low energies ($\gamma_{\mathrm{min,e}} \simeq 1$), radio weak.

B*: The high magnetic field is in equilibrium with neither the electrons nor the protons (Poynting flux, $k_{\mathrm{e+p}} \leq 0.01$), maximal jet with high internal and kinetic energy flow ($q_{\mathrm{j/l}} \leq 1$), radio weak or even quiet.

Q-: Like **Bpe** but with less total energy (therefore on an absolute scale a smaller magnetic field) relative to the disk luminosity ($q_{\rm j/l} \ll 1$) and despite being radiatively very efficient classified as radio weak if compared to the disk.

B-: Non-maximal jet where the internal energy (magnetic field) is much lower than the kinetic energy ($\beta_{\rm s} \sim 0.03c$) but electrons and protons are still in equipartition like in the **Bpe** model. This is the case if all thermal electrons are accelerated ($x_{\rm e} \simeq 1$) into a powerlaw distribution starting at $\gamma_{\rm min,e} \simeq 1$. The jet is radio weak and relatively narrow.

Only model **Bpe** is able to explain the powerful radio emission of the cores of radio loud quasars. This represents the most efficient case, where all parameters are set to their extremes (e.g. high jet power $q_{\rm j/l} \simeq 1$ and high fraction of relativistic electrons $x_{\rm e} \simeq 1$) and implies 'total equipartition', namely $L_{\rm disk} \geq Q_{\rm jet} \geq Q_{\rm B} \simeq Q_{\rm e} \simeq Q_{\rm p}$ (the latter denotes the energy flow in relativisitic electrons and protons). Model **Bpe** is in principle also capable to explain distance and emission of extended lobes. One interesting consequence is that the relativistic electrons must have an unusual energy distribution peaking somewhere above 50 MeV inhibiting the usually assumed – but never observed – $\nu^{2.5}$ self-absorption spectrum at low frequencies. This quasi low-energy cut-off in the electron population was proposed first to avoid Faraday depolarization (Jones & O'Dell 1977, Wardle 1977) and later to explain the high kinetic powers of radio loud jets (Celotti & Fabian 1993). This minimum electron energy should be regarded as a lower limit as we only determine the product $x_{\rm e}\gamma_{\rm min,e}$. If only 10% of the electrons are relativistic then the minimum energy is a factor 10 higher. Perley et al. (1993) for example independently find a minimum Lorentz factor of $\gamma_{\rm e} \sim 450$ for the electrons by fitting spectral aging models to high sensitivity data of Cygnus A.

The finding by Rawlings & Saunders (1991) that the extended lobes of radio jets carry a kinetic energy comparable to the disk luminosity together with the similar finding here and by Celotti & Fabian (1993) to explain the core and hotspot emision fix the problem at both sides (from cores to lobes) and set a well constrained framework for the understanding of radio jets.

For radio weak quasars the situation is more ambiguous. The results of Chapter 6 and similar results by Miller et al. (1993) – the scaling of radio core emission with $L_{\rm disk}$ and the existence of possibly boosted radio weak objects – seem to support the idea that the radio emission in radio weak quasars is due to relativistic jets as well with velocities similar to radio loud jets. Principally all other models are equally well suitable to explain the compact radio emission of radio weak quasars (see chapter 6). All except one (**Q-**) of these (radio-weak) models still require a powerful jet with $Q_{\rm jet}/L_{\rm disk}$ of the order unity mainly due to the power stored in bulk motion, relativistic protons and magnetic field.

In our simple picture also radio loud jets have to start as quiet jets (low electron energies, high magnetic fields) in order to avoid strong synchrotron losses and establish themselves as radio-loud through reacceleration a few 10^{17-18} cm away from the central black hole. One could suggest that all jets start with similar properties and follow a simple evolutionary track as depicted in Figure 5.6. First one has a pure Poynting flux (**B***) converging towards an equilibrium state where protons are (shock) accelerated (**Bp**) and finally relativistic electrons are produced (**Bpe**). Our motive to include the second stage is the minimum energy of the electrons of $\sim 50/x_{\rm e}$ MeV which is close to the energy of electron/positron pairs produced in the pion decay and one could further suggest that all electrons are in fact secondary pairs made by relativistic protons (Biermann & Strittmatter 1987, Mannheim & Biermann 1989, Sikora et al. 1987, Biermann et al. 1994).

As this process should happen some 10^{17} cm from the origin it could be influenced by environmental effects (Chap. 7; Falcke, Gopal-Krishna, Biermann 1994), either because of the external photon flux or interactions of the jet with the ambient medium in a shear layer – a possible acceleration site (Ostrowski 1993). In radio quiet objects this mechanism simply might not be triggered towards an efficient production of secondaries and only the 'thermal' electrons are accelerated in the 'usual' way leaving the jet in the **Bp** or eben **B*** stage. Such a model avoids the need for a bimodal state of the disk to explain the difference between radio loud and radio weak jets (i.e. model **B-** and **Q-**).

An evolutionary scheme without secondaries (and without the second stage **Bp**) would be to assume that protons and plasma electrons both are accelerated by shock acceleration producing a flat electron spectrum ($p < 2$) until equipartition is reached at $\gamma \geq 100$ where the distribution steepens again to $p = 2$. The only problem is that the injection of electrons is still unsolved. It is much more difficult to accelerate electrons and protons and if there is a certain threshold energy needed to shock accelerate electrons then the deficiency in the electron injection alone would be the prime reason for the dichotomy between radio loud and radio weak jets.

Finally we note that another natural explanation for high electron energies could be thermalization of electrons at high temperatures. If the bulk of the electron population is heated to temperatures $T_e > 10^{11}$ K with an additional non-thermal power law tail we have exactly the distribution needed.
The different models for radio weak jets could be distinguishable by their extended emission. One could speculate that models **B*** and **Bp** terminate at similar distances as their radio loud counterparts and produce dim extended emission like in FR I and FR II galaxies only a factor > 100 fainter. Here the only problem is whether in these jets – with a deficiency in electron acceleration – enough high energy electrons with $\gamma_e > 10^4$ are present to produce observable radio emission in the lobes. More promising therefore seem to be X-ray observations where one looks for interactions (shock fronts) with the IGM/ISM. Recent ROSAT observations of NGC 1275 (Böhringer et al. 1993) reveal such a X-ray emission and pressure equilibrium demands an proton/electron ratio of ~ 100 as in the **Bp** model.
The non-maximal jets (model **B-**) on the other hand would be virtually invisible as they either pierce through the ISM with a thin pencil-like beam or terminate further inside without noticeable radio emission leaving us only with the core emission. Finally, the low power jets (**Q-**) are likely to appear as miniature editions of FR I galaxies on the kpc-scale.

5.7 Summary

In this chapter we have applied the simple Blandford & Königl (1979) model for the flat spectrum core emission of radio jets in light of a link between the jet and an accretion disk as the source for energy and matter: we just demand mass and energy conservation of the jet-disk system as a whole. By expressing all quantities, including the plasma parameters, in terms of dimensionless parameters to be scaled with the disk accretion rate we describe the jet as an conically expanding relativistic plasma ($\Gamma = 4/3$) confined only by its own bulk velocity. This allows us to calculate a variety of observational features for different models. Despite many simplifications our jet model can describe the overall appearance of radio jets including sizes and fluxes of cores and lobes surprisingly well. Via the SSC effect this model naturlly accounts also for the X-ray emission of radio loud and possibly also for radio weak quasars. A schematic broadband spectrum is presented in Figure 5.
The models are limited by the requirement that the jet should not expel more matter and energy than is provided by the accretion disk. This limit strongly restricts models for radio-loud jets. At a disk (UV-bump) luminosity of 10^{46} erg/sec and core luminosities of $2\cdot 10^{31} - 6\cdot 10^{32}$ erg/sec/Hz for radio-loud quasars only the most efficient case is able to produce the observed radio emission. This implies a high total jet power ($Q_{\rm jet} \leq L_{\rm disk}$) where a large fraction of the total power is in magnetic fields and relativistic particles ('total equipartition'). Given the limited number of electrons from the accretion flow one needs an electron distribution starting at high energies (≥ 50 MeV) and/or a large number of pairs. Heavy jet models with initial bulk velocities $\gamma_j \gg 10$ seem to be excluded – the kinetic energy demand would be too high. We note that these conclusions are fairly independent of the details of any jet or disk model.
An electron distribution with low energy cut-off (> 50 MeV) is a natural consequence of hadronic interactions and the pion decay, so that the electrons might in fact be secondary pairs. The high amount of energy required to be channeled from the disk into the jet suggest that the jet is produced in the very inner parts of an accretion disk by a mechanism somehow linked to the dissipation process.
The models described in this chapter are also able to explain the compact radio emission in radio weak quasars. In contrast to their radio-loud counterparts the parameters for radio-weak quasars can not be constrained much stronger and therefore the deeper reason for the dichotomy of quasars in radio-loud and radio-weak is still unclear (but see Chap. 7). Yet, the possible answers can be reduced to two possibilities. Firstly, there might be a bimodality in the disk structure, especially at the boundary layer between disk and black hole (e.g. caused by different angular momenta of the black hole) leading to different power supplies for the jet (Models **Bpe** $\leftrightarrow$ **Q-** or **B-**) and secondly, the bimodality could be caused by different acceleration mechanisms for the electrons (Models **Bpe** $\leftrightarrow$ **Bp** or **B***). The latter appears to be the most elegant way as it requires only changes in the microphysics which could easily be caused by environmental effects, e.g. by interactions between the jet and the ambient medium in a shear layer. This speculation then would suggest that jets in radio-loud quasars produce the dominant electron/positron population as secondary particles through hadronic interactions, whereas jets in radio-weak quasars contain only the directly accelerated population of electrons.
The model can be used without modification of the parameters to calculate the SSC emission from radio jets. The expected spectrum around one keV can be either flat ($\nu^{-0.5}$) or even inverted and is dominated by emission from one region at a distance of $\sim 10^{18}$ cm. SSC emission from the nozzle region could produce another spectral

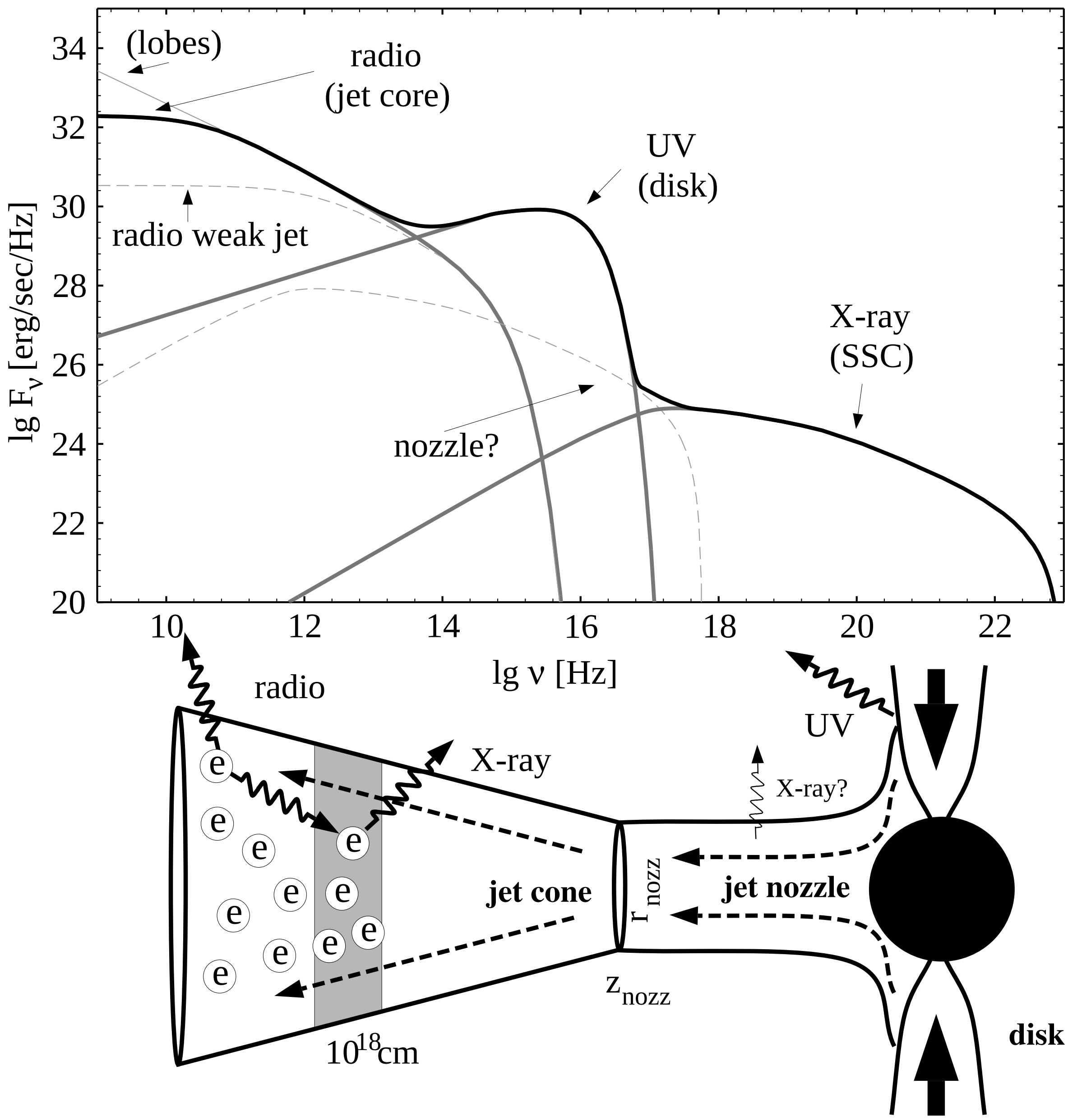

Figure 5.4: Schematic broadband spectrum of a maximal jet-disk combination with three basic components (grey lines): core radio spectrum, disk spectrum, SSC spectrum. The full line gives the composite spectrum. Possible SSC emission from primary electrons in the nozzle is given by a dashed line as is the radio spectrum of a radio weak quasar. For comparison we also inserted a $\nu^{-.75}$ lobe spectrum (thin grey line). The core radio spectrum extends up to the frequency $\nu^*_{\rm max,2}$ corresponding to the spatial scale $Z^*_{\rm max,2}$ where it is assumed to steepen to ν^{-1}; a general cut-off at $10^{14.5}$ Hz is also assumed (Biermann & Strittmatter 1987). As parameters we took $m_8 = 1$, $L_{46} = 1$, $q_{\rm j/l} = 0.3$, $\gamma_{\rm min,e} = 300$, $\gamma_{\rm j} = 5$ $\ln(\gamma_{{\rm max},e}/\gamma_{{\rm min},e}) = 3.5$, $x_{\rm e} = 0.3$, for the nozzle (and the radio weak jet) we have assumed $\gamma_{\rm min,e} = 3$, $r_{\rm nozz} = 10$ and $z_{\rm nozz} = 100$. The inclination angle is $i = 35°$ so that the Doppler factor is close to unity. Boosted quasars will show a higher level of radio and X-ray emission in comparison to the blue bump. The disk spectrum for a maximally rotating Kerr hole ($a = 0.9981$) is taken from Falcke et al. (1993a).
Below the spectrum we sketched the general idea of the model where a part of the accretion disk flow is expelled by a jet. At a scale of $> 10^{17}$ cm a highly energetic electron population is produced being responsible for X-ray and radio emission in radio loud quasars. We suggest that the same picture holds for radio weak quasar but without the additional electron population.

component which might be of interest for X-ray emission of radio weak quasars and X-ray selected BL Lacs.

5.8 Appendix

Here we give some of the equations derived in the main body of this chapter for a different electron powerlaw index of $p = 2.5$.

Eqs. (5.51,5.52)

$$z_{\rm ssa} = 10\,{\rm pc}\,\frac{{x'_{\rm e}}^{2/13}\beta_{\rm j}^{9/26}\left(q_{\rm j/l}L_{46}\right)^{17/26}}{\sqrt{u_3}\gamma_{\rm j,5}^{4/13}f^{2/13}\sin i^{4/13}}\frac{\rm GHz}{\nu_{\rm s,obs}/\mathcal{D}} \tag{5.98}$$

$$z^*_{\rm ssa} = 35\,{\rm pc}\,\frac{{x'_{\rm e,100}}^{4/13}\beta_{\rm j}^{9/26}\left(q_{\rm j/l}L_{46}\right)^{17/26}}{\gamma_{\rm j,5}^{4/13}u_3^{9/26}\sin i^{4/13}}\frac{\rm GHz}{\nu_{\rm s,obs}/\mathcal{D}} \tag{5.99}$$

Eqs. (5.55,5.56)

$$L_{\nu_{\rm s,obs}} = 5.8\cdot 10^{30}\,\frac{\rm erg}{\rm s\,Hz}\,\left(q_{\rm j/l}L_{46}\right)^{18/13}\frac{\mathcal{D}^{29/13}\sin i_{\rm obs}^{3/13}f^{3/26}{x'_{\rm e}}^{23/26}}{\sqrt{u_3}\gamma_{\rm j,5}^{23/13}\beta_{\rm j}^{5/13}} \tag{5.100}$$

$$L^*_{\nu_{\rm s,obs}} = 8.7\cdot 10^{32}\,\frac{\rm erg}{\rm s\,Hz}\,\left(q_{\rm j/l}L_{46}\right)^{18/13}\frac{\mathcal{D}^{29/13}\sin i_{\rm obs}^{3/13}{x'_{\rm e,100}}^{10/13}}{\gamma_{\rm j,5}^{23/13}\beta_{\rm j}^{5/13}u_3^{8/13}} \tag{5.101}$$

Eqs. (5.57,5.58)

$$T_{\rm b} = 3.7\cdot 10^{10}\,{\rm K}\left(\frac{x'_{\rm e}q_{\rm j/l}L_{46}}{f\gamma_{\rm j,5}^2\beta_{\rm j}}\right)^{1/13}\sin i^{11/13} \tag{5.102}$$

$$T^*_{\rm b} = 6.6\cdot 10^{10}\,{\rm K}\left(\frac{{x'_{\rm e,100}}^2u_3q_{\rm j/l}L_{46}}{\gamma_{\rm j,5}^2\beta_{\rm j}}\right)^{1/13}\sin i^{11/13} \tag{5.103}$$

Eqs. (5.60,5.61)

$$\nu_{\rm max} = 1.9\cdot 10^{12}\,{\rm Hz}\;\eta_{03}\frac{f^{23/26}\gamma_{\rm j,5}^{23/13}\beta_{\rm j}^{5/13}{x'_{\rm e}}^{3/26}u_3^{3/2}}{\left(q_{\rm j/l}L_{46}\right)^{5/13}\sin i^{3/13}} \tag{5.104}$$

$$\nu^*_{\rm max} = 1.9\cdot 10^{12}\,{\rm Hz}\;\eta_{03}\frac{\gamma_{\rm j,5}^{23/13}\beta_{\rm j}^{5/13}u_3^{8/13}}{{x'_{\rm e,100}}^{10/13}\left(q_{\rm j/l}L_{46}\right)^{5/13}\sin i^{3/13}} \tag{5.105}$$

Eq. (5.69)

$$\frac{\nu^*_{\rm s}}{\nu^*_{\rm c}} = 1.6\;\gamma_{\rm min,100}^{-20/13}\left(\frac{q_{\rm j/l}L_{46}x_{\rm e}^2}{\beta_{\rm j}\gamma_{\rm j,5}^2\sin i^2}\right)^{2/13} \tag{5.106}$$

Eq. (5.78)

$$L^*_{\rm lobe} = 3.3\cdot 10^{33}\,\frac{\rm erg}{\rm s\,Hz}\,\left(\frac{\rm GHz}{\nu}\right)^{0.75}\frac{\beta_{\rm j}^{3/8}P_{-12}^{3/8}x'_{\rm e,100}\left(q_{\rm j/l}L_{46}\right)^{3/2}}{\gamma_{\rm j,5}^{15/8}u_3^{7/8}} \tag{5.107}$$

Chapter 6

Jet and disk in quasars

6.1 Introduction

The release of energy due to the infall in the gravitational potential is thought to be responsible for the enormous energy output seen in the optical to ultraviolet (UV) regime of quasars which is able to dominate the total emission of the underlying galaxy. While for individual sources the spectral energy distribution (SED) may be dominated by other contributions, e.g. gamma-rays, the UV emission in general is assumed to be the major channel for the energy release of quasars. High gamma-ray fluxes occur only in a few sources and are obviously boosted. However, recently it was pointed out that relativistic jets in radio loud quasars may be another important channel for expelling high amounts of energy from the central engine (Rawlings & Saunders 1991, hereafter RS91; Falcke, Mannheim, Biermann 1993b, hereafter FMB; Falcke & Biermann 1994b; Celotti & Fabian 1993; Chap. 5). Although the radiative contribution of jets to the SED in the radio and gamma regime is small, their energy flow in bulk relativistic motion, magnetic energy and relativistic particles may be a substantial fraction of the total energy released from the central engine. Such a powerful jet suggests that this kind of outflow is directly coupled to the accretion process in the very vicinity of the black hole – where most of the energy is released – having a strong impact on the disk itself.

In the previous chapter we studied the standard theory for the radio emission of compact radio cores produced by radio jets in quasars considering especially the link between the jet and an accretion disk as the basic source for energy and matter. This is simply the Blandford & Königl (1979) theory plus energy and mass conservation in the jet-disk sytem.

A necessary consequence of this jet-disk link is the scaling of the emission from the compact radio core in galactic nuclei with the disk luminosity radiated in the UV where the scaling is not necessarily linear. Another conclusion was that for a given accretion rate, the core emission of radio loud jets is already close to the maximum efficiency, and brighter emission is only possible by relativistic boosting. Moreover we introduced the concept of a jet-disk symbiosis and started with the basic ansatz that jets are necessary partners of accretion disks around compact objects, and not fortuitous by-products of disks. In this context the question was raised whether the radio emission of radio-weak quasars could be explained by the same kind of relativistic jets as well but being less efficient in accelerating electrons. The predictions are that UV and radio core emission should be strongly correlated in radio weak quasars as well and that boosted radio weak jets with enhanced variable radio emission are found. Obviously the dichotomy of the radio emission depends on the host galaxy (radio loud: elliptical, radio weak: spiral) and it is hard to understand why the basic parameters of jet flows should differ as a function of the host galay when the production happens very close to the black hole where the effects of the host galaxy should be negligible.

In this chapter we now want to test some of these ideas and see if they contradict available observational data. If there is indeed a fundamental process linking accretion process and jet production, it should be insensitive to the environment and the host galaxy except for the bimodality between radio loud and radio weak quasars. As was shown in Chapter 5, the pressure of the inner jet cone dominates every plausible pressure of the interstellar medium (ISM), hence the radio core emission should be a good indicator of the state of the jet. Further out the environmental impact of the host galaxy will inevitably change the appearance of jet and disk and modify the emission region. Therefore one has to select carefully the observational data for each object and must make sure that the observed radiation reflects the physical situation of the center and not of the outer region. To achieve this we can follow two extreme strategies, one is to have very high spatial resolution of the observation, e.g. by looking at nearby galactic nuclei. The other extreme would be to look at very luminous objects, where the central engine outshines all other sources in a galaxy like in quasars. Here we will follow the second approach and leave the nearby nuclei – with the exception of our Galactic Center, which is discussed in Falcke et al. (1993a&b) and Falcke & Biermann (1994a&c), to future work. All other galactic nuclei, e.g. Seyfert and radio galaxies, are very difficult to use as test candidates as it requires an elaborated scheme to separate the contributions from different parts of the galaxy (e.g. starburst and AGN).

We build on the work by Miller et al. (1993a, MSR) who investigated the optically selected PG bright quasar sample and found correlations between radio and optical line emission luminosities of radio weak quasars. We now extend this analysis by enlarging the sample with more sources and comparing it with FR II galaxies in light of current unification theories. Moreover we try to determine the disk luminosities of the quasars in our sample as accurately as possible from existing data to compare disk and radio power in absolute terms. This allows us to constrain strongly the parameter range of radio jets and also to give a solid classification for the radio properties of quasars.

In Sec. 6.2 of this chapter we introduce our sample and present our method to estimate the disk luminosity of the individual quasars and calibrate different other indicators to obtain empirical conversion factors, e.g. from line luminosities to disk luminosities. Section 6.3 describes the available radio data and Sec. 6.4 the UV-radio diagram and its implication for the different classes of quasars. In Sec. 6.5 we discuss the constraints this diagram imposes on jet parameters like Lorentz factor and total jet power. Section 6.5 discusses the implication of our estimated parameters for the unification of quasars and FR II radio galaxies and provides a simple method to estimate the hidden disk luminosity in radio galaxies.

For consistency with some of the observational papers we use $q_0 = 0.5$ and $H_0 = 50$ km/sec/Mpc as cosmological parameters.

6.2 The disk luminosity

6.2.1 The quasar sample

Most quasars show a fairly homogenous SED with two important features – an infrared (IR) and an UV-bump (Edelson and Malkan 1986; Sanders et al. 1989). While the IR seems to be due to thermal emission from dust, the dominant UV bump probably reflects the spectrum of an accretion disk around a supermassive black hole (Malkan & Sargent 1982, Malkan 1983). We now estimate this UV-bump luminosity – which hereafter we will also refer to as 'disk luminosity' ($L_{\rm disk}$) – as accurately as possible.

We take the observationally best studied sample of quasars namely the PG sample of bright quasars (Schmidt & Green 1983) with redshift $z < 0.5$ and a multitude of published observational data. Boroson & Green (1992, hereafter BG92) presented a thorough study of the emission line properties of this sample while Sun & Malkan (1989, hereafter SM89) determined the disk luminosity from fitting disk spectra to optical and UV data for a sample containing many of the PG quasars. Kellermann et al. (1989, hereafter KSSSG) and Miller et al. (1993, hereafter MSR) published radio data obtained with the VLA. MSR also tried to classify the morphological structure of the radio maps and studied correlation between radio fluxes and emission lines.

The low redshift PG sample ($z < 0.5$), we will mainly base our arguments on is given in Tab. 1 and contains 87 sources (#1-#87). We did not include the recent addition PG 1001+054 (not included in BG92) or PG 0119+229, since it shows no broad lines. In addition we will consider an extended sample which cannot be used for statistical purposes, as it is not complete and has no clear defined selection criterion. Sources #88-#113 in Tab. 1 are the PG quasars with $z > 0.5$ which were measured by KSSSG as well but not discussed by MRS. It is known that there are some selection effects for the PG sample with $z > 0.5$ (Wampler & Ponz 1985). Beyond the whole PG sample we have the sources #113-#131 which (with the exception of 1821+643) were included in the sample of SM89 and had disk fits available.

Besides quasars we will briefly discuss a sample of Fanaroff-Riley type II (FR II) radio galaxies with $z < 0.5$ which are selected from the 3C-based sample of Laing et al. (1983) and were investigated further by Rawlings et al. (1989) and RS91. It contains 39 FR II galaxies and is listed in Tab. 2 (#132-#170). The Laing et al. (1983) sample is 96% complete to a flux density limit of 10 Jy at 178 Mhz for sources smaller than 10' and can be considered as fairly unbiased because unboosted lobe emission dominates the whole spectrum at this low frequency. We also included in our figures the seven FR I radio galxies used in RS91 and treated them just the same way as the FR II sample. The references for the core fluxes are those used in RS91.

6.2.2 The UV-bump

SM89 fitted accretion disk spectra to a variety of quasars. They collected IR to UV data and used standard relativistic thin accretion disk models including the effects of rotating black holes for their fits of the 'UV-bump'. They also assumed an underlying powerlaw, which is no longer state of the art, but does not invalidate neither their nor our conclusions although it might introduce a slight and systematic shift in the luminosities.

From this detailed study we will mainly use one important number, namely the *fitted* luminosity of the UV-bump. This number may differ from the total integrated luminosity of the measured UV-bump, as the fitted spectra do not always interpolate the observed data perfectly well, indicating the presence of other components not explained by and not necessarily linked to a standard accretion disk. In column 6 ('UV') of Tab. 1 we listed this number from SM89 for all objects, where we assumed an average inclination angle of 40° for the disks.

Unfortunately, SM89 did not include all PG quasars in their investigation. We therefore looked into the archived data of this study and found a few more PG quasars with yet unpublished data. Using exactly the same method as SM89, we were able to obtain some more disk fits for these objects and included them in our list. The new sources are indicated with an asterisk in Table 1: PG 0007+106, 0232−042, 0906+484, PG 1352+011, PG 1411+442, PG 1501+106, PG 1522+101, PG 1613+658, PG 1634+706, 2041−105, and PG 2302+029. We will refer to the whole sample of sources having UV-bump fits available (published or unpublished) simply as the SM89 sample.

In the following we assume that the luminosities derived from the UV-bump fits are indeed the 'disk luminosity'. Because the PG sample is so well studied we now have a large number of quasars having both disk fits and several other luminosity indicators available, such as emission line luminosities and monochromatic continuum luminosities. Because it is generally accepted that these emission lines are produced through ionization by the central source we can now compare UV-bump fits and emission lines to get empirical conversion factors. For sources where no fits are available we can later use these empirical conversion factors to get estimates for the disk luminosity from monochromatic luminosities and emission line luminosities alone. For an individual source there may be discrepancies between the 'real' value and the estimated disk luminosity but in a statistical sense we will get reliable numbers.

Of course this works only if the correlations are almost linear and depend on one single parameter, namely the disk luminosity. That this is indeed the case is not obvious a priori. For example, an emission line responds not only to an increase in the luminosity, but also to a frequency shift of the exciting spectrum which in accretion theory happens due to a shift in mass and accretion rate of the black hole. Fortunately, the dependence of the shift in frequency ($T_{\rm eff}$) is weak – $T_{\rm eff} \propto \dot{M}_{disk}^{.25}/M_\bullet^{.5}$ while $L_{\rm disk} \propto \dot{M}_{\rm disk}$. If all quasars radiate close to the Eddington luminosity, then we have $T_{\rm eff} \propto M_\bullet^{-.25}$. In this sense the PG quasars are relatively uniform – they have comparable effective temperatures of several 10^4 Kelvin – and the expected relations should be fairly independent of the black hole mass, but one has to remember that they will become inadequate if $T_{\rm eff}$ changes appreciably. Some Seyfert galaxies for example show a bump which peaks somewhere in the soft X-ray regime and they should deviate systematically from such correlations. The reason for the uniformity of the PG quasars is obvious as they were selected as objects with a blue excess.

6.2.3 Monochromatic continuum luminosities

A very good indicator for the disk luminosity are the absolute blue magnitude $M_{\rm b}$ – which is not surprising as it was used to select the quasars in this sample – and the absolute magnitude $M_{\rm v}$ of the continuum at $\lambda5500$ of the core spectrum in the restframe of the quasar (BG92). We corrected the magnitudes given in BG92 for the different value $q_0 = 0.5$ we use here. The flux F_ν at $\nu = 5.45 \cdot 10^{14}$ Hz ($\lambda = 5500$Å) can be converted to $M_{\rm v}$ by the formula

$$M_{\rm v} = -0.4\,\lg\left(\frac{F_\nu}{3.53\cdot10^{-20}\mathrm{erg/sec/Hz}}\right) + 5\,\lg\left(\frac{D_{l_\nu}}{\mathrm{pc}}\right) - 5 \tag{6.1}$$

and the monochromatic luminosity distance for our set of cosmological parameters as a function of redshift is

$$D_{l_\nu} = 1.2\cdot10^{10}\,\mathrm{pc}\,\left(\sqrt{1+z}-1\right) \tag{6.2}$$

.

In Fig. 6.2.4a+b we plotted the relation between these colors and the disk luminosity from SM89. In all cases the slope of the correlation between color and luminosity found with linear regression is within the errors 0.4 –

compatible with a direct proportionality between the luminosity in the blue color and the total luminosity. We therefore fixed the slope at that value and determined the intersection to a high precision.

$$\lg L_{\mathrm{disk}}\,(M_{\mathrm{b}}) = (-0.4 M_{\mathrm{b}} + 35.90 \pm 0.04) \pm 0.29 \tag{6.3}$$
$$\lg L_{\mathrm{disk}}\,(M_{\mathrm{v}}) = (-0.4 M_{\mathrm{v}} + 35.70 \pm 0.04) \pm 0.24. \tag{6.4}$$

The first error gives the uncertainty in the determination of the offset and the second error the standard deviation of the sample. As one can see in Fig. 6.2.4 the correlation indeed is very tight and at least for our sample we can expect that the disk luminosities inferred from M_{b} with help of Eq.(6.3) will be close to the fitted one. Two sources (PG 1008+133 & PG 1206+459) showed extremely high deviations (more than a factor 10 above the median deviation) in the $L_{\mathrm{disk}} - M_{\mathrm{b}}$ correlation and we excluded them from this fit.

6.2.4 Emission lines

Another often used indicator for the disk luminosity is the luminosity of the emission lines seen in the optical spectrum. BG92 published a list of spectral data of all low redshift PG quasars and once again we use the SM89 quasars as calibrators for the disk luminosity. In Fig. 6.2.4c-e we show the relations between the luminosity in the emission lines (He II, Hβ and O III) and the luminosity of the disk. We make use of the definition in BG92 where for an emission line EL with equivalence width EW the absolute magnitude of this line is given by $M_{[\mathrm{EL}]} = M_{\mathrm{v}} - 2.5\lg(\mathrm{EW[EL]})$.

$$\lg L_{\mathrm{disk}}\,(M_{\mathrm{HeII}}) = (-0.4 M_{\mathrm{HeII}} + 34.93 \pm 0.08) \pm 0.41 \tag{6.5}$$
$$\lg L_{\mathrm{disk}}\,(M_{\mathrm{H}\beta}) = (-0.4 M_{\mathrm{H}\beta} + 33.70 \pm 0.04) \pm 0.22 \tag{6.6}$$
$$\lg L_{\mathrm{disk}}\,(M_{\mathrm{OIII}}) = (-0.4 M_{\mathrm{OIII}} + 34.45 \pm 0.08) \pm 0.44 \tag{6.7}$$

For our use it may be simpler but equally effective to use a total luminosity of all lines and calculate a total emission line luminosity. By adding all lines together

$$M_{\mathrm{lines}} = M_{\mathrm{v}} - 2.5\lg\left(EW[\mathrm{HeII}] + EW[\mathrm{H}\beta] + EW[\mathrm{O\ III}]\right) \tag{6.8}$$

we get (Fig. 6.2.4f)

$$\lg L_{\mathrm{disk}}\,(M_{\mathrm{lines}}) = (-0.4 M_{\mathrm{lines}} + 33.60 \pm 0.04) \pm 0.24. \tag{6.9}$$

We found that the exact combination of the different line luminosities (i.e. by using certain weights) did not really influence the result. The good correlations we find show that we are not subject to severe orientation dependent effects as far as the determination of the disk luminosity is concerned although some of the line luminosities usually are considered isotropic and others not. Nevertheless, H_β shows the tightest correlation and due to its large luminosity it dominates $L_{\mathrm{disk}}\,(M_{\mathrm{lines}})$. Comparing the correlation of the emission lines with the M_{v} correlation one can see that there is neither a tremendous gain nor a big loss in accuracy by using emission line fluxes instead of continuum fluxes. Both methods therefore seem to be equally suitable to estimate the disk luminosity.

6.2.5 Average disk luminosity

For the comparison between disk luminosity and radio emission we make use of an average disk luminosity obtained by taking the geometrical mean from all available luminosity indicators (UV-bump, M_{v}, M_{b}, M_{lines}) of each source where the disk fit was weighted by a factor three. As seen in Tab. 1 in most quasars all methods to derive the disk luminosity yield similar results with a scattering smaller than a few tenth in the log. This confirms our optimism in anticipating that the luminosity indicators are fairly reliable in a statistical sense. Only a few exceptional cases show deviations larger than a factor three. These quasars, indicated with daggers in Tab. 1, have shown large continuum variations between their photographic measurement in the PG survey and the later spectrophotometry used for disk model fitting.

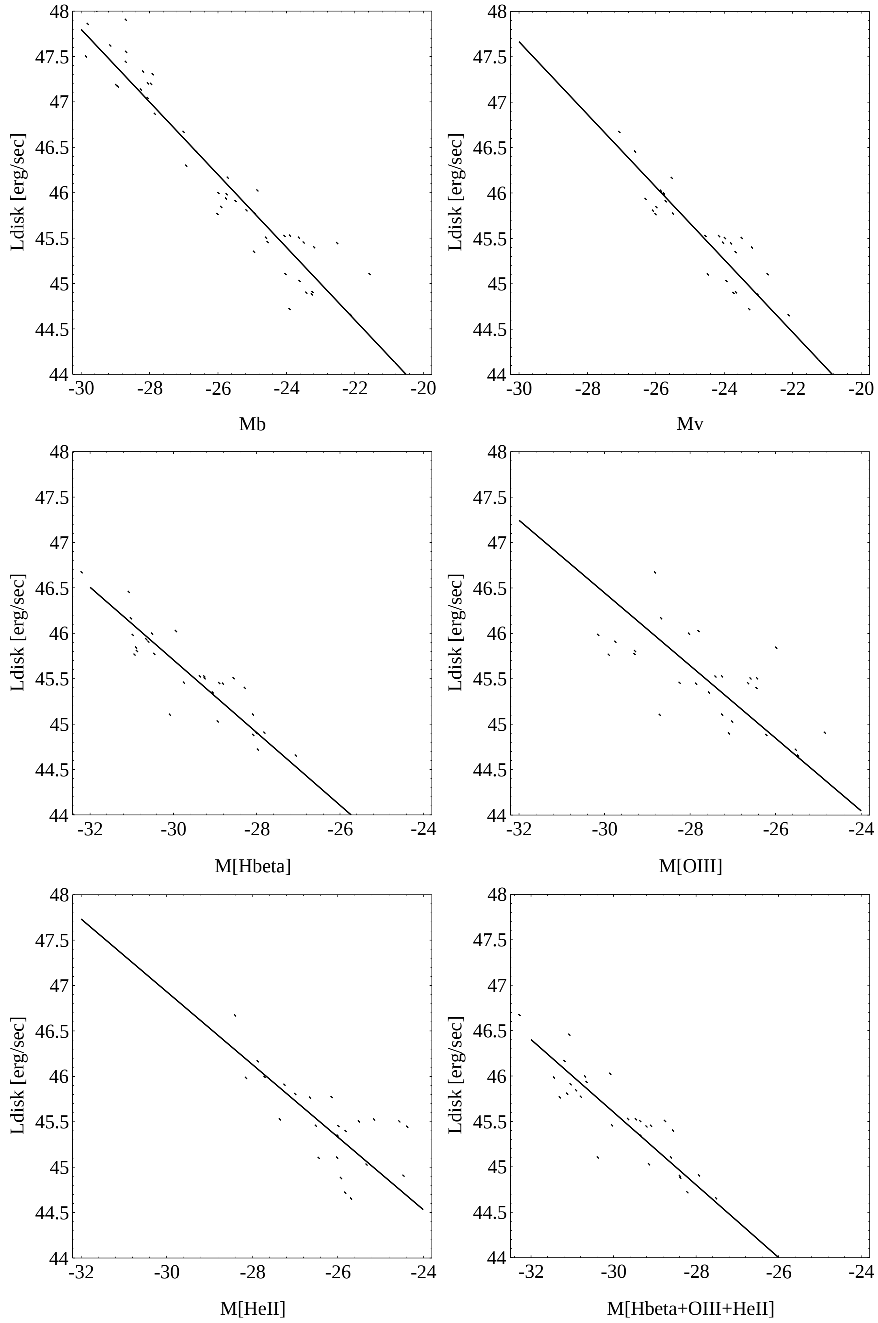

Figure 6.1: Relation between the disk luminosity obtained from accretion disk fits to the UV-bump by SM89 and (a) the blue magnitude, (b) the visual magnitude and (c-e) emission line luminosities (He II, H β, O III and (f) sum of all lines $M_{\rm lines}$) measured by Boroson & Green (1992) for PG quasars (from top left to bottom right).

6.3 The radio data

From observations we know that the radio spectrum of the compact cores in radio loud quasars is completely flat and independent of the frequency. This is readily explained as the overlap of several synchrotron spectra in a gradually declining magnetic field along the jet cone (Blandford & Königl 1979). Generally the observation of a core at one frequency is equivalent with probing the jet at a certain distance from the origin but as long as the spectrum is basically flat, one frequency tells as much as any other. In contrast to a black body spectrum the shift of the flat non-thermal spectrum in frequency would hardly make any difference in the observed flux. Hence we do not need to integrate the whole spectrum to get a radio luminosity in analogy to the UV luminosity. For our comparison the monochromatic luminosity at one radio frequency alone is adequate. In Chapter 5 we speculated that the compact radio emission in radio weak quasars might be due to jets as well following the same basic principles as their radio loud counterparts. Consequently this and the following considerations may apply to radio weak quasars as well. Unfortunately only a few radio weak cores have been measured reliably at high radio frequencies. Antonucci & Barvainis (1988) for example find a high frequency excess in 9 out of 17 objects at $\lambda 2$ cm which could be attributed to a flat spectrum core.
The radio data we took are primarily from Miller et al. (1993) for the low redshift PG sample and from Kellermann et al. (1989) for the rest of the sample; they give a list of VLA fluxes at 5 GHz. 79 out of 89 quasars were detected and in 50 cases a central compact core was also clearly seen. We added, if available, photometric radio data from the NASA Extragalactic Database (NED), from a catalog of Markarian galxies available at the MPIfR (Sherwood, W. p.c.) and other available literature (see Notes). We then transformed the spectra into the rest frame of the quasars and fitted powerlaws or 3rd order polynomials for each source. In cases where multiple photometric datapoints were available at one frequency and the source was variable, we took the geometric mean of the data. For sources without spectral informations we assumed an spectral index of $\alpha = -0.5$. Thus we obtained fairly accurate total fluxes at 5 GHz in the rest frame of the quasar. For the core fluxes we did the same, however, as we have data only at one frequency we simply assumed a flat spectrum ($\alpha = 0$) to get the 5 GHz rest frame flux. In cases where the extended emission swamped the core or the quasar was not detected at all, we took the limits for the core fluxes or the limits of the total fluxes respectively. For a few sources among those not belonging to the PG sample where no core fluxes were available, we either estimated an upper limit for a flat spectrum core flux from the steep spectrum at high frequencies or assumed a median value of the core/lobe ratio of 0.72 found from our (radio weak) sample for Mkn 132, Mkn 679 and 1821+643 and of 0.15 (from double lobed sources) for 3C 110 and 3C 232. We classified the radio spectra, which are shown in Fig. 6.2, according to their slope at 5 GHz in the rest frame as flat (F) or steep (S) and also marked obviously variable (V) spectra. These classifications and the monochromatic core luminosities are presented in Tab. 1 as well.

6.4 The UV-radio correlation

In Fig. 6.4a we plotted the 5 GHz radio core flux versus the average disk luminosity determined from all available luminosity indicators for each quasar (Sec. 6.2.5). Figure 2b gives a 'finding chart', where the same plot is repeated but using our ID numbers from Tab. 1 instead of symbols to easily locate the position of individual sources.
In Fig. 6.4a radio cores of radio weak quasars are represented by black dots and an arrow indicates upper limits for the detection of a compact core. In the few cases where the quasar was not detected at all, we used only the arrow. Radio weak quasars showing extended emission are marked with a grey shade around the black dot. Cores of radio loud quasars are given by open circles and boxes. Point sources are marked with a 'P', double lobed sources with a 'D' and flat spectrum sources by a grey filling.
To complete the picture, we also added the sources belonging to the extended sample in grey. Those sources belonging to the high redshift PG quasar sample are marked with an additional cross.
The quasars fall in at least three distinct categories: radio weak, radio loud lobe dominated quasars (LDQ) and flat spectrum core dominated quasars (CDQ). The distinction between radio-loud and radio-weak holds not only for the total flux, but also for the core fluxes. The separation needs to be understood relative to the disk luminosities. There may be radio weak quasars with a high accretion rate which have more luminous radio cores than some low accreting radio loud objects. Considering only the core fluxes, CDQ are the brightest population. This diagram confirms the well accepted idea that flat spectrum CDQ are the consequence of orientation effects in conjunction with relativistic boosting, which leads to a strong enhancement of the core flux relative to the

					$L_{\rm disk}$				Radio at 5 GHz		
#	name	z	class	$L_{\rm disk}$	UV	Mb	Mv	lines	νL_ν	$f_{\rm c}$(%)	α
1	0003+158,PG	0.45	L,S,D	46.3	-	46.3	46.4	46.4	42.5	30.	-0.8
2	0003+199,PG,Mkn335	0.025	Q,P	44.6	44.6	44.7	44.5	44.6	38.6	80.	-0.29
3	0007+106,PG,IIIZw2*	0.089	L,F,V	45.3	45.4	44.8	45.2	45.3	41.6	50.	0.62
4	0026+129,PG	0.142	Q,E	45.6	-	45.7	45.5	45.5	<39.2	<7.	-0.5
5	0043+039,PG	0.384	Q	46.	45.8	46.2	46.1	46.	39.7	90.	-0.5
6	0049+171,PG	0.064	Q,P	44.6	-	44.6	44.4	44.7	38.7	100.	-0.5
7	0050+124,PG,IZW1	0.06	Q,P	45.	44.9	45.2	45.2	45.	39.1	70.	-0.77
8	0052+251,PG	0.155	Q,E	45.5	-	45.6	45.5	45.5	39.3	60.	-0.5
9	0157+001,PG,MK1014	0.164	Q,P	45.6	-	45.7	45.5	45.6	40.4	60.	-1.
10	0804+761,PG	0.1	Q,E	45.4	-	45.3	45.4	45.5	39.3	40.	-0.5
11	0838+770,PG	0.131	Q	45.	-	45.1	45.	45.	<38.7	<90.	-0.5
12	0844+349,PG,TON 951	0.064	Q	44.9	44.7	45.4	45.	44.9	<38.4	<100.	-0.5
13	0921+525,PG	0.035	Q,E	44.3	-	44.2	44.2	44.5	38.7	50.	-0.87
14	0923+129,PG,Mrk705	0.029	Q,P	44.3	-	44.3	44.3	44.3	38.7	30.	-0.5
15	0923+201,PG	0.19	Q	45.5	-	45.5	45.5	45.6	<39.2	<90.	-0.5
16	0934+013,PG	0.05	Q,E	44.3	-	44.2	44.2	44.4	<38.2	<60.	-0.5
17	0947+396,PG	0.206	Q	45.4	-	45.4	45.3	45.4	<39.3	<90.	-0.5
18	0953+414,PG	0.239	Q,E	46.1	46.2	46.1	45.9	46.1	<39.2	<9.	-0.5
19	1001+054,PG	0.161	Q,E	45.3	-	45.3	45.3	45.2	<39.4	<60.	-0.5
20	1004+130,PG,4C13.41	0.24	L,S,D	45.9	46.	45.7	46.	45.6	41.4	5.	-1.
21	1011−040,PG	0.058	Q,P	44.6	-	44.7	44.7	44.5	38.3	100.	-0.5
22	1012+008,PG	0.185	Q,P	45.6	-	45.5	45.5	45.6	39.7	70.	-0.5
23	1022+519,PG	0.045	Q,E	44.2	-	44.2	44.2	44.1	38.	60.	-0.5
24	1048−090,PG	0.344	L,S,D	46.	-	46.	45.9	45.9	42.	7.	-0.88
25	1048+342,PG	0.167	Q	45.5	-	45.5	45.2	45.6	<39.	<90.	-0.5
26	1049−005,PG	0.357	Q,E	46.1	-	46.1	46.	46.1	<39.7	<60.	-0.5
27	1100+772,PG,3C249.1	0.313	L,S,D	45.9	45.9	46.	46.	46.	42.	8.	-0.99
28	1103−006,PG	0.425	L,S,D	46.	46.	46.2	46.	45.9	42.4	20.	-0.55
29	1114+445,PG	0.144	Q	45.1	45.	45.3	45.2	45.3	<38.9	<90.	-0.5
30	1115+407,PG	0.154	Q	45.1	-	45.3	45.1	44.9	<39.	<70.	-0.5
31	1116+215,PG	0.177	Q,P	45.9	-	45.8	45.9	46.1	40.	70.	-0.5
32	1119+120,PG	0.049	Q,E	44.7	-	44.9	44.7	44.5	<38.2	<30.	-0.5
33	1121+422,PG	0.234	Q	45.5	-	45.7	45.4	45.4	<39.2	<90.	-0.5
34	1126−041,PG	0.06	Q	44.8	-	44.7	44.9	44.9	<38.4	<70.	-0.5
35	1149−110,PG	0.049	Q,E	44.5	-	44.6	44.4	44.6	38.8	50.	-0.5
36	1151+117,PG	0.176	Q	45.5	45.5	45.6	45.3	45.3	<39.	<90.	-0.5
37	1202+281,PG,GQ COM	0.165	Q,P	45.4	45.3	45.8	45.1	45.3	39.5	80.	-0.5
38	1211+143,PG	0.085	Q	45.5	45.5	45.4	45.5	45.5	<39.	<60.	-0.5
39	1216+069,PG	0.334	Q,P	46.1	-	46.1	46.1	46.1	40.8	90.	-0.5
40	1226+023,PG,3C273	0.158	L,F,V	46.6	46.7	46.6	46.5	46.5	44.1	70.	-0.085
41	1229+204,PG,TON 1542	0.064	Q	44.9	44.9	45.1	44.9	45.	<38.7	<90.	-0.5
42	1244+026,PG	0.048	Q,E	44.1	44.	44.3	44.4	44.2	38.4	60.	-0.5
43	1259+593,PG	0.472	Q	46.4	46.5	46.5	46.3	46.	<39.8	<80.	-0.5

Table 6.1: The quasar sample used in this chapter. (#1-#87) is the PG sample with $z < 0.5$, (#88-#113) is the rest of the PG sample, and (#114-#131) are quasars from the sample of SM89. Col. (1): ID number, Col (2): IAU name; Col. (3): redshift, Col. (4): radio classification Q – radio weak, L – radio loud, S – steep spectrum ($\alpha \leq -0.5$), F – flat spectrum ($\alpha > -0.5$), V – variable spectrum, P – point source, E - extended emission, D – (double) lobe structure; Col. (5): average disk luminosity; Col. (6-9): disk luminosities derived from (6) UV-bump fits, (7) $M_{\rm b}$, (8) continuum at $\lambda 5500$ rest frame, (9) emission lines; Col. (10): radio luminosity of the core at 5 GHz rest frame, Col. (11): ratio of core flux to total flux at 5 GHz rest frame in per cent; Col. (12): differential spectral index of fitted spectrum at 5 GHz rest frame. An asterisk (*) marks quasars with yet unpublished accretion disk fits and a dagger (†) marks the 2 quasars with strong variations between $M_{\rm b}$ and the UV.

					$L_{\rm disk}$				Radio at 5 GHz		
#	name	z	class	$L_{\rm disk}$	UV	Mb	Mv	lines	νL_ν	$f_{\rm c}$(%)	α
44	1302−102,PG	0.286	L,F,V	46.1	-	46.2	46.3	45.8	43.	100.	0.035
45	1307+085,PG	0.155	Q	45.5	45.5	45.6	45.5	45.6	39.2	90.	-0.5
46	1309+355,PG	0.184	L,F,P	45.5	-	45.7	45.5	45.3	41.4	90.	-0.5
47	1310−108,PG	0.035	Q	44.3	-	44.2	44.2	44.5	<37.8	<100.	-0.5
48	1322+659,PG	0.168	Q	45.4	-	45.5	45.3	45.3	39.	90.	-0.5
49	1341+258,PG	0.087	Q	44.8	-	44.8	44.7	44.8	<38.5	<100.	-0.5
50	1351+236,PG	0.055	Q,E	44.4	-	44.5	44.6	44.1	<38.2	<40.	-0.5
51	1351+640,PG	0.087	L,F,P	45.2	-	45.1	45.3	45.2	40.7	100.	-0.14
52	1352+183,PG	0.158	Q	45.4	-	45.5	45.3	45.4	39.	90.	-0.5
53	1354+213,PG	0.3	Q	45.5	-	46.	45.3	45.2	<39.3	<90.	-0.5
54	1402+261,PG	0.164	Q,P	45.4	-	45.6	45.4	45.3	39.3	70.	-0.5
55	1404+226,PG	0.098	Q,P	44.8	-	45.	44.8	44.5	39.1	70.	-0.5
56	1411+442,PG*	0.089	Q,P	45.3	45.5	45.3	45.1	45.1	38.9	90.	-0.5
57	1415+451,PG	0.114	Q	45.	-	45.2	45.	44.7	<38.8	<70.	-0.5
58	1416−129,PG	0.129	Q,E	45.3	45.1	45.4	45.5	45.8	39.4	20.	-0.5
59	1425+267,PG,TON 202	0.366	L,S,D	45.9	45.8	46.2	46.1	46.1	41.9	20.	-0.75
60	1426+015,PG,Mkn1383	0.086	Q,P	45.3	45.4	45.2	45.3	45.2	39.2	90.	-0.5
61	1427+480,PG	0.221	Q	45.4	-	45.5	45.2	45.5	<39.2	<90.	-0.5
62	1435−067,PG	0.129	Q	45.4	-	45.4	45.3	45.4	<38.8	<90.	-0.5
63	1440+356,PG	0.077	Q,E	45.	-	45.1	45.	44.9	38.8	40.	-1.1
64	1444+406,PG	0.267	Q	45.7	-	45.8	45.7	45.5	<39.2	<90.	-0.5
65	1448+273,PG	0.065	Q,P	44.9	-	45.	45.	44.7	38.9	100.	-0.5
66	1501+106,PG,Mkn841*	0.036	Q,E	44.9	45.1	44.4	44.8	45.	38.3	50.	-0.81
67	1512+370,PG,4C37.43	0.371	L,S,D	46.	46.	46.1	46.	46.2	42.1	20.	-0.71
68	1519+226,PG	0.137	Q,E	45.2	-	45.2	45.1	45.1	<39.1	<30.	-0.5
69	1534+580,PG	0.03	Q,P	44.3	-	44.1	44.2	44.5	38.5	90.	-0.81
70	1535+547,PG	0.038	Q	44.5	-	44.4	44.5	44.6	38.1	100.	-0.5
71	1543+489,PG	0.4	Q,P	45.9	-	46.1	45.8	45.7	40.2	60.	-0.5
72	1545+210,PG,3C323.2	0.266	L,S,D	45.8	45.8	45.8	45.9	45.9	41.7	4.	-0.98
73	1552+085,PG	0.119	Q,E	45.	44.9	45.1	45.1	44.8	<38.9	<40.	-0.5
74	1612+261,PG	0.131	Q,E	45.3	-	45.2	45.2	45.6	39.7	30.	-0.5
75	1613+658,PG*	0.129	Q,E	45.5	45.5	45.4	45.3	45.4	39.3	30.	-0.45
76	1617+175,PG	0.114	Q,E	45.2	-	45.3	45.2	45.3	<39.4	<50.	-0.5
77	1626+554,PG	0.133	Q,P	45.1	-	45.1	45.1	45.2	38.7	90.	-0.5
78	1700+518,PG	0.292	Q,E	46.	45.9	46.1	46.2	45.9	40.4	20.	-0.86
79	1704+608,PG	0.371	L,S,D	46.	-	46.1	46.2	45.8	41.1	0.5	-0.84
80	2112+059,PG	0.466	Q,P	46.5	-	46.5	46.5	46.5	40.3	70.	-0.5
81	2130+099,PG,IIZw 136	0.062	Q,E	45.2	45.4	45.1	44.9	45.	38.9	40.	-0.51
82	2209+184,PG	0.07	L,F,V	44.9	-	44.7	44.9	45.	41.2	100.	0.15
83	2214+139,PG	0.067	Q	45.	-	45.	45.	45.	38.3	100.	-0.5
84	2233+134,PG	0.325	Q,E	45.7	-	46.	45.7	45.5	39.7	60.	-0.5
85	2251+113,PG	0.323	L,S,D	45.9	45.8	45.9	46.1	46.1	41.5	3.	-0.72
86	2304+042,PG	0.042	Q,P	44.4	-	44.4	44.3	44.4	38.4	100.	-0.5
87	2308+098,PG	0.432	L,S,D	46.1	-	46.2	46.1	46.1	42.2	20.	-0.89

(Table 6.1 continued.)

#	name	z	class	$L_{\rm disk}$	$L_{\rm disk}$ UV	Mb	Mv	lines	Radio at 5 GHz νL_ν	f_c(%)	α
88	0044+030,PG	0.624	L,S	46.6	-	46.6	-	-	42.1	40.	-0.82
89	0117+213,PG	1.49	Q	47.3	-	47.3	-	-	<40.5	<60.	-0.5
90	0946+301,PG	1.22	Q	47.1	47.1	47.1	-	-	<40.1	<70.	-0.5
91	1008+133,PG†	1.29	Q	47.3	47.7	46.3	-	-	<40.2	<70.	-0.5
92	1115+080,PG	1.72	Q	47.6	47.6	47.5	-	-	<40.3	<60.	-0.5
93	1138+040,PG	1.88	Q	47.4	47.4	-	-	-	<40.3	<60.	-0.5
94	1148+549,PG	0.969	Q	47.1	47.2	47.	-	-	40.7	40.	-0.5
95	1206+459,PG†	1.16	Q	45.6	45.1	47.2	-	-	<40.	<70.	-0.5
96	1222+228,PG,TON 1530	2.05	Q	47.6	47.5	47.7	-	-	42.2	50.	-0.5
97	1241+176,PG	1.27	L,S/F	47.2	47.2	47.4	-	-	43.2	50.	-0.50
98	1247+267,PG	2.04	Q	47.8	47.9	47.7	-	-	41.1	40.	-0.5
99	1248+401,PG	1.03	Q	46.9	46.9	46.9	-	-	<40.1	<70.	-0.5
100	1254+047,PG	1.02	Q	47.	47.	47.	-	-	40.3	70.	-0.5
101	1329+412,PG	1.93	Q	47.2	47.2	47.4	-	-	40.5	50.	-0.5
102	1333+176,PG	0.554	L,?	46.6	-	46.6	-	-	41.9	80.	-0.5
103	1338+416,PG	1.22	Q	47.3	47.3	47.1	-	-	<40.1	<70.	-0.5
104	1352+011,PG*	1.12	Q	47.2	47.2	47.	-	-	<40.1	<70.	-0.5
105	1407+265,PG	0.944	Q	47.	47.	-	-	-	41.3	30.	-0.5
106	1522+101,PG*	1.32	Q	47.7	47.9	47.3	-	-	40.4	60.	-0.5
107	1538+477,PG	0.77	L,S	46.7	-	46.7	-	-	42.1	40.	-1.
108	1630+377,PG	1.47	Q	47.4	47.4	47.3	-	-	<40.2	<60.	-0.5
109	1634+706,PG*	1.33	Q	47.9	48.	47.6	-	-	41.1	40.	-0.5
110	1715+53,PG	1.92	Q	47.4	-	47.4	-	-	40.9	40.	-0.5
111	1718+481,PG	1.08	L	47.5	47.5	47.3	-	-	42.9	50.	-0.5
112	2302+029,PG*	1.04	Q	47.2	47.3	47.	-	-	40.2	40.	-0.5
113	2344+092,PG	0.677	L,F,V	46.4	46.3	46.6	-	-	43.8	90.	-0.18
114	0134+329,3C48	0.367	L,S	45.7	45.7	-	-	-	41.8	0.5	-0.94
115	0232−042,PHL1377*	1.44	L,S	47.3	47.3	-	-	-	43.4	20.	-0.77
116	0237−233,PKS,MRC	2.22	L,S	47.5	47.5	-	-	-	<43.8	<5.	-0.15
117	0405−123,PKS	0.574	L,S	46.9	46.9	-	-	-	<43.2	<20.	-0.52
118	0414−060,3C110	0.781	L,S	46.6	46.6	-	-	-	42.4	10.	-0.75
119	0710+458,Mkn376	0.056	Q	44.4	44.4	-	-	-	39.	7.	-0.5
120	0742+318,4C31.30	0.462	L,F	46.3	46.3	-	-	-	43.3	70.	-0.23
121	0906+484*	0.118	Q	45.6	45.6	-	-	-	<39.	<90.	-0.5
122	0955+326,3C232	0.533	L,S	46.2	46.2	-	-	-	42.6	10.	-0.53
123	0958+551,Mkn132	1.76	Q	47.7	47.7	-	-	-	<41.5	<40.	-0.5
124	1011+250,Ton490	1.63	L,F,V	46.9	46.9	-	-	-	43.9	100.	0.34
125	1317+277,Ton153	1.02	Q	47.	47.	-	-	-	<40.6	<70.	-0.5
126	1421+330,Mkn679	1.9	Q	47.4	47.4	-	-	-	41.7	40.	-0.5
127	1435+638	2.06	L,F,V	47.4	47.4	-	-	-	44.2	80.	-0.17
128	1821+643,E1821+643	0.297	Q	46.6	-	46.6	-	-	41.1	60.	-0.5
129	2041−109,Mkn509*	0.036	Q	45.	45.	-	-	-	38.8	30.	-0.56
130	2145+067,4C06.69	0.99	L,F,V	46.8	46.8	-	-	-	44.4	100.	0.029
131	2201+315,4C31.63	0.297	L,F,V	46.1	46.1	-	-	-	43.4	80.	-0.025

(Table 6.1 continued. The extended sample.)

			$L_{\rm disk}$	Radio at 5 GHz		
#	name	z	$f \cdot Q_{\rm jet}$	νL_ν(core)	$f_{\rm c}$(%)	α
132	0106+13,3C33	0.059	45.4	40.2	0.6	-0.77
133	0109+49,3C35.0	0.066	44.4	40.1	2.	-0.85
134	0152+28,3C42	0.395	45.9	40.8	0.2	-0.9
135	0132+37,3C46	0.437	46.	40.7	0.5	-0.87
136	0221+27,3C67	0.31	45.7	42.6	20.	-0.91
137	0307+16,3C79	0.255	46.2	41.	0.6	-1.1
138	0356+10,3C98	0.03	44.9	39.2	0.2	-0.65
139	0410+11,3C109	0.307	46.2	42.6	20.	-0.7
140	0411+14,4C14.11	0.38	45.1	41.7	2.	-0.77
141	0433+29,3C123	0.218	46.1	42.	0.6	-0.89
142	0702+74,3C173.1	0.292	46.1	41.	0.7	-1.
143	0734+80,3C184.1	0.119	45.	40.2	0.5	-1.3
144	0745+56,4C+56.16	0.035	44.4	40.7	20.	-0.98
145	0802+24,3C192	0.06	45.1	39.6	0.3	-0.69
146	0917+45,3C219	0.174	45.4	41.4	2.	-1.
147	0936+36,3C223	0.137	45.7	40.5	0.7	-0.78
148	0944+73,4C73.08	0.058	45.2	40.1	3.	-0.93
149	0958+29,3C234	0.185	45.9	41.9	7.	-0.97
150	1003+35,3C236	0.099	45.4	41.9	30.	-0.65
151	1030+35,3C244.1	0.428	45.9	<40.2	<0.04	-1.
152	1308+27,3C284	0.239	45.4	40.5	0.7	-1.1
153	1319+42,3C285	0.08	44.4	39.9	0.8	-0.82
154	1409+52,3C295	0.461	46.2	41.4	0.1	-1.1
155	1420+19,3C300	0.27	45.4	40.9	0.5	-0.99
156	1441+52,3C303	0.141	45.1	41.7	10.	-0.61
157	1522+54,3C319	0.192	45.	<39.8	<0.1	-1.
158	1529+24,3C321	0.096	45.4	40.7	2.	-0.92
159	1550+20,3C326	0.098	45.4	40.4	3.	-2.1
160	1626+27,3C341	0.448	46.7	40.3	0.1	-1.
161	1658+47,3C349	0.205	45.7	41.2	2.	-0.81
162	1832+47,3C381	0.161	45.7	40.4	0.3	-0.8
163	1833+32,3C382	0.058	44.9	41.1	9.	-0.65
164	1842+45,3C388	0.092	44.9	41.	3.	-0.93
165	1845+79,3C390.3	0.057	45.1	41.3	8.	-0.87
166	1939+60,3C401	0.201	45.4	41.4	2.	-1.
167	2141+27,3C436	0.215	45.4	41.1	1.	-1.
168	2153+37,3C438	0.29	45.9	41.1	0.4	-1.2
169	2243+39,3C452	0.082	45.2	41.2	4.	-0.87
170	2309+18,3C457	0.31	46.4	40.6	0.5	-0.91

Table 6.2: The FR II sample used in this chapter. Col. (1): ID number, Col (2): IAU name; Col. (3): redshift, Col. (4): disk luminosity, derived by multiplying the lobe power calculated by RS91 with a factor 10; Col. (5): radio luminosity of the core at 5 GHz rest frame, Col. (6): ratio of core flux to total flux at 5 GHz rest frame in per cent; Col. (7): differential spectral index of fitted spectrum at 5 GHz rest frame.

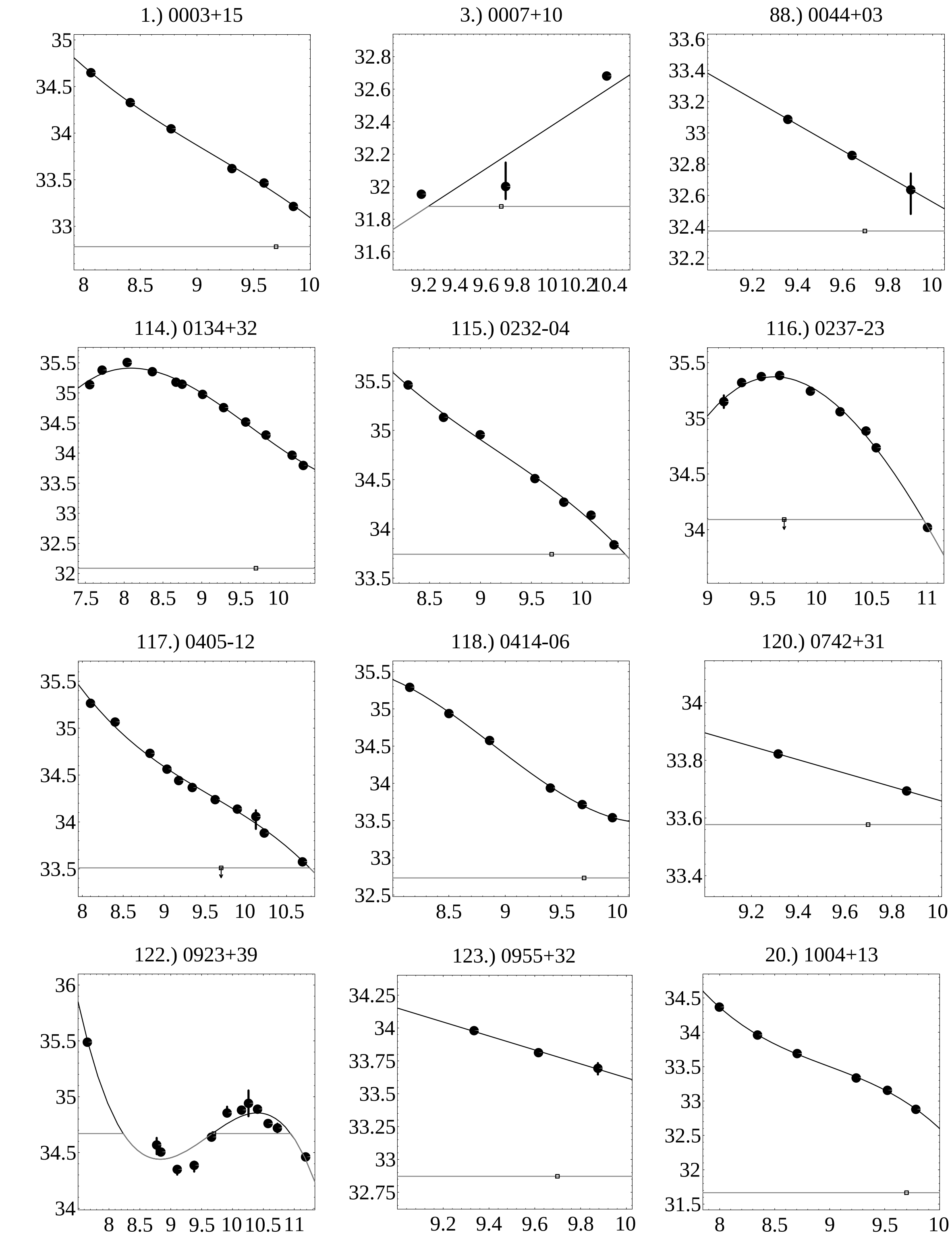

Figure 6.2: Radio spectra of the radio loud quasars in our sample in the rest frame of the quasar multiplied by $4\pi D^2$. The horizontal logarithmic frequency scale is in Hz while the vertical scale gives $\lg L_\nu$ in erg/sec/Hz. The upper solid line shows the polynomial fit we have used. Bars indicate variability as we have combined multiple observations at one frequency. The lower straight line gives the contribution of the core.

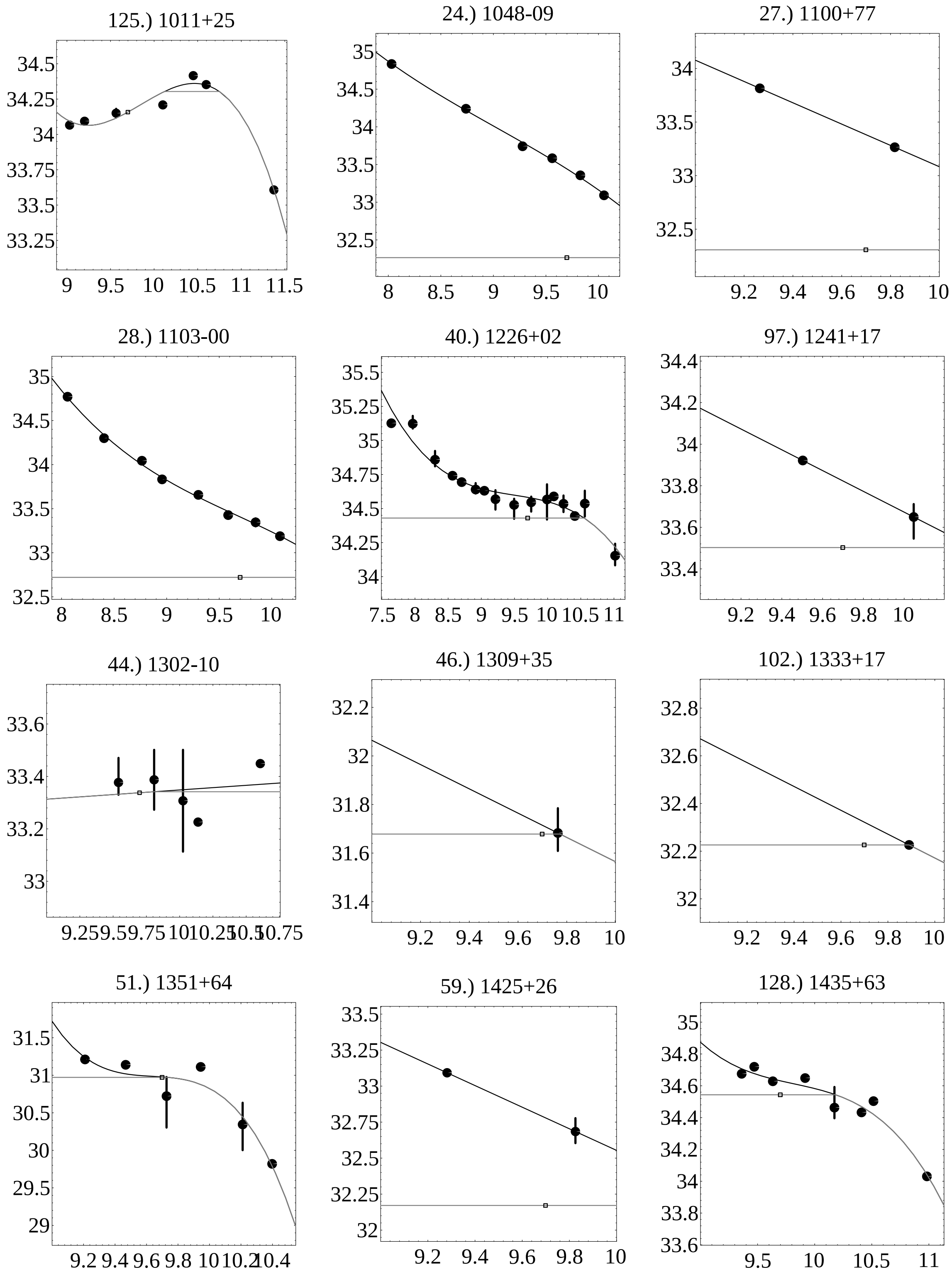

(Figure 6.2 continued.)

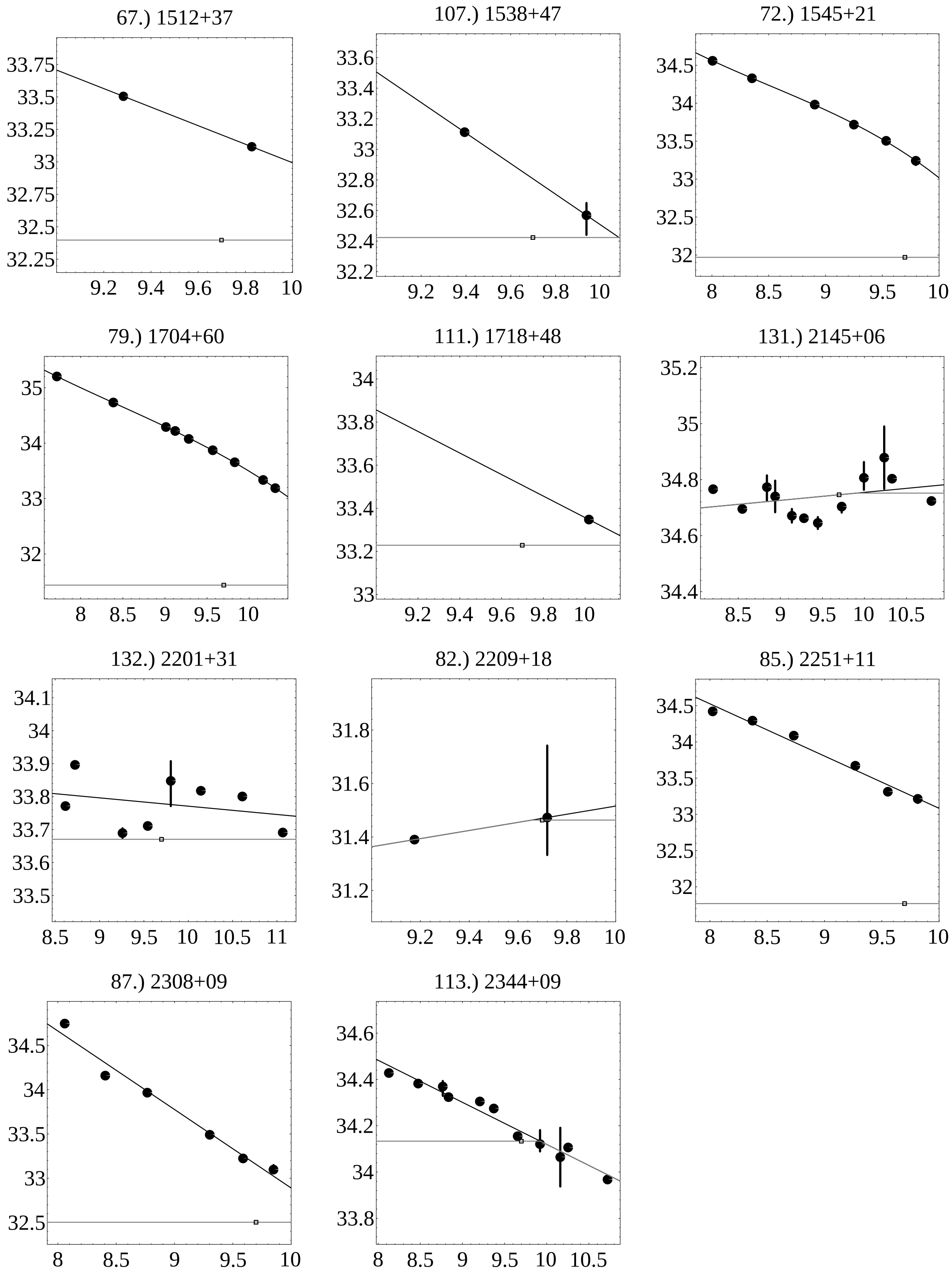

(Figure 6.2 continued.)

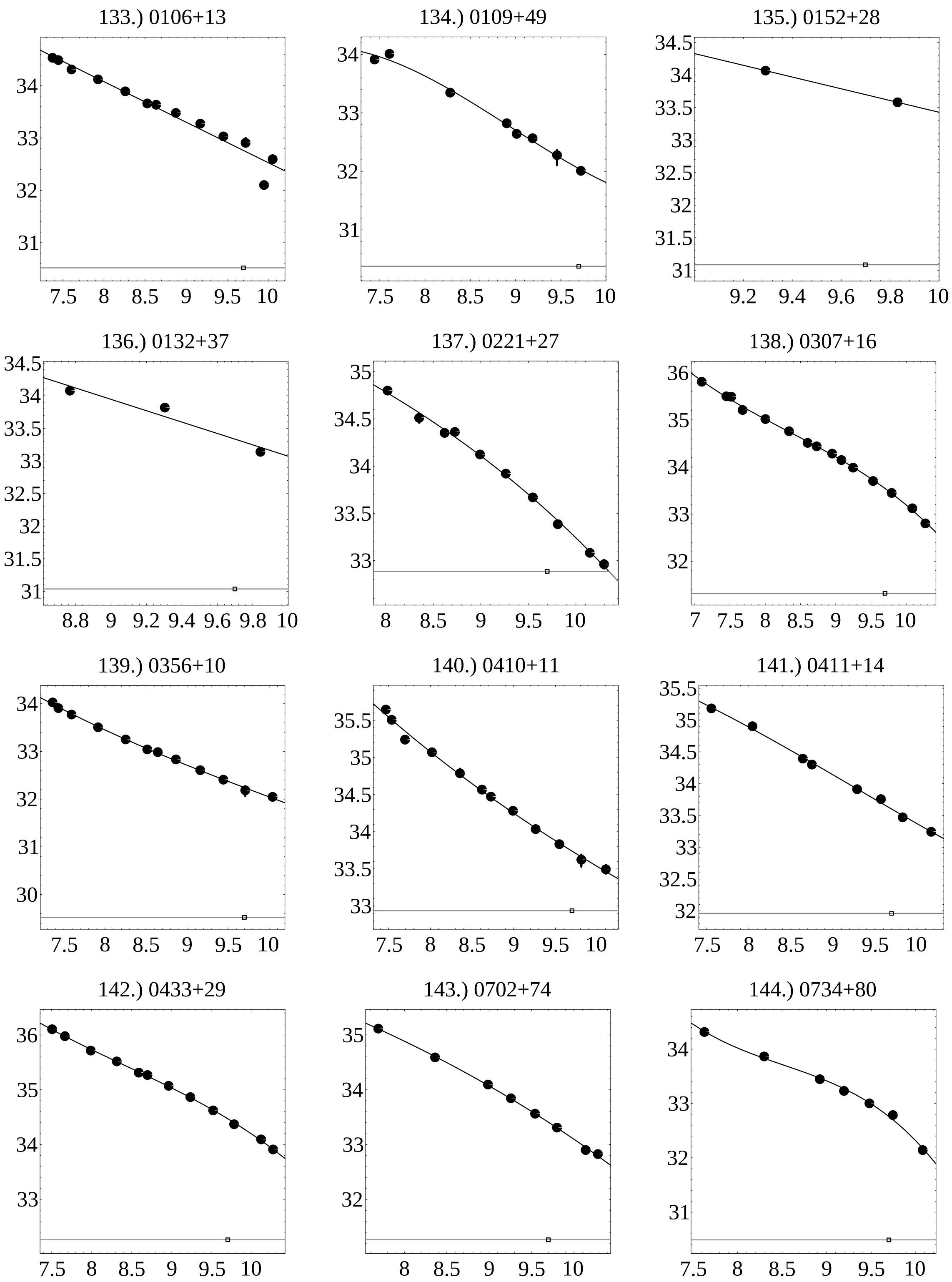

Figure 6.3: Radio spectra of the FR II galaxies in our sample in the rest frame of the quasar multiplied by $4\pi D^2$. The horizontal logarithmic frequency scale is in Hz while the vertical scale gives lg L_ν in erg/sec/Hz. The upper solid line shows the polynomial fit we have used. Bars indicate variability as we have combined multiple observations at one frequency. The lower straight line gives the contribution of the core.

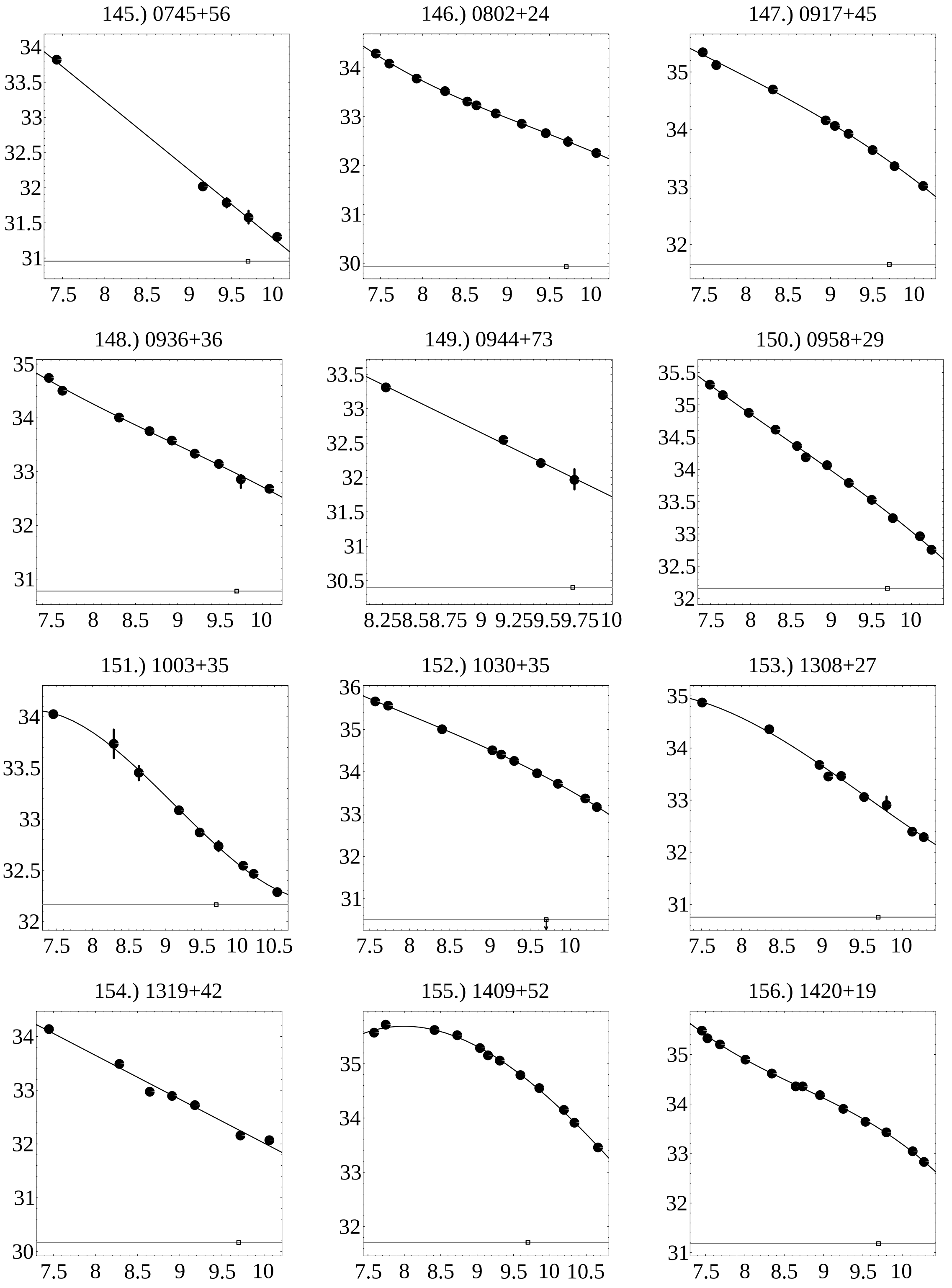

(Figure 6.3 continued.)

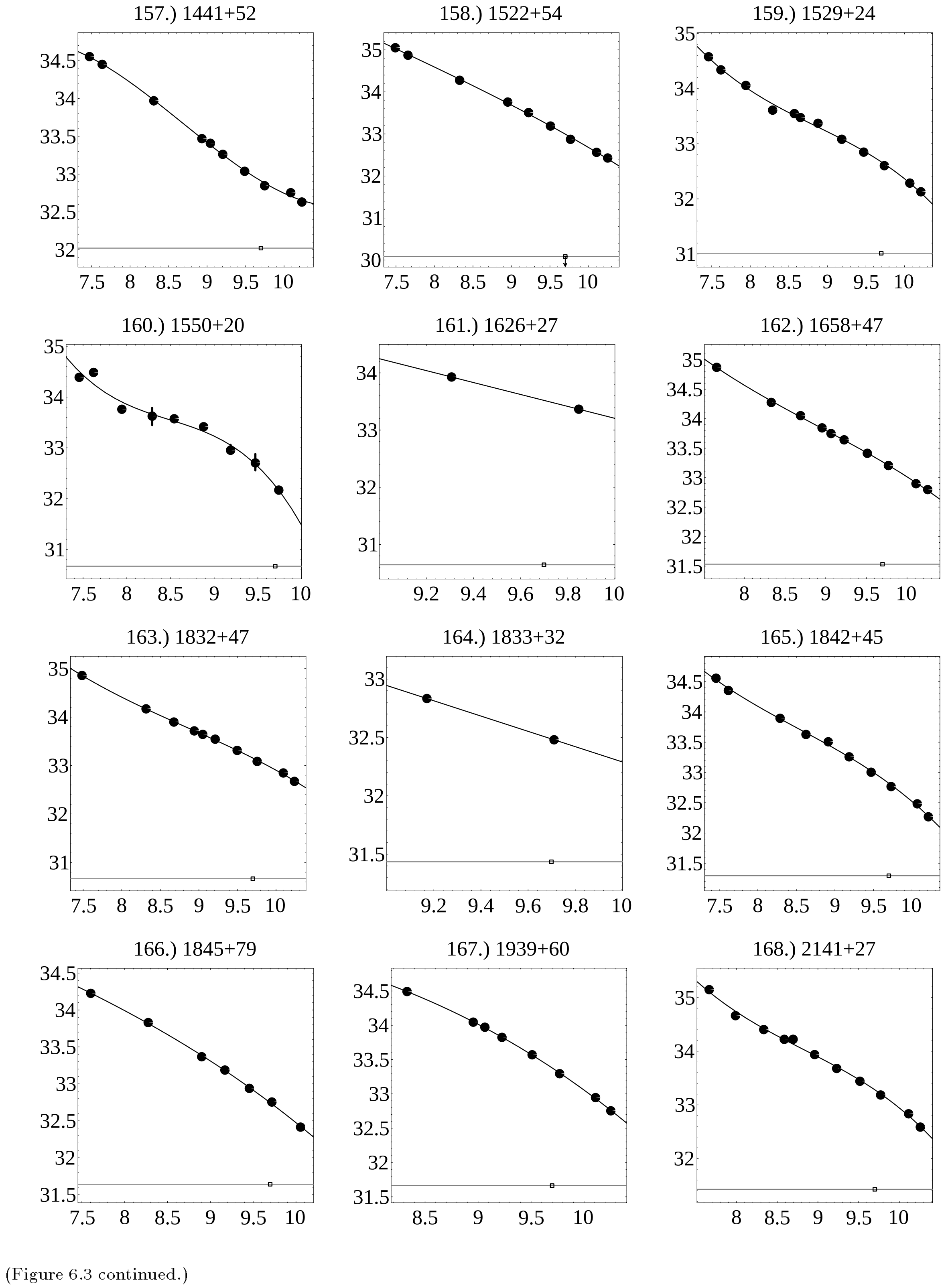

(Figure 6.3 continued.)

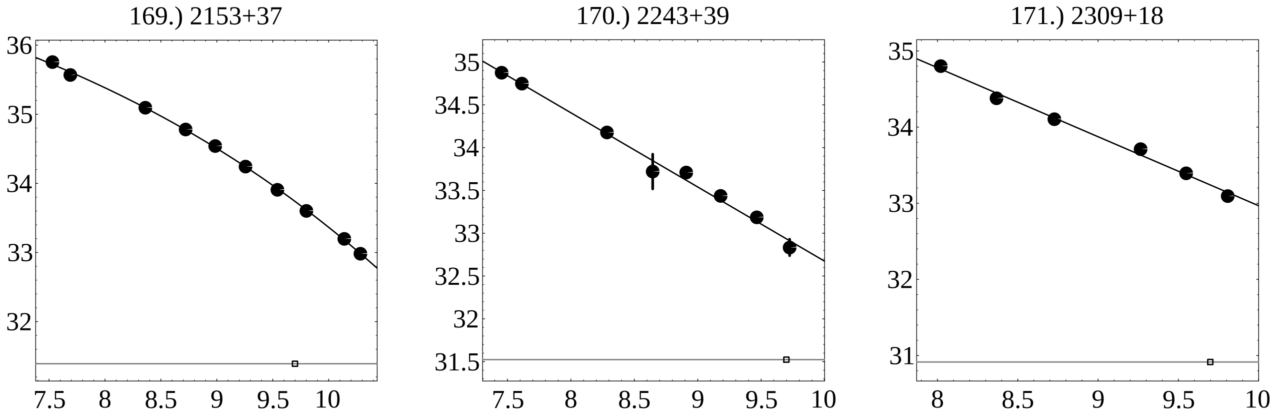

(Figure 6.3 continued.)

un-boosted lobes and disk luminosities.

A few sources do not fit into this general trend: the flat spectrum variable point sources with no sign of large scale lobe structure and a relatively low accretion rate with $L_{\rm disk} < 10^{46}$ erg/sec (boxes in Fig. 2). They have overall properties of (boosted) CDQ but are relatively less luminous and rather seem to fall on the extrapolation of LDQ. Following MRS, we will call these sources radio-intermediate quasars (RIQ) and discuss them in more detail later.

There is a clear correlation between the disk luminosity and the radio core fluxes in each subgroup. Despite the many uncertainties involved, this correlation is remarkably good for extragalactic astrophysical data. It is noteworthy that the upper limits also agree well with the general trend so that a non-detection does not necessarily mean that there is no radio emission, but that the sensitivity was insufficient to measure a radio jet which belongs to a quasar with this redshift and accretion rate. Our theoretical arguments imply that they should be detectable with higher sensitivity (below the 100μJy level). All correlations remain when fluxes, rather than luminosities, are plotted.

We stress that the cores of radio loud quasars (i.e. LDQ and CDQ) are brighter than the cores of radio weak quasars. As we know from numerous VLBI observations that the bulk of the core emission in radio loud quasars comes from a very compact region on the parsec scale it is evident that the difference between radio loud and radio weak quasars is established already at this small scale.

Finally we note that radio loud quasars with lobe emission (morphologically similar to FRII radio galaxies) exist only at disk luminosities $L_{\rm disk} \geq 10^{46}$ erg/sec although radio weak sources with 100 times lower accretion rate do exist in large numbers. Unless there is a strange selection effect – this is an optically selected sample – it means that disks must have luminosities larger than a threshhold luminosity of $\sim 10^{46}$ erg/sec to produce a quasar with FRII type radio jet (Chap. 7).

6.5 Confronting theory with data

6.5.1 Scaling with disk luminosity and velocity

What kind of correlation do we expect between radio core and UV emission? If we base our answer on the idea of a jet-disk symbiosis than we find from Chap. 5 that for a statistical sample the radio flux scales with disk luminosity, bulk Lorentz factor $\gamma_{\rm j}$, and Doppler factor $\mathcal{D}$ as

$$F(\text{radio core}) \propto \mathcal{D}^{2.2}\gamma_{\rm j}^{-1.8}L_{\rm disk}^{1.42} \tag{6.10}$$

for radio loud and radio weak quasars.

There are a few more parameters involved like the relativistic electron number density $x_{\rm e}$ in units of the total (proton) particle density and the mimimum energy of the electrons $\gamma_{\rm min,e}m_{\rm e}c^2$, the total jet power $q_{\rm j/l}$ mormalized to the disk luminosity and the inclination angle i. For homogenous classes of objects we assume that all these parameters will scatter around a constant value and specifically we will also assume that the

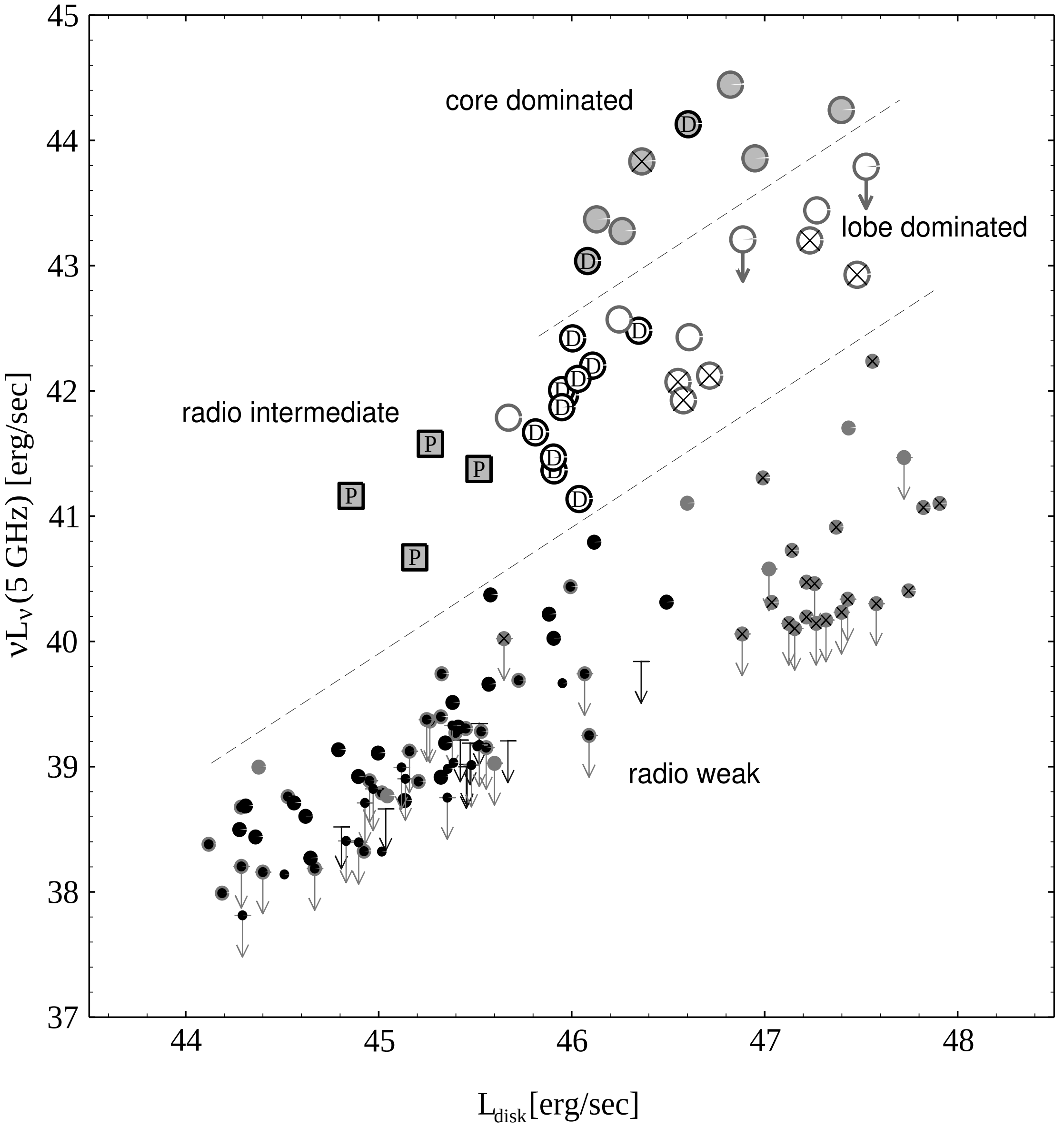

Figure 6.4a: Monochromatic luminosity of the compact radio core vs. the disk luminosity (see text) for PG quasars with $z < 0.5$. 'D': PG quasars showing lobes, 'P': radio loud PG quasars appearing as point sources, *boxes*: RIQ, *black dots*: radio weak point sources, *dots with shades*: radio weak sources with extended emission, *grey dots with cross*: radio weak PG quasars with $z > .5$, *grey dots without cross*: radio weak quasars from SM89, *grey open circles with cross:* radio loud PG quasars with $z > 0.5$, *grey open circles without cross:* radio loud quasars from SM89, *circles and boxes with grey background:* flat spectrum sources.

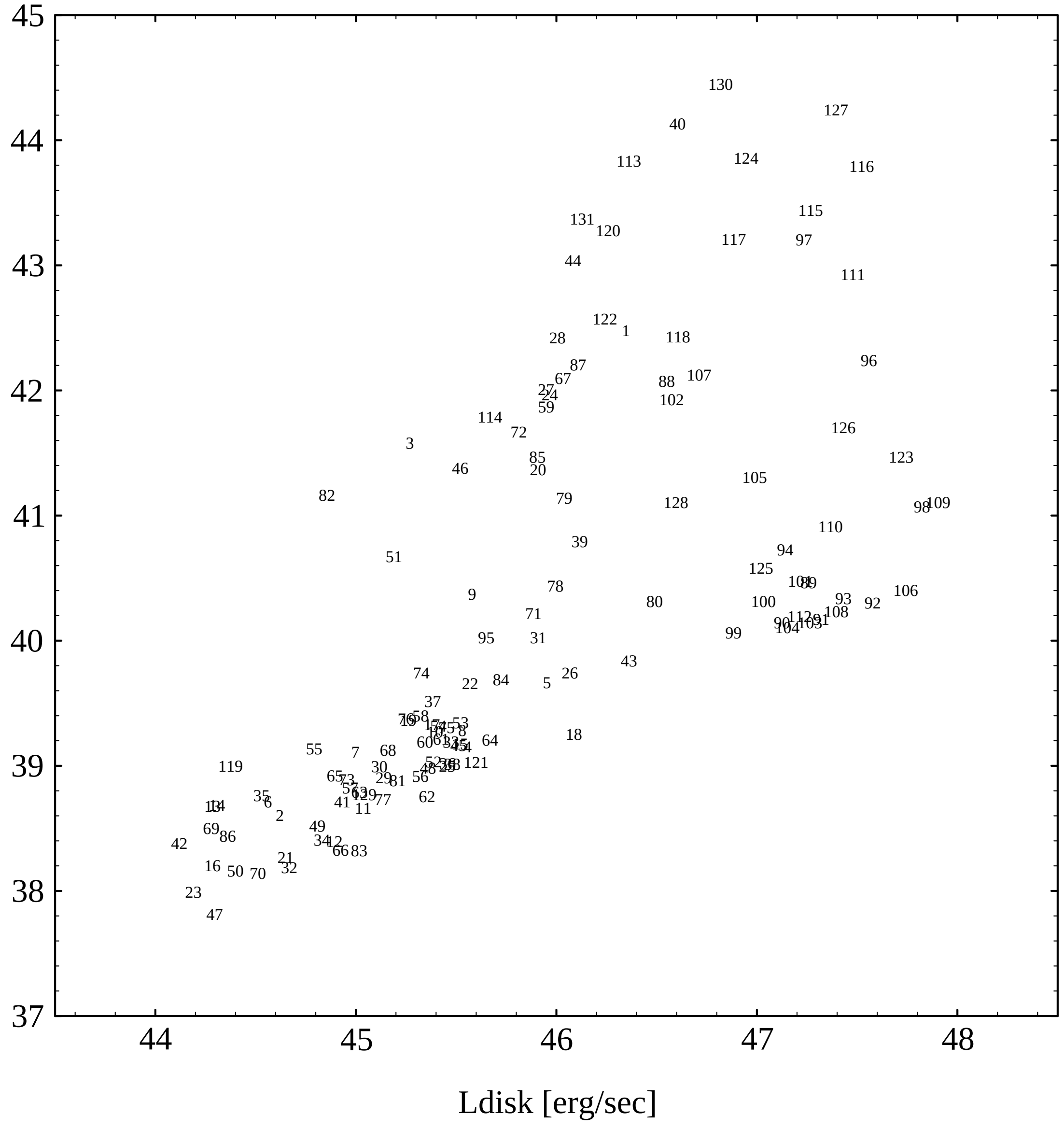

Figure 6.4b: The plot of Fig. 6.4a is repeated in the lower panel but using the ID numbers of Table 1 as labels to make it easier to locate individual sources.

dominant reason for scattering will be the randomly oriented inclination angle with the consequence of strong Doppler boosting. In the earlier discussions on the nature of the quasar radio emission it was suggested that relativistic beaming was responsible for the scatter of all quasars (radio loud and radio weak) but as Strittmatter et al. (1980) showed this is inconsistent with the flux density distribution of optically selected quasar samples and there is a real dichotomy in the radio flux. Hence, we suggest that the scatter within each population is dominated by relativistic boosting and there is an additional discrete process producing an offset between radio loud and radio weak.

The scaling over several orders of magnitudes in the radio luminosity thus will reflect mainly the change in the accretion rate which indeed may vary over 4 orders of magnitudes in the quasars alone and even more if one later includes Seyfert galaxies and stellar mass black holes. The non-linearity between disk luminosity and radio flux is a consequence of the non-linear response of the synchrotron emissivity to a change in the magnetic energy density. Nevertheless, there still remains one uncertainty in the discussion of the scaling, namely, we have no idea whether the jet velocity also depends on the mass accretion rate. We only can argue that this dependence is not very strong because the observed Lorentz factors in jets are usually estimated to be in the range 3-30 (Ghisellini et al. 1993) with a mean value of ~ 10, despite a large range of mass accretion rates of at least 2 orders of magnitudes for radio loud quasars. One could also argue that the escape velocity around black holes is a substantial fraction of the speed of light, so that jets with speed $\ll 0.5c$ from black holes are difficult to achieve unless there is a perfect fine-tuning in the acceleration mechanism. On the other hand the Compton drag of disk photons will decelerate the jet if it starts at $\gamma_{\rm j} \gg 10$ (Melia & Königl 1989). In light of this discussion we make the ansatz that the bulk proper velocity of the jet depends on the accretion rate and thus on the disk luminosity[1] as

$$\gamma_{\rm j}\beta_{\rm j} = \gamma_{\rm j,0}\beta_{\rm j,0}\left(\frac{L_{\rm disk}}{10^{46}{\rm erg/sec}}\right)^{\xi} \tag{6.11}$$

with the additional assumption that for quasars $|\xi|$ is a small number (< 0.5), $\beta_{\rm j,0} \simeq 1$ and $\beta_{\rm j} \simeq 1$ (see above). Following our general philosophy that disks and jets are basically the same everywhere we assume the same scaling for radio weak quasars.

6.5.2 Obscuring dust torus

The PG quasars we use are selected by their blue color and not by their radio flux. In our context this part of the spectrum is produced by the accretion disk and should be relatively free of any substantial selection effect like boosting. We only have to take into account that an obscuring dust torus surrounding the nucleus could prevent us from seeing edge on disks. This, on the other hand, is even helpful because the disk luminosity is then even less dependent on the inclination angle if we deal with maximally rotating black holes as central objects (Cunningham 1975): the light bending and a moderate amount of boosting due to the high rotational velocity compensate the effects of decreasing apparent surface with higher inclination angles.

It is not really known what the opening angle of the viewing cone permitted by the torus for each quasar population actually is which itself might depend on other parameters (i.e. jet power and z, see Kapahi 1990; Falcke et al. 1994b). We pick for the assumed obscuring dust torus of radio weak quasars deliberately a viewing cone with semi-opening angle of $60°$ – saying that we do not detect 50% of the quasars because of obscuration – and obtain as an average inclination angle for the jet axis with respect to the line of sight in this sample $i \approx 40°$. In the range $60° > i > 18°$ we should find 90% of our sample. This value for the obscuring torus is taken from McLeod & Rieke (1994) who investigated the host galaxies of a subsample of the PG quasars.

Studies of the ratio between FR II galaxies and radio loud quasars suggest that this torus might there even cover a larger area than for radio weak quasars and we take $45°$ as a default value (Barthel 1989). Which means, we miss more than 2/3 of all sources and the 90% dividing line is at $14°$. However, none of our conclusions depends sensitively on these assumptions; we will later see that those numbers are able to explain the UV-radio correlation in a consistent manner.

6.5.3 Parameter space for radio loud jets

We now discuss the range of parameters needed to explain the UV-radio correlation as being due to a link between jet and disk. In Chapter 5 we presented the most simple minded model for the jet emission and its

[1] One should understand this scaling in statistical terms. If the jet velocity depends on the ratio $L_{\rm disk}/L_{\rm edd}$ and the average of this ratio has a slight dependence on the total power (see SM89) this could produce such a scaling indirectly.

parameters and noted that in order to explain the high radio flux of radio loud cores we get close to the limits imposed by energy and mass conservation in a jet-disk system. We will fit the model step by step to the data and discuss the range of possible parameters. Among all possible models only the most efficient case, a 'total equipartition jet' — implying rough equipartition between energy stored in magnetic field, electrons and protons and bulk kinetic motion — is able to explain these radio fluxes. Let us now first fix the plasma parameters of this type of jet such that they yield maximum efficiency (see Chapter 5) which implies:

a) a minimum Lorentz factor of the relativistic electron distribution of $\gamma_{\rm e} \approx 100$ for a powerlaw distribution with $p = 2$,

b) a relativistic electron fraction $x_{\rm e} \approx 1$ which means that in a proton/electron jet all electrons get accelerated or that for every thermal electron one additional secondary particle (electron or positron) is created and

c) a proton/electron ratio of $\mu_{\rm p/e} \approx 2$ meaning equal energy in relativistic proton and electron distribution ($u_3 \approx k_{\rm e+p} \approx 1$ and $\ln(\gamma_{\rm e,max}/\gamma_{\rm e,min}) \approx 3.6$)

According to the discussion in Chapter 5 one may vary some of these 'microscopic' parameters but there is no way to further increase the emitted flux of the jet other than by changing the 'macroscopic' parameters which are

a) the jet Lorentz factor $\gamma_{\rm j}$, assumed to be of the order 10 ($\Rightarrow \beta_{\rm j} \simeq 1$),

b) the disk luminosity L_{46} in units of 10^{46} erg/sec which varies in our sample from 10^{-2} to 10^{2} and

c) the total jet power $q_{\rm j/l}$ in units of the disk luminosity which we consider to be < 1.

When the parameters are fixed in this way and one calculates the emitted flux for a supersonically expanding jet with maximal internal energy contents one gets (Chapter 5)

$$\nu L_\nu(5{\rm GHz}) \quad = \quad 6.7\cdot 10^{42}\,{\rm erg/sec}\;\mathcal{D}(L_{46}, i_{\rm obs})^{2.17} \sin i_{\rm obs}^{0.17} \left(\frac{\gamma_{\rm e,min}\, x_{\rm e}}{100}\right)^{0.83} \left(\frac{6}{\gamma_{\rm j,0}}\right)^{1.8} q_{\rm j/l}^{1.42} L_{46}^{1.42-\xi}. \quad (6.12)$$

where we have already made use of the possible velocity scaling (Eq. 6.11) and the parameter setting discussed above. The Doppler factor $\mathcal{D}$ is defined as usual

$$\mathcal{D} = 1/\gamma_{\rm j}(1-\beta_{\rm j}\cos i_{\rm obs}). \quad (6.13)$$

For our comparison with the data we will assume that all jets are two-sided.
In order to fix the parameters we first try to fit the cores of the lobe dominated radio loud quasars at $L_{\rm disk} \simeq 10^{46}$ erg/sec and find that already there the possible parameter range is very narrow. The quasars can not be fitted with bulk Lorentz factors $\gamma_{\rm j,0} \geq 10$ and $q_{\rm j/l} < 1$ as with increasing Lorentz factor the radiative efficieny is decreased and the boosting effect reduces the visible radio flux for the bulk of the population even further. Together this makes a very strong effect which depends on the Lorentz factor roughly as $\gamma_{\rm j,0}^{-4}$.
We also can get an approximate lower limit for the Lorentz factor from our prerequisite that the width of the distribution is mainly given by the scatter in inclination angles. A small Lorentz factor would yield only a narrow band for the scattering width of the UV-radio correlation and some sources would fall outside this band so we conclude that $\gamma_{\rm j,0} \geq 3$ ($q_{\rm j/l} \geq 0.05$). The width (and therefore the scattering) of the radio flux distribution is represented in Fig. 6.5 by grey lanes. Quasars with larger inclination angle (below the lane) are assumed to be missing in our sample due to an obscuring dust torus and smaller inclination angles (above the lane) will lead to a strong boosting effect hence $\sim 10\%$ of each sample should lie close to or above this lane.
In a second step we include the remaining sources and first adopt the velocity gradient by varying ξ in Equation (6.11). As noted before the gradient must not be very steep because of the fourth power entering in Equation (6.12); this is highlighted in Fig. 6.5 where we show the expected UV-radio correlation for ξ as large as 0.5. It is not possible to determine this evolution in more detail from the few radio loud sources in our sample, especially as the high power sources do not belong to the well defined subsample of PG quasars with $z < 0.5$. We only can hope that the distribution of the high power sources is not completely misleading and estimate that $0 \leq \xi \leq 0.25$.
Finally we include the CDQ in our analysis. A strict upper limit of the radio flux as a function of disk luminosity is given by those models with maximum boosting ($i = 0$) and no source in our diagram should be far above

this line. This condition gives us additional limits on the Lorentz factor and also ξ. Moreover should most of the CDQ cluster around a line representing sources at the boosting cone thus inclined to line of sight by $i \simeq 1/\gamma_{\rm j}$. This restricts the margins for the Lorentz factor even further. Figure 6.5 shows different parameter combinations and our best fit model with estimated errors.

$$\gamma_{\rm j} = 6^{+2}_{-2},\ q_{\rm j/l} = 0.15^{+.2}_{-.1},\ \xi = 0.15^{+0.1}_{-0.15} \tag{6.14}$$

The best fit parameter set implies that indeed the microphysical state of the plasma must not be too far away from the radiatively most efficient state, i.e. $x_{\rm e}\gamma_{\rm min,e} \approx 100$, otherwise we will have to increase $q_{\rm j/l}$ substantially. Accordingly we have an indirect argument that the electron distribution in radio loud quasars either must have a low energy cut-off or consists of additionally created pairs. We suggested in Chapter 5 that both effects might naturally arise if the electron population is dominated by pairs produced in the $\pi-$decay of hadronic cascades initiated by pp or $p\gamma$ collisions.

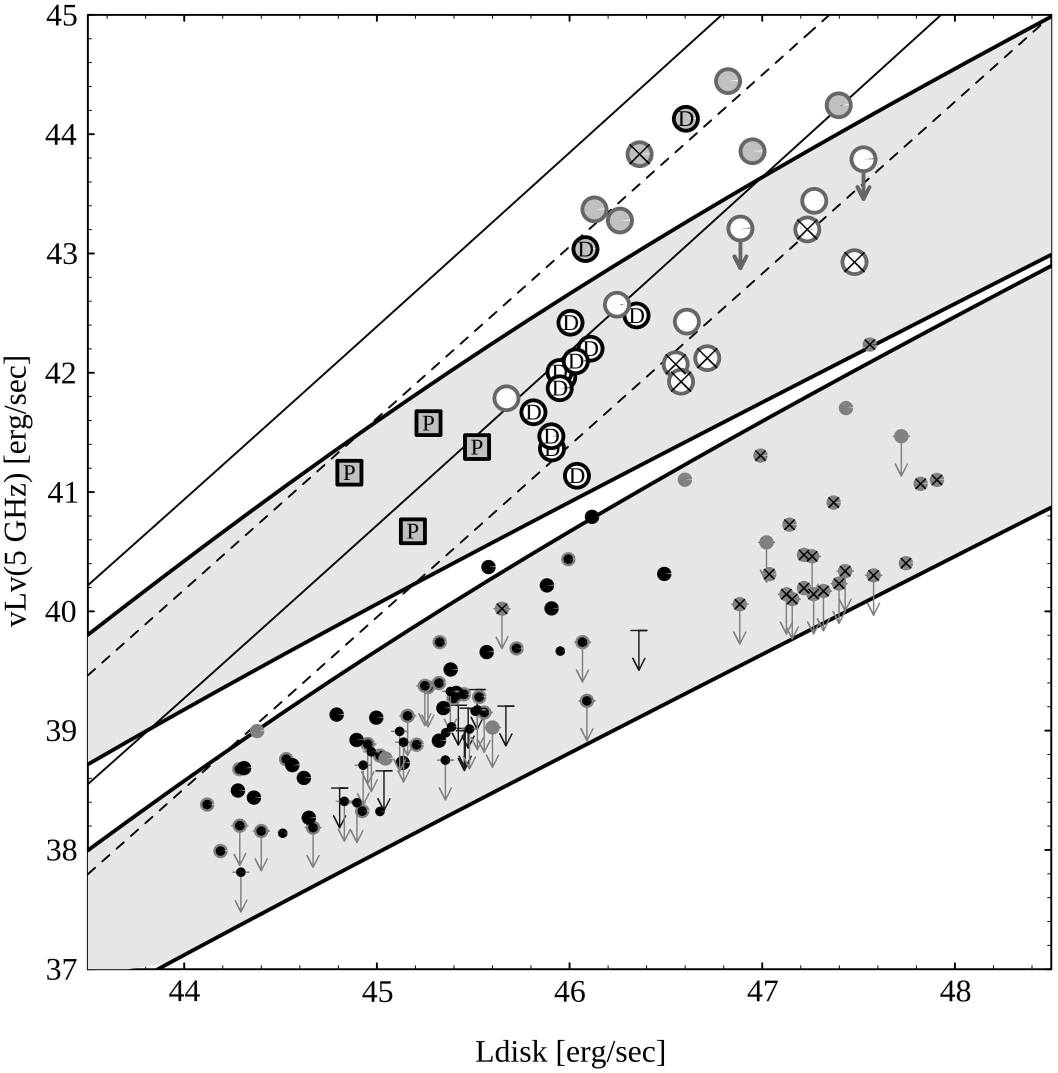

Figure 6.5a: Models (Figs. 6.5a-b) for the UV-radio correlation (Fig. 6.4) for different Lorentz factors $\gamma_{\rm j,0}$ and velocity evolution power index ξ. The jet power $q_{\rm j/l}$ is adjusted such that the bulk of radio loud quasars at $L_{\rm disk} = 10^{46}$ erg/sec are always fit. Upper lane: 'total equipartition' jet. Lower lane: 'protonic' jet. The widths of the grey lanes is given by different inclination angle. Dashed line: boosted sources with $i = 1/\gamma_{\rm j}$. Solid line: maximum possible boosting ($i = 0$). Here we have:
(a) Best fit: $\gamma_{\rm j} = 6$, ($q_{\rm j/l} = 0.15$), $\xi = 0.15$.

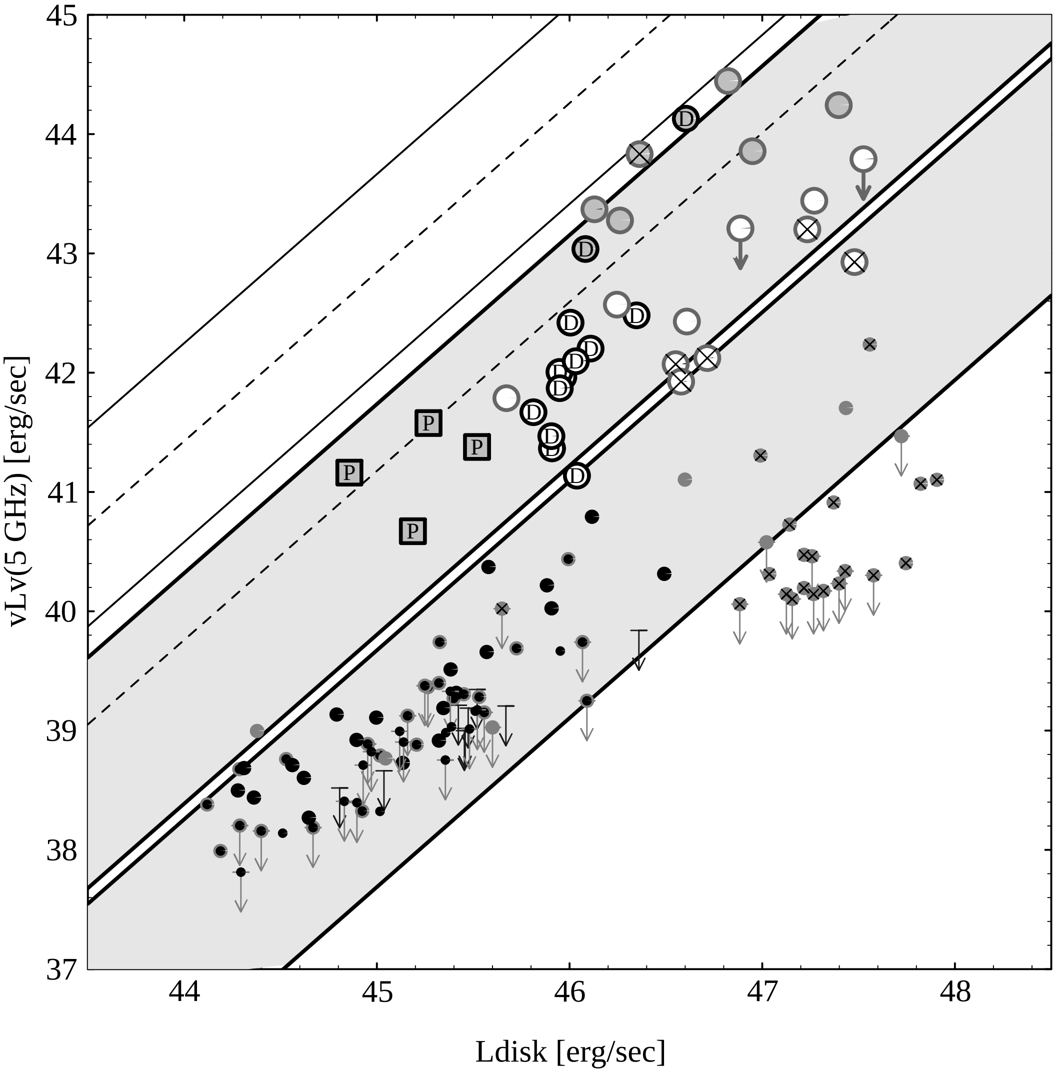

Figure 6.5b: Lorentz factor too high: $\gamma_j = 10$, ($q_{j/l} = 1$), $\xi = 0$ (CDQ are too low).

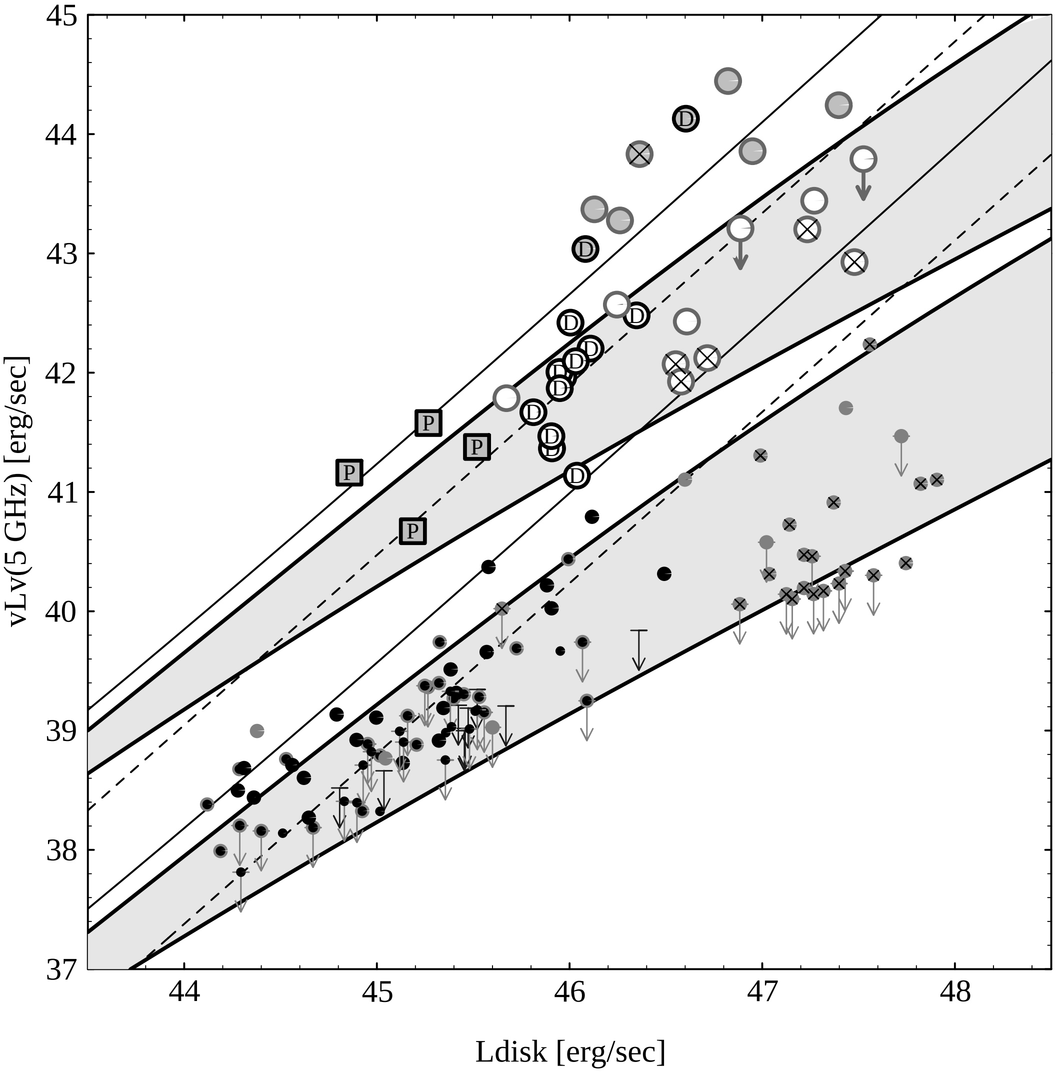

Figure 6.5c: Lorentz factor too low: $q_{j/l} = 0.025$, $\gamma_j = 2.5$, $\xi = 0.15$ (CDQ too high and distribution too narrow).

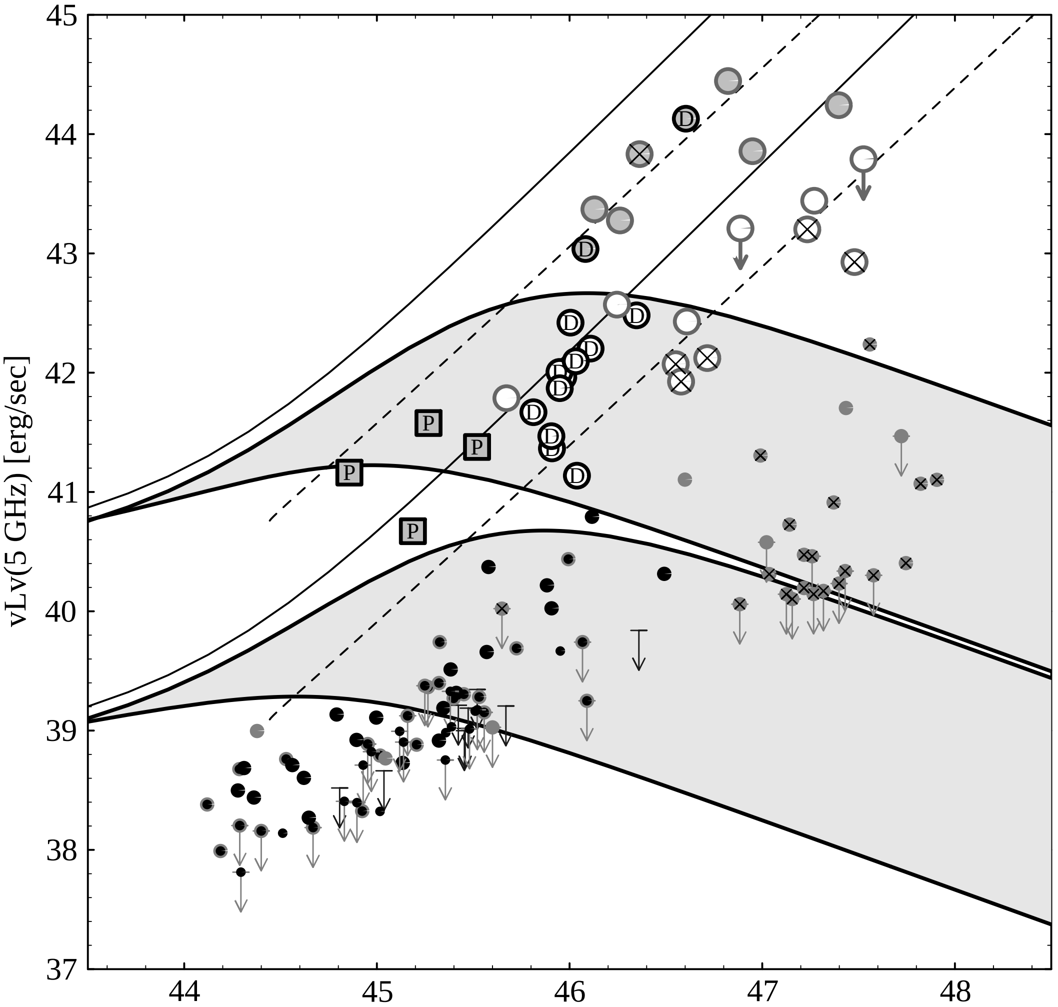

Figure 6.5d: Velocity evolution too strong: $\gamma_{\rm j} = 6$, ($q_{\rm j/l} = 0.15$), $\xi = 0.5$.

6.5.4 Applying the parameters to radio weak jets

As discussed in Chapter 5 we proposed to test if the radio emission from radio weak sources could be explained with emission from jets similar to those observed in radio loud quasars. Based on the idea that quasars are all powered by accretion disks around black holes, it is hard to understand how the jet production in the accretion disk very close to the black hole ($\ll 1$ pc) should depend on environmental effects (e.g. type of galaxy). We noted that a difference in the efficiency of electron acceleration (e.g. production of secondary pairs) could naturally account for the different radio luminosities. The acceleration of these electrons must happen at a larger scale (≥ 1 pc) because of strong synchrotron losses further in, and might well be triggered by environmental effects (e.g. interaction between jet and ISM in a shear layer). But as radio weak quasars, unlike their radio loud siblings, do not all populate the extreme parts of the parameter space, observations are not yet able to decide what is the true distinction between radio loud and radio weak. In Chapter 5 we suggested at least another 3 alternative scenarios. For the discussion in this Chapter we will confine our attention only to the case of a 'protonic' jet (**BP** model in Chapter 5). Nevertheless, all other proposed models would yield similar results; only the interpretation of the microscopic parameters would change.
The protonic jet is obtained by increasing the relativistic proton/electron ratio $\mu_{\rm p/e}$ by a factor 100 which means we reduce the energy stored in relativistic electrons by the same factor, but leave everything else in the jet unchanged. The magnetic field would still be in equipartition with relativistic particles, namely the protons, and both still constitute a major fraction ($\sim 50\%$) of the total jet power (the other half is in kinetic motion). The value for $\mu_{\rm p/e}$ is not ad-hoc but a natural configuration in cases where all electrons are accelerated from their thermal distribution ($x_{\rm e} \simeq 1$) into a powerlaw distribution starting at $\gamma_{\rm e,min} \approx 1$. From Chapter 5 we obtain as the core luminosity

$$\nu L_\nu(5{\rm GHz}) \quad = \quad 1.0 \cdot 10^{41}\,{\rm erg/sec}\,\mathcal{D}(L_{46}, i_{\rm obs})^{2.17} \sin i_{\rm obs}^{0.17} (\gamma_{\rm e,min} x_{\rm e})^{0.83} \left(\frac{6}{\gamma_{\rm j,0}}\right)^{1.8} q_{\rm j/l}^{1.42} L_{46}^{1.42-\xi}. \quad (6.15)$$

There is no way to definitively prove this notion, but we could easily falsify it. We just take the parameters derived for radio loud jets, apply them to Eq.(6.15) and insert this in our diagram without further fitting. The lower bands in Figure 3 represent the protonic jet model where we only have changed the proton/electron ratio by a factor 100 and the opening angles of the torus to 60° to be consistent with other findings as discussed before. The agreement is surprisingly good and indeed we can easily match all three populations (CDQ, LDQ, radio weak quasars) with a single model where the difference is only due to relativistic boosting and different relativistic electron populations.
We have to comment on one additional effect seen in this data. There seems to be a slight curvature in the radio weak population towards high powers. Unlike the case for the extended emission, there is no reason to suppose that any kind of cosmological evolution in this diagram would produce that effect. The core luminosity depends only on the accretion rate and not on the environment. A change in the accretion rate with z should shift a quasar only parallel to the distribution. Strong evolution effects in this diagram would be a serious argument to falsify our theoretical understanding of the radio core. However, the curvature is only minimal and could easily be caused by technical or selection effects, especially as this curvature is mainly seen in the high redshift PG sample where strong selection effect are known to exist (Wampler & Ponz 1985). Should selection effects not be the main cause for this curvature one might argue that this is indeed a sign of a velocity gradient index $\xi \neq 0$, but this is the only indication, and still $\xi = 0$ gives a good approximation to the data. One may test this in the future by incorporating larger complete samples for radio loud and radio weak quasars with high powers. A direct consequence would be that Seyfert galaxies have only mildly relativistic jets without pronounced boosting effects.

6.5.5 RIQ: boosted radio weak quasars?

One inevitable consequence of our "relativistic jets in all quasars" hypothesis is that a fair fraction of all radio weak quasars are boosted and appear as radio loud quasars. For the following discussion we only refer to the PG sample with $z < 0.5$ if not stated otherwise.
The cores of the 11 steep spectrum LDQ appear as radio loud, these quasars obviously form a separate subclass, which is physically different from radio weak quasars already in the cores. The rest of 5 objects, however, is a possible sample of beamed radio weak quasars, because they show all characteristics one might expect from a boosted source: strong compact core, high variability and flat spectrum. Two of them (PG 1226+023 and

PG 1302−102) show a lobe structure themselves and therefore are likely to be boosted specimen of radio loud quasars whereas the remaining 3 objects (PG 0007+106, PG 1309+355, PG 2209+184) apparently do not show any extension and are candidates for boosted radio weak quasars. We use these sources to define a subclass of radio quasars, the radio-intermediate quasars (RIQ). To be classified as such we demand a variable flat spectrum compact core without a large scale lobe structure that in a UV-radio core diagram are found among, or on the extrapolation of, the cores of LDQ. Two other candidates for this kind of sources are PG 1351+640 and PG 1333+176 (see Notes).

We have now three independent means to check the idea that RIQ are boosted radio weak quasars: the number of beamed sources, the offset between boosted and normal quasars and the emission line characteristics.

a) The ratio of the number of boosted to non-boosted objects reflects the angle of the boosting cone which is arcsin $1/\gamma_{\mathrm{j}}$. For a sample of N objects with a boosting cone of $1/\gamma_{\mathrm{j}}$ and an obscuring dust torus with semi-opening angle of ϕ_{torus} we expect

$$n = N\left(1 - \cos \arcsin\left(1/\gamma_{\mathrm{j}}\right)\right) / \cos\phi_{\mathrm{torus}} \tag{6.16}$$

strongly boosted objects. Here we have $N = 73$, $n = 3 \pm 1.7$ and assume $\phi_{\mathrm{torus}} \simeq 60^{\circ}$ which corresponds to a γ-factor for the jet of $\gamma_{\mathrm{j}} = 5^{+2.7}_{-1}$. Inclusion of the fourth source will reduce this value slightly.

b) The offset of the boosted from the non-boosted population is a function of the Doppler factor as well. Alas, despite the major popoulation being called 'non-boosted' it is still affected by boosting and we do not know exactly what the average inclination angle actually is, as we obviously have only upper limits in the high inclination part of our diagram. We first fit a straight line with *fixed slope* to both populations. The 3 boosting candidates are a factor 153 more luminous in the radio. Using the Doppler factors from our model, we find γ-factors in the range $\gamma_{\mathrm{j}} = 1.7$ to $\gamma_{\mathrm{j}} = 4.8$ for the range of inclination angles ($60^{\circ} - 20^{\circ}$) we attribute to the bulk of our parent population. Here we assumed that all boosted jets show no inclination to the line of sight; a more reasonable value for the inclination angle will lead to slightly higher values of γ_{j}. In Fig.6.5 the area between the lower pair of dashed and full line represents the expected region for boosted-radio weak quasars, for the parameter set discussed before. Indeed, taking the uncertainties into account, the RIQ are compatible with this model prediction. Of course, an association with the extrapolation of the radio loud CDQ is not completely excluded but is less likely.

c) BG92 found one significant emission line indicator, which separated radio loud from radio quiet objects in so far that radio loud objects show almost no evidence for Fe II emission lines, whereas radio weak quasars do. Our sample of suspected boosted radio weak quasars clearly shows enhanced level of Fe II emission, in agreement with being radio weak, in marked contrast to the double lobe sample which shows no significant FeII emission. In addition there are some other differences between radio loud and radio quiet and taking all together BG92 come to the conclusion that the sample of flat spectrum sources – which was dominated by the RIQs – has emission properties like radio quiet quasars but unlike radio loud quasars.

The hypothesis of boosted radio weak quasars passed all three tests reasonably well. Both estimates for the Lorentz factor are in agreement with each other and our previous estimate and support the hypothesis of having relativistic jets in radio weak quasars.

6.5.6 FIR emission

Another consequence of having jet emission in radio weak quasars is the possibility to see this emission at higher frequencies. In *Chapter 5* we showed that we can expect non-thermal emission in the rest frame up to the mm regime. Unfortunately the expected flux is on the mJy level which is difficult to observe with current detectors. Chini et al. (1989) observed a subsample of the PG quasars at 230 GHz, showing that the IR emission at higher frequencies in quasars is of thermal origin. They detected only 5 quasars at 230 GHz and concluded from the spectrum that the emission up to this frequency is non-thermal while beyond 230 GHz thermal dust emission takes over. We give a table of spectral indices α between these fluxes and the 5 GHz VLA core and total fluxes (except for 2041−109 where we take the flux referenced in Chini et al. 1989) of the 5 objects being in our extended sample. We define the spectral index to be positive for inverted spectra ($F_{\nu} \propto \nu^{\alpha}$).

All spectral indices are flat or inverted as expected if there indeed is a strong flat (inverted) spectrum core. In our picture the non-thermal emission at this frequency should come from a very small region of the order 10^{18} cm away from the disk and therefore we are allowed to peek into the region where the jet establishes itself and may still be in a state of accelerating its inital electron population. Interestingly the Galactic Center source Sgr A* shows a similar inverted spectrum in the mm to submm range where we explained this qualitatively as being radiation coming from the jet nozzle (FMB; Falcke & Biermann 1994a; Chap. 4).

Table 6.3: High frequency spectral indices for radio weak quasars detected at 1.3 mm: $\alpha_{\rm core}$ is the spectral index between the coreflux at 6 cm and the total flux at 1.3 mm while $\alpha_{\rm total}$ is the spectral index between the total flux at 6 cm and 1.3 mm.

Name	$F_{230\rm GHz}[mJy]$	$\alpha_{\rm core}$	$\alpha_{\rm total}$
0007+106	3.9 ± 1	$0.51^{+0.06}_{-0.08}$	$0.48^{+0.06}_{-0.08}$
1411+44	3.9 ± 1	$0.51^{+0.06}_{-0.08}$	$0.48^{+0.06}_{-0.08}$
2041–10	4.0 ± 1	–	$-0.08^{+0.05}_{-0.08}$
2130+09	2.1 ± 0.7	$0.23^{+0.08}_{-0.1}$	$0.01^{+0.08}_{-0.1}$
2214+13	3.5 ± 0.6	–	$0.7^{+0.04}_{-0.05}$

6.6 Unification with FR II galaxies

6.6.1 Core emission

An often used assumption is that FR II radio galaxies and quasars are basically the same objects but seen under different aspect angles. Seen edge on, the obscuring dust torus will prevent us from observing UV bump and broad line region, and we cannot classify the radio source as a quasar. In fact, if an obscuring dust torus is indeed present, and the widths of the lanes in Fig. 3 do support such a concept, this bimodality is a necessary consequence.

However, a big problem of an optically selected sample is the scarcity of radio loud objects which inhibits detailed statistical studies of their properties and we supplement our sample with a sample of radio selected FR II galaxies used by RS91. The problem with these is that per definition it is almost impossible to measure the disk luminosity. Rawlings et al. (1989) tried to use the OIII narrow line as an indicator, but found only weak correlations. Later RS91 used a combination of narrow lines to obtain a better indicator for the central luminosity and indeed found a good correlation between the luminosity of these lines and the power stored in the radio lobes divided by the age of the lobe. Unfortunately, they did not tabulate these narrow line luminosities, and in any case it is difficult to calibrate this indicator to an absolute value of the disk luminosity as we did for our sample.

Fortunately we do not really need this information because with our analysis so far, we are able to estimate the hidden disk luminosity of FR II radio galaxies and have also a way to check if this estimate is consistent with the general model and the unification theory. The idea, we have followed throughout this chapter, is that the average ratio between jet power and disk luminosity is constant within our sample. So if this and the value $q_{\rm j/l}$ we derived previously is correct, we obtain the hidden disk luminosity of FR II radio galaxies simply by dividing the jet power derived from the radio lobes by this conversion factor. Given the jet power $Q_{\rm jet,RS91}$ derived by RS91 the disk luminosity of the FR II source is

$$L_{\rm disk} = 10\, Q_{\rm jet,RS91} \left(\frac{f_{\rm RB93}}{3}\right) \left(\frac{q_{\rm j/l}}{0.15}\right)^{-1}. \tag{6.17}$$

There is a factor $2q_{\rm j/l}$ in this equation because jets are generally two-sided and $q_{\rm j/l}$ accounts only for one cone. The factor $f_{\rm RB93}$ is to correct the RS91 minium energy estimates for the presence of relativistic protons. Rachen & Biermann (1993, RB93) and Rachen et al. (1993) made arguments about the ultra-high energy tail of the cosmic ray population and found that the cosmic ray ratio in hotspots of FR II galaxies should be of the order 20. RS91 neglected any proton content in the lobes to get a truly minimum energy value. RB93 and Rachen et al. (1993) therefore corrected the energy estimates of RS91 for their more reasonable cosmic ray ratio yielding a factor 3 increase in total lobe energy.

Now we can use the hidden disk luminosity Eq.(6.17), proceed as before and plot radio core luminosities versus disk luminosity. We used the core fluxes listed in Rawlings et al. (1989) and total fluxes from the NED database and converted them into the rest frame just the way we did for quasars. If our estimate for $q_{\rm j/l}$ and our conversion is correct, then the FR II cores should coincide with the quasar cores with one exception: following unification theory, FR II radio cores should mainly occupy a region below the quasar cores as their inclination angles are supposed to be higher.

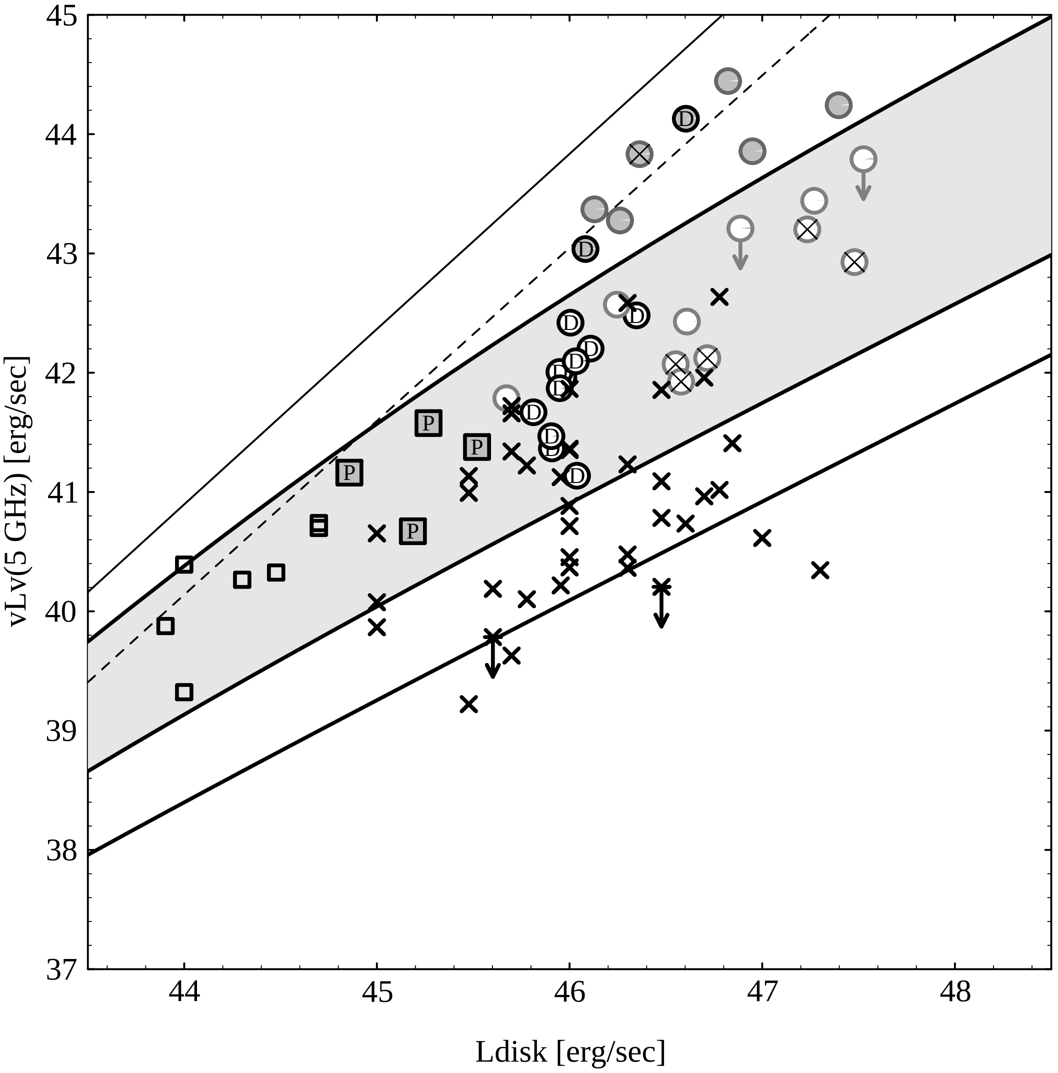

Figure 6.6: Monochromatic luminosity of the compact radio core versus disk luminosity (see text) for radio loud quasars (circles and boxes – see Fig. 6.4) and FR II galaxies with $z < 0.5$ (crosses). The 'disk luminosity' for FR II galaxies was obtained by applying a general conversion factor $L_{\rm disk} = 10 Q_{\rm jet}$ to their lobe powers estimated by RS91. For orientation, we also added the FR I sources used by RS91 (boxes). The shaded band gives our radio loud model for inclination angles of 15° to 45°. The lower grey line is the extension of the band for 90° inclination.

With the conversion factor $q_{\rm j/l} = 0.15$ and $f_{\rm RB93} = 3$ we reproduced our diagram in Fig. 6.6.1 for the radio loud sources only, where small crosses represent the FR II cores. The theoretical 'best fit' radio loud model from Fig. 6.5 is redrawn and the grey line below gives the widening of the band for including up to 90° (edge-on) orientation.
The expected coincidence between FR II radio galaxies and quasars is indeed present. The overlap of these two populations was obtained without further adjusting previously constrained parameters and therefore is an independent test for several conclusions drawn before, e.g. the high jet power $2Q_{\rm jet}/L_{\rm disk} \sim 0.3$. This is also a check for the consistency of the unification theory, and we conclude that the implied scaling of the jet cores with disk luminosity seems to be correct in quasars, as well as in FR II galaxies. Double lobed quasars and FR II galaxies have similar jet properties. A major parameter to influence the core brightness is the inclination angle, and as expected the FR II cores cluster at the lower end of the distribution, such that approximately 2/3 of the FR II cores are close to or below the 45° line of the model.
This effect is highlighted by the core to lobe ratio at 5 GHz (restframe) in both populations for the quasars where the median values are

$$\left\langle \frac{L_{\rm core,quasars}}{L_{\rm lobe,quasars}} \right\rangle = 15\% \qquad \left\langle \frac{L_{\rm core,FR\,II}}{L_{\rm lobe,FR\,II}} \right\rangle = 0.8\% \,. \tag{6.18}$$

If we exclude the two CDQ one would get 8% for the quasars, still the quasars have substantially brighter cores compared to FR II galaxies. This was originally one of the reasons to propose the quasars/FR II unification scheme. Only one of the radio cores (3C341) falls far below the theoretically expected range and one should re-examine the determination of the jet power or look for other pecularities. On the other hand this offset might only indicate the larger uncertainty in determining the hidden disk luminosity.

6.6.2 Extended emission

Does the coincidence of FR II and quasar fluxes also hold if one compares the extended fluxes? Figure 6.6.2 shows the total flux of all sources plotted versus the disk luminosity. FR II sources are again incorporated using the conversion parameter $2q_{\rm j/l} = 0.3$ as before. We used the total luminosity as it is in most cases dominated by the lobes and it is by far the most reliable datum we have. As the lobe emission is assumed to be unaffected by boosting we expect that the total flux of LDQ and FR II show exactly the same distribution. The fact that this is indeed the case is another independent check of the consistency of unification and of our parameter $q_{\rm j/l}$. The distribution scales with the disk luminosity and is very narrow; it scatters only by a factor 3 in both directions – much less than for the core fluxes where different inclination angles broaden the distribution. CDQ are still at the upper end of the distribution, however, they are no longer clearly separated.
We also plotted as a full line the lobe luminosity $2 \cdot L^*_{\rm lobe}$ derived in Chapter 5 from extrapolating the physical situation in the core out to the lobes; the dashed lines are each offset by 0.5 in the log to indicate the scatter. Although the agreement is fairly good, one should be careful with the interpretation as the derivation was very simplified (e.g. the dissipation of kinetic energy is still unclear) and serves only as an order of magnitude check. In our sample consisting of sources with $z < 0.5$ we do not expect strong cosmological evolution, for sources with higher redshift it appears as if indeed there is a tendency for PG quasars to have lower radio flux, perhaps caused by cosmological evolution. Lobes of quasars at higher redshift may be relatively fainter although equally bright in absolute terms, but statistical statements seem to be problematic with this small number of sources and it is suspicious that radio loud and radio weak high redshift PG quasars seem both to be shifted to relatively lower radio emission whereas the other soures do not show this trend.

6.6.3 Extended emission in radio weak quasars

For the radio weak population there also is a correlation between total radio luminosity at 5 GHz and disk luminosity, but the scatter of the distribution is larger than in the radio loud quasars and slightly larger than in the cores alone. In these sources we obviously have a mixture of many contributions. A popular idea is that the diffuse emission is caused by starbursts or starburst-driven superwinds (Baum et al. 1993), but in this case starburst and AGN activity must be strongly linked by the large scale accretion flow in the galaxy to provide this correlation. The alternative explanation than is that a large fraction of the extended emission is caused by diffuse emission from the terminating or disrupting jet flow as seen in many Seyfert galaxies (e.g. NGC1275, see Böhringer et al. 1993 and refs.). This would require the jet to terminate at the kiloparsec scale, which is difficult to explain with the assumption of equal powers for jets in radio loud and radio weak quasars. One

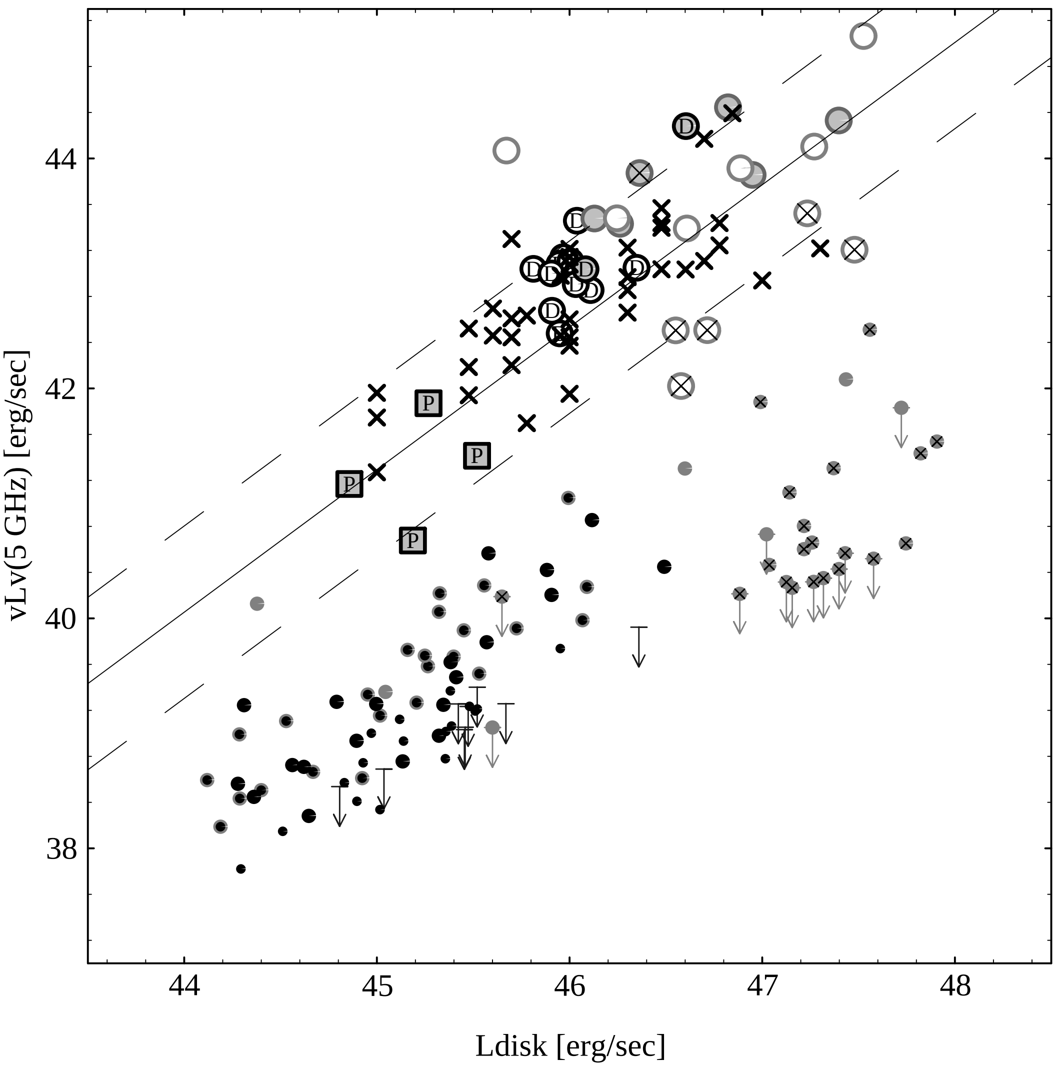

Figure 6.7: Monochromatic total luminosity of quasars (boxes, circles and points – see Fig. 6.4) and FR II galaxies (crosses). The 'disk luminosity' for FR II galaxies was obtained by applying a general conversion factor basing on our analysis to the jet powers (RS91). The radio loud quasar sticking out from the general distribution is the CSS source 3C48.

would have to favour a dichotomy in the jet production itself with a lower $Q_{\rm jet}/L_{\rm disk}$ in radio weak quasars and not a dichotomy in the electron acceleration. On the other hand radio weak quasars are mostly spiral galaxies having a completely different density profile along the rotation axis than elliptical galaxies where radio loud quasars are found, and one might speculate that jets in spirals either terminate almost invisibly far out or very close to the center. Interestingly half of the detected radio weak quasars show no extended emission at all.

6.7 Summary

We used an optically selected quasar sample to test our idea that jet and disk are symbiotic features which are equally important for the overall energy budget of the AGN and are present in radio loud and radio weak quasars. From UV-bump fits we derived empirical relations between disk luminosity and other luminosity indicators (optical continuum, $M_{\rm b}$, OIII, He II and H_β). We then plotted the average disk luminosity of each quasar versus the radio luminosity at 5 GHz of its compact core and find good correlations. This suggests that *compact core radio emission and the UV bump have a common energy source in all quasars.* Using the disk luminosity one has an absolute reference scale to compare objects according to their accretion power. In our UV-radio diagram the quasars split into 4 groups separated by their radio core brightness relatively to the disk luminosity: core dominated quasars (CDQ), lobe dominated quasars (LDQ), radio-intermediate quasars (RIQ) and radio weak quasars.

- For a given disk luminosity the cores of radio loud quasars are brighter than those of radio weak quasars, hence the difference between radio loud and radio weak quasars is established already in the inner parsecs.
- For a given disk luminosity CDQ have the brightest cores due to relativistic boosting.
- AGN must have a disk luminosity $\geq 10^{46}$ erg/sec to be able to become a radio loud quasar and produce a FR II type jet.
- The radio core emission of radio weak quasars scales with the central disk luminosity as well.
- A subsample of flat spectrum variable point sources (RIQ) is substantially fainter than CDQ but almost as bright as the cores of LDQ in a disk luminosity regime $< 10^{46}$ erg/sec, we interpret these sources as boosted radio weak quasars
- The one CSS (3C48) quasar in our sample has a core luminosity comparable to other quasars of the same disk luminosity but a tremendously enhanced total radio flux – the jet is undisturbed in the core but disrupted by environmental effects further out

Together with our previously developed model for the jet core emission, where we added energy and mass conservation of the jet-disk system to the standard emission model, we now can strongly constrain the parameter range for jet models.

- Radio loud cores are the most efficient case of a jet and, given the constraints from the disk luminosity, can only be explained if the energy in magnetic field and relativistic particles represent a large fraction ($\sim 50\%$) of the total jet energy.
- This high power of the relativistic particle distribution in radio loud cores can not be explained by accelerating thermal plasma electrons smoothly into a powerlaw distribution but requires a low-energy cut-off of the relativistic electrons around 50 MeV or the presence of a large population of pairs or both.
- The power of the jet approaches 1/3 of the disk luminosity, therefore the jet is energetically important for the disk structure and evolution.
- The bulk Lorentz factor of the jets are between 3 and 10 and can not be much higher because Doppler boosting would reduce the radio luminosity of the bulk of the population too much, and the width of the distribution would be strongly increased by the random orientation of inclination angles.
- For the same reason the dependence of the bulk Lorentz factors on the disk luminosity must not be very strong ($\gamma_{\rm j} \propto L_{\rm disk}^{\xi}$ and $|\xi| \ll 0.5$).

- The distribution of cores of radio weak quasars can be explained with the same type of relativistic jets as in radio loud quasars but either the ratio $Q_{\rm jet}/L_{\rm disk}$ is lower or radio weak quasars simply do not reach the extreme efficiency in accelerating electrons.
- The properties of CDQ and RIQ are consistent with being the boosted counterparts of radio loud and radio weak quasars respectively.

We conclude that the difference between radio loud and radio weak quasars need not necessarily arise from different kinds of jets and disks but may simply be due to the presence of a highly energetic electron population in the jets of radio loud quasars. Given the limits from mass and energy conservation in the accretion flow and assuming that electrons are accelerated from the thermal regime into a powerlaw distribution it is impossible to get more radio emission than what is seen in radio weak quasars. To produce radio loud cores an additional process is required that either shifts the whole relativistic electron distribution towards higher energies or creates lots of additional particles, i.e. pairs. In Chapter 5 we suggested that hadronic cascades initiated by high energy proton pp or $p\gamma$ collisions might be such a process that could be additionally switched on in radio loud quasars (e.g. due to interactions in the shear layer between jet and ISM). Interestingly, hadronic cascades could explain the high energy gamma-ray emission seen in these objects as well (Mannheim 1993).
With our estimate of the ratio between jet power and disk luminosity, we are also able to estimate the hidden disk luminosity in FR II radio galaxies. By virtue of this method we can insert FR II sources in our UV-radio correlation and show that LDQ and FR II cores as well as LDQ lobes and FR II lobes coincide in this diagram. This demonstrates consistency of our parameter set and of the FR II/quasar unification scheme. In this context we point out that the lack of FR I quasars in our sample – especially in the low power regime below 10^{46} erg/sec – shows that the difference between FR I and FR II can not simply be due to a decrease in disk or jet power alone. There appears to be a critical power of $L_{\rm disk} \approx 10^{46}$ erg/sec below which only extremely few – if any – radio loud quasars with FR II morphology exist.

6.8 Notes on individual sources

PG 0007+106 (III Zw 2): A very unusual quasar which attracted a lot of interest in the past (Kaastra & Korte 1988 and refs. therein). The radio flux density varies more than a factor 30 and shows flare like events on a timescale of one year. Variability is found at all other wavelengths as well from infrared to X-rays. Past VLBI experiments found some 80% of the total flux in a compact core and a jet like extension at PA 148°. Unger et al. (1993) found a weak component 30 kpc away from the core with the VLA at 1.5 GHz not seen at 5 GHz. The core flux density has varied from 425 mJy to 40 mJy at 8.4 GHz between June 1991 and Oct. 1992 (Patnaik, A., p.c.). Large and fast changes of the polarization angles at 4.8 GHz and 8 GHz, outbursts on a month timescale and variability $<$ 10 days at 37 GHz have been found (Aller et al. 1985, Teräsranta et al. 1992). These are typical signs for boosted jet emission, however, III Zw 2 seems to fall on the extrapolation of the lobe dominated quasars and not of the CDQ. We consider this source as the archetype of RIQs.
PG 0044+030: This source has a relatively low total flux and appears diffuse elongated on a recent VLA map at 20 cm while at 6 cm only the core prevails (Price et al. 1993).
PG 0157+001: We regard the core flux given by KSSSG (5.9 mJy) of this compact source as an upper limit for a flat spectrum core. The spectrum by Barvainis & Antonucci (1989) of the VLA peak flux does show a very steep spectral index ($\alpha \sim -1$) and there is no indication of a flat component above 1 mJy. In addition the KSSSG core flux would make 0157+001 also a possible candidate for being a RIQ which we think is not justified in light of the spectral form. On the other hand 0157+001 has a host galaxy which is almost face on (Hughes et al. 1993) and hence if the jet axis is related to the rotation axis of the galaxy there is a high probability for getting enhanced emission due to boosting.
0232-042: A triple radio source at VLBI scales with a strong bent. The core flux is from Saikia et al. (1984).
0237-233: This is a GPS source with two components (lobes?) at the VLBI scale. The spectrum continues to be steep up to 31 GHz and we can only estimate an upper limit for a flat component of $f_{\rm c} \approx 0.1$ which seems to be consistent with the overall picture.
0134+329, 3C 48: is a famous CSS. High resolution maps (Wilkinson et al. 1991) show a compact core and a hotspot plus a huge amount of diffuse emission making this source outstandingly bright in total flux. Due to an unusually low core/lobe ratio of 0.007 the core flux is consistent with other radio loud objects. This strengthens the idea that 3C 48 is powered by an ordinary radio jet where disruption by environmental effects close to the nucleus causes an enhancement of the (lobe) radio emission.

0414-060, 3C 110: This source is unresolved (Ekers 1969) and the mean value of .11 for the lobe to core ratio we assigned to this source may be inappropriate (see 3C48) but the spectrum is steep with a slight flattening at higher frequencies which might indicate the presence of a weak flat component.
0710+457, Mkn 376: We took 1.6 mJy as VLA core flux at 5 GHz from Neff & Hutchings (1992). The source is compact (< 0.8") and if the total flux of 21 mJy is correct than Mkn 376 has relatively bright extended emission.
0955+326, 3C232: Akuyer et al. (1994) show a map of a compact ~ 1" source and quote a flattening of the spectrum to $\alpha = -0.2$ between 1.4 GHz and 408 MHz therefore it might be a compact steep spectrum source (CSS) or even a GHz peaked source (GPS) and the assumed value for the core lobe ratio is very uncertain although the source fits into the general trend. The total emission however is at the upper end of the distribution
PG 1008+133: UV-bump fit and M_{b} yield disk luminosities which differ by more than a factor 20 so that the average disk luminosity is completely uncertain. We excluded this source from our fit to the $L_{\mathrm{disk}} - M_{\mathrm{b}}$ correlation.
PG 1206+459: UV-bump fit and M_{b} disk estimates differ by a factor 100 (same as PG 1008+133).
PG 1309+335: MRS report a total flux density of 54 mJy concentrated in a single core component. The flux was $\sim 35\%$ brighter than in previous surveys (Gregory & Condon 1991: 40 mJy, Becker et al. 1991: 35 mJy). The spectrum is flat and it is a point source at the VLA. In our diagram it occupies the region around III Zw 2; we consider it a RIQ as well.
PG 1211+143: This source was obviously misidentified in KSSSG and we take the fluxes given by MRS.
PG 1333+176 has a core/lobe ratio of 1.2 in KSSSG indicating variability and very weak extended emission. Nevertheless this source is at the lower end of the radio loud sources and one might speculate that this is another example of a RIQ quasar. The total emission is at the extreme lower end for radio loud sources.
PG 1351+640: This is a variable point source. The flux dropped by a factor of 6 within 4 years (Barvainis & Antonucci 1989). In Fig. 6.4 it clearly stands out from the normal population but does not quite reach the RIQ. One is tempted to call this source an intermediate RIQ source. The fact that the light curve showed a steady decline over 4 years and not a wiggling around an average value makes it difficult to classify the source at present because our averaging procedure gives a biased result. Using the data of KSSSG only lowers the radio flux substantially although it would still be well above the radio weak population. Like 1333+176 one will need more data to come to an unambigious conclusion. Interestingly McLeod & Rieke (1994) find that this is one out of three sources where the luminosity profile is better fitted by an elliptical than by a disk galaxy.
PG 1407+265: was classified as radio loud by Sanders et al. (1989) which is in clear contradiction to its position in Fig. 6.4 and we labeled it radio weak especially as the core/lobe ratio (~ 0.4) is fairly high.
1501+106: This source had originally a fitted disk luminosity which was a factor 10 higher than what we estimated from the other luminosity indicators because it was the only object where SM89 made an extreme (high $\dot{M}$) fit to try to hit the strong soft X-ray excess. We now redid this and went only for a good fit to the optical/UV data which lowered the disk luminosity estimate substantially.
PG 1634+706: Barvainis & Antonucci (1989) find a slightly inverted spectrum for the VLA peak flux; thus at least here the assumption of a flat spectrum core seems to be justified.
PG 1700+518: A broad absorption line (BAL) quasar like PG 1411+442, was labeled a RIQ by MRS because of its high total flux which is caused by two compact knots separated by 0.9"where the optical nucleus is close to the brighter radio peak. Considering its core flux this source is not outstanding at all and also lacks the other characteristic features of a RIQ as we define it (pointlike appearance and variability). It appears more likely that like in CSS and GPS environmental effects cause the enhancement of the total radio flux by disrupting a weak radio jet.
E1821+643: This is a giant elliptical galaxy in the center of a rich cluster with a very luminous AGN. Radio core and jet structure are seen in the center but the total radio flux is very low (Hills et al. 1992). In our diagram it is placed on the upper end of the radio weak distribution supporting the impression that this is a radio weak jet in an environment usually producing radio loud quasars.
2041-109,Mkn 509: VLA data by Barvainis & Antonucci (1989) indicate a flattening of the spectrum beyond 5GHz so that there is indeed a flat component. We took 1.8 mJy as core flux at 5GHz from Neff & Hutchings (1992).
PG 2209+184: VLA total fluxes for this source (z=0.07) at 5 GHz are reported to be between 120 mJy (MRS) and 290 mJy (KSSSG, claimed to be in error by Miller et al.) with a VLA core flux $> 95\%$ of the total flux and a low brightness knot ($S_{4.8\mathrm{GHz}} \simeq 3$mJy/beam). The spectrum is inverted between 5 GHz and 1.4 GHz ($\alpha = -0.24$). Only recently Machalski & Magdziarz (1993) explicitly identified this source as variable with total

fluxes at 5GHz between 116 mJy and 326 mJy. Like III Zw 2 we classify it as a RIQ.

Chapter 7

Unified unification

7.1 Introduction

Mass accretion onto a compact massive object is assumed to power all energetic phenomena seen in active galaxies like bright non-stellar contiuum emission (either directly observed indirectly inferred from the presence of broad and narrow emission lines), high energy (γ-ray) emission, and large scale bipolar outflows (radio jets). Interestingly these different signatures of activity are rarely seen all together and the variety of active galaxies is somehow confusing. Numerous attempts try to unify different classes by arguing that relativistic beaming and an obscuring dust torus may provide completely different views of the same object if seen under different aspect angles. The work by Lawrence & Elvis (1982), Mushotzky (1982) and Antonucci & Miller (1985) suggested that Seyfert 2 galaxies are just Seyfert 1 galaxies where an obscuring torus blocks our view of the central engine. Barthel (1989) extended the same idea to unify quasars and FR II radio galaxies. The enigmatic BL Lacs could be understood if they are the relativistically boosted counterparts of FR I radio galaxies seen under small aspect angles (Blandford & Rees 1978; Padovani & Urry 1990). More detailed reviews on these topics were given by Antonucci (1993), Wilson (1992) and Gopal-Krishna (1994).

In this work and in related papers (Falcke & Biermann 1994, hereafter FB94; Falcke et al. 1994, hereafter FMB; see also Falcke et al. 1993 a&b) we have attacked the problem from another side, starting with the basic ansatz that jet and disk in quasars form a closely coupled, symbiotic system which basically should be the same in all galaxies except for different accretion rates and black hole masses, while the host galaxy is expected to influence the central engine only at scales beyond ~ 1 pc eventually leading to different tori. This ansatz would imply the presence of initially powerful and relativistic jets in all active nuclei and explains the close correlation between radio emission and disk luminosity in radio loud and radio weak quasars (Rawlings & Saunders 1991; FMB).

We now want to show that the different unification schemes and our ansatz can be combined to yield one homogenous concept for active galaxies by postulating a slightly different geometry of the obscuring torus in ellipticals.

7.2 The radio loud quasar void

Although signs of activity in quasars come in all possible combinations there is one striking exception to that rule: *the jets of radio loud quasars never appear with FR I type morphology.* This statement can easily be verified by studying a quasar sample we have used in this work (Chap. 6), e.g. the PG quasar sample (Schmidt & Green 1983). Miller et al. (1993) have investigated the radio morphology of this sample for sources with $z < 0.5$ using the VLA. Out of 89 quasars 13 can be considered as radio loud and all of them show a core/lobe morphology rather typical for FR II radio galaxies. Four radio-intermediate quasars (RIQ) are flat spectrum variable point sources while the remaining 72 radio weak quasars have either pointlike or diffuse emission in the center. Not a single quasar has anything comparable to a FR I type jet.

This becomes even more peculiar if one inspects the radio/optical diagram of the whole PG sample (Fig. 7.2 & 6.4) where the radio core luminosity was plotted vs. the 'disk luminosity'. Radio weak quasars occupy the whole range from 10^{44} erg/sec to 10^{48} erg/sec in disk luminosity while there is not a single radio loud quasar below $\sim 10^{46}$ erg/sec with extended radio emission. The four RIQ found in this regime have radio properties typical for boosted radio sources (core dominated quasars) and have been interpreted as *boosted radio weak quasars*

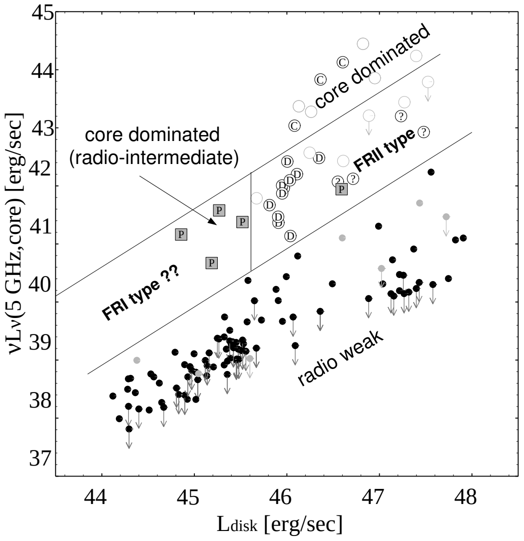

Figure 7.1: Radio core luminosity vs. the disk luminosity of PG quasars. Below $L_{\rm disk} \sim 10^{46}$ erg/sec no radio loud quasars of FR II type are found (see Chap. 6 for details) – *open circles*: radio loud quasars, 'D' marks FR II morphology and 'C' marks core dominated quasars; *dots*: radio weak quasars; *boxes*: variable flat spectrum points sources, interpreted as boosted radio weak quasars; *grey symbols:* non-PG quasars from the extended sample of FMB.

(Miller et al. 1993; FMB; Cahp. 6). On the other hand we can not yet completely exclude the possibility that these are the very rare cases of (BL Lac-like) FR I type quasars seen under small aspect angles[1].
The absence of low-luminosity FR II type radio loud quasars can not be a selection effect because the low-luminosity region is crowded by 68 radio weak quasars of this optically selected sample. If there would have been any FR II type radio loud quasars with lower disk luminosity than 10^{46} erg/sec they would have easily been detected. This break in disk luminosity directly reminds one of the FR I/FR II radio luminosity break (Fanaroff & Riley 1974). Below a critical radio luminosity FR II morphologies disappear and FR I morphologies appear. A straight forward interpretation of the radio break is that below a critical jet power the originally well collimated and supersonic jet is slowed down (external pressure, mass entrainment) and becomes a low Mach number jet producing the irregular FR I type morphology (Gopal-Krishna 1991, Bridle 1992). Jets above the critical power remain highly supersonic and terminate far away in a strong shock producing lobes and hotspots. This picture implies a transition from FR II to FR I with decreasing power and – believing that jet and 'UV-bump' in quasars are produced by the same engine – we naively would expect the same effect to happen in quasars: lower accretion power (i.e. disk luminosity) implies lower jet power (i.e. radio power) and below a critical disk luminosity FR II jets should turn into FR I jets. Obviously this is not true. The disappearance of FR II quasars below a critical luminosity is observed but there is no appearance of FR I quasars at any lower power. Hence we are lead to the speculation that *the void of radio loud quasars below* 10^{46} *erg/sec is actually the void of FR I quasars.*

7.3 Unified unification scheme

7.3.1 The closed torus

How is it possible to *directly* link the disappearance of the quasar activity with the transition between the two jet morphologies? It was suggested that FR I have qualiatively different engines where most of the power is channeled into the jet and not into disk radiation (cf. Rees et al. 1982; Heckman et al. 1994) but FR I and FR II look very similar close to their cores (Bridle 1992).
What if an obscuring torus is resposible for this effect as well? In the FR II/quasar unification scheme the ratio of quasars to FR II galaxies gives the opening angle of the torus ($\sim$ 60deg). The same logic strictly applied to

[1] This would falsify our hypothesis of relativistic jets in all quasars but strengthen our conclusion of a closing torus.

quasars and FR I galaxies would yield an opening angle of $\sim$ 0deg – there are no FR I quasars. Considering that FR I galaxies will appear as BL Lacs for small aspect angles the opening angle will actually have a non-zero value.

7.3.2 Consequences for FR I/FR II dichotomy

Hence, we infer a power dependent opening angle of the obscuring dust torus in radio galaxies (see also Gopal-Krishna 1994) such that below a critical power of the central engine the torus is almost closed. This would have several interesting effects for quasars below the critical power:

- The optical emission from the nucleus is effectively blocked by the closed torus, almost irrespectively of the inclination angle – similar to the 'hidden quasar' picture (Sanders et al. 1988) for evolving quasars.
- The jet will strongly interact with the torus, slow down and entrain matter from the torus. This can change the jet morphology to FR I type (see Bicknell 1994).
- The intrinsically weak FR I jets with narrow torus opening angle ($< 10^{\mathrm{deg}}$) would be identified as radio galaxies from most of the viewing directions, except when viewed almost down the jet where beaming would lead to a BL Lac classification (Gopal-Krishna 1994, Gopal-Krishna et al. 1994); the closed torus could still obscure a substantial fraction of thermal continuum and emission lines.

The *closed torus* concept is only a subtle change to the general picture as an obscuring torus will be present in FR I if they are low-power counterparts to FR II. The big advantage, however, is that there is no need for different engines in FR I & FR II. We will not specify the nature of the torus any further as it could be anything, from the inner edge of an extended dusty disk to a spherical distribution of clouds or even of stellar envelopes.

7.3.3 Opening the closed torus

What could be the reason for the different opening angles? Following our arguments it should be linked to the engine power. The simplest possibility is that 'tori' in active elliptical galaxies are always closed and the jet first has to plow through the matter. For a gas mass of $M_9 10^9 M_\odot$ which is compatible with the IR spectrum (see Chini et al. 1989, Niemeyer & Biermann 1993), i.e. a density of $n_{10}10^{10}\mathrm{cm}^{-3}$ within a radius of $R_\mathrm{c} = r_\mathrm{pc}pc$, the jet may entrain matter until it is slowed down to the escape velocity of $\sim 3000\,\mathrm{km/s}\,\sqrt{M_9/r_\mathrm{pc}}$ – which is a typical velocity for FR I jets (Bicknell 1994). The momentum of the jet $\leq 1/3\, L_{46}/c\, 10^{46}$ erg/s (Chap. 5) than provides a lower limit for the time scale

$$t_\mathrm{open} \geq 2 \cdot 10^8\,\mathrm{yr}\, M_9^{3/2} L_{46}^{-1} r_\mathrm{pc}^{-1/2} \tag{7.1}$$

on which the jet can push a substantial amount of matter outwards. Consequently quasars with luminosities $L_\mathrm{disk} \ll 10^{46}$ erg/sec would never be able to open the torus on a reasonable time scale while quasars with $L_\mathrm{disk} \gg 10^{46}$ erg/sec could.

7.4 Difference between radio loud and radio quiet

7.4.1 A closed torus only in ellipticals?

What are the consequences of this concept for the difference between radio loud and radio quiet quasars? To answer this question the difference of the host galaxies may become important. While FR I/FR II radio galaxies and radio loud quasars are almost exclusively found in ellipticals most radio quiet quasars and all Seyfert nuclei reside in spiral galaxies (e.g. McLeod & Rieke 1994). The exact way of the mass transport from the large scales to the center within both types of galaxies is not yet exactly clear, nevertheless, it is quite obvious that in spiral galaxies the mass transport will happen within the disk, perhaps stirred by starbursts (Biermann et al. 1993). The core radii of these galaxies are very small and as we know from our Galaxy and M31 a disk structure can be found down to the pc scales. Therefore it is no surprise that matter flowing into the center will have large angular momentum and maintain a disk structure. The torus may never get closed.

In ellipticals the situation is very different. Their core radii can be much larger ($\geq$ 200pc) than in spirals (see Gerhard 1992) and the gravitational potential will be more or less spherical. The formation of ellipticals may be connected to violent merging of two galaxies, with effective matter and angular momentum transport. It is imaginable that under these cirumstances formation of a more spherical matter distribution occurs (Camenzind 1993). Jet/torus interaction would then be important only in elliptical galaxies.

7.4.2 Jet collimation

In theoretical studies (Appl & Camenzind 1993 a&b) of jet formation it was pointed out that after the initial phase external pressure is needed to confine the jet, but for this mechanism to work pressures 10^{10} times higher than normal ISM pressures are needed. This can be avoided if dynamical interaction with the dense torus is considered instead. The proposed closed torus in ellipticals necessarily will confine the jet while the open torus in spirals will not, thus making the diffuse radio emission in quasars and broad uncollimated outflows in Seyferts understandable.

7.4.3 Making a jet radio loud

Radio loud jets are extremely efficient radio emitters. Considering mass and energy conservation in the jet/disk system the amount of electrons needed to produce the observed synchrotron emission is a factor 100 higher than what is available in the jet plasma (Chap. 4). We suggested that injection of pairs with a low-energy cut-off could solve this problem and noted that because of strong synchrotron losses at small scales the pair creation must take place $\sim 10^{18}$ cm from the nucleus. As injection mechanism we proposed the pion decay following *pp* collisions which results in a relativistic $e^{\pm}$ spectrum with low energy cut-off around 100 MeV.
As dense targets for the shock accelerated relativistic protons in the jet (Biermann & Strittmatter 1987, Sikora et al. 1987) we suggested either stars, BLR clouds or a dense boundary layer between jet and ISM. In the FR I scenario outlined in this chapter the dense torus would be another natural target for the relativistic protons. Taking the *pp* cross section of $\sigma_{\rm pp} = 6 \cdot 10^{-26}{\rm cm}^2$ we find that the optical depth to *pp* collision is $\tau_{\rm pp} = 2 \cdot 10^3 n_{10} r_{\rm pc}$. Thus, only a low probability that relativistic protons enter the high density regime is required to produce a large population of seconary pairs.
The situation in FR II appears more complicated as we require an optically thin regime between torus and jet. Nevertheless, the torus is still very close and interaction between jet and torus may still take place. This could be due to either an instable configuration of the hollowed torus or due to a wind initiated by heating through the central source (e.g. Balsara & Krolik 1993 scaled to FR II). However, the jet may not pick up much more matter as it contains itself without being strongly disturbed. This corresponds to a massflow of $\sim 0.01\dot{m}_{-2}M_{\odot}/{\rm yr}$ (i.e. 1% of accretion rate, see Chap. 4) in shear layer and jet for an engine at the FR I/FR II break. If the pick-up is caused by the magnetic field $B = (b \cdot {\rm Gauss})(r_{\rm pc} \cdot {\rm pc})^{-1}$ in the jet the scale for the interaction zone will correspond to the gyro radius of the thermal matter with respect to the relativistic jetflow with Lorentz factor $10\gamma_{10}$ and width $r/10$. Hence the density of the turbulent, thin shear layer is expected to be of the order

$$n_{\rm sl} = 2 \cdot 10^{10}\,{\rm cm}^{-3}\; b\,\dot{m}_{-2}\gamma_{10}^{-2} r_{\rm pc}^{-2}, \qquad (7.2)$$

providing a possible collision site at least for low energetic protons *along* the jet. The details of this will also depend on the local magnetic field topology and the acceleration and diffusion processes for relativistic particles which is far beyond the scope of this work. We finally remark that FR I, though having stronger interactions, will not be radiatively more efficient than FR II as the energy of the newly created pairs is limited by the proton energy density.
In spiral galaxies with a strongly reduced jet/torus interaction *pp* collisions might be very inefficient so that the relativistic electrons are limited to the number of particles in the jet plasma which is just enough to explain radio weak quasars (Chap. 5&6). If neither shear layer nor torus are the main targets for *pp* collisions but stars or BLR clouds then one would have to postulate a different geometry of stars or BLR in spirals and ellipticals to explain the different radio emission. As a consequence the link between the FR I/FR II/quasar picture described here and the radio loud/quiet dichotomy would be less direct – if present at all.

7.5 Conclusions

Current unification schemes can only be reconciled with the 'FR I quasar void' if the transition from FR II to FR I jet morphology is *directly* linked to the disappearance of the quasar signature. This is possible if the *obscuring torus in most ellipticals is almost closed*, i.e. the opening angle is a few degrees or less. Although

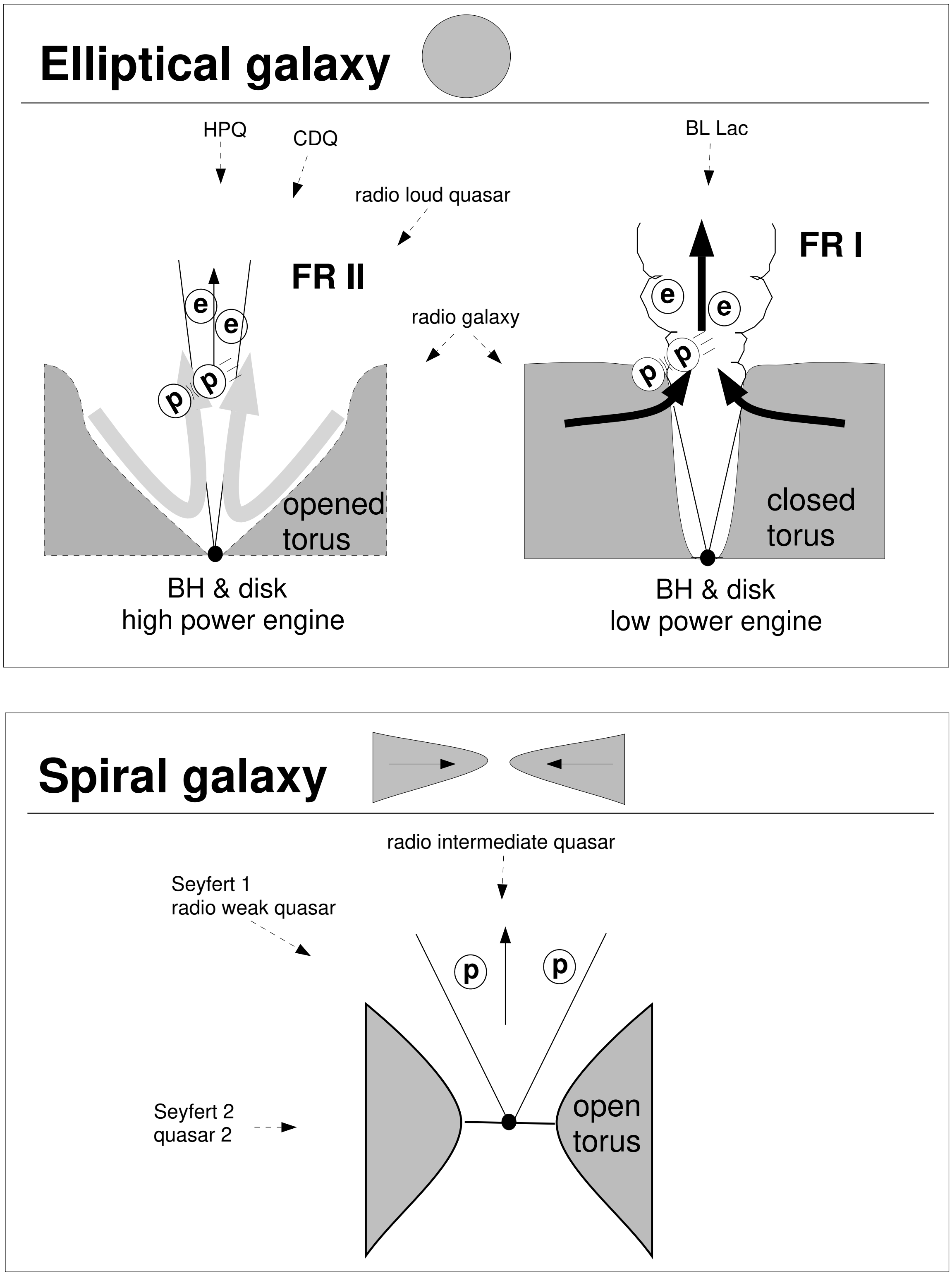

Figure 7.2: *Upper panel* – elliptical galaxies with initially closed torus: a low-power (FR I) jet is slowed down by the torus which also obscures the central engine while a high-power (FR II) jet carries away a large part of the torus. Proton-proton collisions produce an excess population of secondary $e^{\pm}$ pairs making the jet radio loud. The jet/torus interaction might also help to collimate the jet.
Lower panel – spiral galaxy with initially open torus: The lack of jet/torus interaction neither leads to jet collimation nor to pp collisions producing excess secondaries, leaving the jet radio weak.

being only a subtle change to existing theories this concept seems promising – *the jet/torus interaction can explain simultaneously FR I/FR II structure and efficient injection of $e^{\pm}$ pairs (radio loudness).* The closed torus will block optical and line emission in FR I and BL Lacs, interaction with a jet (entrainmnet) changes the jet morphology below a critical jet/disk power and opens the torus above making the quasar visible only for high power engines. The torus could also collimate the jet and serve as a target for pp collisions. The latter leads to injection of an excess population of relativistic $e^{\pm}$ pairs explaining the high radiative efficiency of the radio cores. This would not happen if the torus is initially open (in spirals?) leaving the jet uncollimated and radio weak. Consequently one can attribute all differences in the AGN zoo to the pc scale where an influence of the host galaxy is much more reasonable and allow the same type of engine (e.g. black hole/disk/jet) to be present in every nucleus (see 7.5).

Here we are only able to outline the basic concept for a unified unification scheme. Future work needs to concentrate on the stability and formation of the torus in different host galaxies and its interaction with a jet. It also has to be discussed how the accretion rate depends on the galaxy type to explain the apparent differences in host galaxies between FR I and FR II (e.g. Smith & Heckman 1989).

Observational consequences are expected mainly in the high energy regime, i.e. production of X-rays and gamma-rays (Mannheim 1993) as consequence of the jet/torus interaction. Because of entrainment FR I jets should be much heavier than FR II jets. From the different torus geometries one expects a luminous warm dust component (radiating shortwards of $10\mu m$) and a cold dust component in FR I yielding a more bumpy infrared spectrum while the FR II infrared spectrum could be much smoother (see Heckman et al. 1994). The power dependence of the torus opening angle also predicts a luminosity (and redshift) dependence of the ratio between quasars and radio galaxies (see Gopal-Krishna 1994). If radio weak quasars have similar engines one expects a population of boosted (flat spectrum) radio weak quasars as well.

Chapter 8

Discussion

As a consequence of this thesis a model capable of explaining the diversity of active galaxies emerges based on only four fundamental ingredients. The basic concept is an accretion disk around a black hole producing a jet which interacts with a dense, obscuring torus – none of these ingredients can be treated separately but one has to consider all four in an integrated system. The overall scheme we have developed obeys a few principles:

- The active engine in the very center of galaxies is basically the same everywhere – including black hole, disk and jet – except for different black hole masses and accretion rates.
- Jet and disk are closely coupled and of comparable importance for the overall energy budget.
- The presence of a nearly closed, obscuring torus in ellipticals can modify the appearance of jets strongly and leading to the difference between FR I & FR II, quasars & radio galaxies and radio loud & radio weak.
- An important mechanism for the injection of relativistic electrons is pair creation in hadronic cascades following *pp* collisions producing a low-energy cut-off around 100 MeV.

We have modified the standard paradigm only slightly by considering the consequences of coupling and interaction between the basic ingredients. But although the parametrization of the coupling is very simple, this modification promises substantial progress as it appears possible to naturally unify the whole zoo of active galaxies. If the obscuring torus in ellipticals is indeed almost closed as a consequence of angular momentum mixing in the process of galaxy merging, the jet/torus interaction can lead to a disruption of low power jets while completely obscuring the nucleus (i.e. FR I radio galaxy), the production of a large population of $e\pm$ pairs to explain radio loudness and might also serve to collimate the jet. Thus it would be understandable why there are no FR I quasars and why radio loudness depends so strongly on the host galaxy.
Here it is important that one model can explain the characteristics of a variety of AGN – the monsters – as well as the Galactic Center source Sgr A* – a monster on a starvation diet. We can not claim to have proven beyond any doubt that the standard paradigm for nuclear activity is correct but it is able to explain the observed phenomena over a luminosity range of 10 orders of magnitude and over at least 8 orders of magnitude in frequency – to highlight this Fig. 8 presents an overview over the whole range of disk and radio luminosities covered in this thesis withh the addition of a few more sources to stimulate further investigations. Moreover, the parameters we have derived here for the central engines are in agreement with the results of many other studies before and as a byproduct of this line of thinking we obtain a grossly extended unification scheme. Therefore one should not easily abandon the one paradigm (black hole/disk/jet/torus) in favour of a variety of exotic models because not every detail does yet fit into the general picture. We have to remember that the number of parameters we really can constrain by observation is still fairly small and hence the predictive power of AGN models remains very limited. We may get an idea about gods creation but we will never be able to rebuild it in our computers.

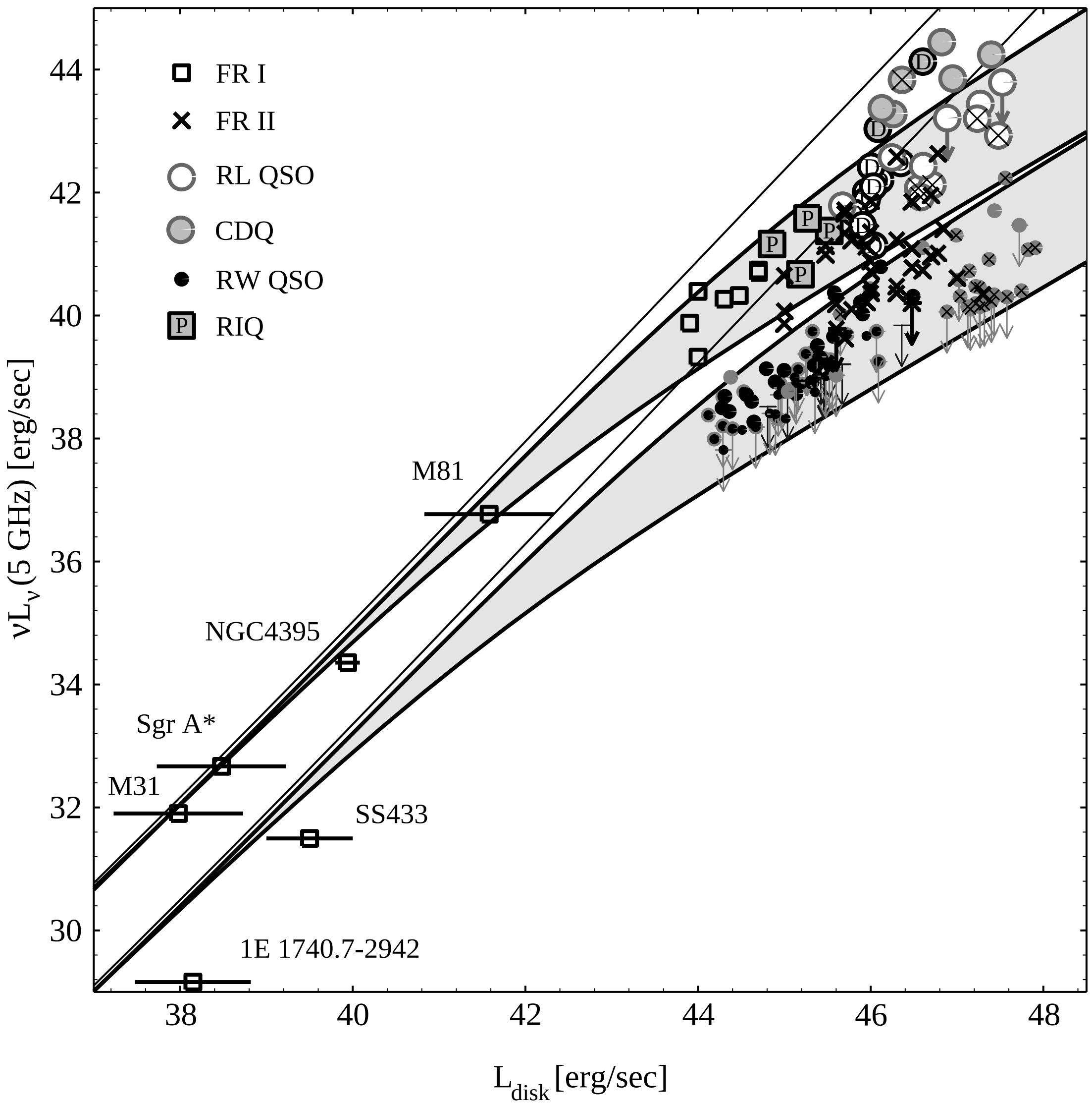

Figure 8.1: Monochromatic luminosity of the compact radio core versus disk luminosity (see text) of various sources of astrophysical interest: radio loud and radio weak quasars (circles and dots), FR II & FR I radio galaxies (crosses and boxes) where $L_{\rm disk}$ was estimated as described in Chapter 6. The shaded band represents our best fit model derived for quasars in Chapter 6 giving reasonable fits also for the low power sources (boxes with error bars) which were selected randomly. Vertical error bars reflect systematic uncertainties in the determination of $L_{\rm disk}$ rather than statistical errors; the available radio flux measurements of the radio cores (VLBI or VLA) were averaged without indicating this variability in the plot. A more detailed treatment of the low power regime will be presented elsewhere, it seems however interesting that the two galactic jet sources with stellar mass central objects separate from the four supermassive black hole candidates in the nuclei of nearby galaxies.

Chapter 9

Publications

This is a list of publications and ongoing projects which have emerged from this thesis or are otherwise related.

1.) Falcke H., Biermann P.L., Duschl W. J., Mezger P. G. 1993a, A&A 270, 102 (FBDM)
"A rotating black hole in the galactic center"

2.) Falcke H., Mannheim K., Biermann P.L. 1993b, A&A 278, L1
"The Galactic Center radio jet"

3.) Falcke H., Biermann P.L. 1994c, to appear in the proceedings of the conference on "Mass Transfer Induced Activity in Galaxies", Shlosman I. (ed.), Lexington 1993
"The Galactic Center - An AGN on a starvation diet"

4.) Falcke H., Biermann P.L. 1994a, A&A, in press
"The jet/disk symbiosis I. Radio to X-ray emission models for quasars"

5.) Falcke H., Malkan M., Biermann P.L. 1994, A&A, submitted "The jet/disk symbiosis II. Interpreting the Radio/UV correlations in quasars"

6.) Falcke H., Heinrich O. 1994, A&A, in press
"Starved disks in the center of galaxies: The examples of Sgr A* and M31"

7.) Falcke H., Gopal-Krishna, Biermann P.L. 1994, A&A Letters, submitted
"The missing FR I quasars – a clue for unifying unification schemes"

8.) Biermann P.L., Strom R., Falcke H. 1994, A&A, submitted
"Comic rays V. The nonthermal radioemission of the old nova GK Per – a signature of hadronic interactions"

9.) Bednarek W., Falcke H. 1994, to be submitted to A&A "Gamma-rays from Sgr A*"

11.) Falcke H., Biermann P.L. 1994b, in preparation
"The jet/disk symbiosis III. Sgr A* and the AGN connection"

10.) Falcke H. 1994, invited contribution to the IAU Symp. 169, in preparation
"What is Sgr A*?"

12.) Falcke H., Scherer H., Schmutzler T., Biermann P.L., 1994, in preparation
"Heating the ambient medium of Sgr A* and the effects of a Kerr hole"

13.) Marecki A., Falcke H., Patnaik A. 1994, in preparation
"A complete sample of GHz-peaked sources"

Chapter 10

References

Abramowicz M.A., Piran T. 1980, ApJ 241, L7

Akuyer C.E., Ludke E., Browne I. et al. 1994, A&A in press

Aller H.D., Aller M.F., Latimer G.E., Hodge P.E. 1985, ApJS 59, 513

Antonucci R. 1993, ARA&A 31, 473

Antonucci R., Barvainis R. 1988, ApJ 332, L13

Antonucci R., Miller J. 1985, ApJ 297, 621

Appl S., Camenzind M. 1993a, A&A 274, 699

Appl S., Camenzind M. 1993b, A&A 270, 71

Böhringer H., Voges W., Fabian A.C., Edge A.C., Neumann D.M. 1993, MNRAS 264, L25

Backer D.C., Zensus J.A., Kellermann K.I., Reid M., Moran J.M., Lo K.Y. 1993, Sci 262, 1414

Balick B., Brown R. L. 1974, ApJ 194, 265

Balsara D.S., Krolik J.H. 1993, ApJ 402, 109

Bardeen J.M. 1970, Nat 226, 64

Barthel P.D. 1989, ApJ 336, 606

Barvainis R., Antonucci R. 1989, ApJS 70, 257

Becker R.L., White R.L., Edwards A.L. 1991, ApJS 75, 1

Bednarek W., Falcke H. 1994, to be submitted to A&A

Bicknell G.V. 1994, ApJ 422, 542

Biermann P.L., Duschl W.J., Linden S.v., 1993, A&A 275, 153

Biermann P.L., Strittmatter P.A. 1987, ApJ 322, 643

Biermann P.L., Strom R., Falcke H. 1994, A&A, submitted

Blandford R.D., Königl A. 1979, ApJ 232, 34

Blandford R.D., Znajek R.L. 1977, MNRAS 179, 433

Blandford R.D., Rees M. 1978, in: "Pittsburgh Conference on BL Lac Objects", Kluwer, Wolfe A.M. (ed.), p. 328

Blumenthal G.R., Gould R.J. 1970, Rev. Mod. Phys. 42, 237

Boroson T.A., Green R.F. 1992, ApJS 80, 109 (BG92)

Bridle A.H. 1992, in: "Testing the AGN Paradigm", AIP, Holt, Neff & Urry (eds.), p. 386

Bridle A.H., Perley R.A. 1984, ARAA 22, 319

Brunner H., Lamer G., Staubert R., Worrall D.M. 1994, A&A, in press

Camenzind M. 1986, A&A 156, 137

Camenzind M. 1993, talk presented at the Kolloquium "Gamma-Emission von Quasaren und BL Lac Objekten", Landessternwarte Heidelberg-Königsstuhl, Nov. 1993

Carter B. 1968, Phys. Rev. 174, 1559

Celotti A., Fabian A. 1993, MNRAS 264, 228

Chini R., Biermann P.L., Kreysa E., Gemünd H.-P. 1989b, A&A 221, L2

Chini R., Kreysa E., Biermann P.L. 1989a, A&A 219, 87

Clarke C.J., Lin D.N.C., Pringle J.E. 1990, MNRAS 242, 439

Cox P., Laureijs R. 1989, in: Morris M. (ed.), The Galactic Center. Proc. IAU Symp. 136, p. 121

Cox P., Mezger P.G., 1989, A&AR 1, 49

Cunningham C. 1975, ApJ 202, 788

Dermer C.D., Schlickeiser R. 1993, ApJ 416, 458

Dermer C.D., Schlickeiser R. 1994, ApJS, in press

Drury L.O'C. 1983, Rep. Prog. Phys. 46, 973

Duschl W.J., Lesch H. 1994, A&A, in press

Duschl W.J., Tscharnuter W.M., 1991, A&A 241, 153

Eckart A., Genzel R., Krabbe A., Hofmann R., van der Werf P.P., Drapatz S. 1992, Nat 355, 526

Ekers R. 1969, Aust. J. Phys. Astrophys. Suppl. 7, 1

Falcke H. 1992, Diploma Thesis, RFW Universität Bonn

Falcke H. 1994, Proc. of the IAU Symp. 169, in prep.

Falcke H., Gopal-Krishna, Biermann P.L. 1994, A&A Letters, submitted

Falcke H., Biermann P.L. 1994a, A&A, in press

Falcke H., Biermann P.L. 1994b, in preparation

Falcke H., Biermann P.L. 1994c, to appear in the proceedings of the conference on "Mass Transfer Induced Activity in Galaxies", Shlosman I. (ed.), Lexington 1993

Falcke H., Biermann P.L., Duschl W. J., Mezger P. G. 1993a, A&A 270, 102 (FBDM)

Falcke H., Heinrich O. 1994, A&A, in press

Falcke H., Malkan M., Biermann P.L. 1994, A&A, submitted

Falcke H., Mannheim K., Biermann P.L. 1993b A&A 278, L1 (FMB)

Falcke H., Scherer H., Schmutzler T., Biermann P.L. 1994, in preparation

Fanaroff B.L., Riley J.M. 1974, MNRAS 167, 31P

Fanti R., Fanti C., Schilizzi R.T. et al. 1990, A&A 231,333

Fath E. A. 1909, Lick Obs. Bull. 5, 71

Genzel R., Townes C.H. 1987, ARA&A 25, 377

Gerhard O. 1992, in: "Physics of AGN", Springer Verlag, Duschl & Wagner (eds.), p. 273

Ghisellini G., Guilbert P.W., Svensson R. 1988, ApJ 334, L5

Ghisellini G., Maraschi L., Treves A. 1985, ApJ 146, 204

Ghisellini G., Padovani P., Celotti A., Maraschi L. 1993, ApJ 407, 65

Gopal-Krishna 1991, A&A 248, 415

Gopal-Krishna 1994, to appear in the Proc. of the 6th Asian-Pacific Regional Meeting of the IAU at Pune 1993

Gopal-Krishna, Kulkarni V.K., Mangalam A.V. 1994, MNRAS, in press

Gregory P.C., Condon J.J. 1991, ApJS 75, 1011

Haardt F., Maraschi L. 1991, ApJ 380, L51

Hartmann D.L., Bertsch D.L., Fichtel C.E. et al. 1992, ApJ 385, L1

Heckman T., O'Dea C.P., Baum S.A., Laurikainen, E. 1994, ApJ (10 June 1994), in press

Hessman F.V. 1991, A&A 246, 137

Hubble E. 1926, ApJ 54, 369

Hughes D.H., Robson E.I., Dunlop J.S., Gear W.K. 1993, MNRAS 263, 607

Jones T.W., O'Dell S.L. 1977, A&A 61,29

Jones T.W., O'Dell S.L., Stein W.A. 1974, ApJ 188, 353

Kaastra J.S., de Korte P.A.J. 1988, A&A 198, 16

Kapahi V.K. 1990, in: "Parsec Scale Radio Jets", Zensus J.A. & Pearson T.J. (eds.), Cambridge University press, p. 304

Kato S., Fukue J., Inagaki S., Okazaki A.T. 1982, PASJ 34, 51

Kellermann K.I., Pauliny-Toth I.I.K. 1969, ApJ 155, L71

Kellermann K.I., Sramek R., Schmidt M., Shaffer D.B., Green R. 1989, AJ 98, 1195 (KSSSG)

Kembhavi A., Feigelson E.D., Singh K.P. 1986, MNRAS 220, 51

Kerr R. 1963, Phys.Rev.Lett. 11, 237

Königl A. 1980, Phys. Fluids 23, 1083

Königl A. 1981, ApJ 243, 700

Krabbe A., Genzel R., Drapatz S., Rotaciuc V. 1991, ApJ 382, L19-L22

Krichbaum T.P., Zensus J.A., Witzel A., Mezger P.G., Standke K. et al. 1993, A&A 274, L37

Kühr H., Nauber U., Pauliny-Toth I.I.K., Witzel A. 1981, A&AS 45, 367

Lacy M., Rawlings S., Hill G.J. 1992, MNRAS 258, 828

Laing R.A., Riley J.M., Longair M.S. 1983, MNRAS 204, 151

Lawrence A., Elvis M. 1982, ApJ 256, 410

Lind K.R., Blandford R.D. 1985, ApJ 295, 358

Machalski J., Magdziarz P. 1993, A&A 267, 363

Malkan M.A. 1983, ApJ 268, 582

Malkan M.A., Falcke H. 1994, in preparation

Malkan M.A., Sargent L.W. 1982, ApJ 254, 22

Mannheim K. 1993, A&A 269, 67

Mannheim K., Biermann P.L. 1989, A&A 221, 211

Maraschi L., Celotti A., Ghisellini G. 1992, in: "Physics of AGN", Springer Verlag, W. Duschl & S.J. Wagner (eds.), p. 605

Marecki A., Falcke H., Patnaik A. 1994, in prep.

Marscher A.P. 1987, in: "Superluminal Radio Sources", Cambridge University press J.A. Zensus & T.J. Pearson (eds.), p. 280

Marscher A.P. 1992, in: "Physics of AGN", Springer Verlag, W. Duschl & S.J. Wagner (eds.), p. 510

Marscher A.P., ApJ 264, 296

Marscher A.P., Gear W.K. 1985, ApJ 298, 114

McLeod K.K., Rieke G.H. 1994, ApJ 420, 58

Meisenheimer K. 1992, in: "Physics of AGN", Springer Verlag, W. Duschl & S.J. Wagner (eds.), p. 525

Melia F., Jokipii J.R., Narayanan A. 1992, ApJ 395, L87

Melia F., Königl A. 1989, ApJ 340, 162

Mezger P. G., Wink J.E. 1986, A&A 157, 252

Miller P., Rawlings S., Saunders R. 1993a, MNRAS 263, 425 (MRS)

Miller P., Rawlings S., Saunders R., Eales S. 1993b, MNRAS 254, 93

Müller T., Rosa M.R., Röser S. 1994, A&A 283, L29

Mushotzky R.F. 1982, ApJ 256, 99

Neff S.G., Hutchings J.B. 1992, AJ 103, 1746

Niemeyer M., Biermann P.L. 1993, A&A 297, 393

Novikov I.D., Thorne K.S. 1973, in: "Les astres occlus", DeWitt C. & DeWitt B. (eds.), Gordon & Breach, New York p. 343-450

Osterbrock D.E. 1991, Rep. Prog. Phys. 54, 579

Ostrowski M. 1993, preprint

Padovani P., Urry C.M. 1990, ApJ 368, 373

Page D.N., Thorne K.S. 1974, ApJ 191, 499

Perley R.A., Carilli C.L., Leahy J.P. 1993, in: "Jets in Extragalactic Radio Sources", Röser & Meisenheimer (eds.), Springer Verlag, p. 217

Phinney E.S. 1982, MNRAS 198, 1109

Pogge R.W. 1989a, AJ 98, 124

Pogge R.W. 1989b, ApJ 345, 730

Price R., Gower, A.C., Hutchings J.B., Talon S., Duncan D., Ross G. 1993, ApJS 86, 365

Rachen J.P., Biermann P.L. 1993, A&A 272, 161 (RB93)

Rachen J.P., Stanev T., Biermann P.L. 1993, A&A 273, 377

Rawlings S., Saunders R. 1991, Nat 349, 138 (RS91)

Rawlings S., Saunders R., Eales S.A., Mackay C.D. 1989, MNRAS 240, 701

Rees M., Begelman M., Blandford R., Phinney E. 1982, Nat 295, 17

Roberts D.A., Goss W.M., van Gorkom J.H., Leahy J.P. 1991, ApJ 366, L15

Rosa M.R., Zinnecker H., Moneti A., Melnick J. 1992, A&A 257, 515

Rybicki G.B., Lightman A.P. 1979, “Radiative Processes in Astrophysics”, John Wiley & Sons, New York

Saikia D.J., Shastri P., Sinha R.P., Kapahi V.K., Swarup G. 1984, JA&A 5, 429

Sanders D.B., Phinney E.S., Neugebauer G., Soifer B.T., Matthews K. 1989, ApJ 347, 29

Sanders R.H. 1992, Nat 359,131

Sanders R.H., Lowinger Th., 1972, AJ 77, 292

Schmidt M. 1963, Nat 197, 1037

Schmidt M., Green R. 1983, ApJ 269, 352

Schmutzler T. 1987, PhD Thesis, RFW Universität Bonn

Schmutzler T., Tscharnuter W.M. 1993, A&A, 273, 318

Schwarzschild K. 1916, Sitzungsber. Dtsch. Akad. Wiss. Berin, Kl. Math. Phys. Tech., p. 189

Sellgren K. 1988, in: “The Galctic Center”, Morris M. (ed.), Proc. IAU Symp. 136, p. 477

Seyfert C.K. 1943, ApJ 97, 28

Shakura N.I., Sunyaev R.A., 1973, A&A 24, 337

Sikora M., Kirk J.G., Begelman M.C., Schneider P. 1987, ApJ 320, L81

Slipher V. M. 1917, Lowell Obs. Bull. 3, 59

Smith E., Heckman T. 1989, ApJ 341, 658

Sofue Y., Reich W., Reich P. 1989, A&A 341, L47

Strittmatter P.A., Hill P., Pauliny-Toth I.I.K., Steppe H., Witzel A. 1980, A&A 88, L12

Sun W.H., Malkan M.A. 1989, ApJ 346, 68 (SM89)

Tamblyn P., Rieke G.H. 1993, ApJ 414, 573

Teräsranta H., Tornikoski M., Valtaoja E. et al. 1992, A&AS 94, 121

Terlevich R., Melnick J. 1985, MNRAS 224, 193

Thorne K. S. 1974, ApJ 191, 507

Unger S.W., Lawrence A., Wilson A.S., Elvis M., Wright A.E. 1993, MNRAS 228, 52

von Weizsäcker C.F. 1948, Zeitschrift f. Naturf. 3 a, 524

Wampler E.J., Ponz D. 1985, ApJ 298, 448

Wardle J.F.C. 1977, Nat 269, 563

Wilkinson P.N., Tzioumis A.K., Benson J.M. et al. 1991, Nat 352, 313

Wilson A.S. 1992, in: "Physics of AGN", Springer Verlag, Duschl & Wagner (eds.), p. 307

Witzel A. 1992, in: "Physics of AGN", Springer Verlag, Duschl & Wagner (eds.), p. 484

Zdziarski A.A., Ghisellini G., George I.M., Svensson R., Fabian A.C., Done C. 1990, ApJ 363, L1

Zylka R., Mezger P.G. 1988, A&A 190, L25

Zylka R., Mezger P.G., Lesch H., 1992, A&A 261, 119 (ZML92)

Zylka R., Mezger P.G., Wink J.E., 1990, A&A 234, 133

Danksagungen

Als aller erstes möchte ich mich bei meinem Betreuer Prof. Dr. P.L. Biermann ganz herzlich für seine intensive Begleitung bedanken. Seine andauernde Neugier, seine stetige Diskussionsbereitschaft und sein schier unerschöpflicher Erfahrungsschatz waren für mich eine wertvolle und lehrreiche Unterstützung. Dem Koreferenten Herrn Prof. Dr. H.J. Fahr danke ich für die Durchsicht dieser Arbeit und seine wohlwollende Begleitung in den vergangenen zwei Jahren.

Finanziert wurde ich aus Mitteln der DFG (Bi 191/9, SP Kosmische Plasmen). Die positive internationale Akzeptanz meiner Arbeit wäre aber nicht möglich gewesen ohne die großzügige Unterstützung von Reisen und Arbeitsmaterialien durch das Max-Planck-Institut für Radioastronomie und unserem Direktor Prof. Dr. G. Weigelt, dem ich dafür noch einmal ganz besonders danken möchte.

Neben den materiellen Rahmenbedingungen waren für mich die vielen Diskussionen die ich führen konnte von besonderer Bedeutung. Herr Prof. Dr. P.G. Mezger hat mit seinem Interesse für das Galaktische Zentrum diese Arbeit ganz entscheident beeinflußt und viele neue Fragestellungen motiviert. Dr. W. Duschl, Dr. K. Mannheim und Prof. Dr. Gopal-Krishna haben ebenfalls wichtige Beiträge zu den verschiedenen Kapiteln geleistet. Prof. Dr. M. Malkan (UCLA) hat darüberhinaus auch noch unveröffentlichte Daten zur Verfügung gestellt. Dr. T. Schmutzler (ITA Hdbg.), Dr. R. Zylka, Dr. T. Krichbaum, Prof. Dr. G. & M. Rieke (Steward Obs., Tucson), Dr. O. Heinrich (ITA Hdbg.), Dr. R. Schlickeiser, Dr. H. Scherer, Prof. Dr. W. Kundt und Dr. H. Lesch haben in unterschiedlicher Weise durch Daten und Diskussionen zur Klärung vieler Sachverhalte beigetragen. Ihnen allen gilt mein herzlicher Dank.

Darüberhinaus gilt ein besonderes Dankeschön meinen Zimmerkollegen Dipl. Phys. Jörg Rachen, Dipl. Phys. M. Niemeyer, Dr. Biman Nath und zuletzt auch Henning Seemann, mit denen eine hervorragende und oft lehrreiche Zusammenarbeit möglich war. Für viele Tips und gelegentliche Tischtennis Spiele danke ich unserem Nachbarzimmer, insbesondere Dr. R Wegener, Dipl. Phys. C. Naundorf, Dipl. Phys. K. Otterbein und Dipl. Phys. W. Steffen.

Schließlich möchte ich es nicht versäumen meiner Familie, insbesondere meinen Eltern, Großeltern, meiner Schwiegermutter und meinem Bruder für ihre kontinuierliche Förderung und Begleitung meines Studiums zu danken. Eine ganz besondere Unterstützung und Motivation waren mir aber meine Frau Dagmar und unsere Tochter Jana. Unsere gemeinsame Liebe und unser gemeinsamer Glaube sind trotz aller Größe und Erhabenheit des Universums das Wichtigste für mich geblieben.

Lebenslauf

Name:	F a l c k e
Vornamen:	Heino Dietrich Erhard
Geburtsdatum:	26. September 1966
Geburtsort:	Köln
Anschrift:	Heinrich-Imig-Str. 31, D-50226 Frechen
Stand:	Verheiratet seit 12. Mai 1989 mit Dagmar Falcke, geb. Freiburg, Lehramtsanwärterin, geb. am 28. November 1966
Kinder:	Jana Lena, geb. 10.11.1992
Eltern:	Dr. Sigurd Falcke, Facharzt für Orthopädie und Erika Falcke, geb. Hemmersbach, Lehrerin
Geschwister:	Carsten, 24 Jahre, Student
Schulbesuch:	Besuch der Grundschule in Köln 1972 bis 1974; (1974 Umzug nach Frechen) Besuch der Grundschule in Frechen 1974 bis 1976; Besuch des Gymnasiums der Stadt Frechen 1976 bis 1985 mit Abschluß Abitur
Zivildienst:	20 Monate von Juli 1985 bis Februar 1987 in der Biometrischen Abteilung der Universitätsklinik Köln, anschließend ein weiteres halbes Jahr als Honorarkraft in der selben Abteilung
Studium:	Studium der Physik an der Universität Köln 3 Semester (WS86/87 bis WS87/88); 5 Semester an der Universität Bonn (SS88-WS90/91); Vordiplom am 4.4.1989; nach 7 Semestern mündliche Hauptdiplom-Prüfung in Physik (im SS90), im Anschluß Diplomarbeit "Zur Theorie strahlungsgetriebener Scheibenwinde in Quasaren", Erlangung des Diploms am 13. Februar 1992; von März 1992 bis Juni 1994 Promotionsstudium im Fach Astronomie an der Universität Bonn
Weitere Tätigkeiten:	Freiberuflicher Dozent für Fortran bei der Firma DIGITAL (DEC) 1987 bis 1988; Tutor (Computer/theor. Physik) an der Universität Bonn (WS89/90); Honorarkraft (Diplomand) am Max-Planck-Institut für Radioastronomie in Bonn Juli 1990 bis Februar 1992; seit April 1993 wissenschaftlicher Angestellter an der Universität Bonn mit Gastvertrag am MPIfR Bonn und Finanzierung durch DFG, Erziehungsurlaub von Dezember 1993 bis Mai 1994; im Juni 1993 Teilnahme an der internationalen Sommerschule der Vatikansternwarte in Castel Gandolfo; ehrenamtlicher Prediger in der ev. Kirche seit 1992; Vorsitzender des CVJM Frechen e.V. seit 1987